NATIONAL CENTER FOR EARTHQUAKE ENGINEERING RESEARCH

ISSN 1088-3800

Computational Strategies for Frames with Infill Walls: Discrete and Smeared Crack Analyses and Seismic Fragility

by

K.M. Mosalam, R.N. White and P. Gergely

Technical Report NCEER-97-0021

December 31, 1997

This research was conducted at Cornell University and was supported in whole or in part by the National Science Foundation under grant number BCS 90-25010 and other sponsors.

NOTICE

This report was prepared by Cornell University as a result of research sponsored by the National Center for Earthquake Engineering Research (NCEER) through a grant from the National Science Foundation, and other sponsors. Neither NCEER, associates of NCEER, its sponsors, Cornell University nor any person acting on their behalf:

a. makes any warranty, express or implied, with respect to the use of any information, apparatus, method, or process disclosed in this report or that such use may not infringe upon privately owned rights; or

b. assumes any liabilities of whatsoever kind with respect to the use of, or the damage resulting from the use of, any information, apparatus, method, or process disclosed in this report.

Any opinions, findings, and conclusions or recommendations expressed in this publication are those of the author(s) and do not necessarily reflect the views of NCEER, the National Science Foundation, or other sponsors.

NATIONAL CENTER FOR EARTHQUAKE ENGINEERING RESEARCH
Headquartered at the State University of New York at Buffalo

Computational Strategies for Frames with Infill Walls: Discrete and Smeared Crack Analyses and Seismic Fragility

by

K.M. Mosalam[1], R.N. White[2] and P. Gergely[3]

Publication Date: December 31, 1997
Submittal Date: July 21, 1997

Technical Report NCEER-97-0021

NCEER Task Numbers 93-3111, 94-3111, 94-3112 and 95-3111

NSF Master Contract Number BCS 90-25010

1 Assistant Professor, Department of Civil and Environmental Engineering, University of California, Berkeley; former Lecturer, School of Civil and Environmental Engineering, Cornell University
2 James A. Friend Family Professor of Engineering, School of Civil and Environmental Engineering, Cornell University
3 Professor of Structural Engineering (deceased), School of Civil and Environmental Engineering, Cornell University

NATIONAL CENTER FOR EARTHQUAKE ENGINEERING RESEARCH
State University of New York at Buffalo
Red Jacket Quadrangle, Buffalo, NY 14261

PREFACE

The National Center for Earthquake Engineering Research (NCEER) was established in 1986 to develop and disseminate new knowledge about earthquakes, earthquake-resistant design and seismic hazard mitigation procedures to minimize loss of life and property. The emphasis of the Center is on eastern and central United States *structures*, and *lifelines* throughout the country that may be exposed to any level of earthquake hazard.

NCEER's research is conducted under one of four Projects: the Building Project, the Nonstructural Components Project, and the Lifelines Project, all three of which are principally supported by the National Science Foundation, and the Highway Project which is primarily sponsored by the Federal Highway Administration.

The research and implementation plan in years six through ten (1991-1996) for the Building, Nonstructural Components, and Lifelines Projects comprises four interdependent elements, as shown in the figure below. Element I, Basic Research, is carried out to support projects in the Applied Research area. Element II, Applied Research, is the major focus of work for years six through ten for these three projects. Demonstration Projects under Element III have been planned to support the Applied Research projects and include individual case studies and regional studies. Element IV, Implementation, will result from activity in the Applied Research projects, and from Demonstration Projects.

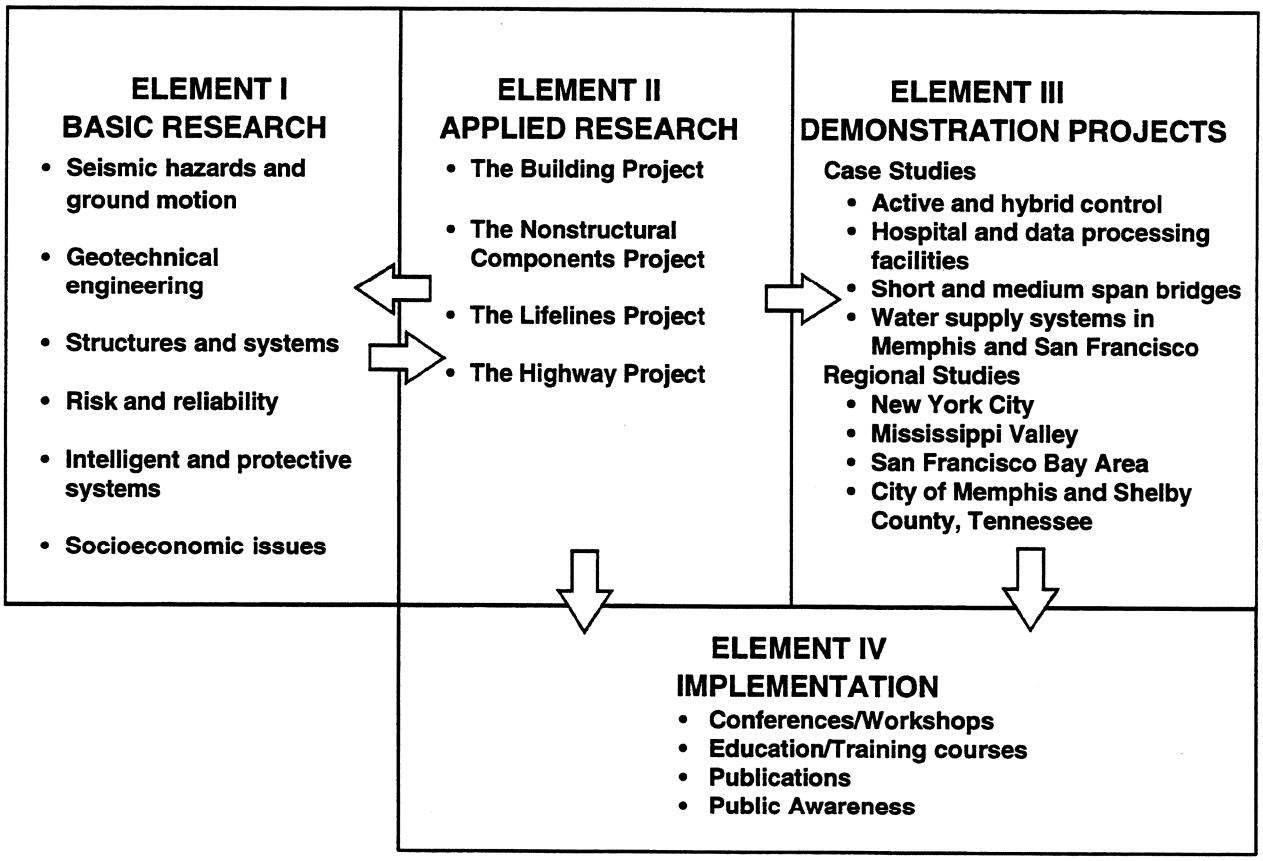

Research in the **Building Project** focuses on the evaluation and retrofit of buildings in regions of moderate seismicity. Emphasis is on lightly reinforced concrete buildings, steel semi-rigid frames, and masonry walls or infills. The research involves small- and medium-scale shake table tests and full-scale component tests at several institutions. In a parallel effort, analytical models and computer programs are being developed to aid in the prediction of the response of these buildings to various types of ground motion.

Two of the short-term products of the **Building Project** will be a monograph on the evaluation of lightly reinforced concrete buildings and a state-of-the-art report on unreinforced masonry.

The **structures and systems program** constitutes one of the important areas of research in the **Building Project**. Current tasks include the following:

1. Continued testing of lightly reinforced concrete external joints.
2. Continued development of analytical tools, such as system identification, idealization, and computer programs.
3. Perform parametric studies of building response.
4. Retrofit of lightly reinforced concrete frames, flat plates and unreinforced masonry.
5. Enhancement of the IDARC (inelastic damage analysis of reinforced concrete) computer program.
6. Research infilled frames, including the development of an experimental program, development of analytical models and response simulation.
7. Investigate the torsional response of symmetrical buildings.

This work proposes a model of behavior of mortar joints including fracture after a peak of nonlinear strength is achieved. The model is calibrated using information from rigorous testing of masonry subcomponents and materials. The model was used in a finite element analysis using a complex computational platform, DIANA, to determine the contribution of masonry infills to the behavior of framed structures. The analytical method of super-convergent path recovery is compared with a smeared crack model approach and with experiments (pseudo-dynamic and seismic simulation using the shaking table). The model was then used to generate fragility curves for infill frames with various properties resulting from variability of materials and modeling parameters. The work presents a comprehensive analytical and experimental approach which allows a complete picture of advanced analysis of masonry structures. The work integrates the efforts of NCEER in seismic loss assessment, providing reliable fragility curves for the probabilistic cost analysis. The work was part of phase one of "Loss Assessment of Memphis Buildings," and provides a strong engineering basis for the evaluation.

ABSTRACT

Several computational strategies for masonry structures, and particularly for frames with masonry infills, are presented. Three levels of details for the computational models are explored. *Micro-modeling* of masonry is presented first where the mortar joints are modeled using interface elements. Subsequently, a different approach is provided where various techniques for masonry composite are discussed. These models may be considered of an intermediate level of detail (*meso-modeling*) where damage mechanisms are accounted for in the form of smeared cracking using homogeneous properties for masonry. Numerical simulations involving smeared cracking face several problems due to mesh-sensitivity. To circumvent these problems, the standard smeared cracking is reformulated to allow for a systematic adaptation of the crack band width. This idea led to the development of the evolutionary characteristic length method, along with an adaptive strategy for the finite element discretization with mesh enrichment. This technique can handle nonlinearities produced by both smeared cracking and interface conditions. The third level of modeling (*macro-modeling*) is special for masonry infill walls where equivalent nonlinear truss elements are used to replace the effect of the walls on the bounding frames. This modeling technique is useful as a design approach for masonry infills. Finally, further simplification of modeling frames with and without masonry infills is considered by using equivalent single degree of freedom systems based on the dynamic plastic hinge method. This approximate computational approach is utilized for the seismic fragility evaluation.

ACKNOWLEDGEMENTS

The financial support of the National Center for Earthquake Engineering Research, Buffalo, New York is gratefully acknowledged. The computational work of this study was conducted using the finite element code DIANA of TNO Building and Construction Research, Delft, The Netherlands. The assistances of Dr. Ton van den Boogaard of TNO and Dr. Paulo Lourenço of Delft University of Technology in the understanding and use of DIANA are acknowledged. Special thanks to Dr. Glaucio H. Paulino, for his help and contributions with the evolutionary characteristic length method and the adaptive finite element method.

TABLE OF CONTENTS

1 INTRODUCTION 1

2 FINITE ELEMENT MODELS FOR INFILLED FRAMES: DISCRETE APPROACH 5

2.1 Literature Review on Finite Element Analysis of Infilled Frames 5

2.2 Modeling of Masonry Infills 10

2.3 Discrete Modeling of Mortar Joints 13

2.3.1 Interface elements for masonry composite 13

2.3.2 Mode-I fracture model and normal direction behavior of mortar joints 15

2.3.3 Pre-peak model and tangential direction behavior of mortar joints . 17

2.3.4 Determination of the material parameters 19

2.3.5 Post-peak model and tangential direction behavior of mortar joints 22

2.3.6 Verification of the interface constitutive model 24

2.4 Application to an Infilled Frame 24

2.4.1 Frame/wall interface modeling 27

2.4.2 Comparison between experimental and numerical results 29

2.5 Summary 29

3 FINITE ELEMENT CONTINUUM APPROACHES FOR MASONRY INFILLS 31

3.1 Review of Homogenization Techniques 31

3.2 Elastic Properties For Masonry as a Composite Material 34

3.2.1 Rheological model for masonry composites 34

3.2.2 Verification of the 1D model for masonry using the FEM 37

3.3 Parameter Estimation Using Experimental Displacement Fields 39

3.3.1 Theoretical background 39

TABLE OF CONTENTS (Cont'd)

3.3.2 Experimental setup and observation data for system identification . 41

3.3.3 Numerical model for system identification 41

3.3.4 Identification results 43

3.4 Continuum Modeling of Masonry Infills 44

3.4.1 Calibration and verification of the truss model 47

3.4.2 Effect of opening size on the lateral stiffness of infilled frames . . . 53

3.4.3 Motivation for evolutionary methods in smeared cracking 55

3.5 Summary 55

4 EVOLUTIONARY METHODS FOR SMEARED CRACKING 57

4.1 Smeared Crack Framework 58

4.2 Strain Softening and Fracture Energy 64

4.3 Adaptive FEM For Problems With Smeared Cracking 66

4.3.1 Review of error estimation and adaptivity 66

4.3.2 Error estimation for linear problems 67

4.3.3 Modified superconvergent patch recovery 69

4.3.4 Identification of patches 72

4.3.5 Adaptivity 72

4.3.6 Mesh enrichment 75

4.3.7 Numerical results 77

4.4 Evolutionary Characteristic Length Method For Smeared Cracking 79

4.4.1 Nonlocal apparent fracture energy and systematic evaluation of Λ . 79

4.4.2 Convergence property 82

4.4.3 Simplified forms for the evolution equation 83

4.4.4 Nonlocal forms and superconvergent patch recoveries 84

4.4.5 Numerical implementation 85

4.4.6 Mesh sensitivity study 85

TABLE OF CONTENTS (Cont'd)

4.4.7 Numerical applications 88

4.5 Summary 99

5 APPROXIMATE MODELS FOR SEISMIC FRAGILITY 101

5.1 Seismic Fragility 101

5.1.1 Seismic hazard 102

5.1.2 Limit states 103

5.2 The Dynamic Plastic Hinge Method 108

5.3 Description of The Investigated Structure 110

5.4 Validation of The Dynamic Plastic Hinge Method 113

5.5 Random Properties 115

5.6 Simulation Method 116

5.7 Results 118

5.8 Summary 120

6 CONCLUDING REMARKS 121

6.1 Summary and Conclusions 121

6.2 Suggestions for Future Research 122

7 REFERENCES 123

A Derivation of Equivalent Elastic Properties of Masonry 137

A.1 Vertical Direction 137

A.2 Horizontal direction 138

B Fracture Energy and Damage Mechanics 141

C Characteristics of LRC Frame 143

LIST OF ILLUSTRATIONS

1-1 Study program of infilled frames. 3

2-1 Finite element models for masonry infills. 12

2-2 Modeling of masonry composite; (a) Detailed model; (b) Approximate model. 14

2-3 4-noded 1D interface element. 15

2-4 Normal stress versus relative displacement relation. 16

2-5 Pre-peak shear stress versus relative displacement relation. 18

2-6 Effect of the peak ratio (R_p) on the tangent shear stiffness. 20

2-7 Mohr-Coulomb failure envelope of the interface element. 22

2-8 Post-peak shear stress versus relative displacement relation. 23

2-9 Finite element model for the masonry diagonal tension example. 25

2-10 Interface elements as mortar joints for the masonry diagonal tension example. 25

2-11 Deformed shape at crack initiation of the masonry diagonal tension example. 26

2-12 Deformed shape at full cracking of the masonry diagonal tension example. 26

2-13 Comparison between FE results and experimental results for the masonry diagonal tension example. 27

2-14 Determination of the lateral stiffness of the two-bay single-story bare frame. 28

2-15 Material model for the frame/wall interface element. 28

2-16 Comparison between the FE results (top) and the experimental (bottom) crack patterns for the two-bay single-story infilled frame. 29

3-1 Two-step homogenization techniques. 32

3-2 Masonry as a composite material; (a) Periodic unit in a masonry wall; (b) Dimensions of block and mortar; (c) Rheological model in the vertical direction; (d) Rheological model in the horizontal direction. 35

3-3 Variation of the elastic modulus of masonry composite with the elastic modulus of the concrete block masonry. 37

3-4 Variation of stiffness in vertical direction with E_b. 38

LIST OF ILLUSTRATIONS (Cont'd)

3-5 Setup for system identification experiment. 40

3-6 Generic loading cycle at a system identification location of the wall panels. 41

3-7 Finite element model for system identification. 42

3-8 Convergence of identification algorithm; (a) Estimated parameter; (b) Norm of the residuals. 45

3-9 Experimental versus calculated displacement fields. 46

3-10 Finite element results of the two-bay, two-story infilled steel frame before wall cracking at $\Delta_r = 0.1\%$; (a) Deformed shape [Amplification factor = 100]; (b) Normal relative displacement along the interface [max $\approx$ 0.025 in]; (c) Normal compressive stress along the interface [max $\approx$ 2.65 ksi]. 48

3-11 Finite element results of the two-bay, two-story infilled steel frame after wall cracking; (a) Stress trajectories at $\Delta_r = 0.12\%$ [compression (max = 2.64 ksi), tension (max = 0.99 ksi)]; (b) Initiation of cracks in the top story at $\Delta_r = 0.12\%$; (c) Initiation of major cracks in the bottom story at $\Delta_r = 0.22\%$. 50

3-12 Finite element results of the two-bay, two-story infilled steel frame at the last converged loading increment; (a) Incremental deformation at $\Delta_r = 0.33\%$ [Amplification factor = 485]; (b) Crack pattern in the infill walls [all cracks]; (c) Crack pattern in the infill walls [fully open cracks]. 51

3-13 Approximate analysis of semi-rigidly connected steel frame with and without infills; (a) Truss model and its deformed shape with top floor displacement = 0.08 in [Amplification factor = 57]; (b) Bending moment diagram for infilled frame [max = 18.8 kip.in, min = -20.2 kip.in]; (c) Bending moment diagram for bare frame [max = 74.5 kip.in, min = -71.4 kip.in]. 52

3-14 Finite element model and material parameters for studying the effect of windows on the lateral stiffness. 54

3-15 Effect of opening size on infilled frame lateral stiffness for different applied inter-story drift (SD). 54

3-16 Spurious kinematic mode (top) and corresponding cracks (bottom). 55

4-1 Smeared cracking in a typical patch of finite elements; (a) Example of a patch of finite elements; (b) Mohr circle; (c) Tension cut-off in 2D principal stress space; (d) Strain decomposition; (e) Total fracture energy density (full cracking). 62

4-2 Strain decomposition and apparent fracture energy density. 63

LIST OF ILLUSTRATIONS (Cont'd)

4-3 Different patches for the SPR method. 73

4-4 Refinement level used in the adaptivity procedure. 76

4-5 Identification of constraint nodes during mesh enrichment. 76

4-6 One-level-rule. 77

4-7 Results of the adaptive procedure before wall cracking; (a) Deformed shape; (b) Adapted mesh without the One-level-rule; (c) Adapted mesh enforcing the One-level-rule. 78

4-8 Results of the adaptive procedure after wall cracking; (a) Crack pattern; (b) Adapted mesh without the One-level-rule; (c) Adapted mesh enforcing the One-level-rule. 80

4-9 4-point bending notched plain concrete beam for the study of mesh sensitivity. 87

4-10 Results of the 4-point bending notched plain concrete beam; (a) Constant Λ; (b) Adapting Λ. 89

4-11 Distribution of the adapted crack band width along the beam ligament. . 90

4-12 Results of Example 1; (a) Finite element model and fully developed smeared cracks; (b) Model for discrete cracking; (c) Comparison of load-deflection relations for different cracking approaches. 92

4-13 Load-deflection relations of Example 2. 93

4-14 Example 2: finite element model and its results; (a) Model; (b) Crack patterns with constant Λ; (c) Crack patterns with adapted Λ. 94

4-15 Crack-Line-Wedge-Loaded Double-Cantilever-Beam (CLWL-DCB) specimen; (a) Dimensions, boundary conditions and material properties; (b) Finite element mesh. 96

4-16 CLWL-DCB results; (a) Wedge force versus CMOD; (b) CMSD versus CMOD; (c) Notations. 98

4-17 CLWL-DCB results; (a) Contour plot for g^t; (b) Contour plot for $\bar{g}^t$; Note: (left) actual scale and (right) distorted scale. 100

5-1 Definition of probability of failure for fragility analysis. 102

5-2 Distribution of the PGA of the synthetic records. 103

5-3 Time histories of a sample of earthquake records used for the fragility analysis. 104

LIST OF ILLUSTRATIONS (Cont'd)

5-4 Response spectra of a sample of earthquake records used for the fragility analysis; (a) $R_e = 40$ km; (b) $M_m = 7.0$. 105

5-5 Finite element model of the investigated two-bay, two-story LRC infilled frame. 111

5-6 Reinforcement details of the finite element model of the investigated two-bay, two-story LRC infilled frame. 112

5-7 Pushover curve for the bare frame. 113

5-8 Comparisons between the results of finite element analysis and the equivalent SDOF based on the DPHM under Taft scaled to $0.175g$. 114

5-9 Pushover curves obtained from the finite element analysis. 116

5-10 Range of variation of the pushover parameters for the trilinear approximate model; (a) Bare frame; (b) Infilled frame. 117

5-11 Fragility curves for the LRC frame; (a) Bare frame; (b) Infilled frame. . . 119

B-1 Relation between damage parameter and apparent fracture energy density for different value of the crack band width. 142

C-1 Concrete dimensions and reinforcement details of the LRC frame. 144

C-2 Typical stress-strain relation of the concrete used in constructing the LRC frame. 145

C-3 Variation of the splitting tensile strength with the compressive strength. . 145

C-4 Variation of the modulus of rupture with the compressive strength. 146

C-5 Variation of the modulus of elasticity with the compressive strength. . . . 146

C-6 Typical result of a bond slip test. 147

C-7 Experimental results of the crack width versus the applied vertical load in three point bending experiments. 147

LIST OF TABLES

3-I Geometrical properties of the 1/4 scale concrete blocks (dimensions in inches). 36

3-II Parametric studies and results of the system identification technique. . . . 43

3-III Calibration results of continuum model and equivalent truss model of masonry infills. 47

5-I An example of the damage states. 107

5-II Random properties of the basic parameters of the analyzed LRC frames. . 115

5-III Random properties of additional parameters of the analyzed LRC frames. 118

SECTION 1

INTRODUCTION

A common type of construction in urban centers is low-rise and mid-rise building frames with unreinforced masonry walls filling the spaces bounded by their structural members. The walls, usually referred to as infill walls, are built after the frame is constructed as partitions or as cladding. Unreinforced masonry infill walls are usually classified as non-structural components, *i.e.* their structural contribution is neglected during the design process of the frames. Under this assumption, the bounding structural frame should be designed to withstand *all* forces: vertical due to gravity loads and lateral due to wind pressure and/or seismic ground motion.

Ignoring the contributions of infill walls during the design of the bounding frames may lead to erroneous design as the frame/wall interaction under extreme loading conditions always occurs. The effects of neglecting the infill walls are accentuated in high seismicity regions where the frame/wall interaction may cause substantial increase of stiffness resulting in possible changes in the seismic demand due to the significant reduction in the natural period of the structural system. Also, the composite action of the frame/wall system changes magnitude and distribution of straining actions in the frame members, *i.e.* critical sections in the infilled frame differ from those of the bare frame, which may lead to unconservative or poorly detailed designs. Moreover, these designs may be uneconomical since an important source of structural strength (particularly beneficial in regions of moderate seismicity) is wasted.

As a matter of fact, there is no resemblance between the responses of the infilled frame and the bare one, as the former is substantially stronger and stiffer than the latter. The performance shown by infilled frames is advantageous especially when the capacity (and ductility) of the frame itself is suspected to be inadequate. This is the case of frames mainly designed for gravity loads without or with little attention to lateral loads (usually due to wind effects) when subjected to moderate or severe lateral loads due to earthquakes.

Lessons from recent damaging earthquakes illustrate the consequence of ignoring the contribution of infill walls. In some cases, the real structure (*i.e.* the infilled frame) is subjected to demands smaller than those considered during design. Unfortunately, in other cases, the contrary occurs, *i.e.* design forces may be significantly exceeded increasing the seismic damage vulnerability of the structure. In all cases, the changes in the distribution of straining actions may render the structural detailing ineffective.

The problem of considering infill walls in the design process is partly attributed to incomplete knowledge of the behavior of *quasi-brittle* materials such as masonry and to a lack of conclusive experimental and analytical results to substantiate a reliable design procedure for this type of structure.

A series of three reports addresses the definition and investigation of experimental and computational strategies to evaluate the behavior of infilled frames subjected to earthquake loading. These reports are based on a study at Cornell University which is divided into three parts as schematically illustrated in Figure 1-1. In **Part I**, the static experiments on infilled frames are presented together with an investigation of the properties of concrete block masonry and its constituents. In **Part II**, the pseudo-dynamic experimentation and the corresponding results for a two-story infilled frame are presented. Finally, in **Part III**, different computational strategies are introduced and critically investigated.

The first two reports of this series essentially involved experimental approaches to study the seismic behavior of frames with masonry infill walls. Although experiments provide invaluable findings, they can be quite expensive and time consuming. Also, the limitations enforced by the available testing facilities may make it impossible to experimentally investigate all the required parameters. In the present report, which is the third in this series, several computational strategies for masonry structures, and particularly for frames with masonry infills, are presented.

In **SECTION 2**, *micro-modeling* of masonry is presented where the mortar joints are modeled using interface elements. A different approach is provided in **SECTION 3** where various techniques for masonry composite (*meso-modeling*) are discussed. Brief presentation of the use of nonlinear truss elements to replace the effect of the walls on the bounding frames (*macro-modeling*) is also presented in **SECTION 3**. The standard smeared cracking, used to account for damage in quasi-brittle materials, is reformulated to allow for a systematic adaptation of the crack band width in **SECTION 4**. Also in this section, an adaptive strategy for the finite element discretization with mesh enrichment is presented. **SECTION 5** introduces an approximate computational approach for the seismic evaluation of frames with and without infill walls using fragility analyses. Finally, concluding remarks are given in **SECTION 6**.

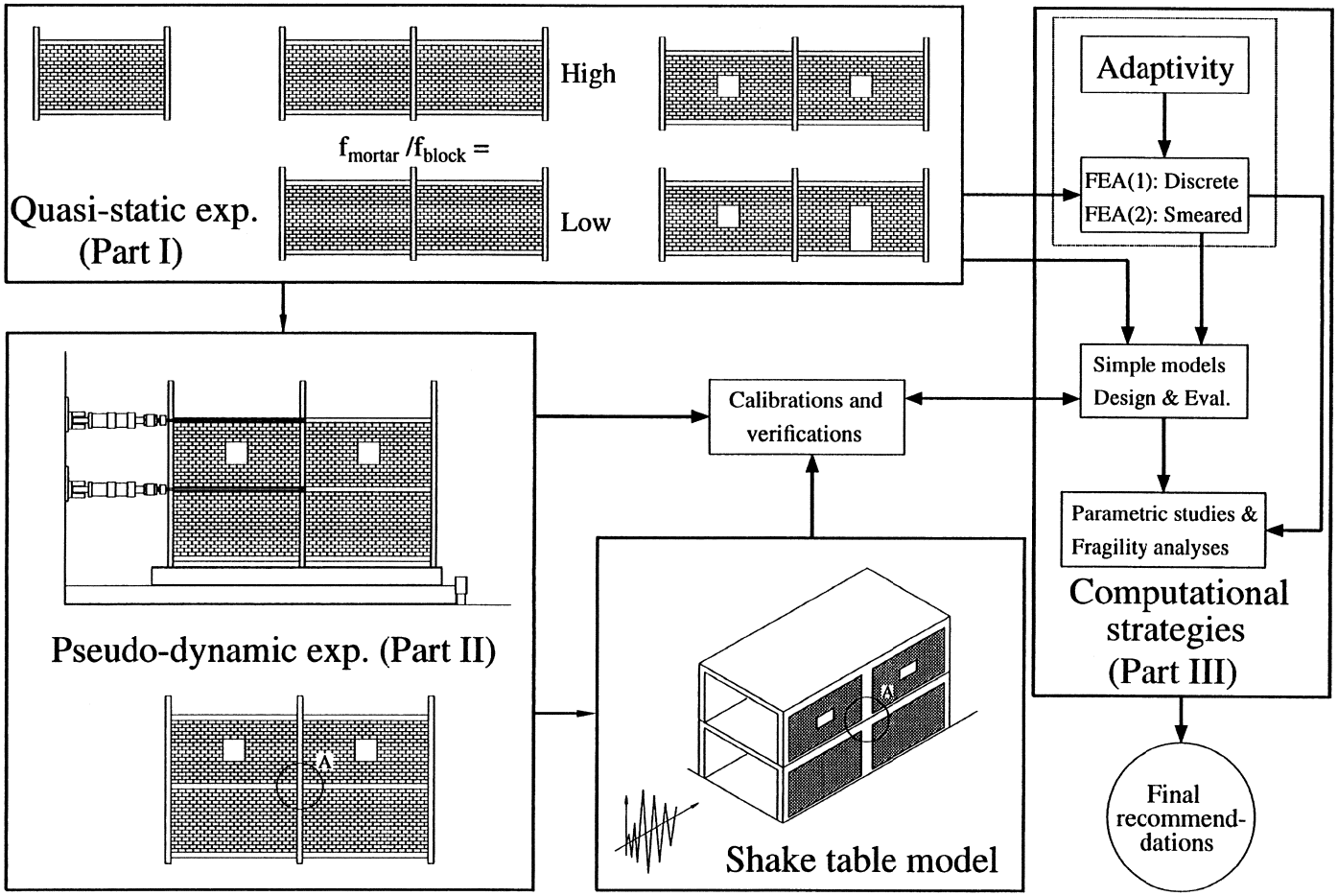

A: Typical lightly reinforced concrete joint detail, f: Compressive strength, FEA: Finite Element Analysis

FIGURE 1-1 Study program of infilled frames.

SECTION 2

FINITE ELEMENT MODELS FOR INFILLED FRAMES: DISCRETE APPROACH

The Finite Element Method (FEM) is used to model the structural behavior of frames with masonry infills. This method has been extensively used in the analysis and design of nearly all kinds of structures. A literature review of the studies conducted on infilled frames using FEM is presented first. This is followed by a discussion of the different methods for modeling masonry in the context of the FEM. The main thrust of this section is to introduce a discrete model for masonry. The model is formulated and applied to the analysis of a Gravity Load Designed (GLD) steel frame infilled with UnReinforced concrete block Masonry (URM) walls under the effect of lateral loading.

2.1 Literature Review on Finite Element Analysis of Infilled Frames

Several researchers have used the FEM to investigate the behavior of frames with infill walls. The FEM is considered as a *microscopic* modeling approach to complement more global *macroscopic* methods such as the equivalent strut techniques. In the absence of reliable experimental data, the microscopic approach is needed to develop and particularly to calibrate the corresponding macroscopic models [84].

The FEM was used for the first time to analyze infilled frames by Karamanski [80] in 1967. Using FE, Mallick and Severn [106] pioneered the treatment of frame/wall interface conditions by considering gap formation, slip and friction between the frame members and the infill walls. They modeled single- and multi-story infilled frames using linear plane stress elements for the infill walls. Mallick and Garg [107] considered the axial deformations of the windward column and assumed that the beam and the leeward column were axially rigid. They also examined the effects of openings and their location on the infilled frame behavior using linear elastic material models. Other researchers have focused also on the use of linear FE models, *e.g.* Liauw [94] assumed that infills were bonded to the frame, Yong [167] considered the pre-cracking behavior treating the frame/wall gap formation, and Achyutha *et al.* [1] [2] studied the effect of opening size, position and shape with and without stiffeners of different types around the openings on the behavior of infilled frames.

Thiruvengadam [161] utilized FE analysis to evaluate the first few natural frequencies and the associated mode shapes of infilled frames. He compared his results with two approximate methods, namely, the multiple strut model and the shear-flexure cantilever analogy. Based on the approximate models, the effect of frame/infill separation in reducing the fundamental frequency was investigated and an empirical relation was presented. Another

interesting contribution on the use of linear FE analysis of infilled frames was given by Reflak and Fajfar [141] where each infill is treated as a *substructure* and all degrees of freedom corresponding to the infill, with the exception of those at the contact with the frame, are eliminated using the *static condensation* procedure. Based on parametric studies of single-bay, single-story infilled frames with different types of openings, they concluded the following:

- Masonry infills can drastically alter the structural response of infilled frames.
- A model with an equivalent diagonal strut, although often used, may fail in the case of infill with openings and usually does not provide correct results for shear forces and bending moments in the columns of the frame.
- Provided that an appropriate mesh is used, a FE model yields reasonable results for displacements, internal forces in the frame and stresses in the infill, except in the vicinity of the contact between the frame and the infill.
- The feasibility of the FE analysis is greatly enhanced when substructuring techniques are considered especially for the analysis of multi-bay, multi-story infilled frames[1].

In a recent paper, Doudoumis *et al.* [44] developed a macroelement for the simulation of the elastic behavior of the infill panels in multi-story frames under horizontal seismic actions. The macroelement has 4 external and 4 internal nodes and consists of an isoparametric plane stress element with unilateral contact bonds at the corner nodes. They demonstrated the effectiveness of the developed macroelement through comparative parametric studies related to the geometry of the infilled frame, the relative stiffness of the frame and infill, the effects of vertical loads at the columns, the isotropy or orthotropy of the infill, and the friction coefficient between the frame and the infill.

Since the early attempts to use FEM in the analysis of infilled frames [106], modeling of the frame/wall interface conditions has received significant attention. Riddington and Stafford-Smith [144] introduced short stiff linking members between nodes on the interface to simulate cracking along the interface. King and Pandey [83] used friction elements to model the interface between the frame and the wall. Liauw and Kwan [96] used three different types of elements for the interface, panel and frame to study the behavior of infilled frames subjected to monotonic loading. They later extended their work to study the static as well as the cyclic behavior of multi-story infilled frames with different interface conditions [98].

The bracing action provided by the infill wall to the frame leads to reasonably high transverse tension field in the wall panels. The wall material usually has low tensile strength as it is made of plane concrete or unreinforced masonry; therefore, cracking is an important issue in modeling the material behavior of infill walls. This fact led several researchers

[1]Computational models such as those in the program COMBAT (COMprehensive Building Analysis Tool) consider these techniques [35].

to consider modeling of crack initiation and propagation among other sources of material and geometric nonlinearities in infill walls. Liauw and Kwan [95] [97] assumed that the infill panel *anisotropy* is mainly due to cracking. In tension, the material is treated as elastic/brittle whereas in compression, a nonlinear *uniaxial* stress-strain relation was assumed. They consider that the biaxial stress state may be approximated by a uniaxial state because one principal stress is much smaller than the other. From their experimental investigation, they confirmed this claim using strain gage measurements. The model was used to examine the behavior of multi-story infilled frames. Two cases for frame/wall interface conditions were treated: with and without shear connectors. The former led to no-slip behavior while the latter led to friction mobilization. They concluded that shear connectors improved the behavior by reducing the joint moments and the stress concentrations at the loaded corners.

The consideration of the material nonlinearity of the infill walls under dynamic loading may have started with the work of Natarajan and Wen [118] who studied the effect of walls on the dynamic response of infilled frames to earthquakes. Their analysis extended beyond the elastic range. The nonlinearities of the structural response produced by the formation of plastic hinges in the frame members and crack propagation in the wall elements were taken into account. The filler walls were idealized by finite elements in plane stress, interacting with the moment-resisting frame such that the joint displacements were compatible. In the dynamic analysis, the mass of the system is handled by a lumping procedure. Numerical results were reported for a three-story steel frame with concrete filler walls subjected to selected portions of the ground motion of the El-Centro earthquake of May, 1940. They concluded the following:

- The modeling of the wall panel of a floor as a *single rectangular finite element* interacting with the frame could reasonably account for the contribution of the walls to the overall lateral stiffness of a structure.

- The contribution of walls to the lateral stiffness and consequently the fundamental frequency and the dynamic response of a structure appears to be too considerable to be ignored, even when the walls are cracked.

- Elimination of the axial and rotational modes makes possible the use of a much larger time step in the numerical integration procedure and thus a considerable saving of computation time without any appreciable loss of accuracy.

Another important nonlinear FE model, developed by Rivero and Walker [148], was applied for dynamic analysis of infilled frames. They accounted for frame/wall discontinuities and interaction, wall cracking, wall bracing effect on the frame and the frame inelastic behavior. They modeled masonry cracking in the walls using discrete *joint* elements placed at the edges of the isotropic triangular elements representing the solid material of the wall. A special failure surface was assumed for masonry. In two dimensional (2D) stress space, this surface accounts for the effect of the angle between the mortar joints and the principal

stress. They used their model to study the behavior of several one-bay, one- and three-story infilled frames under ground motion. They concluded the following:

- Modeling the frame/masonry wall discontinuity and gap formation is essential.
- The gap size, the infilled frame strength, and the time of the frame maximum response have the most effect on the system behavior.
- The wall braces the frame once contact is made at the opposite diagonal corners.
- The natural period of the bare frame is far greater than that of the infilled frame.

Dhanasekar and Page [38] conducted an experimental research program where they tested 180 half-scale brickwork specimens under biaxial stress states. Based on their experimental results, they proposed a constitutive model for infill brick masonry which includes elastic properties, an inelastic stress-strain relation and a failure surface. This failure surface consisted of three intersecting elliptical cones in $\{\sigma_p, \sigma_n, \tau\}$ stress space, where σ_n is the normal stress orthogonal to the mortar bed joint, σ_p is the normal stress parallel to the mortar bed joint and τ is the shear stress. They considered this constitutive model in the analysis of infilled frames where one-dimensional (1D) interface elements were used to model frame/infill separation and block/mortar joint cracking. They analyzed square and rectangular panels and concluded the following:

- Diagonal and corner crushing failure modes were predicted for the square and rectangular panels, respectively.
- Nonlinear behavior was primarily caused by cracking and not by the other material nonlinearities.
- The infill modulus of elasticity considerably affected the infilled frame characteristics while Poisson's ratio did not.
- The compressive strength of the infill wall material had significant effects on the ultimate strength of the infilled frame if the failure mode was corner crushing. Consequently, increasing the infill compressive strength would change the failure mode from corner crushing to diagonal cracking failure.
- The infill tensile and shear bond strengths greatly affects the system strength and could also change the failure mode.

Initial gaps between the frame members and the infill walls may result from shrinkage of the wall material or from poor construction. Although this is obviously a highly uncertain parameter, its effect may be studied through the use of FE models where the interface conditions are idealized using elements that allow the definition of initial gaps. This may be accomplished either at the geometrical level (finite distance between the interface nodes)

or at the constitutive[2] level (zero tensile strength starting at a finite value of compressive deformation as will be discussed in Section 2.4.1). Riddington [145] used FE models to investigate the effect of initial gaps on the behavior of infilled frames. He noticed that even relatively small initial gaps significantly reduce the infilled frame lateral stiffness. However, they do not have a significant effect on the cracking pattern or ultimate strength. He classified the behavior of infilled frames with initial gaps into the following five stages:

1. The system acts as a bare frame.
2. The frame contacts the infill.
3. The infill slips and lifts to wedge into the loaded corners.
4. The infill wedges into the opposite corners of the frame .
5. The infill and the frame start acting together and continue up to the ultimate load.

Obviously, an infilled frame without initial gaps goes through stages 4 and 5 only. For dynamic analysis, Kost and Weaver [86] described a method for calculating the dynamic response of a plane building frame with filler panels and pre-existing gaps at the sides and top of the walls. All parts of the structure were assumed to be linearly elastic, but the response of the structure was nonlinear because of the opening and closing of the gaps. They analyzed a four-story structure where they concluded that the presence of gaps between the frame and the panels can have a major effect on the dynamic response of such structures.

El Hadad [51] used FEM and fracture mechanics techniques to consider cracking and separation phenomena between a reinforced concrete frame and a masonry infill wall. He investigated the redistribution of internal straining actions in the frame elements and stresses in the infill elements due to existing cracks considering the effect of varying the frame/infill contact length and infill/frame relative stiffness. In a more recent paper, Lafuente and Genatios [92] conducted nonlinear FE analysis of confined masonry walls subjected to monotonic loads to study the effect of the most important variables in determining the various possible infill cracking patterns. These variables were: vertical load, wall slenderness, and stiffness ratio between masonry units and mortar and between the masonry infill and the reinforced concrete frame. They proposed interaction curves in order to describe the various possible failure mechanisms in terms of the vertical load and to estimate the resistance of the wall.

The macroscopic behavior of masonry may be derived from the material behavior of its components (bricks or blocks and mortar). This can be accomplished through the use of *homogenization theory for periodic media* [158]. The technique of *homogenization* is becoming increasingly popular among the masonry analysis community [102]. The homogenization technique is meant to provide constitutive relations in terms of averaged stresses and

[2]Constitutive relations are mathematical descriptions of the material behavior.

strains from the constitutive relations of the individual components of masonry. Anthoine [6] used homogenized media to model masonry infill in a reinforced concrete frame. He considered elastic perfectly plastic behavior of the reinforcing steel whereas for concrete and masonry, he used an isotropic model combining plasticity in compression (Drucker-Prager criterion with softening) and smeared cracking along two orthogonal fixed directions in tension (maximum tensile stress criterion with softening). Unilateral contact without friction is assumed at the infill/frame interface. He analyzed two-bay, single-story structures under monotonically increasing lateral load, and observed that the initial lateral stiffness of the infilled frame is about 2.5 times that of the bare frame. Furthermore, the yielding in steel bars did not occur at the same locations as in the bare frame and the damage was spread along the leeward column. The failure in the infill was due to diagonal cracking.

An attempt to adopt both discrete and smeared cracking techniques for the analysis of infilled frames was performed by Mehrabi *et al.* [111] where they analyzed previously tested single-bay, single-story reinforced concrete frames infilled with unreinforced concrete block masonry. They considered interface elements to model the mortar joints, frame/wall interface and bond-slip of the reinforcing bars. They also considered smeared cracking for the concrete frame and the concrete blocks. Regarding the use of the different interface elements, they concluded the following:

- The bond-slip elements are important for capturing the behavior of the bare frame, while the influence of these elements on the behavior of infilled frames is insignificant.

- The interface elements successfully capture the separation at the frame/wall interfaces and the crack propagation along the mortar joints.

This section has shown that some progress has been achieved in computational modeling of infilled frames. This report presents further contributions in this area since much remains to be accomplished.

2.2 Modeling of Masonry Infills

The FEM is adopted to approximate the behavior of masonry structures, in particular frames with masonry infills. For a complete formulation of the finite element method, the reader is referred to textbooks on this subject, *e.g.* [17] [170] [171] and to the documentation of the computer program DIANA[3] [39] [40], which is the basic software used in this study. The behavior of infilled structures depends upon a large number of parameters [33]. For understanding the behavior of infilled frames, numerical tools which are capable of performing parametric studies under different conditions are needed. The FEM is a general technique which can model continuum mechanics phenomena as well as discrete

[3]DIANA: DISplacement ANAlyzer is the finite element code of TNO Building and Construction Research in The Netherlands.

phenomena such as cracks and interfaces. Therefore, the FEM is a good choice to carry out such tasks provided that sufficient validation and calibration of the used FE models are performed using experimental observations and measurements. Unfortunately, the quality of the results of the FE approximation is affected by the type and size of the finite elements, interpolation functions, quadrature rules (the structure stiffness matrix is usually numerically integrated) and by the arrangement of the mesh. Such pathological effects become highly detrimental in problems with strain-softening [149]. Accordingly, careful interpretation of the numerical results is mandatory in such cases.

Masonry exhibits distinct directional properties because mortar joints act as planes of weakness. When masonry walls are built to fill the space defined by a framed structure (*i.e.* as infill walls), the interfaces between the frame members and the walls act as other planes of weakness around the wall panel. Herein, a distinction is made between internal planes of weakness produced by mortar bed and head joints and external planes of weakness occurring at the frame/wall interfaces. For the internal joints, two phenomenological approaches are possible: discrete modeling and (enhanced) continuum modeling. As for the frame/wall interface, only discrete modeling is admissible. From a geometrical perspective, the modeling techniques for the two approaches of internal joints and that for the boundary interface are schematically illustrated in Figure 2-1. This figure illustrates two possible FE models for the two-bay, one-story semi-rigidly connected steel frame infilled with masonry walls. The infill walls have asymmetric openings to represent a window in one bay and a door in the other. This structure, tested using the quasi-static experimentation technique, was described in the first report of this series. In Figure 2-1, P and Δ are respectively the lateral load and displacement applied at the top of the central column. The stiffness of the frame/wall interface element in the normal and tangential directions are denoted as $\mathcal{D}_n$ and $\mathcal{D}_t$, respectively. The superscripts (comp) and (tens) refer to the value of the quantity in compression and in tension, respectively.

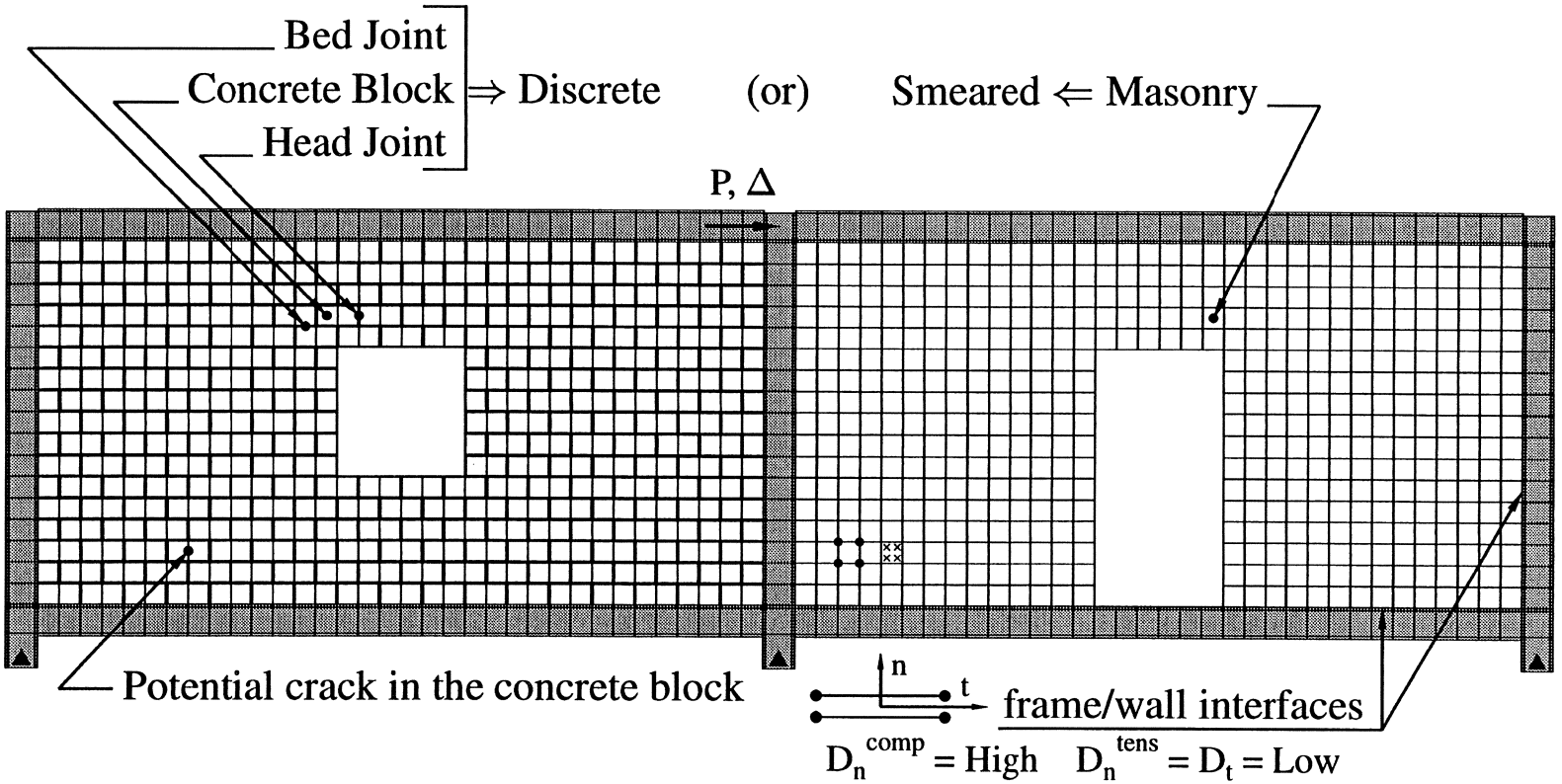

FIGURE 2-1 Finite element models for masonry infills.

2.3 Discrete Modeling of Mortar Joints

In the discrete approach, the softening characteristics are attributed to appearance of discrete cracks at interfaces, in which continuity of deformation is no longer satisfied because there are jumps in the displacement field. To represent this behavior, interface elements are introduced between continuum elements representing the masonry units. The constitutive relations for the interfaces define the relation between stress and relative displacements rather than stress and strain as in the standard continuum finite elements. This is intrinsically associated to the discrete nature of the crack model.

In general, the behavior of unreinforced hollow concrete block masonry structures cannot be treated with the well established concepts of concrete structures. In the latter, it is acceptable to assume homogeneous isotropic behavior [120]. This assumption may be justified for reinforced masonry where the concrete block masonry cells are grouted and reinforced. In unreinforced masonry, mortar joints must be treated properly. These joints represent planes of weakness and sources of material damping. The existence of such joints render the masonry composite a heterogeneous and anisotropic material.

Several methods are available in the literature for the treatment of discontinuities embedded in continuous systems. The pioneering researchers in this field are the rock mechanicians (*e.g.* Goodman, Ghaboussi and Isenberg). Within the context of the FEM, joints are usually treated using special joint elements. These elements differ from conventional elements in their geometrical configuration as well as their constitutive models. Some of the commonly used joint elements are those by Goodman *et al.* [63], Ghaboussi *et al.* [62], Desai *et al.* [37], Rots [150], Lotfi and Shing [100], Gambarotta and Lagomarsino [59] and Lourenço [102].

In the present study, interface elements are considered to model the mortar joints between hollow concrete masonry blocks. In this treatment, a new constitutive model is formulated and implemented in the finite element system DIANA.

2.3.1 Interface elements for masonry composite

Two levels of detail may be considered in the FE modeling of masonry composite to represent either of the following:

- Both masonry units and mortar joints are modeled using continuum elements with interfaces between the units and the joints, as illustrated by Figure 2-2(a).

- The lumped mortar joints in addition to the masonry units/mortar joints interfaces where continuum elements are considered in modeling *expanded masonry units* (regular masonry unit plus half a mortar joint in each side of the unit), as illustrated by Figure 2-2(b).

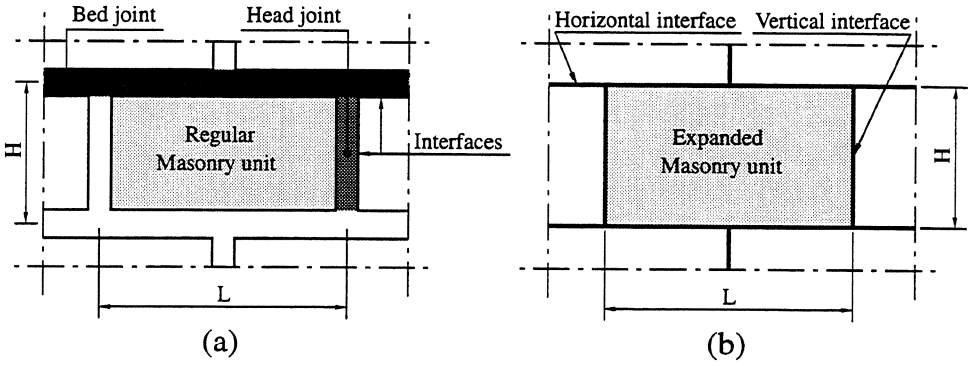

FIGURE 2-2 Modeling of masonry composite; (a) Detailed model; (b) Approximate model.

From computational point of view, note that the second alternative is more efficient than the first one. Therefore, the second alternative is employed in the present study where application is confined to the use of 1D interface element (for 4-noded case, see Figure 2-1). This element is depicted in Figure 2-3 and its detailed formulation can be found in Section 4.3 of reference [149].

The material model associated with the interface element used in the simplified model shown in Figure 2-2(b) is discussed in the present section. This material model reflects the following:

1. The elastic normal and shear behaviors of the mortar joint.
2. Crack initiation when normal tensile stress exceeds the tensile strength of the mortar joint (mode-I fracture).
3. Crack development produced by softening behavior in tension.
4. Full separation beyond the stress-free crack opening.
5. Nonlinear pre-peak response of the mortar joints subjected to shear loading.
6. The effect of pre-compression on the peak and residual shear strengths of the joints.
7. Post-peak shear strength evolution from peak value to residual value (mode-II fracture).
8. Dilatancy, which is the normal expansion of the mortar joints, particularly the bed joints, during shearing.

This model may be classified as a mixed mode crack model for masonry composite using interface finite elements. From a theoretical point of view, this model is in fact a cohesive zone type model. Essentially, it is an extension of the Dugdale-Barenblatt model (see, for

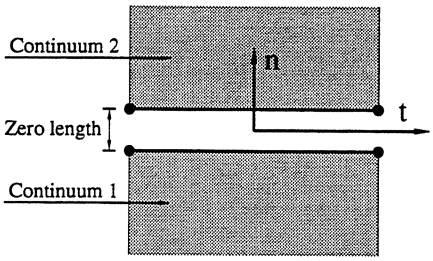

FIGURE 2-3 4-noded 1D interface element.

example, Section 5.1 of the book by Kanninen and Popelar [79]) applied to cracking in the masonry composite. From a computational point of view, the crack model using interface elements can be considered simply as nonlinear springs along the normal and the tangential directions of the interface (*i.e.* the mortar joint). The material parameters of this model were given in the first report of this series.

In the *elastic* stage, it is assumed that there is no coupling between the normal and the tangential directions, *i.e.*

$$\left\{ \begin{array}{c} \sigma \\ \tau \end{array} \right\} = \left[\begin{array}{cc} \mathcal{D}_n & 0 \\ 0 & \mathcal{D}_t \end{array} \right] \left\{ \begin{array}{c} u_n \\ u_t \end{array} \right\} \tag{2.1}$$

where σ, τ and u are, respectively, normal stress, shear stress and relative displacement between the two sides of the interface. Subscripts n and t, respectively refer to the local normal and tangential directions to the interface, as illustrated in Figure 2-3. The determination of the stiffness coefficients $\mathcal{D}_n$ and $\mathcal{D}_t$ will be discussed in the following paragraphs.

2.3.2 Mode-I fracture model and normal direction behavior of mortar joints

The material behavior of the interface element in the normal direction is governed by the normal stress versus relative displacement relation shown in Figure 2-4. From this figure, three distinct stages can be identified, namely

1. Contact

   $$\mathcal{D}_n = \mathcal{D}_n^{init} \qquad u_n \leq u_n^{cr} \tag{2.2}$$

   where superscript (init) refers to the initial value (*i.e.* value at zero displacement).

2. Development of separation

   $$\mathcal{D}_n = \mathcal{D}_n^{sec} \qquad u_n^{cr} \leq u_n \leq u_n^{ul} \tag{2.3}$$

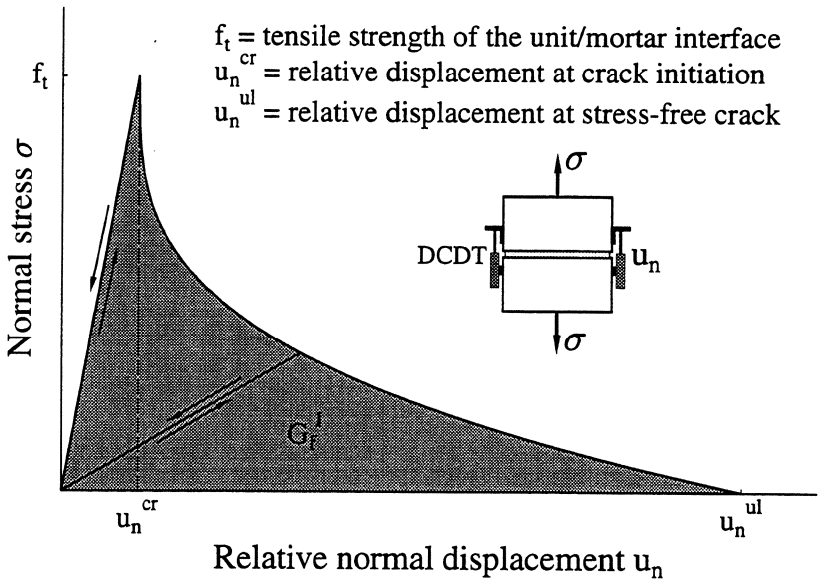

FIGURE 2-4 Normal stress versus relative displacement relation.

where $\mathcal{D}_n^{sec}$ is the secant stiffness.

3. Complete separation

$$\mathcal{D}_n = 0 \qquad u_n^{ul} \leq u_n \tag{2.4}$$

The second stage corresponds to the tension *softening* stage which is controlled by three parameters as shown in Figure 2-4, *viz.* the tensile strength (f_t) of the masonry unit/mortar interface, which is the weakest plane, the shape of the softening diagram and the mode-I fracture energy (G_f^I) which is defined as the amount of energy required to create a unit area of a crack in mode-I. In the present model the total relative displacement in the normal direction of the interface element is decomposed into the elastic (el) and inelastic (ie) parts. This additive decomposition means that

$$u_n = u_n^{el} + u_n^{ie} \tag{2.5}$$

The inelastic part is related to the normal stress using the following relation

$$\sigma = f_t \left[1 - (u_n^{ie}/u_n^{ul})^k\right] \tag{2.6}$$

where k is a material constant. From Figure 2-4, G_f^I is defined as the area under the softening diagram, *i.e.*

$$G_f^I = \int_0^{u_n^{ul}} \sigma du_n^{ie} \tag{2.7}$$

From Eqs. (2.6) and (2.7), the stress-free crack opening (u_n^{ul}) is related to the fracture energy G_f^I, which is assumed to be a material property[4] by the following relation

$$u_n^{ul} = \frac{1+k}{k}\frac{G_f^I}{f_t} \tag{2.8}$$

The linear softening is a special case of the previous model which is reproduced by setting $k = 1$ in Eq. (2.6). Once a crack is initiated, *i.e.* $u_n^{cr} \leq u_n$, it is assumed that the shear stress transmitted parallel to the crack plane will depend on either the pre-peak (Section 2.3.3) or post-peak (Section 2.3.5) situation where *indirect coupling* between the normal and the tangential directions is provided. This implies that

$$\begin{Bmatrix} \sigma \\ \tau \end{Bmatrix} = \begin{bmatrix} \mathcal{D}_n^{cr} & 0 \\ 0 & \mathcal{D}_t \end{bmatrix} \begin{Bmatrix} u_n \\ u_t \end{Bmatrix} \tag{2.9}$$

where $\mathcal{D}_n^{cr}$ is either $\mathcal{D}_n^{sec}$ or 0 depending on the current stage of the crack, stage 2 or 3, respectively. $\mathcal{D}_t$ is determined as discussed in Sections 2.3.3 and 2.3.5.

2.3.3 Pre-peak model and tangential direction behavior of mortar joints

In the tangential direction, the stress versus relative displacement relationship is assumed nonlinear elasto-plastic following the Mohr-Coulomb yield criterion supplemented with softening criteria for cohesion and for internal friction. To allow a dilatancy angle different from the angle of internal friction, in accordance with experimental findings (*e.g.* [137]), the plasticity formulation uses a non-associated plastic potential.

The response of masonry bed joints in direct shear has been studied by many researchers, *e.g.* Hegemier *et al.* [65], Drysdale *et al.* [45], Pook *et al.* [138], Atkinson *et al.* [8], Guo [64], and Van der Pluijm [137]. Based on the findings of Atkinson *et al.* [8] and using a hyperbolic model similar to that proposed by Duncan and Chang [47] for soils and investigated further by Kulhawy [89] for rock joints, the pre-peak response of the masonry joints subjected to shear loading is given by the following hyperbolic representation

$$\tau = \frac{u_t}{f + s u_t} \qquad \tau < \tau_p \tag{2.10}$$

where τ_p is the peak shear stress to be discussed later.

[4]For discussions on the validity of such assumption, the reader is referred to Section 3.1.2 of reference [149] and to reference [68].

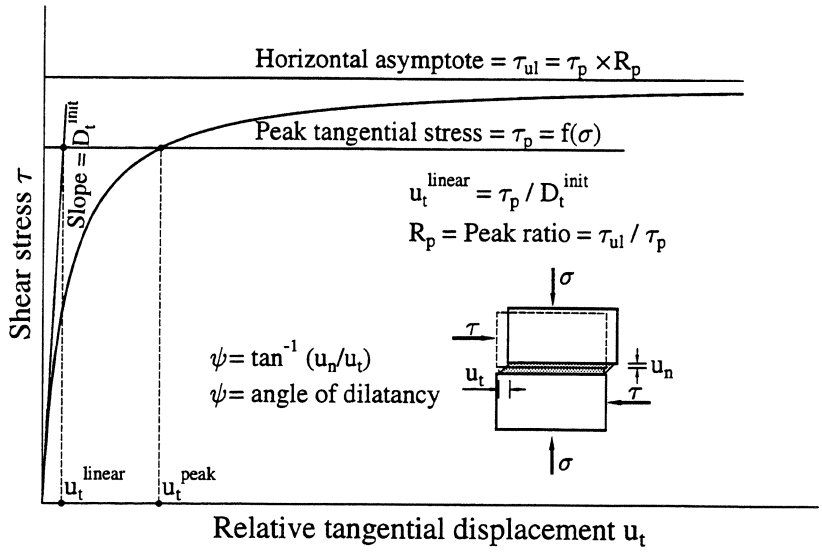

FIGURE 2-5 Pre-peak shear stress versus relative displacement relation.

From Eq. (2.10), the tangent shear modulus $\mathcal{D}_t$ is obtained as follows

$$\mathcal{D}_t = \frac{\partial \tau}{\partial u_t} = \frac{f}{(f + s u_t)^2} \tag{2.11}$$

The parameters (f) and (s) are obtained from Eqs. (2.10) and (2.11) by

$$\mathcal{D}_t^{init} = \mathcal{D}_t|_{u_t=0} = \frac{1}{f} \tag{2.12}$$

$$\tau_{ul} = \lim_{u_t \to \infty} \tau = \lim_{u_t \to \infty} \frac{1}{f/u_t + s} = \frac{1}{s} \tag{2.13}$$

Accordingly, the parameter (f) is the reciprocal of the initial joint shear stiffness $(\mathcal{D}_t^{init})$, whereas the parameter (s) is the reciprocal of the horizontal asymptote (τ_{ul}) to the τ-u_t hyperbolic relation illustrated in Figure 2-5. Straightforward manipulations of Eqs. (2.11), (2.12) and (2.13) lead to the following expressions

$$\mathcal{D}_t = \frac{\mathcal{D}_t^{init}}{(1 + \mathcal{D}_t^{init} u_t / \tau_{ul})^2} \tag{2.14}$$

$$\mathcal{D}_t^{init} u_t = \frac{\tau \tau_{ul}}{\tau_{ul} - \tau} \tag{2.15}$$

Upon substitution from Eq. (2.15) into Eq. (2.14), one obtains, after simplification, the following expression

$$\mathcal{D}_t = \mathcal{D}_t^{init}\left[1 - \frac{\tau}{\tau_{ul}}\right]^2 \tag{2.16}$$

This expression is recast in terms of the peak shear stress by introducing the peak ratio (R_p) defined as follows

$$R_p = \frac{\tau_p}{\tau_{ul}} \tag{2.17}$$

This peak ratio ranges from 0 to 1 and the higher its value, the higher the nonlinearity of the pre-peak behavior. Therefore, Eq. (2.16) becomes

$$\mathcal{D}_t = \mathcal{D}_t^{init}\left[1 - \frac{\tau}{\tau_p}R_p\right]^2 \tag{2.18}$$

Equation (2.18) represents the tangent shear modulus in terms of the shear stress only and not of the relative displacement. This is a useful form for analysis involving *arbitrary initial stress conditions*. The effect of R_p on the variation of $\mathcal{D}_t$ with τ (see Eq. (2.18)) is illustrated in Figure 2-6(a). In this figure, the stiffness is normalized by its initial value whereas the stress is normalized by its peak value. The peak ratio R_p may be selected such that a chosen value of the shear stiffness is maintained at the peak stress. This value should be checked to make sure that the relative displacement in the tangential direction of the interface at the peak stress is "reasonable". This verification may be carried out using Figure 2-6(b) where the normalized stiffness (as in Figure 2-6(a)) is plotted against the normalized relative tangential displacement. The latter is normalized with respect to the linear displacement (u_t^{linear}), shown in Figure 2-5, and defined as

$$u_t^{linear} = \tau_p/\mathcal{D}_t^{init} \tag{2.19}$$

2.3.4 Determination of the material parameters

The presented material model for mortar joints depends on several material parameters that can be determined from simple experiments performed on small specimens. The initial stiffness coefficients are adjusted according to the dimensions and properties of the masonry units and mortar joints while keeping the properties of the 'expanded masonry units' the same as those for the "regular masonry units" (see Figure 2-2). Considering stack

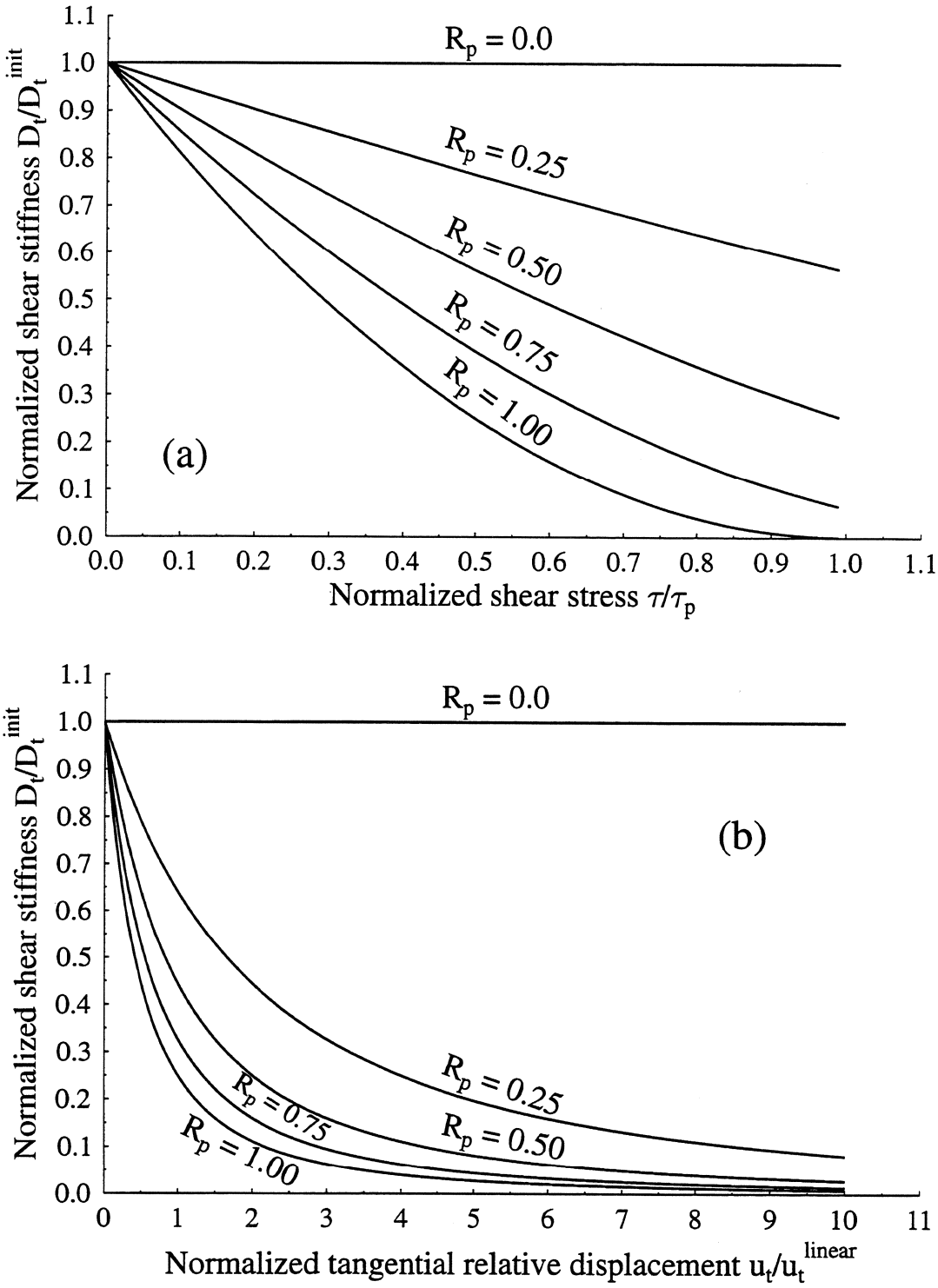

FIGURE 2-6 Effect of the peak ratio (R_p) on the tangent shear stiffness.

bond (*i.e.* a serial chain connection of the components) and uniform stress distributions in the masonry unit and the mortar joint, the initial stiffness coefficients are

$$\mathcal{D}_n^{init} = \frac{E_m E_u}{t_m(E_u - E_m)} \quad \& \quad \mathcal{D}_t^{init} = \frac{G_m G_u}{t_m(G_u - G_m)} \tag{2.20}$$

where E_m and G_m are, respectively, the Young's modulus and the shear modulus for the mortar joint, E_u and ν_m are, respectively, the Young's modulus and shear modulus for the masonry unit and t_m is the mortar joint thickness. As usual, the shear moduli are related to the Young's moduli by

$$G_m = \frac{E_m}{2(1+\nu_m)} \quad \& \quad G_u = \frac{E_u}{2(1+\nu_u)} \tag{2.21}$$

where ν_m and ν_u are the Poisson's ratios for the mortar joint and the masonry unit, respectively. Two observations are worth mentioning:

1. The accuracy of the approximation given by Eqs. (2.20) improves upon the increase of the ratio E_u/E_m and decrease of the ratio ν_u/ν_m. The ratios E_u/E_m and G_u/G_m must be strictly greater than unity to ensure validity of Eqs. (2.20).

2. Equations (2.20) do not enforce any contact-surface compatibility (*i.e.* impenetrability and pre-sliding stick constraints). Accordingly, the stiffness coefficients defined by Eqs. (2.20) cannot be regarded as *penalty numbers* [136].

In general, one should assume that the initial shear stiffness of the interface element ($\mathcal{D}_t^{init}$) is dependent upon the normal stress applied to the interface. This sophistication is relaxed in the present model for two main reasons. First, experimental data needed to quantify the effect of normal stress on the initial shear stiffness of mortar joints are scarce. To the best of the authors' knowledge, the only available experimental data are those of Atkinson *et al.* [8] and they show a large scatter which makes it impossible to fit a reasonable relation. Second, the crude linear regression of the experimental data given by Atkinson *et al.* [8] leads to only a 75% increase of $\mathcal{D}_t^{init}$ upon a nine-fold increase of σ.

The peak value of the shear stress (τ_p) is obtained from the failure envelope of mortar joints under uniform constant normal stress combined with increasing shear stress. This failure envelope is obtained experimentally using masonry triplet specimens as discussed in the first report of this series. In the next section, the use of such an envelope as a yield surface in the context of plasticity theory will be discussed.

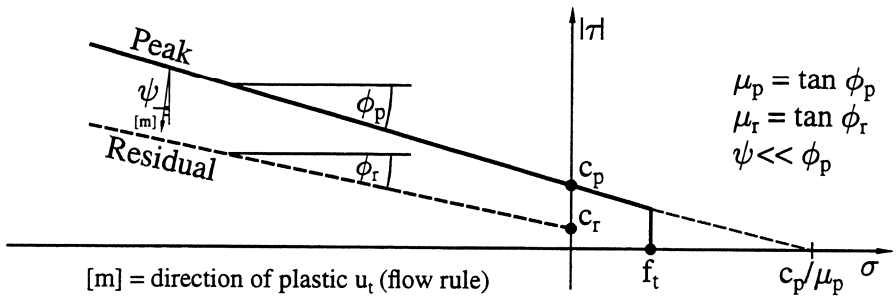

FIGURE 2-7 Mohr-Coulomb failure envelope of the interface element.

2.3.5 Post-peak model and tangential direction behavior of mortar joints

The linear regression of the experimental results presented in **Chapter 2** from tested masonry triplets led to the following Mohr-Coulomb yield criteria at the peak and residual shear stresses

$$\tau_p = c_p - \mu_p \sigma \quad \& \quad \tau_r = c_r - \mu_r \sigma \tag{2.22}$$

where c is the cohesion, $\mu = \tan\phi$ is the coefficient of friction, and ϕ is the corresponding angle of internal friction. Subscripts p and r indicate, respectively, that the quantity in question corresponds to the peak and residual shear stresses. From the experimental results ($c_p = 0.04$ ksi, $\mu_p = 1.3$, $c_r = 0.01$ ksi, and $\mu_r = 0.9$). These envelopes are supplemented by a tension cut-off to limit the normal tensile stress to the tensile strength of the masonry unit/mortar joint interface. The envelopes for the peak and residual shear strength are depicted in Figure 2-7. For compatibility with the Mohr-Coulomb failure envelope, the tension cut-off at $\sigma = f_t$ must satisfy the following inequality

$$f_t \leq c_p/\mu_p \tag{2.23}$$

The cohesion (c) and coefficient of friction (μ) are assumed to be *linear* functions of the plastic part of the relative tangential displacement. Similarly to the behavior in the normal direction of the interface, *cf.* with Eq. (2.5), the tangential relative displacement is decomposed into elastic (el) and plastic (pl) parts, *i.e.*

$$u_t = u_t^{el} + u_t^{pl} \tag{2.24}$$

Referring to Figure 2-8, one can propose the following forms of c and μ

$$c = \begin{cases} c_p - (c_p - c_r)u_t^{pl}/u_t^{resid} & 0 \leq u_t^{pl} < u_t^{resid} \\ c_r & u_t^{resid} \leq u_t^{pl} \end{cases} \tag{2.25}$$

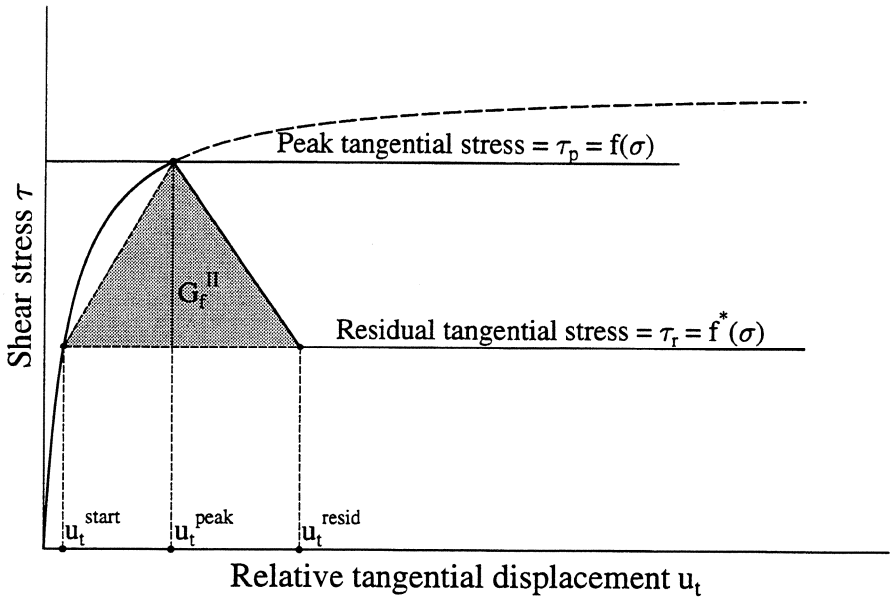

FIGURE 2-8 Post-peak shear stress versus relative displacement relation.

$$\mu = \begin{cases} \mu_p - (\mu_p - \mu_r)u_t^{pl}/u_t^{resid} & 0 \le u_t^{pl} < u_t^{resid} \\ \mu_r & u_t^{resid} \le u_t^{pl} \end{cases} \tag{2.26}$$

where all the above parameters are defined in Figures 2-7 and 2-8.

The mode-II fracture energy (G_f^{II}) is defined[5] in Figure 2-8. From this figure, one can easily calculate an expression for u_t^{resid} in terms of G_f^{II} as follows

$$u_t^{resid} = u_t^{start} + \frac{2G_f^{II}}{\tau_p - \tau_r} \tag{2.27}$$

where u_t^{start} is determined from the pre-peak behavior by solving Eq. (2.15) for u_t at $\tau = \tau_r$.

The post-peak behavior is governed by the previously discussed Mohr-Coulomb friction model with softening. This model is formulated within the context of *non-associated plasticity*. The basic ingredients of such formulation are the yield function Y and the plastic potential function P which read

$$Y = \tau + \sigma \tan\phi - c \qquad \& \qquad P = \tau + \sigma \tan\psi - c \tag{2.28}$$

The angle of dilatancy (ψ) is defined in the insert of Figure 2-5. As reported by Van der Pluijm [137] and as pointed out in the first report of this series, masonry joints exhibit

[5]To the best of the authors' knowledge, the definition of G_f^{II} was proposed by Stankowski *et al.* [153] and implemented by them in [154]. Based on experimental findings, this definition was simplified, in a manner similar to the present model, by Van der Pluijm [137].

much smaller ψ than ϕ. Accordingly, the direction of the plastic flow $[m]$ is not normal to the yield surface (refer to Figure 2-7), *i.e.* the flow rule is non-associated. This formulation will produce a non-symmetric stiffness matrix. The derivation of the plasticity equations is fairly standard[6].

2.3.6 Verification of the interface constitutive model

The proposed model for interface elements to simulate the behavior of mortar joints in masonry structures is implemented in the finite element package DIANA. The model and its implementation is verified using the standard diagonal tension test of masonry assemblages (ASTM-E519) [3]. This test is widely used in the evaluation of the masonry tensile strength. The specimen was tested and the mode of failure was diagonal failure which is governed mainly by the tensile strength characteristics of mortar joints. Once cracking is initiated, sliding along these cracks occurs.

The finite element mesh of the analyzed specimen is illustrated in Figures 2-9 and 2-10. This mesh consists of 36 8-noded quadrilaterals (Q8) elements for the expanded masonry unit (2 elements for each masonry unit as shown in Figure 2-9), 30 6-noded bed joints interface elements (elements 37-66 in Figure 2-10), 15 6-noded rigid linear interface elements[7] between each pair of Q8 elements forming one masonry unit to provide the necessary displacement compatibility (elements 67-81), and 15 6-noded head joint interface elements (elements 82-96 shown in Figure 2-10). The plots of the calculated deformed shapes at the initiation of diagonal cracking and at the full cracking are shown in Figures 2-11 and 2-12, respectively. The FE results are compared with the experimental results in Figure 2-13.

From the plotted load-deformation relations and the deformed shapes of the diagonal tension specimen, one may conclude that the implemented interface model is capable of capturing the basic failure mechanisms for the behavior of mortar joints in masonry subassemblages.

2.4 Application to an Infilled Frame

The discrete finite element model shown in the left-hand-side of Figure 2-1 for the steel frame with masonry infill is considered for the application of the proposed interface model for the mortar joints. The crack patterns obtained from the experimental investigation and those from the numerical results are compared. The failure of the structure was governed by mortar cracking without any visible cracking or crushing of the concrete block masonry

[6]For brevity, the theoretical and numerical formulation of the plasticity theory will be omitted. For details, the reader is referred to Lotfi and Shing [100] and **Chapter 3** of Lourenço's Ph.D. dissertation [102].

[7]High values for $\mathcal{D}_n$ and $\mathcal{D}_t$ are assigned for these elements without any possible nonlinearities.

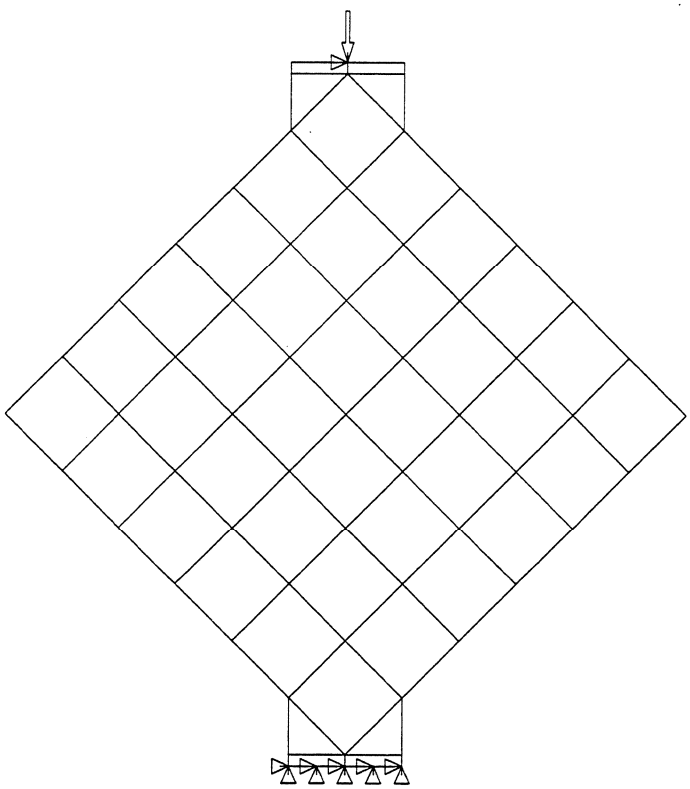

FIGURE 2-9 Finite element model for the masonry diagonal tension example.

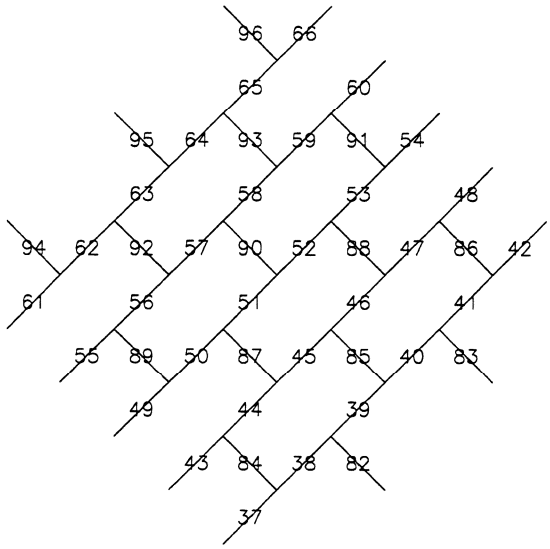

FIGURE 2-10 Interface elements as mortar joints for the masonry diagonal tension example.

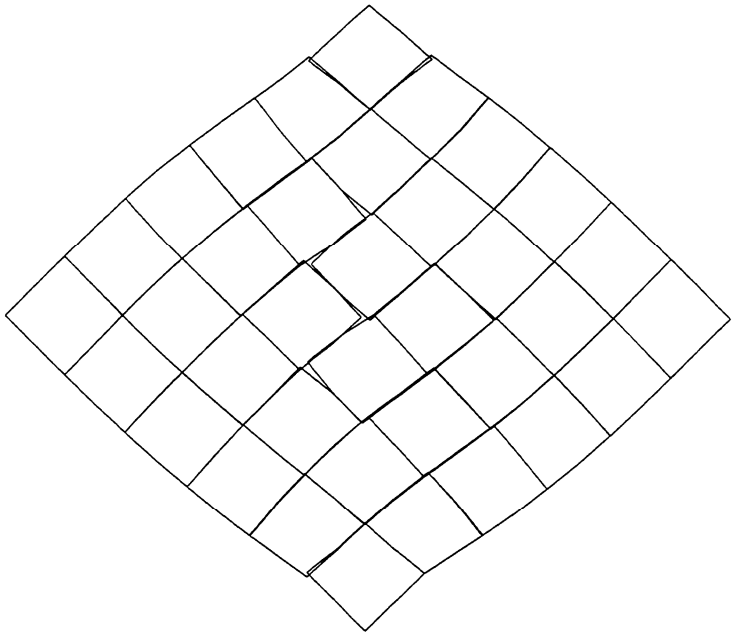

FIGURE 2-11 Deformed shape at crack initiation of the masonry diagonal tension example.

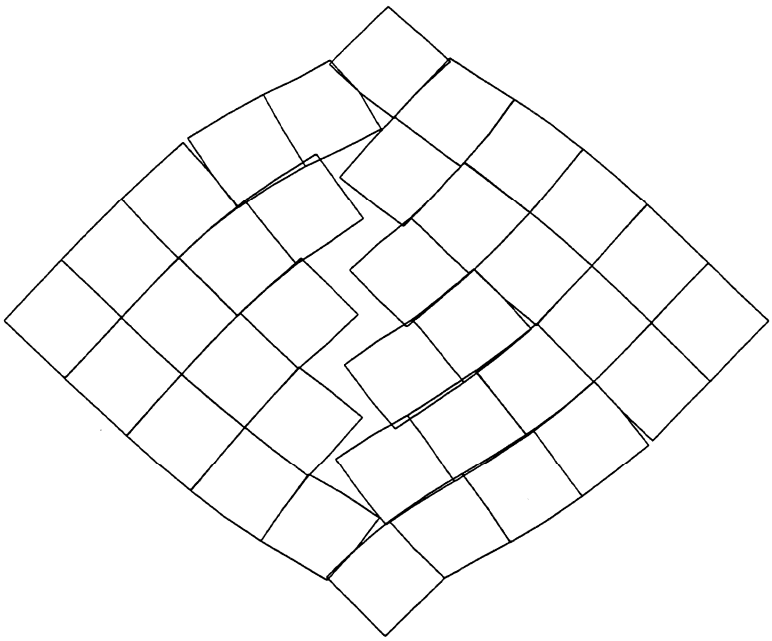

FIGURE 2-12 Deformed shape at full cracking of the masonry diagonal tension example.

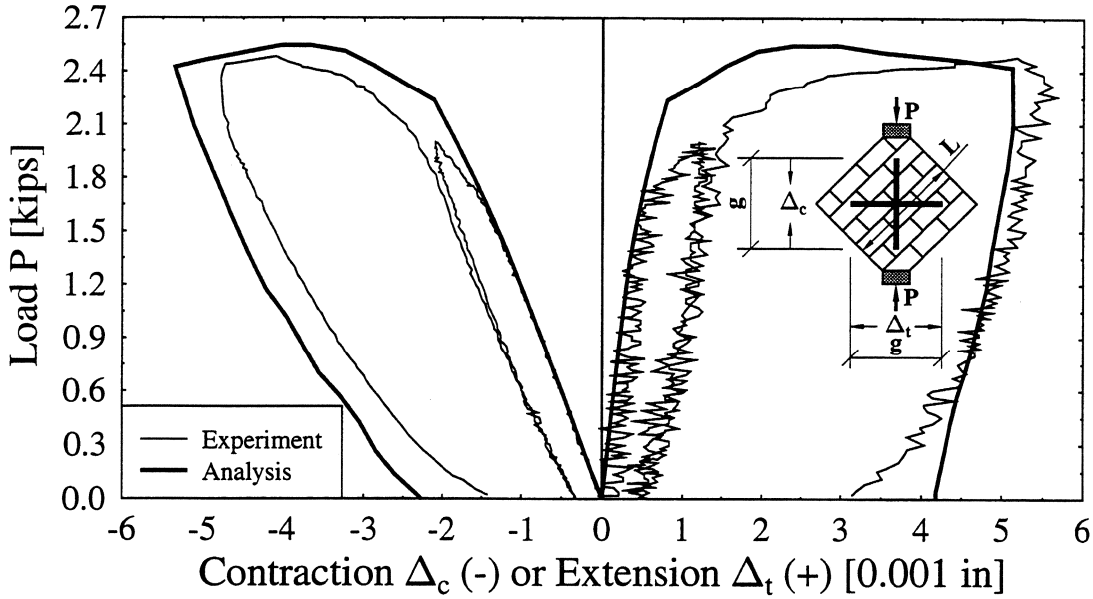

FIGURE 2-13 Comparison between FE results and experimental results for the masonry diagonal tension example.

units. The steel frame was modeled with 4-noded plane stress elements having *linear* properties. The treatment of the frame/wall interface will be given in the next section. The beam/column connections of the steel frame were modeled with interface elements with stiffnesses in the normal and the tangential directions to simulate the nature of the *semi-rigid connections*. These finite stiffnesses were obtained by calibration to match the experimentally determined lateral stiffness of the bare frame shown in Figure 2-14.

2.4.1 Frame/wall interface modeling

The interfaces between the frame members and the infill walls are modeled by the interface elements illustrated in Figure 2-1. A relatively small value of shear stiffness was assigned to these interfaces because of the smooth surface between steel frame members and the infills[8]. In the normal direction of these interface elements, the material behavior is governed by the constitutive model shown in Figure 2-15. This model allows for the consideration of initial *gaps* between the frame members and the walls. The zone characterized by the slope, D_n^{tran}, represents the transition from a zero stiffness in tension, D_n^{tens}, to a very high stiffness in compression, D_n^{comp}. The size of the initial gap (g) defines the beginning of this transition zone. The end of the transition zone (s) is the summation of the gap size and the amount of deformation required to degrade the roughness of both the wall and the frame along the interface.

[8]This assumption may be not acceptable for reinforced concrete frames infilled with masonry walls.

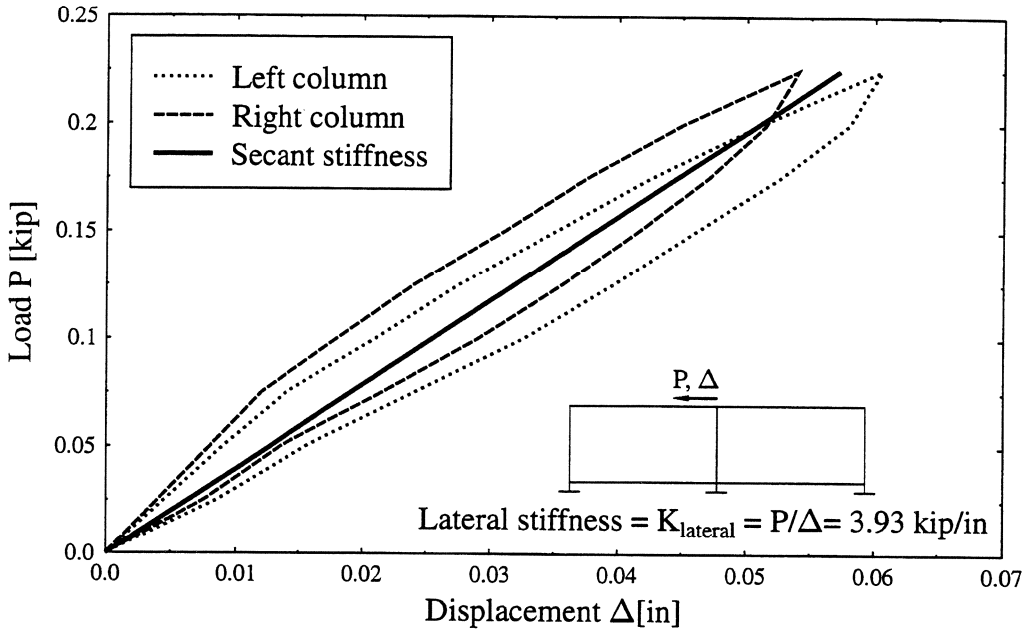

FIGURE 2-14 Determination of the lateral stiffness of the two-bay single-story bare frame.

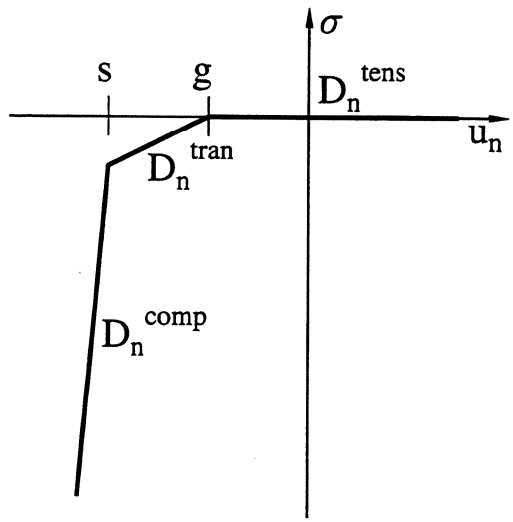

FIGURE 2-15 Material model for the frame/wall interface element.

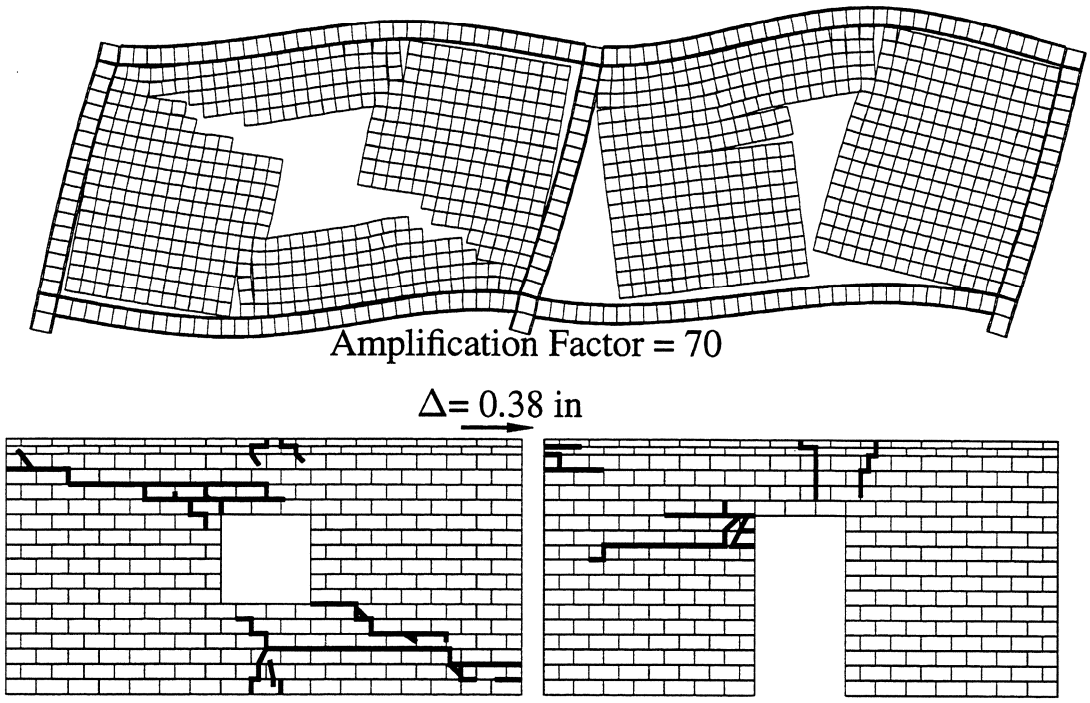

FIGURE 2-16 Comparison between the FE results (top) and the experimental (bottom) crack patterns for the two-bay single-story infilled frame.

2.4.2 Comparison between experimental and numerical results

The comparison between the crack patterns obtained from the quasi-static experiment and the deformed shape of the corresponding FE analysis, showing the cracking, are presented in Figure 2-16. Reasonable agreement can be observed in this figure. This agreement is achieved because of the appropriate modeling of the mortar joint cracking as well as the frame/wall interface conditions. It should be noted that the analysis presented herein preceded all the experiments including those for the determination of the material properties. Therefore, comparison of the load-displacement relations obtained later from the experiment and that obtained analytically is not possible because of (1) the real elastic properties of the masonry infills were not used in the analysis, and (2) cyclic loading was applied in the experiment while the analysis was performed under monotonic loading.

2.5 Summary

Review of literature for the use of FEM in the analysis of infilled frames is presented. In the literature, special attention is given to the treatment of the frame/wall interface

conditions. A discrete model for mortar joints in masonry structures is formulated. The model accounts for mode-I and mode-II fracture along the mortar joints which form planes of weakness in the masonry composite.

The results of standard diagonal tension test are used to validate the proposed model. Finally, analysis of an infilled frame with asymmetric openings in the wall panels is performed using the presented model. As experimentally determined, the most important source of material nonlinearity is cracking and sliding along the mortar joints. Comparison between the experimental and numerical crack patterns indicate the reliability of the proposed model to capture the basic failure mechanisms in masonry structures.

SECTION 3

FINITE ELEMENT CONTINUUM APPROACHES FOR MASONRY INFILLS

The discrete model presented in the previous section embodies all the necessary aspects for accurate modeling of masonry infills. Although the approach is accurate, the computational effort involved in such models may prevent their use, especially in the analysis of large structures. This drawback is even more pronounced when the analysis is performed under dynamic loading. Accordingly, one needs to resort to continuum models (meso-models) where relations between average stresses and strains are established and homogeneous properties are considered.

In the present section, an exploration of the various homogenization techniques to obtain average properties for masonry composites is reviewed. In these techniques, masonry structures are treated as a *periodic composite continua.* Since the masonry composite is made up of two different materials (blocks or bricks and mortar) arranged in a periodic pattern, masonry may be modeled as a continuum made of periodic repetition of an elementary cell, called Representative Volume Element (RVE). The typical length scale of the RVE should be much smaller than the structural length scale. This is the fundamental hypothesis in the idealization of masonry assemblages via *homogenization procedures.* Here, a simple homogenization technique to evaluate average elastic properties of masonry is presented and assessed using the FEM. A *system identification technique* is presented to evaluate the average material parameters using iterative finite element analysis of an infilled structure. The infilled structure was tested to obtain the complete displacement field of the masonry panels. In the identification procedure, the iterative process attempts to adjust the material parameters to match the finite element solution with the experimental data.

Homogenized properties of masonry infills are applied to analyze the two-bay, two-story infilled frame discussed in the second report of this series. The results are utilized to verify the equivalent truss model for infills which is introduced in the second report of this series. Preliminary investigation of the effect of openings on the lateral stiffness of infilled frames is presented. The application of smeared cracking concepts with the estimated homogeneous properties for the analysis of infilled frames leads to numerical difficulties due to the mesh-dependency of the smeared cracking technique. Remedies to such problems are suggested in the next section.

3.1 Review of Homogenization Techniques

The Homogenization Theory for Periodic Media (HTPM) was first proposed in 1974 by Sanchez-Palencia [151]. Since then, the theory has been described and extensively applied

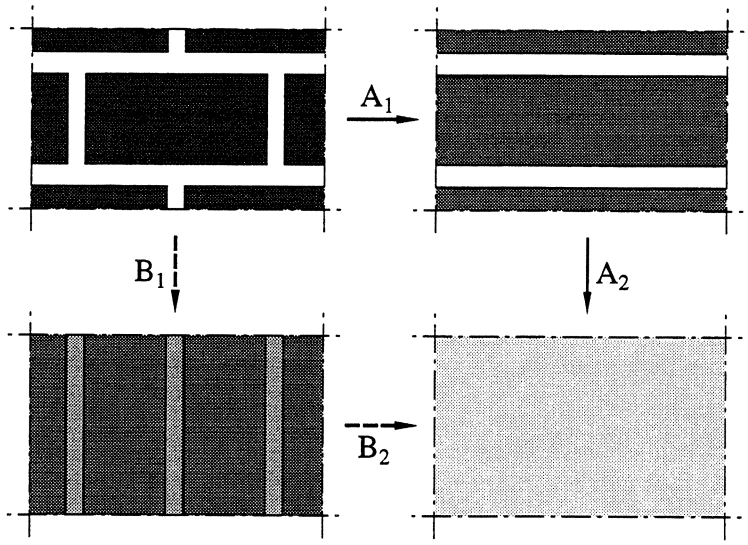

FIGURE 3-1 Two-step homogenization techniques.

by many researchers. In this theory, calculation of the effective constitutive parameters (homogenization) is performed on the basic cell which describes the periodic material. This basic cell is the smallest repetitive unit of the material. Complete and technical presentations based on asymptotic analysis have been performed by Bensoussan *et al.* [23] and Sanchez-Palencia [152]. The homogenization theory was revisited for nonlinear behavior by Suquet [158].

Many researchers attempted to use homogenization techniques in masonry to establish constitutive relations in terms of averaged stresses and strains from the constitutive relations of the individual components. Naturally, the determination of the elastic characteristics received the most attention. The common approximate approach is to perform two-step homogenization procedure (as shown in Figure 3-1), under the assumption of layered material. Liang *et al.* [93] and Pande *et al.* [128] proposed to homogenize first in the horizontal direction to include the masonry units and the vertical (head) joints, then vertical homogenization is performed to account for the material obtained from the first step and the horizontal (bed) joints (path $A_1 \rightarrow A_2$ in Figure 3-1). On the other hand, Papa [129] and Maier *et al.* [105] followed an approach to homogenize in the vertical direction where masonry units, head and bed joints are considered first. Then, horizontal homogenization is followed for the two-phased material obtained from the first step (path $B_1 \rightarrow B_2$ in Figure 3-1).

Similar to the two-step homogenization technique of Pande *et al.* [128], Pietruszczak [134] and Pietruszczak and Niu [135] adopted a two-step homogenization technique with the exception of treating the head joints in the first step of the homogenization process (see Figure 3-1) as aligned, uniformly dispersed weak *ellipsoidal* inclusions embodied in the matrix (*i.e.* the concrete blocks). This simplification allowed them to estimate the components of the constitutive matrix for the first step of the homogenization using Eshelby's [54]

solution to an ellipsoidal inclusion problem combined with Mori-Tanaka's [116] mean-field theory. Anthoine [7] implemented the HTPM in a rigorous way, *i.e.* in a one step rather than two. He also considered the real geometry of masonry in the form of finite thickness and actual bond pattern. Therefore, he avoided the assumptions of very thin media as in [105] and very thick media as in [135]. With all the sophistication he introduced to avoid these assumptions, he arrived at the conclusion that these assumptions only *slightly* affect the in-plane elastic characteristics of masonry, but he speculated that in the non-linear range (plasticity or damage), the same assumptions might lead to erroneous results. Lourenço [102] presented a new matrix formulation for the elasto-plastic analysis of layered materials. From the comparison between the results of the layered and homogenized models, he concluded that the two-step homogenization can successfully predict the elastic characteristics of masonry.

The Theory of Mixtures is one of the most simple and widely used constitutive models for computational tools in composites. Such a theory considers a representative continuum where the stiffness of each phase contributes to the overall stiffness in a measure directly proportional to its volume fraction. For a composite material consisting of n phases, if K_i is the stiffness of the i^{th} phase and v_i the corresponding volume fraction, the stiffness of the composite material is given by

$$K_{overall} = \sum_{i=1}^{n} K_i v_i \tag{3.1}$$

As a consequence of the Theory of Mixtures for two phases characterized by having different stiffnesses, one can show that a uniaxial state of stress will produce a compressive stress in one phase and a tensile stress in the other along directions which are normal to the axis of loading. This was clearly demonstrated experimentally[1] and numerically [150].

In a sequence of three papers, McNiven and Mengi [108] [109] [110] developed a mathematical model, based on the theory of mixtures, for two phase materials with the objective of using it for predicting the response of masonry walls to dynamic inputs. This objective was later [114] [157] achieved in three stages: (1) experimental observations of a brick masonry wall subjected to input earthquake and periodic excitations at the base, (2) selection of a mathematical model, and (3) the determination of the model parameters through optimization analysis.

[1]The experiments were conducted by Beranek and Hobbelman on stacks of masonry units with neoprene as joint material. The actual reference of these experiments is in Dutch and this work was cited by Rots in reference [150].

3.2 Elastic Properties For Masonry as a Composite Material

Masonry can be treated as a *two-phase composite material.* Due to the regular structure of masonry, a repeatable unit can be identified as shown in Figure 3-2(a), where both shaded units are ideally identical. The theoretical model is based on combinations of the series and parallel models for composite materials.

3.2.1 Rheological model for masonry composites

The rheological model for masonry composite is based on combination of series and parallel arrangements of a two-phase composite material. This model is motivated by the experimental findings in the first report of this series. The actual properties of the real composite materials lie between two arrangements identified in Figures 3-2(c) and 3-2(d). Note that these arrangements can carry loading only in one direction. Therefore, they are referred to as one dimensional (1D) models and they are distinguished by the direction of the load they can support.

In the vertical direction shown in Figure 3-2(c), one obtains (see Section A.1 in **Appendix A**)

$$E^v_{com} = \frac{(h_b + t_{mb})(l_b + t_{mh})(t_{mh} l_{mh} E_m + l_b t_b E_b) t_b}{A^v_{com}\,(t_{mh} l_{mh} t_{mb} E_m + l_b t_b t_{mb} E_b + (l_b + t_{mh}) t_b h_b E_m)} E_m \tag{3.2}$$

where E^v_{com}, E_m and E_b are Young's moduli for the composite in the vertical direction, mortar and blocks, respectively. The subscript (com) refers to the composite. All other variables are defined in Figure 3-2. The apparent cross sectional area in the vertical direction (A^v_{com}) of the composite is given by

$$A^v_{com} = \frac{(h_b + t_{mb})(l_b + t_{mh})(t_{mh} l_{mh} + l_b t_b) t_b}{t_{mb}(t_b l_b + t_{mh} l_{mh}) + t_b h_b (l_b + t_{mh})} \tag{3.3}$$

It is interesting to note that, for the case $t_b = l_{mh}$, *i.e.* solid blocks, Eq. (3.3) reduces to the following expected expression

$$A^v_{com} = (l_b + t_{mh}) t_b \tag{3.4}$$

In the horizontal direction shown in Figure 3-2(d), one obtains (see Section A.2 in **Appendix A**)

$$E^h_{com} = \frac{(l_b + t_{mh})}{A^h_{com}} \left[\frac{t_{mb} t_b}{l_b + t_{mh}} + \frac{h_b t_b l_{mh} E_b}{t_b t_{mh} E_b + l_b l_{mh} E_m} \right] E_m \tag{3.5}$$

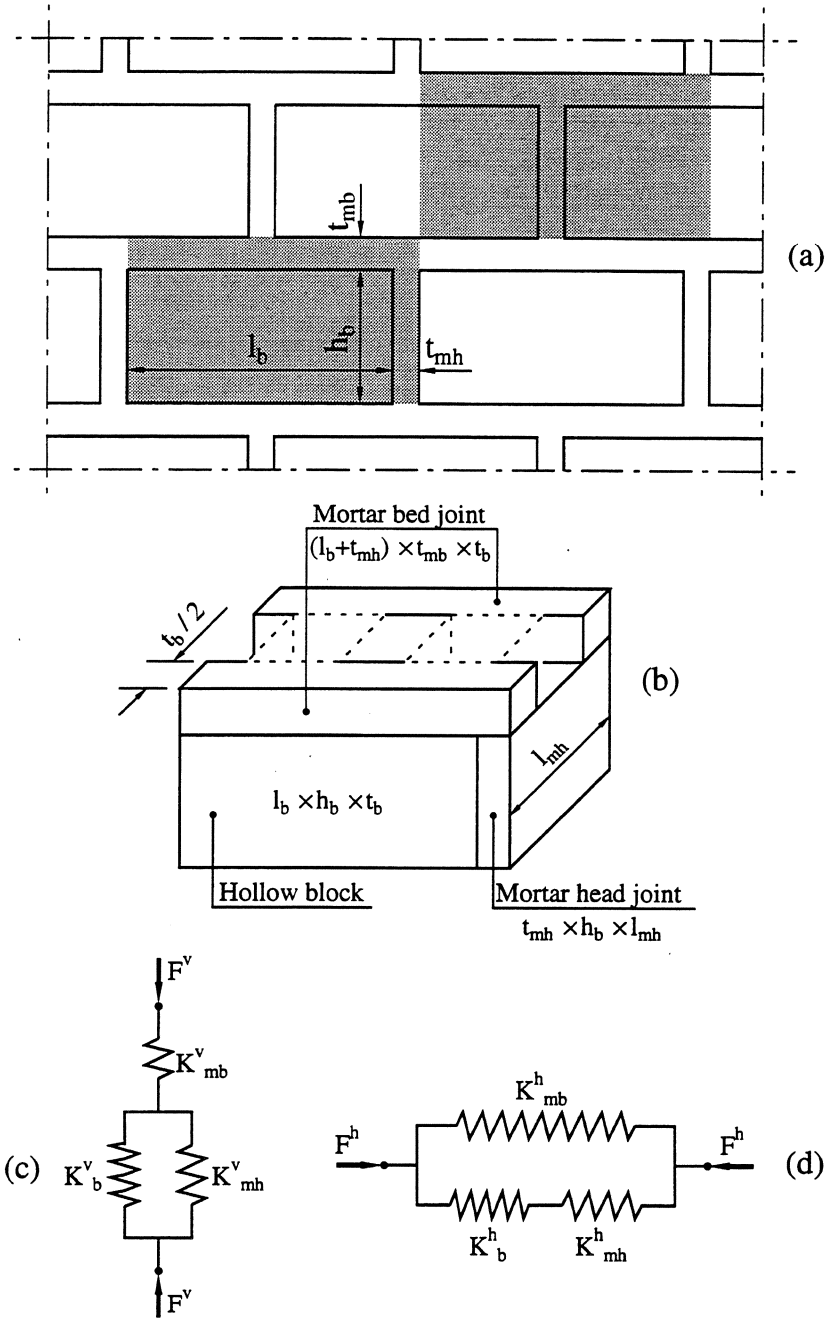

FIGURE 3-2 Masonry as a composite material; (a) Periodic unit in a masonry wall; (b) Dimensions of block and mortar; (c) Rheological model in the vertical direction; (d) Rheological model in the horizontal direction.

TABLE 3-I Geometrical properties of the 1/4 scale concrete blocks (dimensions in inches).

l_b	h_b	t_b	t_{mb}	t_{mh}	l_{mh}
$3\frac{26}{32}$	$1\frac{27}{32}$	$2\times\frac{10}{32}$	$\frac{5}{32}$	$\frac{5}{32}$	$1\frac{27}{32}$

where E^h_{com} is Young's modulus for the composite in the horizontal direction. The apparent cross sectional area in the horizontal direction (A^h_{com}) of the composite is given by

$$A^h_{com} = (l_b + t_{mh})\left[\frac{t_b t_{mb}}{l_b + t_{mh}} + \frac{l_{mh} h_b t_b}{t_{mh} t_b + l_b l_{mh}}\right] \tag{3.6}$$

Also, for the case $t_b = l_{mh}$, *i.e.* solid blocks, Eq. (3.6) reduces to the following expected expression

$$A^h_{com} = t_b(t_{mb} + h_b) \tag{3.7}$$

Table (3-I) lists the geometrical properties of reduced scale (1/4 scale) hollow concrete block masonry. In Table 3-I, the thickness of the blocks t_b is taken as twice the thickness of the face shell. This is the case for partial bedding, *i.e.* mortar of the bed joint is placed on the face shell only. From Table 3-I and Eqs. (3.2), (3.3), (3.5), and (3.6), one readily obtains the following results:

$$A^v_{com} = 2.66 \text{ in}^2 \qquad \& \qquad A^h_{com} = 1.28 \text{ in}^2$$

$$\frac{E^v_{com}}{E_m} = \frac{4.45E_b/E_m + 0.54}{0.37E_b/E_m + 4.62} \qquad \& \qquad \frac{E^h_{com}}{E_m} = \frac{6.59E_b/E_m + 0.53}{0.10E_b/E_m + 7.03}$$

Figure 3-3 illustrates the variation of the composite moduli of elasticity for both the vertical and the horizontal directions versus the concrete block modulus of elasticity. These moduli are normalized with the modulus of elasticity of the mortar. Some relevant remarks from Figure 3-3 are given next.

1. For $E_b > E_m$, which is the realistic case, Young's modulus of the composite is always less than that for the block.
2. For $E_b > E_m$, the homogenization in the vertical direction always yields a lower value of the composite Young's modulus than that obtained from the horizontal direction.
3. For $E_b \lesssim 3E_m$, the Young's moduli obtained from the vertical and horizontal directions are practically the same. This implies that for the considered geometrical configuration and up to a ratio $E_b/E_m \approx 3.0$, masonry composite maybe treated nearly as an *isotropic* material.

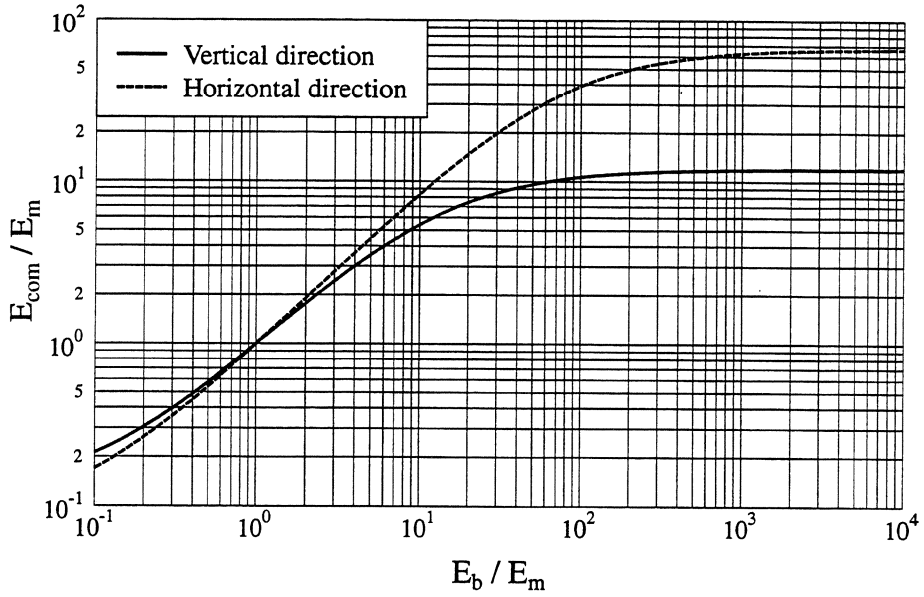

FIGURE 3-3 Variation of the elastic modulus of masonry composite with the elastic modulus of the concrete block masonry.

4. The predicted composite Young's moduli from the vertical and horizontal directions deviate from each other for larger ratios, *e.g.* $E_b/E_m \gtrsim 3.0$, which corresponds to larger deviation from homogeneous material. This is not an academic situation, but represents a quite possible situation where compression normal to the bed joints and tension parallel to the bed joints may exist. Once this stress state occurs, the stiffness of the vertical joints will degrade and tend to zero leading to significant difference between Young's moduli of the blocks and the mortar.

5. In the limit $E_b \gg E_m$, *e.g.* $E_b > 1000E_m$, the difference between the Young's moduli from the horizontal and vertical directions is approximately constant. This situation is more of an academic interest and it is useful for checking the masonry composite formulation.

3.2.2 Verification of the 1D model for masonry using the FEM

The previously discussed 1D model for masonry composite is verified by the FEM applied to the periodic unit shown in Figure 3-2(b) using the FE system DIANA. To obtain the stiffness of the composite material in a certain direction, the masonry cell is subjected to uniform loading along that direction and admissible displacement fields are imposed in the transverse directions by proper constraints. The composite moduli in the vertical (E^v_{com}) and horizontal (E^h_{com}) directions, predicted by Eqs. (3.2) and (3.5), respectively, are used

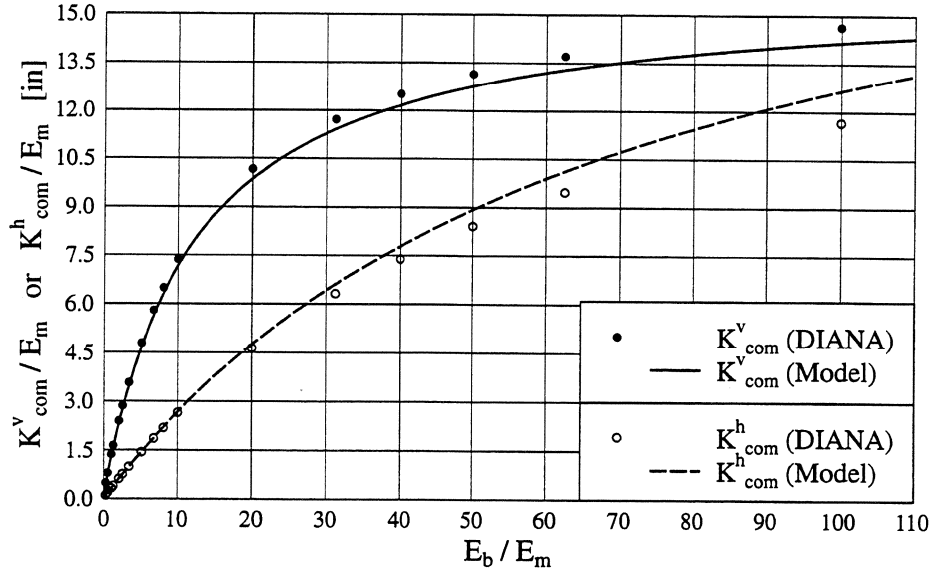

FIGURE 3-4 Variation of stiffness in vertical direction with E_b.

to determine the stiffnesses in these directions as follows,

$$K^v_{com} = \frac{E^v_{com} A^v_{com}}{h_b + t_{mb}} \qquad \& \qquad K^h_{com} = \frac{E^h_{com} A^h_{com}}{l_b + t_{mh}} \tag{3.8}$$

where K^v_{com} and K^h_{com} denote the stiffnesses for the composite in the vertical and horizontal directions, respectively. The variation of K^v_{com} and K^h_{com}, normalized with respect to E_m, obtained from both the 1D and the finite element analysis for different values of the ratio E_b/E_m are shown in Figure 3-4. The terms K^v_{com} and K^h_{com} are based on reasonable constant values for Poisson's ratios

$$\nu_b = 0.1 \qquad \& \qquad \nu_m = 0.2$$

for the blocks and the mortar, respectively. From Figure 3-4, one can reach the following conclusions:

1. Good agreement exists between the 1D model and the FEM results for values of the ratio $E_b/E_m \lesssim 10$.

2. The higher the ratio E_b/E_m, the more influential the effect of Poisson's ratios becomes. Therefore, the results of the 1D model start deviating from the results of the FEM at $E_b/E_m \approx 20$.

3. Considering the FEM results as the reference values, one observes that for the same ratio E_b/E_m, the present model consistently overestimates the normalized stiffness in the horizontal direction and underestimates it in the vertical direction.

3.3 Parameter Estimation Using Experimental Displacement Fields

Parameter estimation is one of the fundamental issues in system identification [122]. In structural engineering, system identification has been applied primarily to dynamic systems. In these systems, the identified parameters are those that cannot be measured directly, such as damping characteristics [119]. Some of the rare applications of system identification in continuum mechanics are those of Distéfano [43], Hendriks [66], Iding *et al.* [73] and Kavanagh and Clough [81]. In these studies, finite elements are used as the numerical model with some material and/or geometrical properties to be identified.

3.3.1 Theoretical background

In this study, the considered identification procedure is the one developed and implement by Hendriks [66]. The method is based on the sequential minimum variance approach and resembles the *Kalman-Bucy theory of filtering* [76] [77]. For discussion of the theory and applications, the reader is referred to the book by Bucy and Joseph [29]. The experimental data, *e.g. displacement of specific points on the tested structure*, is assumed to be collected in a vector $\mathcal{A}_{exp}$. The tested structure is modeled using FEM and the displacements at the same points are calculated and collected in another vector $\mathcal{A}_{fem}$ which is assumed to be a nonlinear function of the required material parameters $\mathcal{M}$, *i.e.*

$$\mathcal{A}_{exp} = \mathcal{A}_{fem}(\mathcal{M}) + \mathcal{E}_{obser} \tag{3.9}$$

where $\mathcal{E}_{obser}$ is a vector of observation errors.

The estimation process requires the following:

1. Observed variables $\mathcal{A}_{exp}$.
2. Uncertainty model for $\mathcal{E}_{obser}$.
3. A-priori knowledge of initial guess of $\mathcal{M}$, *i.e.* $\mathcal{M}_0$.

The initial guess $\mathcal{M}_0$ is related to $\mathcal{M}$ by

$$\mathcal{M} = \mathcal{M}_0 + \mathcal{E}_{estim} \tag{3.10}$$

where $\mathcal{E}_{estim}$ is a vector of estimation errors.

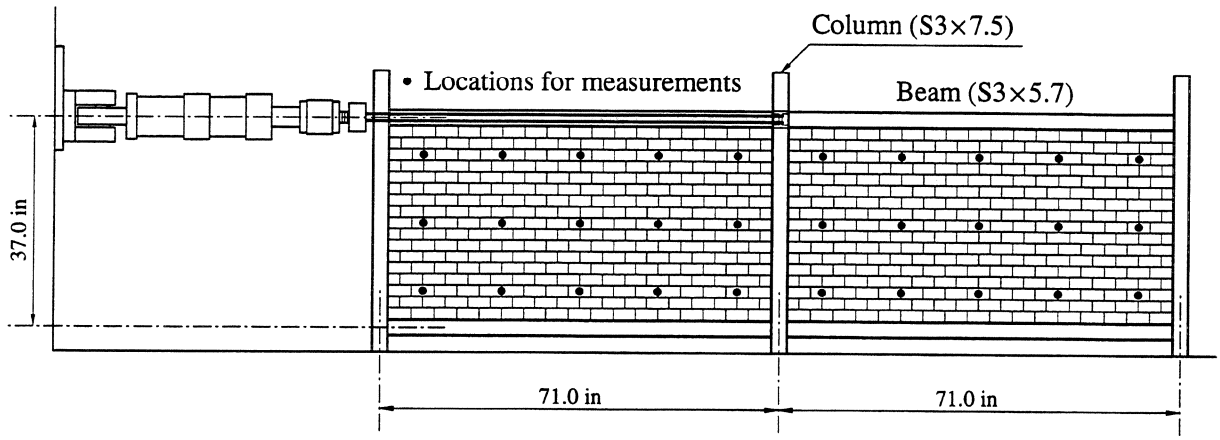

FIGURE 3-5 Setup for system identification experiment.

From the model given by Eqs. (3.9) and (3.10), the optimal parameter vector $\mathcal{M}$ minimizes the following quadratic expression [66]:

$$\begin{aligned} \mathcal{S} &= (\mathcal{A}_{exp} - \mathcal{A}_{fem}(\mathcal{M}))^T \mathcal{R}^{-1} (\mathcal{A}_{exp} - \mathcal{A}_{fem}(\mathcal{M})) + \\ &\quad (\mathcal{M}_0 - \mathcal{M})^T \mathcal{P}_0^{-1} (\mathcal{M}_0 - \mathcal{M}) \end{aligned} \tag{3.11}$$

where superscript T indicates transpose. The weighting matrices $\mathcal{R}$ and $\mathcal{P}_0$ are chosen on the basis of engineering judgement. In minimum variance estimation, $\mathcal{R}$ represents the covariance matrix[2] of the observation error ($\mathcal{E}_{obser}$) and $\mathcal{P}_0$ represents the covariance matrix of the estimation error ($\mathcal{E}_{estim}$). Generally, the larger the terms of the covariance matrix, the smaller the influence of its corresponding error. In the present study, diagonal matrices for $\mathcal{R}$ and $\mathcal{P}_0$ are assumed. Another simplification is obtained by assigning very large values for all the terms of $\mathcal{P}_0$ to indicate large influence of the estimation error in the parameter estimation process. On the contrary, very small values are assigned to the terms of $\mathcal{R}$ representing negligible influence of the observation errors (which are difficult to assess accurately) on the estimation process.

The parameter estimation procedure solves the nonlinear inverse problem which is mathematically defined by Eqs. (3.9), (3.10) and (3.11). For the estimation of n parameters, an iterative scheme is followed where $(n+1)$ finite element analyses are executed for each iteration. The sequential property of the estimation process is utilized when another observation vector with new experimental data becomes available from either a different experiment on the same material or from the same experiment at a different point in time[3]. The new data can be used with the estimate based on the previous data as the initial guess resulting, in general, in an improved estimation.

[2]Probability concepts such as variance and covariance are discussed in many textbooks on probability theory, *e.g.* references [4] [5].

[3]pseudo-time in case of static nonlinear analysis to indicate incremental loading.

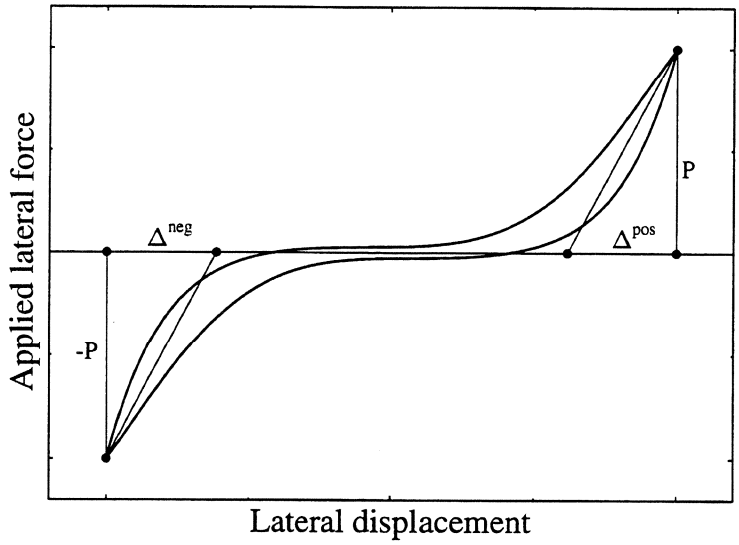

FIGURE 3-6 Generic loading cycle at a system identification location of the wall panels.

3.3.2 Experimental setup and observation data for system identification

The quasi-static experiment of the GLD steel frame with URM infills designated Q21SSB is considered here as the *identification experiment.* General description of this experiment can be found in the first report of this series. The walls were instrumented to provide the necessary displacement field of the masonry panels, *i.e.* the experimental data $\mathcal{A}_{exp}$. The experimental setup and the locations where the experimental data were taken are indicated in Figure 3-5. The loading was applied through reversed cyclic quasi-static lateral displacement as discussed in the first report of this series. A generic plot of the applied lateral load at the top central column of the steel frame versus the measured lateral displacement at one of the locations, shown in Figure 3-5, is shown in Figure 3-6. From this figure, the linear part of the measured deformation, excluding the effect of the frame/wall gap closure and transition zone of wall-stiffness mobilization (refer to Figure 2-15), may be determined as the average of the displacements Δ^{pos} and Δ^{neg} corresponding to the same load level P. The secant slope in each loading excursion is the average tangential slope of the loading and unloading curves at the same load level.

3.3.3 Numerical model for system identification

The experiment discussed in the previous section is modeled using the FEM with 8-noded, isoparametric, plane stress elements. The steel frame members were modeled as in **SECTION 2** to allow rotational stiffness of the joints and to account for the frame/wall interface

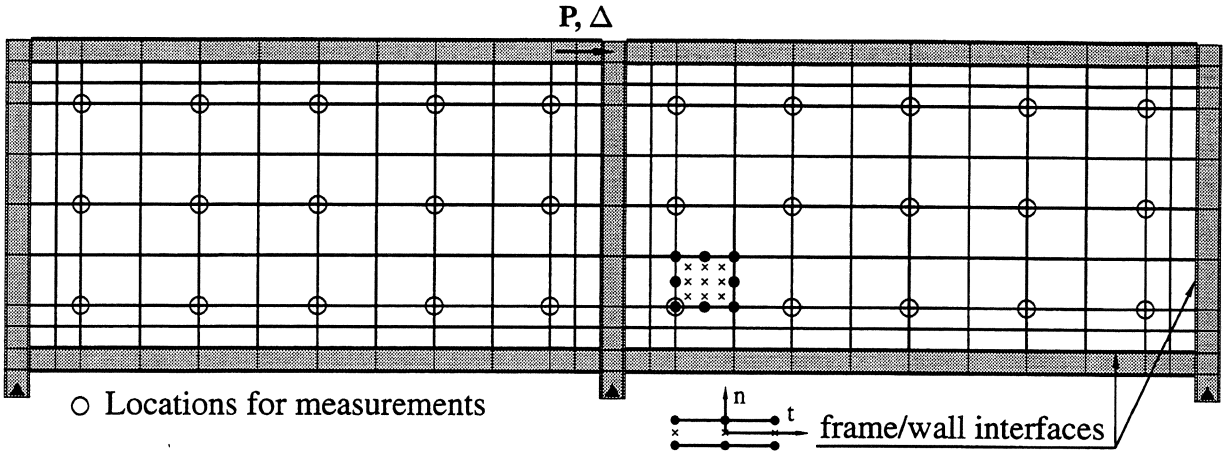

FIGURE 3-7 Finite element model for system identification.

conditions using the previously described model for the interface element (see Figure 2-15). The model used in the FEM is shown in Figure 3-7.

"Linear" finite element analysis is conducted to obtain the vector $\mathcal{A}_{fem}$. The actual performance of the tested structure is nonlinear from the early stages of loading because of the frame/wall interaction mainly due to the gap formation between the frame members and the infill walls. For appropriate modeling of the experiment with linear analysis, the following procedure is conducted:

1. An appropriate guess for the material parameters to be identified is made based on the experimental measurements of the properties from masonry subassemblages or masonry constituents, in addition to the 1D homogenization procedure described earlier.

2. Nonlinear finite element analysis is performed where material nonlinearities are not included and the only source of nonlinearities is the interface gap opening and sliding. The lengths of contact between the frame members and the walls are determined.

3. Full bond between the frame members and the infill walls is provided only along the length of contact determined from the previous step. The system identification procedure is followed to obtain a better estimate of the chosen material parameters using "linear" finite element analysis.

4. The new material parameters determined from the identification procedure are used as the new guess for checking the used lengths of contact. If large difference is detected between the new lengths of contact and the previous values, the whole procedure is repeated.

TABLE 3-II Parametric studies and results of the system identification technique.

			System identification	
Case	Model	Fixed parameters	Initial guess(es)	Final value(s)
1	Isotropic	$\nu = 0.10$	$E = 600$ ksi	$E = 309.3$ ksi
2	Isotropic	$\nu = 0.15$	$E = 600$ ksi	$E = 307.1$ ksi
3	Isotropic	$\nu = 0.10$	$E = 50$ ksi	$E = 309.3$ ksi
4	orthotropic	$\nu_{xy} = 0.10$ $G_{xy} = 140.6$ ksi	$E_x = 600$ ksi $E_y = 60$ ksi	$E_x = 392.0$ ksi $E_y = 78.5$ ksi
5	orthotropic	$\nu_{xy} = 0.15$ $G_{xy} = 140.6$ ksi	$E_x = 600$ ksi $E_y = 60$ ksi	$E_x = 388.5$ ksi $E_y = 75.7$ ksi
6	orthotropic	$\nu_{xy} = 0.10$ $G_{xy} = 210.9$ ksi	$E_x = 600$ ksi $E_y = 60$ ksi	$E_x = 388.9$ ksi $E_y = 56.0$ ksi

3.3.4 Identification results

In the finite element model, the material model for masonry is assumed to be either *isotropic* or *orthotropic*. Table (3-II) summarizes the material model adopted, the fixed parameters during the identification process, and the actual results from the system identification technique. The sensitivity of the identification process to the factors listed below is investigated.

1. Material model (isotropic versus orthotropic).
2. Initial fixed parameters in the material model during the identification process.
3. Initial guess of the identified parameters.

From the results listed in Table 3-II, one may conclude the following:

1. The adopted material model influences the estimated parameters. It is apparent that the wall behaves orthotropically (E_x/E_y varies from 5 to 7) rather than isotropically.
2. The effect of Poisson's ratio on the identified parameters is very small for both isotropic or orthotropic material models.
3. The effect of the shear modulus for the orthotropic model affects the identified Young's moduli, with relatively larger influence in the vertical (E_y) direction than in the horizontal (E_x) direction.
4. Initial guess(es) do not influence the estimated parameters.

5. The estimated E in Table 3-II is about 45% of the masonry prism initial stiffness obtained for material Group A as discussed in the first report of this series. This large difference may be attributed to an overestimation of the actual experimentally determined displacement field using the technique in Figure 3-6. Another suggested explanation is that, for hollow concrete block units, the prism stiffness for compression normal to the bed joints could be higher than the value for compression parallel to the bed joints [46] and obviously, the compression parallel to the bed joints approximates the stress conditions for laterally loaded infill walls better. This implies that the values of the initial stiffness obtained from the masonry prism tests may be overestimated for the tested infill walls.

The robustness of the identification algorithm is assessed by studying the convergence rate of the estimation for different sets of initial guesses of the identified parameters. These results are illustrated in Figure 3-8(a), whereas Figure 3-8(b) indicates the variations of the corresponding Euclidian norm of the residuals ($||e||$) with the iteration number. The residuals are defined as the difference between the experimental displacements and the calculated displacements, *i.e.* $\mathcal{E}_{obser}$. Obviously, the convergence characteristics of the estimation verify the robustness of the technique. Using the estimated parameter from case (1) listed in Table 3-II and performing the finite element analysis, the results shown in Figure 3-9 are obtained. From this figure, the analysis based on the estimated parameter recovers the *pointwise* experimentally determined displacement field to a reasonable accuracy. Therefore, the comparison in Figure 3-9 for case (1) justifies the use of the isotropic model in Table 3-II. It should be noted that vertical displacements were expected to be negligible compared to the horizontal ones. Therefore, they were not measured.

3.4 Continuum Modeling of Masonry Infills

In this section, masonry is modeled as a continuum with assumed homogeneous properties. The nonlinearities introduced in the analytical model are due to the frame/wall interface conditions and cracking in the masonry walls. A smeared crack approach [139] is adopted to model fracture in the homogenized masonry composite. This approach and the relevant material parameters are discussed in the **SECTION 4**. The results presented in the current section have the following purposes:

- Calibrate and verify the truss mechanism presented in the second report of this series. This verification is accomplished through the finite element results in the form of deformed shapes, crack patterns and stress trajectories.

- Evaluate the effect of opening sizes on the lateral stiffness of infilled frames.

- Motivate the use of the evolutionary methods presented in **SECTION 4** for smeared cracking. This is achieved by illustrating some of the numerical problems encountered

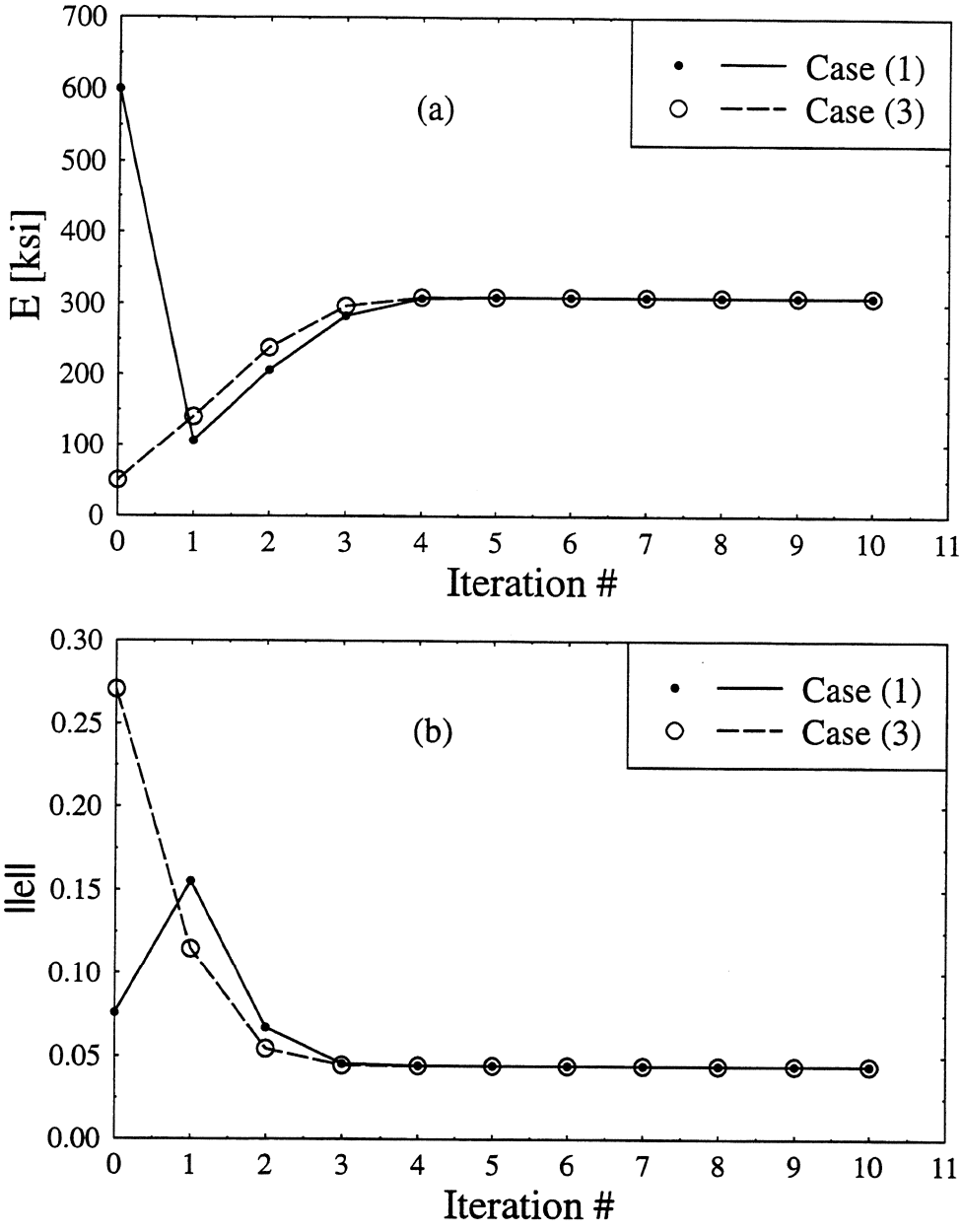

FIGURE 3-8 Convergence of identification algorithm; (a) Estimated parameter; (b) Norm of the residuals.

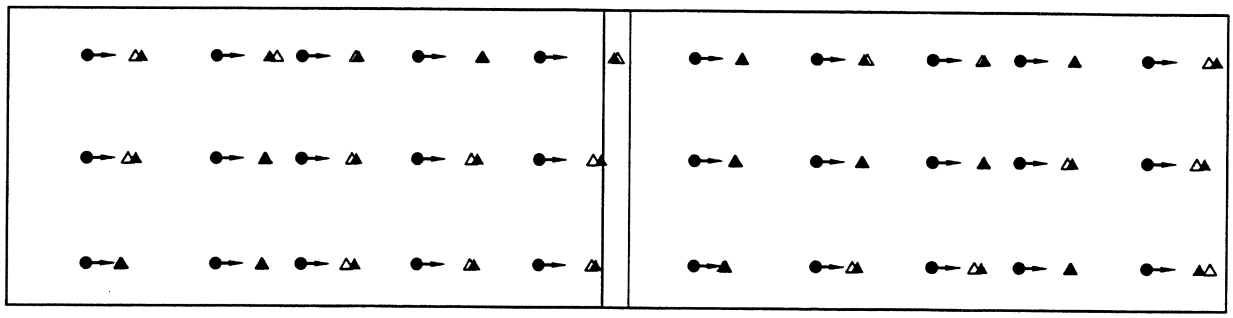

Amplification factor for deformation = 200 — Displacement direction

• Original marks △ Calculated position ▲ Measured position

FIGURE 3-9 Experimental versus calculated displacement fields.

when the standard smeared cracking approach is adopted in the material model of homogenized masonry walls.

The smeared cracking finite element model is illustrated on the right-hand-side of Figure 2-1. The structure considered in the present analysis has some similarities to the one illustrated in Figure 2-16, which was analyzed with the discrete model discussed in the previous chapter. However, the present results are for the case of symmetric openings in the infill walls. Monotonically increasing lateral load is applied at the central column of the frame as shown in Figure 2-1. The load is applied at the floor level. For the two-story case, an equivalent lateral force distribution is applied. This distribution is maintained to satisfy the first mode shape of the structure. This technique of *adapted push-over analysis* is discussed in detail in **SECTION 5.**

The finite element analysis is, once again, performed using the finite element code DIANA. The structure is assumed to be in a state of plane stress. The solution of the resulting nonlinear equations is obtained using the arc-length scheme proposed by Riks [147], which is capable of passing snap-back points, either spurious or not [149]. The importance of the arc-length schemes for softening analyses of localized fracture has been discussed by Crisfield [36]. To study the structural performance in the inelastic stage of the behavior, solution methods based on load control are not valid. For direct displacement control, constraining the degrees of freedom at which the displacements are applied becomes mandatory. This constraining makes the continuous monitoring of the mode shape (obtained from an eigen solution) practically impossible. Therefore, amongst the solution methods available in DIANA, the arc-length technique is the most reliable solution method.

TABLE 3-III Calibration results of continuum model and equivalent truss model of masonry infills.

Continuum model (FEM)				Equivalent truss model			
K_n	f_{bare}	E_m	f_{infill}	K_r	f_{bare}	A_{eq}	f_{infill}
2×10^4	3.08	0.84×10^3	10.86	1×10^4	2.94	50	12.27
2.5×10^4	3.14	1.00×10^3	11.55	1.7×10^4	3.13	46	12.17
2.6×10^4	3.15	1.15×10^3	12.13	1.8×10^4	3.15	45	12.14

All dimensions in inches, kips, seconds and radians

Experimental data are: $f_{\text{bare}} = \mathbf{3.15\ Hz}$ & $f_{\text{infill}} = \mathbf{12.14\ Hz}$

3.4.1 Calibration and verification of the truss model

The two-story Semi-Rigidly Connected Steel (SRCS) frame with URM infill walls was analyzed using continuum modeling of the masonry walls. Homogeneous properties of masonry were determined using the rheological model discussed in Section 3.2.1. The material properties for the bare frame and the infilled frame were adjusted to match the fundamental frequencies given in the second report of this series for the same structures tested pseudo-dynamically. The natural frequency of the bare frame was matched with the experimental value by adjusting the normal stiffness (K_n) of the interface element representing the semi-rigid joints. For the infilled frame, the fundamental frequency is the one that corresponds to the case of a braced frame with partial contact lengths between the frame members and the walls. This structural configuration was achieved by applying a small lateral load to determine these contact lengths and then performing the eigen analysis using the tangent stiffness matrix of the infilled frame with the actual contact lengths. The fundamental frequency of the infilled frame was adjusted to match the experimental observations by changing the value of the Young's modulus of masonry (E_m).

A similar calibration procedure was conducted for the infilled frame[4] where the walls were idealized using the equivalent truss model presented in the second report of this series. In this case, rotational springs were used to model the semi-rigid joints by rotational stiffness (K_r) which is adjusted to match the fundamental frequency of the bare frame. The calibration parameter for matching the fundamental frequency for the infilled frame was the equivalent cross sectional area (A_{eq}) of the truss members. The results of the calibration procedure are summarized in Table 3-III. The results discussed in the following paragraphs are referred to a response quantity selected as the top floor displacement normalized by the height of the structure ($\Delta_r\%$).

The finite element results before the cracking of the infill walls are shown in Figure 3-10.

[4]It was assumed that all frame joints have the same rotational stiffness (K_r) and all truss members have the same cross sectional area (A_{eq}). Obviously, these are approximations to simplify the calibration procedure.

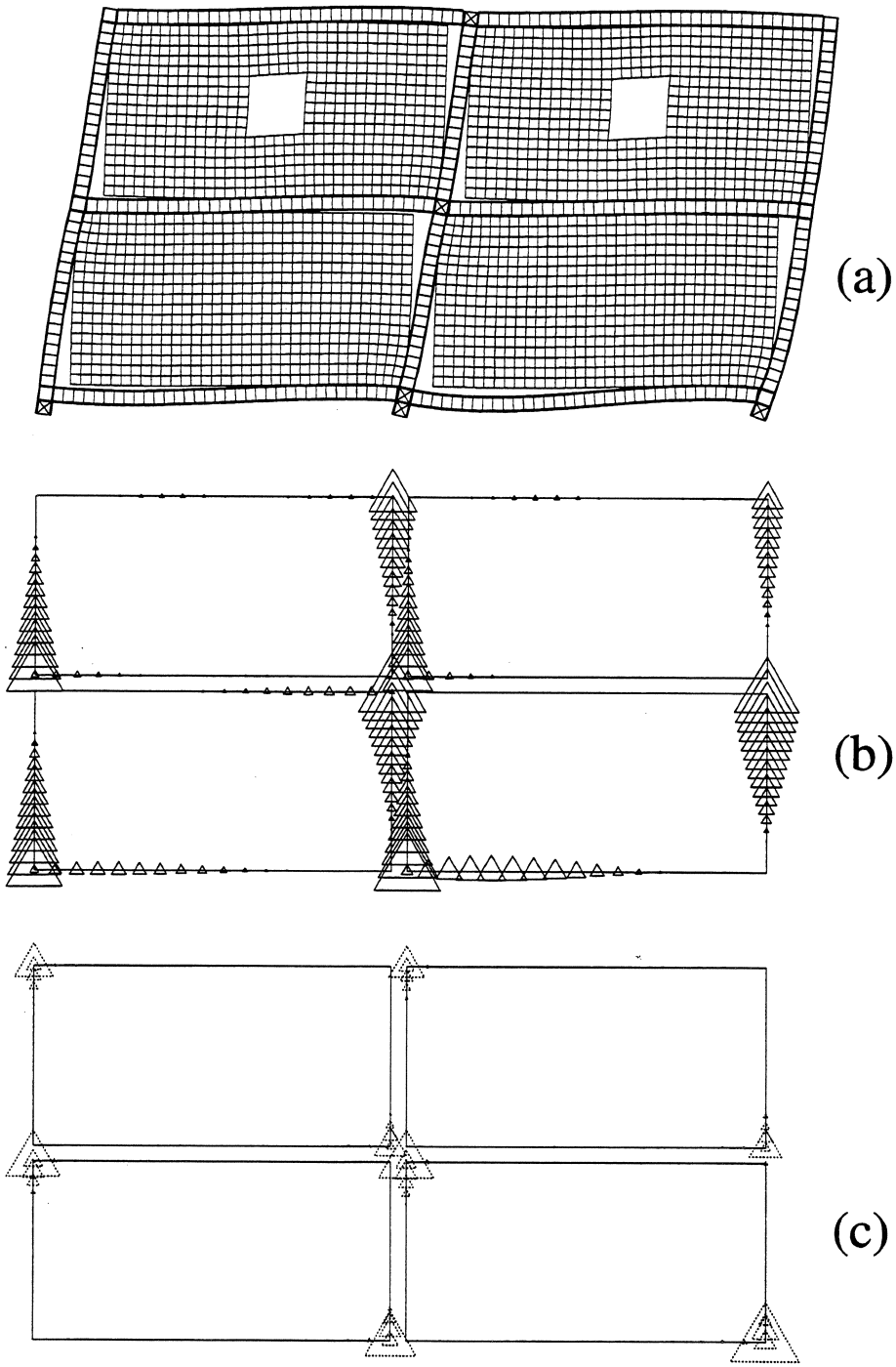

FIGURE 3-10 Finite element results of the two-bay, two-story infilled steel frame before wall cracking at $\Delta_r = 0.1\%$; (a) Deformed shape [Amplification factor = 100]; (b) Normal relative displacement along the interface [max $\approx$ 0.025 in]; (c) Normal compressive stress along the interface [max $\approx$ 2.65 ksi].

These results include the deformed shape of the structure and the frame/wall interface conditions in the form of normal relative displacements and normal stresses along the interface. The figure reflects the non-integral nature of the masonry walls, *i.e.* no tension between the wall and the frame members is allowed. Accordingly, the deformed shape clearly illustrates that the wall and the frame are contacting only in the interface regions where compressive stresses are mobilized. It is interesting to note that the normal relative displacements along the interface between the frame members and the infill walls indicate an obvious contact between the walls and the beams which extends beyond the local frame corners. This justifies the need for off-diagonal load transfer mechanisms to replace the continuum infill walls. With respect to Figure 3-10, the relative displacements and stresses normal to the interface are illustrated using triangles that are proportional in size to the value they are presenting. Dotted triangles indicate compression while solid ones indicate tension.

Figure 3-11 shows the finite element results after cracking occurred in the wall panels. The concentrations of stresses at the wall corners where the frame members contact the walls are clearly presented in the stress trajectories. In these trajectories, the length of the line is proportional to the stress value and compressive stresses dominate the stress field. Because the tensile stresses are much smaller than the compressive stresses, it is difficult to observe the tensile stress bars in Figure 3-11(a) but the major tensile stress fields are in general normal to the crack patterns shown in Figures 3-11(b) and 3-11(c). During the deformation process, the small tension capacity of the masonry walls is soon exhausted and cracks start to appear. First, cracks are initiated at the corners of the windows located in the top story. This is followed by cracks in the solid panels (*i.e.* panels without openings) in the first story. These observations are similar to the experimental results. As mentioned in the previous paragraph the interaction between the walls and the beams occurs not only at the frame connections but also close to the mid-spans of the beams which lead to the vertical cracks on the horizontal edges of the infills shown in Figure 3-11(c). Based on the previous discussions of the finite element results, it may be concluded that the truss idealization, discussed in the second report of this series, is appropriate in capturing the actual stress fields in the infill panels and the frame/wall interaction characteristics.

The final incremental deformation and crack patterns were obtained at $\Delta_r = 0.33\%$, after which convergence of the numerical solution was not achieved anymore, *i.e.* this loading level corresponded to the last converged solution. These results are shown in Figure 3-12. Two crack patterns are shown: all cracks (Figure 3-12(b)) and fully open cracks (Figure 3-12(c)). The fully open cracks are those cracks where the normal stresses are dropped to zero (*i.e.* stress-free cracks). From the localization of deformation (Figure 3-12(a)) and cracks (Figures 3-12(b) and 3-12(c)), one can observe the bracing (truss) actions that the non-integral wall panels provide to the bounding frame. The solid panels undergo compressive and tensile fields that can be characterized by equivalent struts and ties. For the panels with windows the truss model should account for the stress concentrations at the corners of the openings.

From the stress trajectories and crack patterns obtained with the FEM (*e.g.* Figure 3-11),

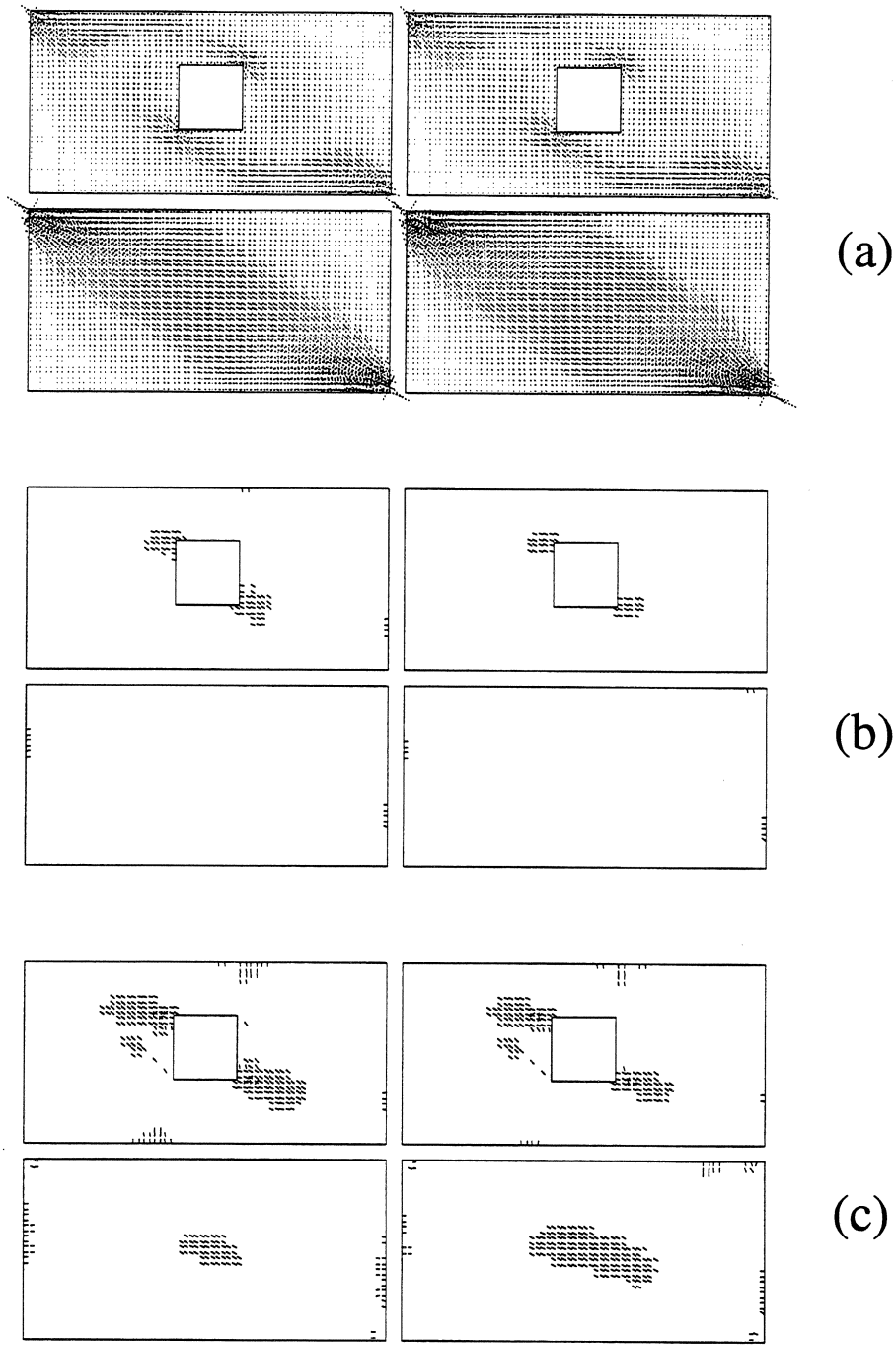

FIGURE 3-11 Finite element results of the two-bay, two-story infilled steel frame after wall cracking; (a) Stress trajectories at Δ_r = 0.12% [compression (max = 2.64 ksi), tension (max = 0.99 ksi)]; (b) Initiation of cracks in the top story at Δ_r = 0.12%; (c) Initiation of major cracks in the bottom story at Δ_r = 0.22%.

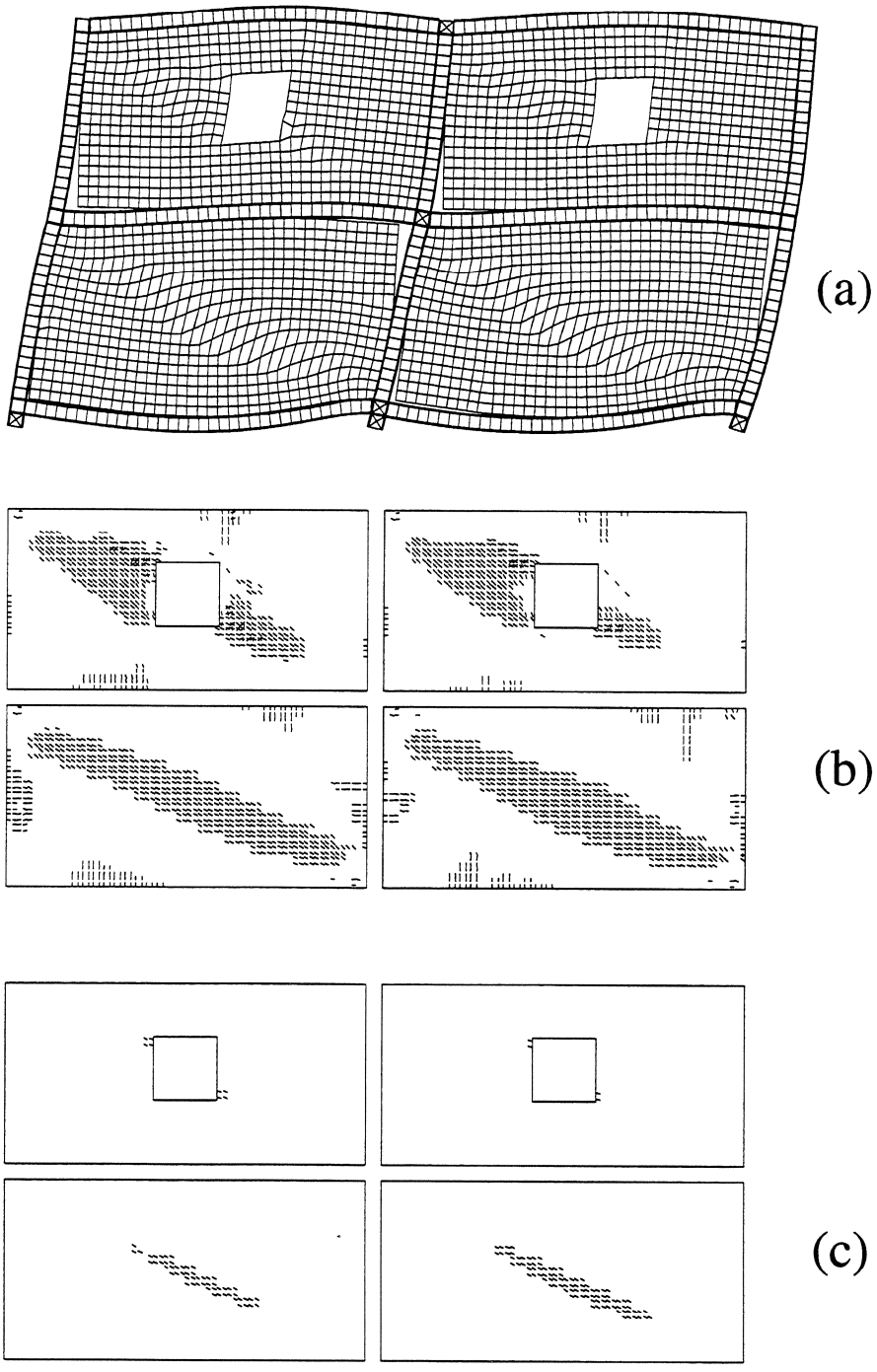

FIGURE 3-12 Finite element results of the two-bay, two-story infilled steel frame at the last converged loading increment; (a) Incremental deformation at $\Delta_r = 0.33\%$ [Amplification factor = 485]; (b) Crack pattern in the infill walls [all cracks]; (c) Crack pattern in the infill walls [fully open cracks].

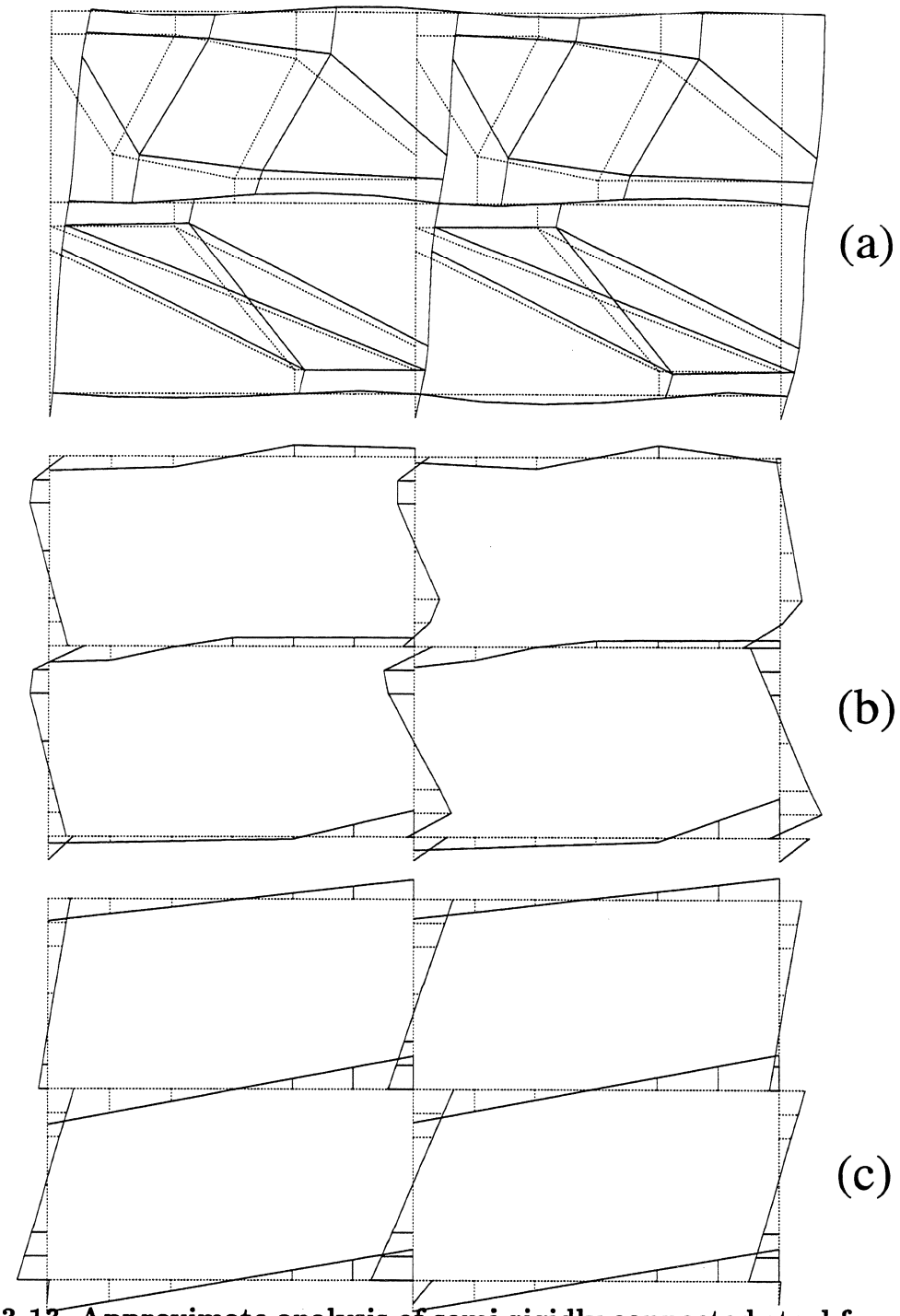

FIGURE 3-13 Approximate analysis of semi-rigidly connected steel frame with and without infills; (a) Truss model and its deformed shape with top floor displacement = 0.08 in [Amplification factor = 57]; (b) Bending moment diagram for infilled frame [max = 18.8 kip.in, min = -20.2 kip.in]; (c) Bending moment diagram for bare frame [max = 74.5 kip.in, min = -71.4 kip.in].

the equivalent widths of the truss members may be determined. The equivalent statical system of the frame with the infills replaced by the truss model is shown in Figure 3-13 together with the obtained deformed shape. The undeformed structure is shown in dotted lines and the deformed shape is given in solid lines. Bending moment diagrams with and without the infills are also shown in the same figure. These results are obtained by applying lateral forces ($F_1 = 3.14$ kips & $F_2 = 6.15$ kips). Comparing the numerical results in Figure 3-13 with experimental findings in the second report of this series, one may conclude that the truss model reasonably reproduces the magnitude and distribution of the bending moments in the frame members. From the bending moment diagrams of the infilled frame (*i.e.* with the equivalent truss replacing the infills) and the bare frame (*i.e.* without the equivalent truss), significant differences in distribution and magnitudes of the bending moments are obvious. This comparison illustrates the importance of accounting for the infill effects on the frame behavior.

3.4.2 Effect of opening size on the lateral stiffness of infilled frames

Openings increase the difficulty in defining a simple model to represent the effect of infill walls on the performance of the bounding frames. A study is conducted here, using the FEM, to investigate the effect of the size of window openings on the lateral stiffness of infilled frames. The used finite element model together with the material parameters are shown in Figure 3-14. This model accounts for the *material* nonlinearity due to wall cracking and the *geometrical* nonlinearity introduced by the change of frame/wall interface conditions during loading. Homogeneous properties are used for the masonry infills. A parameter α, defined as the percentage of the opening area relative to the solid wall panel area, is varied to study the effect of the opening size on the lateral stiffness of the infilled frame. The lateral stiffness is expressed in terms of the parameter κ, defined as the ratio of the stiffness with openings to that without openings.

The results of these finite element analyses are shown in Figure 3-15. Each curve in this figure corresponds to a certain applied inter-story drift (SD) which is defined as the applied displacement at the top central column normalized by the story height. For a single-story structure such as the present case, SD is the same as Δ_r defined in the previous section, but for a multi-story structure, they are different. Distinction is made between the infill wall status before and after cracking. For the range of parameters considered here, it may be observed that for either uncracked or cracked walls, the variation of the wall stiffness ratio is approximately a *linear* function of the opening area. Between the uncracked and cracked states, there is a transition zone which depend on the intensity of the applied inter-story drift. Plots, such as those presented in Figure 3-15, may be generated in more detailed parametric studies to furnish design charts for infilled frames where the effect of wall openings is to be accounted for.

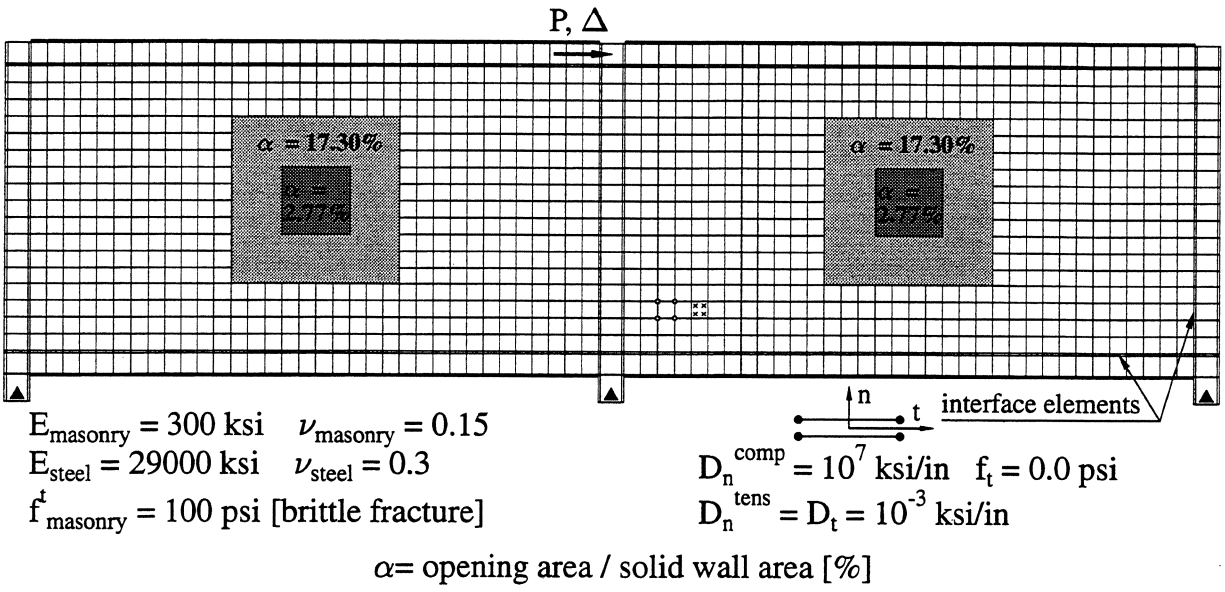

FIGURE 3-14 Finite element model and material parameters for studying the effect of windows on the lateral stiffness.

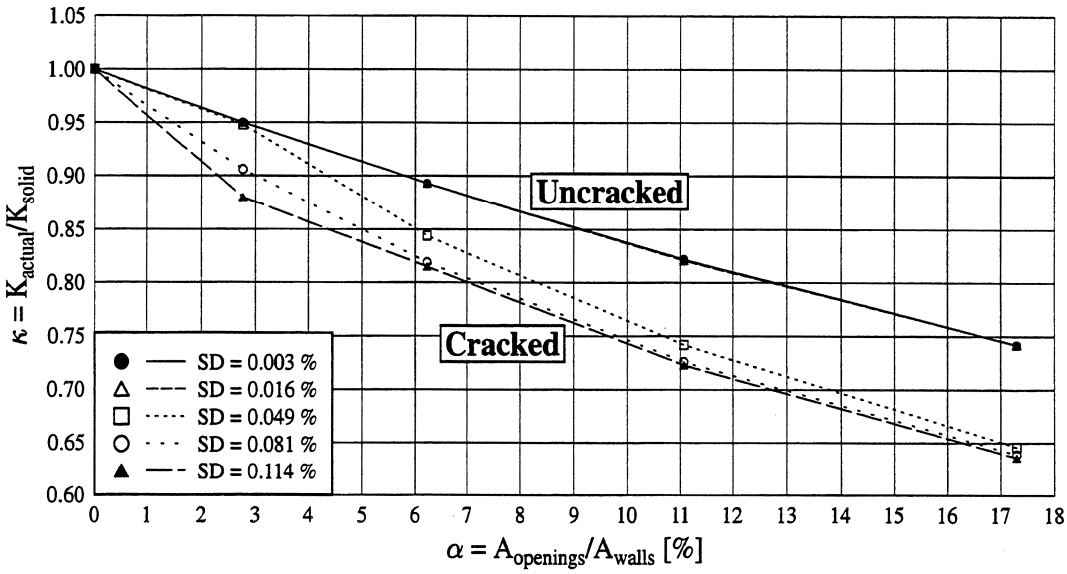

FIGURE 3-15 Effect of opening size on infilled frame lateral stiffness for different applied inter-story drift (SD).

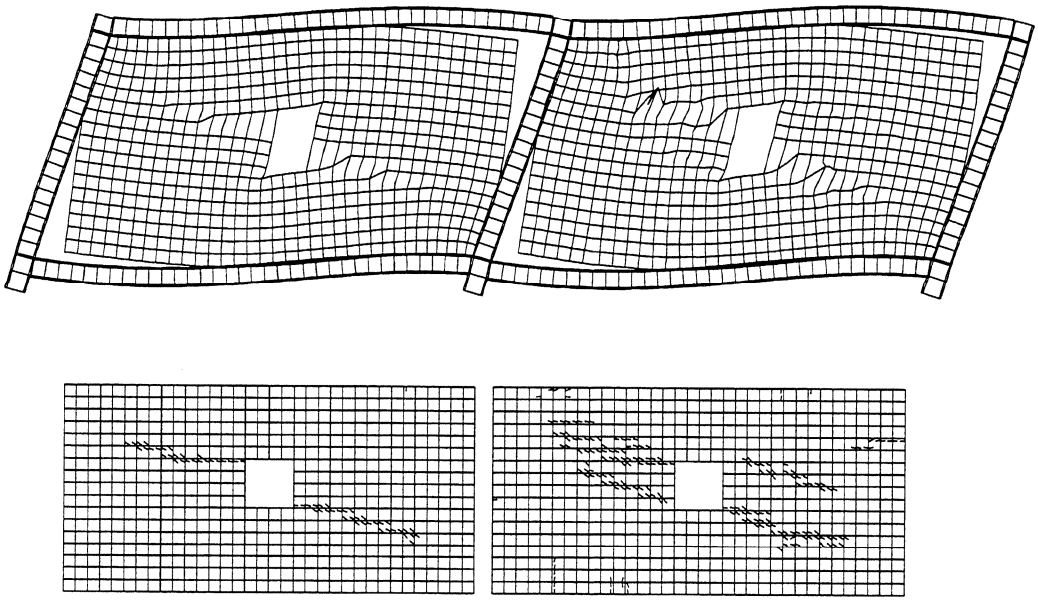

FIGURE 3-16 Spurious kinematic mode (top) and corresponding cracks (bottom).

3.4.3 Motivation for evolutionary methods in smeared cracking

In some cases, the computations involved in the analysis of the infilled frame with continuum modeling of the walls became critical; convergence became difficult and a negative pivot was signaled upon factorizing the tangent stiffness matrix. This situation was also encountered by Rots during the analysis of a Crack-Line-Wedge-Loaded Double-Cantilever-Beam (CLWL-DCB) [149]. Following a procedure similar to the one discussed in reference [149], an eigen value analysis was performed subsequent to the signaling of this negative pivot. The results of this eigen analysis detected a negative eigen value and the corresponding eigen mode represented a *spurious mechanism.* This spurious mechanism and the corresponding crack pattern in the masonry infills are illustrated in Figure 3-16.

The occurrence of the spurious modes is dependent upon the softening characteristics of the constitutive model [149]. In general, these spurious modes may be attributed to the continuous use of the tangent stiffness matrix which may blow up the iterative procedure once this matrix becomes ill-conditioned. Two techniques to overcome this inherent difficulty in smeared cracking analysis are presented in the next section.

3.5 Summary

In this section, masonry infills are treated as a continuum. A review of homogenization techniques for periodic media is presented. Seeking simplicity, an approximate model based on a one dimensional rheological representation of the elastic properties of masonry composite is derived and verified using the FEM. A system identification technique is briefly outlined and applied to estimate the elastic properties of masonry infill walls.

Using homogeneous properties of masonry infills, an application to a two-bay, two-story infilled frame is presented. The equivalent truss model, suggested in the second report of this series, is calibrated and verified. Preliminary investigation of the effect of window openings on the lateral stiffness of the infilled frames is shown to provide realistic trends which may be useful in calibrating simplified models such as the equivalent truss model. Finally, a computational difficulty encountered during the nonlinear finite element analysis including smeared crack representation in masonry infills is shown. The symptom of this problem is identified to be a spurious kinematic mode. Obviously, the development of techniques to circumvent this problem is a must.

SECTION 4

EVOLUTIONARY METHODS FOR SMEARED CRACKING

One of the fundamental components in nonlinear problems undergoing localized damage is the existence of an *internal length parameter.* This *characteristic length* determines the width of the localization zone as discussed by Pamin [127]. In smeared cracking terminology, this length parameter is the *crack band width* (Λ). When this parameter is related to the adopted finite element size, the spurious mesh dependency on the structural response can be reduced. This spurious dependency is mentioned in the previous section and a pathological consequence of it is illustrated in Figure 3-16. The relation between Λ and the finite element size can be determined by a trial-and-error fitting of some reliable results (*e.g.* experimental results or selected discrete crack results [149]). Some *ad hoc* rules depending on the chosen element type, element size, element shape, integration scheme and even on the particular problem considered, can be established to determine Λ as reported by Feenstra [55]. In the existing literature, Bažant [19] and Oliver [124] have attempted to rationalize the arbitrariness of the choice of the crack band width. In [19], Bažant has used strain-localization instability analysis to determine Λ. As he states, this analysis seems useful in principle, but not in practice, as it would be quite complicated in case of a large fracture process zone within a nonhomogeneously stressed specimen. In [124], Oliver has analyzed a singular band in a two-dimensional (2D) domain, in which a crack is modeled as a limiting case of two singular lines with continuous displacements but discontinuous gradients across them. This allowed him to relate the crack band width to the crack orientation and to the characteristics of the finite element interpolation functions. Although this approach is an improvement over the standard method [149], it renders the estimated value of the crack band width *constant* throughout the entire loading history.

In many applications, upon increasing the damage level (given here by the crack strain), cracking tends to *localize in a band of decreasing width.* By simply relating Λ to the finite element size (in 2D problems, the finite element area, A_e), one *cannot* capture such localization during damage evolution. One remedy to such a shortcoming is to *adapt* the finite element mesh to the present level of damage (cracking). Accordingly, the element size is determined in a manner consistent with the nature of the localization process. Upon such automated adjustment of the finite element size, a simple rule for the crack band width, *e.g.* $\Lambda \propto \sqrt{A_e}$, may be sufficient for accurately capturing localization. This adaptation requires continuous modification of the topology of the finite element mesh and needs a robust *transfer operator* [126] to map the state variables to the new mesh. Unfortunately, such a task in a highly nonlinear problem is difficult to execute.

The previous section illustrated some numerical difficulties encountered when the smeared cracking approach was adopted in the analysis of structures made of quasi-brittle materials such as masonry. Two techniques, intended to alleviate such difficulties, are presented

in this section. The first is an adaptive strategy for the finite element mesh in nonlinear problems where the nonlinearities are mainly attributed to smeared cracking. The second is a more practical adaptation of the crack band width, without changing either the topology or the geometry of the original finite element mesh.

4.1 Smeared Crack Framework

Smeared cracking is a continuum approach for the numerical solution of fracture mechanics problems in which local discontinuities are distributed (*i.e.* smeared) over a certain tributary area within the cracked finite element. Accordingly, crack strain can be defined as a function of the relative displacement (displacement jump or displacement discontinuity) of the crack surfaces and some length parameter over which this displacement jump is assumed to be smeared. The introduction of such *characteristic length* allows modeling of the cracked material in terms of stress-strain relations.

The smeared cracking concept has been shown to be a powerful technique for the continuum mechanics solution of damage and fracture problems. Since the advent of the smeared crack concept by Rashid [139], it has been refined by several researchers [120]. Significant improvements of this concept have been provided by *the fictitious crack model* developed by Hillerborg *et al.* [67] and *the crack band theory* presented by Bažant and Oh [20].

In the fictitious crack model, the tensile strength (f_t) and the fracture energy ($\mathcal{G}_f$) are the model parameters. The fracture energy is the amount of energy required to create a unit area of crack surface. The two parameters (f_t and $\mathcal{G}_f$) are also included in the crack band theory, in addition to a third parameter, which is the crack band width (Λ).

In the original formulation of the smeared crack approach [139], the strain vector represented the overall strain of the cracked material. In this way no distinction was made between cracks and the solid material between them. Since cracks are naturally perceived as geometrical discontinuities, it is of advantage to make such distinction in modeling the cracked material. Therefore, the modern approach for smeared cracking is based on the idea of *strain decomposition*, originally proposed by Litton [99]. In this idea, an increment of the total strain vector $\Delta\boldsymbol{\epsilon}$ is decomposed into an increment of the crack strain vector $\Delta\boldsymbol{\epsilon}_{cr}$ and an increment of the solid material (*i.e.* material between cracks) strain vector $\Delta\boldsymbol{\epsilon}_{ma}$, *i.e.*

$$\Delta\boldsymbol{\epsilon} = \Delta\boldsymbol{\epsilon}_{cr} + \Delta\boldsymbol{\epsilon}_{ma} \tag{4.1}$$

In Eq. (4.1), the strain vectors are given with respect to the global coordinate axes $\{x, y\}$. Focusing on the *plane stress* idealization, one can write

$$\Delta\boldsymbol{\epsilon}_{cr} = [\Delta\epsilon_{cr}^{xx}\ \Delta\epsilon_{cr}^{yy}\ \Delta\gamma_{cr}^{xy}]^T \tag{4.2}$$

where $[\cdot]$ indicates a matrix and superscript T denotes transpose. $\Delta\epsilon_{cr}^{xx}$ and $\Delta\epsilon_{cr}^{yy}$ are increments of normal strains and $\Delta\gamma_{cr}^{xy}$ is an increment of shear strain.

Similarly, the vector of incremental stresses in the global coordinate axes $\Delta\boldsymbol{\sigma}$ is given by

$$\Delta\boldsymbol{\sigma} = [\Delta\sigma^{xx}\ \Delta\sigma^{yy}\ \Delta\tau^{xy}]^T \tag{4.3}$$

where $\Delta\sigma^{xx}$ and $\Delta\sigma^{yy}$ are increments of normal stresses and $\Delta\tau^{xy}$ is an increment of shear stress.

Setting a local frame of axes $\{p,\ q\}$ normal and tangential to the crack direction, one can define

$$\Delta\boldsymbol{e}_{cr} = [\Delta\epsilon_{cr}^{pp}\ \Delta\gamma_{cr}^{pq}]^T \tag{4.4}$$

as the local incremental crack strain vector. In fracture mechanics terminology, $\Delta\epsilon_{cr}^{pp}$ is the mode-I crack normal strain and $\Delta\gamma_{cr}^{pq}$ is the mode-II crack shear strain. Associated with the $\{p,\ q\}$ local axes, one can readily define a vector of incremental stresses in the crack direction, $\Delta\boldsymbol{s}$, as

$$\Delta\boldsymbol{s} = [\Delta s^{pp}\ \Delta s^{pq}]^T \tag{4.5}$$

where, in analogy to Eq. (4.4), Δs^{pp} is the mode-I normal stress and Δs^{pq} is the mode-II shear stress.

The transformation from local to global crack strains is

$$\Delta\boldsymbol{\epsilon}_{cr} = \boldsymbol{N}\Delta\boldsymbol{e}_{cr} \tag{4.6}$$

Correspondingly, global stresses are transformed to local stresses by

$$\Delta\boldsymbol{s} = \boldsymbol{N}^T\Delta\boldsymbol{\sigma} \tag{4.7}$$

The transformation matrix $\boldsymbol{N}$ in Eqs. (4.6) and (4.7) is a function of the crack orientation with respect to the global coordinate axes[1]. In the present smeared crack approach, $\boldsymbol{N}$ is assumed to remain fixed upon crack formation (*fixed crack concept*). When the axes of material orthotropy $\{p,\ q\}$, caused by material cracking, are assumed to co-rotate with the axes of principal strains, the *rotating crack concept* is obtained [149].

To relate the incremental stress vector to the incremental strain vector, let $\boldsymbol{D}_{ma}$ be the matrix of instantaneous properties of the solid material between cracks and $\boldsymbol{D}_{cr}$ the matrix

[1]In the local directions, some strain and stress components are omitted because they have no physical meaning. The consequence is a rectangular transformation matrix $\boldsymbol{N}$ rather than a square one. For more discussions on the characteristics of $\boldsymbol{N}$, the reader is referred to **Chapter 2** in reference [149].

incorporating the mode-I, mode-II and mixed-mode properties of the crack. For plane stress problems with isotropic solid material between cracks,

$$\boldsymbol{D}_{ma} = \frac{E}{1-\nu^2}\begin{bmatrix} 1 & \nu & 0 \\ \nu & 1 & 0 \\ 0 & 0 & (1-\nu)/2 \end{bmatrix} \tag{4.8}$$

where E is Young's modulus and ν is Poisson's ratio.

Moreover,

$$\boldsymbol{D}_{cr} = \begin{bmatrix} D_{cr}^{I} & 0 \\ 0 & D_{cr}^{II} \end{bmatrix} \tag{4.9}$$

where D_{cr}^{I} and D_{cr}^{II} are the respective mode-I and mode-II stiffness moduli for a "single smeared crack". For simplicity, the *direct* shear-normal coupling is ignored (zero off-diagonal terms) in Eq. (4.9). The mode-II stiffness modulus D_{cr}^{II} can be related to the elastic shear modulus G by

$$D_{cr}^{II} = \frac{\beta}{1-\beta}G \quad \text{with} \quad G = \frac{E}{2(1+\nu)} \tag{4.10}$$

where β is the shear retention factor introduced to adapt the shear stiffness of the cracked material. In cracked cement-based composites, *e.g.* plain or reinforced concrete or mortar, shear forces can still be transferred through aggregate interlock, shear friction and dowel action. The latter mechanism is available in the case of reinforcing bars crossing the crack. Some of the early attempts to establish the shear force-displacement relations in cracked plain concrete were conducted by Fenwick and Paulay [56], White and Holley [164] and Taylor [160]. Paulay and Loeber [130] conducted a series of displacement-controlled static shear loading tests to study the aggregate interlock in concrete. Based on these experiments, Rots *et al.* [115][2] derived the following expression for β

$$\beta = \frac{1}{1 + 4447\,\epsilon_{cr}^{pp}} \tag{4.11}$$

This expression introduces an *indirect* shear-normal coupling. Based on the same experimental data of Paulay and Loeber [130], Bažant and Gambarova [18] derived a similar expression. In the present study, β is either based on Eq. (4.11) or is assumed to be a very small constant, *e.g.* $\beta \approx 0.0$ meaning that only the opening mode crack is considered.

The mode-I stiffness modulus D_{cr}^{I} is the most important factor in the present material model because it not only governs the crack propagation in mode-I but also indirectly

[2]The original reference of the work by Rots *et al.* is in Dutch. This work is cited by Van Mier *et al.* in reference [115].

affects the shear modulus according to Eq. (4.11). This modulus depends on the selected shape of the descending branch of the stress-strain relation.

The constitutive relations for both solid material between cracks and smeared cracks are given by

$$\Delta\boldsymbol{\sigma} = \boldsymbol{D}_{ma}\ \Delta\boldsymbol{\epsilon}_{ma} \tag{4.12}$$

$$\Delta\boldsymbol{s} = \boldsymbol{D}_{cr}\ \Delta\boldsymbol{e}_{cr} \tag{4.13}$$

The constitutive relation between the increment of total stress vector and that of the total strain vector in global coordinate axes can be easily obtained by algebraic manipulations of Eqs. (4.1), (4.6), (4.7), (4.12) and (4.13) as given in reference [149]. The final relationship is

$$\Delta\boldsymbol{\sigma} = \left[\boldsymbol{D}_{ma} - \boldsymbol{D}_{ma}\boldsymbol{N}\left[\boldsymbol{D}_{cr} + \boldsymbol{N}^T\boldsymbol{D}_{ma}\boldsymbol{N}\right]^{-1}\boldsymbol{N}^T\boldsymbol{D}_{ma}\right]\Delta\boldsymbol{\epsilon} \tag{4.14}$$

Riggs and Powell [146] arrived at a relation similar to Eq. (4.14) with the exception of making a distinction between the stress and strain transformation matrices from local to global coordinates. The resulting constitutive matrix from Eq. (4.14) is a modification of the elasticity matrix $\boldsymbol{D}_{ma}$ with another matrix of a lower rank[3] to account for the material damage introduced by smeared cracking.

A summary of the basic concepts of smeared cracking approach is illustrated by Figures 4-1 and 4-2. For clarity, the superscripts p and q for local coordinates are dropped from these figures. Consider a Gauss point in one element of the finite element mesh as shown in Figure 4-1(a), at which the principal stresses (σ_1, σ_2) are obtained, *e.g.* by means of the Mohr circle as shown in Figure 4-1(b). Next, the principal tensile stress σ_1 is checked against a *cracking criterion*, such as the one given by the Rankine failure surface of Figure 4-1(c). If cracking occurs, the crack orientation, determined by the angle ϕ in Figure 4-1(a), becomes *fixed* and normal to the direction of the principal tensile stress σ_1 at crack initiation. The strains aligned with the crack orientation are decomposed according to Eq. (4.1), as shown in Figures 4-1(d) and 4-2. The stresses normal to the crack direction are related to the crack strains by a nonlinear strain-softening function as indicated in Figure 4-1(e). In case of non-zero shear retention factor, some shear capacity is retained in the constitutive matrix of a cracked element. Therefore, the principal tensile stress direction is no longer normal to the fixed crack. Accordingly, the fixed crack normal stress component is designated by s to distinguish it from the principal tensile stress σ_1 (see Figures 4-1(e) and 4-2).

[3]The rank of a matrix equals the maximal number of independent rows or columns [58].

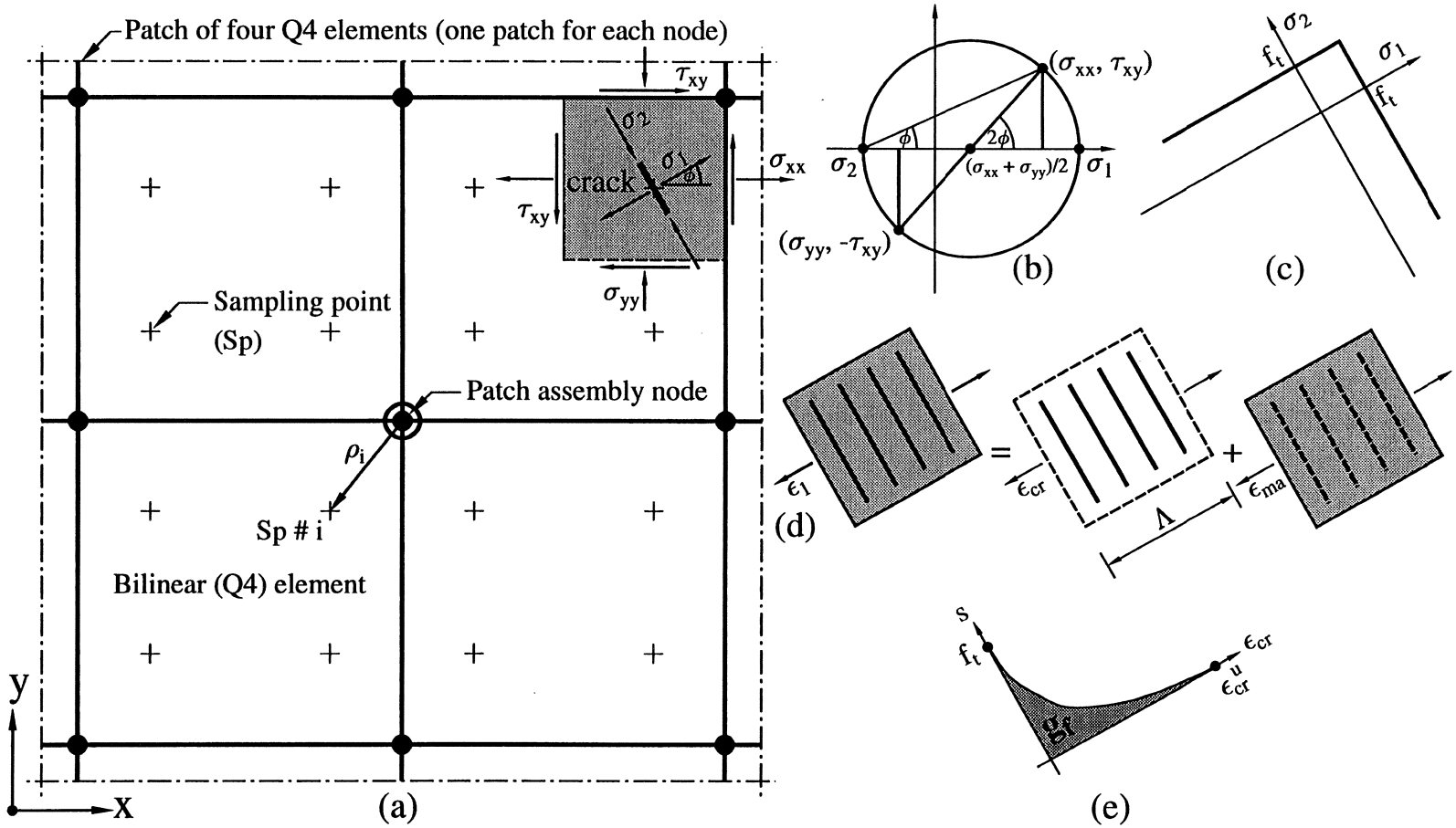

FIGURE 4-1 Smeared cracking in a typical patch of finite elements; (a) Example of a patch of finite elements; (b) Mohr circle; (c) Tension cut-off in 2D principal stress space; (d) Strain decomposition; (e) Total fracture energy density (full cracking).

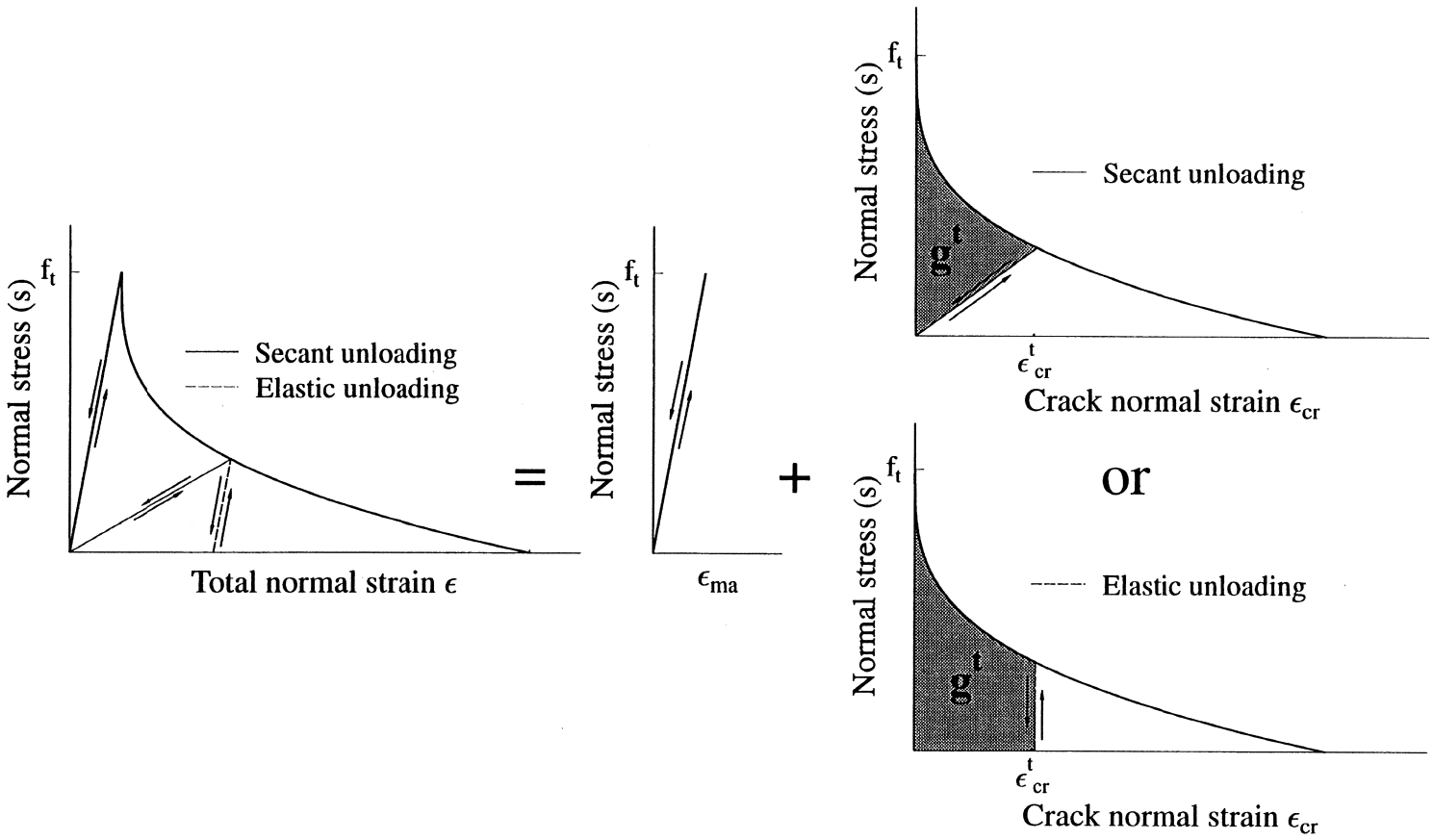

FIGURE 4-2 Strain decomposition and apparent fracture energy density.

4.2 Strain Softening and Fracture Energy

In this section, the behavior of structures made of quasi-brittle materials (*e.g.* rock, concrete, clay brick, mortar or ceramics) in the inelastic stages is considered. In these stages, the structure may undergo *strain softening*, *i.e.* gradual decline of stress at increasing strain mainly due to cracking. Material softening and strain localization have been the focus of significant computational and experimental research efforts directed to elucidate problems such as stability, uniqueness, localization, phenomenological models at the macro-level of observation and micro-mechanical models at the meso-level. A comprehensive treatise of such problems can be found in the review article by Read and Hegemier [140] where an exploration of the physical basis of strain softening in rock, soil and concrete is presented. Bažant *et al.* [21] presented a continuum theory for strain-softening in heterogeneous materials such as concrete or rock. In this theory, they adopt a new type of nonlocal continuum called the *imbricate* continuum which is a limit of a discrete system of imbricated (regularly overlapping) elements which have a fixed length and a cross section area that tends to zero as the discretization is refined. This theory was latter simplified by Bažant and Lin [22] by applying the nonlocal treatment only to those variables which cause strain-softening, while the other variables are kept local. In this way, the differential equations of equilibrium with the boundary conditions retain their standard form.

A family of crack normal stress versus crack normal strain (s-ϵ_{cr}) relations is considered in the present study. This family is based on curve-fitting of a large number of experiments, as reported by Reinhardt [142], to determine the crack normal stress versus crack opening (s-δ_{cr}) relations of concrete. This family of relations is governed by the exponent k in the following equation

$$\frac{s}{f_t} = 1 - \left(\frac{\delta_{cr}}{\delta_{cr}^u}\right)^k \tag{4.15}$$

where δ_{cr}^u is the stress-free crack opening (*i.e.* opening at total loss of load carrying capacity in the normal direction of a crack). This crack opening can be related to *the total fracture energy* ($\mathcal{G}_f$) by considering the following relation

$$\mathcal{G}_f = \int_0^{\delta_{cr}^u} s d\delta_{cr} \tag{4.16}$$

This definition implies that $\mathcal{G}_f$ is the total area under the stress versus crack opening curve. From Eqs. (4.15) and (4.16), one easily obtains

$$\delta_{cr}^u = \frac{(k+1)\mathcal{G}_f}{k f_t} \tag{4.17}$$

Assuming uniform distribution of the crack opening over Λ, one gets the following simple and important relationship for the smeared crack normal strain (see Figure 4-1(d))

$$\epsilon_{cr} = \frac{\delta_{cr}}{\Lambda} \tag{4.18}$$

Substitution of Eqs. (4.17) and (4.18) into Eq. (4.15) leads to

$$s = f_t \left(1 - \left(\frac{k f_t \Lambda \epsilon_{cr}}{(k+1)\mathcal{G}_f} \right)^k \right) \tag{4.19}$$

which gives the softening (descending) branch of a smeared crack in terms of the basic three parameters of the previously mentioned crack band theory [20], namely f_t, $\mathcal{G}_f$ and Λ. From the softening relation of Eq. (4.19), one obtains

$$D^I_{cr} = \frac{\partial s}{\partial \epsilon_{cr}} = -k \left(\frac{k f_t \Lambda}{(k+1)\mathcal{G}_f} \right)^k (\epsilon_{cr})^{k-1} \tag{4.20}$$

From the assumption stated by Eq. (4.18) and for constant Λ, the (total) fracture energy density is

$$g_f = \int_0^{\epsilon^u_{cr}} s d\epsilon_{cr} = \mathcal{G}_f / \Lambda \tag{4.21}$$

where g_f is the total area under the stress versus crack strain curve (*cf.* with Eq. (4.16)), as illustrated by Figure 4-1(e). At a certain load level (t) and in accordance with the adopted unloading/reloading assumption (secant or elastic), the *apparent fracture energy density* (g^t) is defined as shown in Figure 4-2. Therefore,

$$g^t = \int_0^{\epsilon^t_{cr}} s \, d\epsilon_{cr} - \frac{1}{2} \epsilon^t_{cr} \, s^t \qquad \text{Secant unloading} \tag{4.22}$$

$$= \int_0^{\epsilon^t_{cr}} s \, d\epsilon_{cr} \qquad \text{Elastic unloading} \tag{4.23}$$

From these expressions, one may define the so-called apparent fracture energy density g^t as the amount of fracture energy density (energy per unit volume) released up to a certain load level t. The apparent fracture energy density may be related to measures of damage indicating that the evolution of material damage in the form of smeared cracking can be reflected in this quantity. An outline of the relation between the apparent fracture energy density and a simple isotropic measure of damage in plane stress representation is given in **Appendix B**.

4.3 Adaptive FEM For Problems With Smeared Cracking

The solution obtained from any numerical method, *e.g.* FEM [170], Boundary Element Method (BEM) [131] or Finite Difference Method (FDM) [14], is an approximation of the exact solution of the governing differential equations of the problem. Adaptivity is defined as the successive refinement of an approximation to reach predetermined levels of accuracy. In general, adaptivity consists of the following two basic components:

- *A-posteriori* error estimation.
- Adaptive strategy.

Adaptivity for linear elliptic problems has achieved a high level of mathematical and numerical understanding. This technique is now routinely used within finite element computations [169]. Unfortunately, nonlinear problems have received little attention due to their complexity and the special features of each particular problem.

This section presents an adaptive nonlinear finite element method where the nonlinearities are mainly due to smeared cracking. The presentation is a mere illustration of the adaptivity procedure as a possible means to capture strain localization due to accumulation of structural damage. No attempt is made to formulate a complete adaptive nonlinear finite element methodology.

4.3.1 Review of error estimation and adaptivity

There exists an extensive literature on error estimation and adaptive methods. In this section, in the interest of brevity, a short account of the literature is given, and only the publications of major relevance to this work are cited. Several surveys of the literature in error estimation and adaptivity have been written, and the reader is directed to the appropriate references. Only references related to FEM are mentioned here.

The volumes edited by Brebbia and Aliabadi [28] and by Babuška *et al.* [14] [15] review adaptive techniques for FEM. Recent surveys also include articles by Noor and Babuška [121][4], Oden and Demkowicz [123][5], Strouboulis and Haque [155] [156] and Babuška and Suri [16]. A compilation of literature on mesh generation and refinement in the period 1990-1993 was conducted by Mackerle [103][6]. Literature on error analysis and adaptive techniques in the 1992-1993 period was also compiled by Mackerle [104][7]. Recent textbooks

[4] cites 196 references.
[5] cites 184 references.
[6] cites 272 references in FEM.
[7] cites 312 references in FEM.

on FEM emphasize the field of adaptive solution techniques. The book by Zienkiewicz and Taylor [170] includes a chapter on "Error Estimation and Adaptivity" (**Chapter 14**). Also, the recent book by Szabó and Babuška [159] is primarily concerned with adaptivity in the FEM.

Most of the above references dealt with linear elliptic problems. In contrast, relatively few advances have been published for certain classes of nonlinear problems. Some of these advances can be found in reference [15]. General mathematical theory of *a-posteriori* error estimates and adaptive approaches for history-dependent nonlinear problems in solid mechanics are still lacking. Exceptions to the previous statement are the contributions by Rheinboldt [143], Ladeveze *et al.* [90], Johnson and Hansbo [74] [75], Perić *et al.* [132] and Lee and Bathe [91]. To the best of the authors' knowledge, the application of adaptive strategies in nonlinear finite element analysis of problems undergoing damage due to material fracturing has not yet been addressed.

4.3.2 Error estimation for linear problems

The definition of an appropriate error estimator is essential for reliable adaptive FEM. This error estimator is a *local measure* of the deviation of the numerical solution from the exact one. Several sources of such deviation may exist leading to different types of errors (*e.g.* those due to roundoff and uncertainties in material, geometry, and boundary conditions). In the present study, only errors introduced by the discretization process which reduces the continuous mathematical model to one having a finite number of degrees of freedom are considered. These errors are termed discretization errors.

There are two broad classes of error estimation schemes:

- Residual methods.
- Interpolation methods.

To demonstrate these two classes, the following linear elliptic problem which characterizes a wide range of boundary value problems (*e.g.* problems of linear elasticity) is considered. The governing equation for the selected problem is

$$\mathcal{S}^T\boldsymbol{\sigma} + \boldsymbol{b} = \mathbf{0} \quad \text{with} \quad \boldsymbol{\sigma} = \mathcal{D}\boldsymbol{\epsilon} = \mathcal{D}\mathcal{S}\boldsymbol{u} \quad \text{in the domain } \Omega = \Omega_t \cup \Omega_u \tag{4.24}$$

with boundary conditions

$$\boldsymbol{n}\boldsymbol{\sigma} = \check{\boldsymbol{t}} \quad \text{on } \partial\Omega_t\,, \quad \boldsymbol{u} = \check{\boldsymbol{u}} \quad \text{on } \partial\Omega_u \;\&\; \partial\Omega = \partial\Omega_t + \partial\Omega_u \tag{4.25}$$

where superscript T indicates transpose, $\boldsymbol{\sigma}$, $\boldsymbol{\epsilon}$ and $\boldsymbol{u}$ are the generalized stresses, generalized strains and displacements, respectively, $\mathcal{S}$ is a first order strain differential operator, $\boldsymbol{b}$ is

the body force, $\mathcal{D}$ is the elasticity matrix, $\check{\boldsymbol{t}}$ and $\check{\boldsymbol{u}}$ are the assumed generalized tractions and displacements on the boundaries $\partial\Omega_t$ and $\partial\Omega_u$, respectively, and $\boldsymbol{n}$ is the outward unit normal to the boundary of the domain Ω.

Denote the finite element approximation $(\boldsymbol{u}_h,\ \boldsymbol{\sigma}_h)$ of the solution $(\boldsymbol{u},\ \boldsymbol{\sigma})$ obtained by the standard Galerkin procedure [170] as

$$\boldsymbol{u} \approx \boldsymbol{u}_h = \mathcal{N}\hat{\boldsymbol{u}} \qquad \& \qquad \boldsymbol{\sigma} \approx \boldsymbol{\sigma}_h = \mathcal{D}\mathcal{B}\hat{\boldsymbol{u}} \quad \text{with} \quad \mathcal{B} = \mathcal{S}\mathcal{N} \tag{4.26}$$

where $\hat{\boldsymbol{u}}$ is the nodal value of the displacements and $\mathcal{N}$ is the matrix of the finite element basis functions.

Based on the previous equations, it is possible to define the following two kinds of *local* errors:

$$\boldsymbol{e}_u = \boldsymbol{u} - \boldsymbol{u}_h \tag{4.27}$$

$$\boldsymbol{e}_\sigma = \boldsymbol{\sigma} - \boldsymbol{\sigma}_h \tag{4.28}$$

and

$$\boldsymbol{r} = \mathcal{S}^T\boldsymbol{\sigma}_h + \boldsymbol{b} \tag{4.29}$$

$$\boldsymbol{r}_t = \boldsymbol{n}\boldsymbol{\sigma}_h - \check{\boldsymbol{t}} \tag{4.30}$$

The first kind is the *interpolation error* and is given by Eqs. (4.27) and (4.28) and the second kind is the *residual error* and is given by Eqs. (4.29) and (4.30). These error definitions may be stated in a general form by considering a response quantity with exact solution (Γ) which has an approximate solution (Γ_h), then

$$\mathcal{E}_\Gamma = \Gamma - \Gamma_h \tag{4.31}$$

$$\mathcal{R}_\Gamma = \mathcal{F}(\Gamma_h) \tag{4.32}$$

where $\mathcal{E}_\Gamma$ and $\mathcal{R}_\Gamma$ are the respective interpolation and residual error estimators for the response quantity Γ.

For the residual error estimators, it is difficult to suggest a pragmatic form for the functional $\mathcal{F}$. The original contributions in this type of error estimators are attributed to Babuška and Reinboldt [10] [11].

For the interpolation error estimators, the main difficulty in their calculation stems from the fact that no exact solution of the considered problem is available. However, one technique commonly used to overcome such obstacle is to replace the exact solution Γ by a recovered solution $\bar{\Gamma}$ obtained by *interpolation* from the approximate solution Γ_h. The recovered solution $\bar{\Gamma}$ is a smooth field obtained, for example, by nodal averaging (see the technique of Hinton and Campbell [69] and the survey paper by Krizek and Neittaanmakior [88]) or by a projection process which satisfies

$$\int_{\Omega} \Pi \left(\bar{\Gamma} - \Gamma_h \right) d\Omega = 0 \tag{4.33}$$

where some possible choices for the projection matrix Π are listed in references [169] and [170]. Strouboulis and Haque [155], among others, have demonstrated that the error estimates obtained from projection methods may deviate from the true error.

Another approach to obtain recovered solution has recently been published by Zienkiewicz and Zhu [172] and termed the Superconvergent Patch Recovery (SPR). The error estimator obtained from this technique not only converges to the true error but also achieves a convergence rate of $\mathcal{O}(h^4)$ for stresses at the interior nodes of quadratic finite elements, compared to the standard $\mathcal{O}(h^2)$ where h refers to the finite element size. A criticism to the new Zienkiewicz and Zhu [172] [173] error estimator was given by Wiberg and Abdulwahab [165]. They pointed out that, in general, equilibrium is violated, especially at the boundary patches, and they proposed a modification of the original method to add the square of the residuals of the equilibrium equation and natural boundary conditions to the Zienkiewicz-Zhu recovery. In this way equilibrium is enforced. This modification is also reported by Blacker and Belytschko [25]. The original technique by Zienkiewicz and Zhu [172] is adopted in the present study and is explained with extension to nonlinear problems in connection to smeared cracking. The sophistication suggested by Wiberg and Abdulwahab [165] and Blacker and Belytschko [25] is not included in the current implementation of the method.

4.3.3 Modified superconvergent patch recovery

Considering an interpolation error estimator of the form given by Eq. (4.31), one obtains the approximation

$$\bar{\mathcal{E}}_{\Gamma} = \bar{\Gamma} - \Gamma_h \tag{4.34}$$

where the overbar indicates a recovered solution or a quantity based on the recovered solution rather than the exact one. In the present study, the recovered solution is obtained using the SPR [172].

In nonlinear problems, the choice of the response quantity (Γ) in Eq. (4.31) should reflect the sources of material and/or geometrical nonlinearities. Once a reliable error estimator

is established and computed during the nonlinear solution, continuous adaptation of the finite element mesh may be performed to reduce such errors. This adaptation must be accompanied by a means to transfer the state variables (*e.g.* displacements, stresses, strains, damage, ... etc.) from the old mesh to the new (adapted) one.

A new type of error estimator, based on the SPR technique, is proposed here. The standard $\mathcal{L}_2$ norm estimate established for linear elliptic problems will be specialized for a particular response quantity which is naturally related to the accumulation of damage due to distributed (smeared) fracture. For physical reasons, the apparent fracture energy (g^t), defined in Section 4.2, is selected as the required response quantity for the discretization error estimation, *i.e.*

$$\|\mathcal{E}_g\|^2_{e,t} = \int_{\Omega_e} (\mathcal{E}_{g^t})^T (\mathcal{E}_{g^t})\, d\Omega_e \qquad \text{with} \qquad \mathcal{E}_{g^t} = \bar{g}^t - g^t_h \tag{4.35}$$

where $\|\mathcal{E}_g\|_{e,t}$ is the $\mathcal{L}_2$ norm of the local error in the apparent fracture energy at a load level t for a finite element e, $\bar{g}^t$ and g^t_h are the respective recovered and approximate finite element solutions for the apparent fracture energy at the load level t. The choice of g^t as the response parameter implies that the error estimator remains zero until cracking starts. To assess the quality of the mesh before the onset of damage, the energy norm is used rather than the $\mathcal{L}_2$ norm of the apparent fracture energy. This energy norm is given by

$$\|\mathcal{E}_E\|^2_{e,0} = \int_{\Omega_e} (\mathcal{E}_{\boldsymbol{\epsilon}})^T (\mathcal{E}_{\boldsymbol{\sigma}})\, d\Omega_e \quad \text{with} \quad \mathcal{E}_{\boldsymbol{\sigma}} = \bar{\boldsymbol{\sigma}} - \boldsymbol{\sigma}_h \;\&\; \mathcal{E}_{\boldsymbol{\epsilon}} = \bar{\boldsymbol{\epsilon}} - \boldsymbol{\epsilon}_h \tag{4.36}$$

where the load level t is given the value 0 to refer to the initial state, *i.e.* the state before cracking. In regions of damaged finite elements due to fracturing, the error estimator of Eqs. (4.35) governs the adaptive process, while for the rest of the finite element mesh, the error estimator of Eqs. (4.36) must be considered.

Approximating the response quantity Γ, which stands for g^t, σ or ϵ, with a *polynomial expansion*, one obtains

$$\bar{\Gamma} = \boldsymbol{\mathcal{P}}\boldsymbol{a} \tag{4.37}$$

where $\boldsymbol{\mathcal{P}}$ contains the appropriate polynomial terms and $\boldsymbol{a}$ is a set of unknown parameters. For two dimensional problems and bilinear finite elements (4-noded isoparametric elements), the following approximation is recommended [172]

$$\boldsymbol{\mathcal{P}} = [1 \; x \; y \; xy] \tag{4.38}$$

$$\boldsymbol{a} = [a_0 \; a_1 \; a_2 \; a_3]^T \tag{4.39}$$

The unknown coefficients $\boldsymbol{a}$ can be obtained through a *least square fit* of the polynomial expansion given by Eq. (4.37) to the values of $\bar{\Gamma}$ obtained from the finite element solution

at the *sampling points* (Γ_h) (see Figure 4-1(a)). The finite element solution (*e.g.* stresses, strains or a combination of them such as the fracture energy release density) at these sampling points is known to be the most accurate (*i.e.* superconvergent upon enhancing the interpolation or the discretization). Instead of applying the least square fit to the whole domain of the problem (*global fit*), Zienkiewicz and Zhu [172] suggested the use of small *patches* of elements to perform *local* least square fit. This method of least square fitting, in its global and local forms, was originally proposed by Hinton and Campbell [69] to smooth the obtained stress field from the displacement finite element solution.

Consider a patch of finite elements containing n sampling points as illustrated by Figure 4-1(a), in which $n = 16$. For a generic sampling point i in this patch, let $(x_i,\ y_i)$ be the Cartesian coordinates in the global axes. Therefore, the least square problem reduces to the minimization of the following functional

$$\mathcal{F} = \sum_{i=1}^{n} \left(\Gamma_h(x_i, y_i) - \bar{\Gamma}(x_i, y_i)\right)^2 \tag{4.40}$$

Upon substitution of Eq. (4.37) in Eq. (4.40), one obtains

$$\mathcal{F} = \sum_{i=1}^{n} \left(\Gamma_h(x_i, y_i) - \boldsymbol{\mathcal{P}}(x_i, y_i)\boldsymbol{a}\right)^2 \tag{4.41}$$

To solve this minimization problem, one needs to set $\partial\mathcal{F}/\partial\boldsymbol{a} = 0$, *i.e.*

$$\frac{\partial \mathcal{F}}{\partial \boldsymbol{a}} = -2\sum_{i=1}^{n} \boldsymbol{\mathcal{P}}^T(x_i, y_i)\left(\Gamma_h(x_i, y_i) - \boldsymbol{\mathcal{P}}(x_i, y_i)\boldsymbol{a}\right) = 0 \tag{4.42}$$

Therefore,

$$\sum_{i=1}^{n} \boldsymbol{\mathcal{P}}^T(x_i, y_i)\boldsymbol{\mathcal{P}}(x_i, y_i)\boldsymbol{a} = \sum_{i=1}^{n} \boldsymbol{\mathcal{P}}^T(x_i, y_i)\Gamma_h(x_i, y_i) \tag{4.43}$$

which can be rewritten as

$$\boldsymbol{A}\boldsymbol{a} = \boldsymbol{b} \tag{4.44}$$

where

$$\boldsymbol{A} = \sum_{i=1}^{n} \boldsymbol{\mathcal{P}}^T(x_i, y_i)\boldsymbol{\mathcal{P}}(x_i, y_i) \quad \text{and} \quad \boldsymbol{b} = \sum_{i=1}^{n} \boldsymbol{\mathcal{P}}^T(x_i, y_i)\Gamma_h(x_i, y_i) \tag{4.45}$$

Since n is a relatively small number compared to the actual problem size, the set of simultaneous equations given by (4.44) can be easily solved for the unknown vector $\boldsymbol{a}$.

4.3.4 Identification of patches

The minimization of the functional given by Eq. (4.40) is performed over patches of finite elements. In a general finite element mesh, there exist several forms of these patches. The identification of each of these forms is an important step in the error estimation algorithm. Three basic forms of patches are identified in Figure 4-3 which shows the patch assembly nodes and the nodes at which the recovered solution is calculated.

To identify the different patches in the finite element mesh, the following two steps are adopted [162]:

- **Global identification** where the number of occurrences of each node in the finite elements of the whole mesh is determined.

- **Local identification** where the number of occurrences of each node in the finite elements of the current patch is determined.

The previous two-step procedure is sufficient to uniquely identify the patches and the corresponding nodes at which the recovered solution is calculated using the SPR. In this process, nodes may be common to several patches. In these cases, an averaging technique of the recovered solutions from different patches at the same node is considered. Exterior and corner patches may be found at the boundary of the analyzed domain or at the interface between two different materials. In the latter case, smoothing should not be adopted as it is not permissible [174]. Therefore, each side of the material interface is treated separately. This situation is encountered at the interface between the steel frame and the masonry infill walls of the example considered later. This situation mandates some caution in generating the interface elements along such planes of displacement discontinuity. A simple procedure is adopted herein to force the same number of finite elements on both sides of the interface by using the larger of element numbers on both sides.

4.3.5 Adaptivity

Once a local error estimator is established, the level of accuracy of the finite element solution is assessed. An improvement of the solution may be performed using one of the following available techniques:

1. h-method (*e.g.* [113]): refines the finite element model by introducing more elements into the mesh.

2. p-method (*e.g.* [12]): increases the order of interpolating polynomials while keeping the element topology unchanged.

3. h/p-method (*e.g.* [13]): which is a combination of the h-method and the p-method.

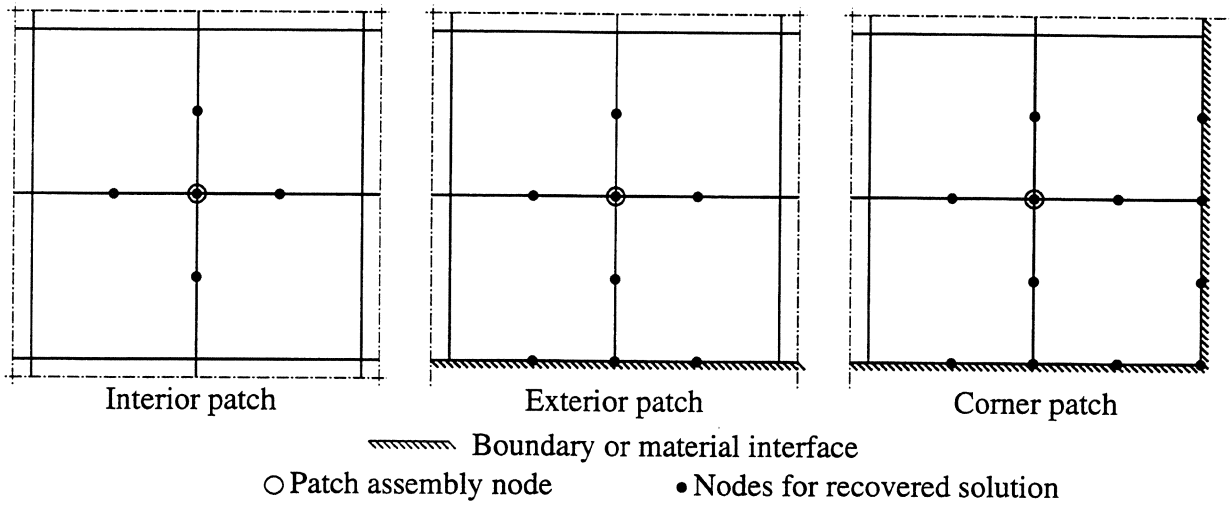

FIGURE 4-3 Different patches for the SPR method.

4. r-method (*e.g.* [41]): relocates the nodal points in a given mesh while keeping the number of degrees of freedom fixed.

5. s-method (*e.g.* [57]): increases the numerical resolution by superimposing meshes rather than by changing them.

In the present study, only the h-method is considered. Two techniques may be used in approaching the corrected element size, namely

- Mesh enrichment (or local mesh refinement).

- Mesh regeneration.

The two approaches have been evaluated and compared using quadrilateral elements by Zhu *et al.* [168]. In the present study, a simple version of the mesh enrichment is implemented. An important characteristic of this technique is that the previous mesh is embedded in the new (adapted) one during the loading process. This feature facilitates the job of the transfer operator to map the older solution into the newer mesh. The adopted mesh enrichment technique is based on the methodologies presented by Zienkiewicz and Zhu [169] and Krishnamoorthy and Umesh [87] which are generalized herein for nonlinear incremental finite element solution.

Define a *global* error estimator at load level t as

$$\|\mathcal{E}\|_t^2 = \sum_{i=1}^{m} \|\mathcal{E}\|_{i,t}^2 \tag{4.46}$$

where the subscript i represents the contribution of element number i in the finite element mesh which has m elements. The local error norm $\|\mathcal{E}\|_{i,t}$ is based on either g^t or $\boldsymbol{\sigma}$ (energy

norm) depending on the load level t and determined by either Eqs. (4.35) or Eqs. (4.36). The *absolute* global error norm determined by Eq. (4.46) has little advantage. On the contrary, the following *relative* global error is more advantageous

$$\eta_t = \left(\frac{\|\mathcal{E}\|_t^2}{\|\mathcal{U}\|_t^2 + \|\mathcal{E}\|_t^2} \right)^{1/2} \tag{4.47}$$

where $\|\mathcal{U}\|_t$ is a reference norm obtained from the finite element solution. For $t = 0$, *i.e.* before cracking, it is chosen as twice the strain energy, accordingly

$$\|\mathcal{U}\|_0 = \left(\sum_{i=1}^{m} \left(\int_{\Omega_i} \boldsymbol{\epsilon_t}^T \boldsymbol{\sigma_t} \, d\Omega_i \right) \right)^{1/2} \tag{4.48}$$

After cracking, the $\mathcal{L}_2$ norm of the apparent fracture energy is used as the reference quantity to calculate the relative global error norm, *i.e.*

$$\|\mathcal{U}\|_t = \left(\sum_{i=1}^{m} \left(\int_{\Omega_i} \left(g^t\right)^T \left(g^t\right) \, d\Omega_i \right) \right)^{1/2} \tag{4.49}$$

For a particular finite element e, the *local* relative error is obtained from Eq. (4.47) as follows

$$\eta_{e,t} = \left(\frac{\|\mathcal{E}\|_{e,t}^2}{\|\mathcal{U}\|_t^2 + \|\mathcal{E}\|_t^2} \right)^{1/2} \tag{4.50}$$

A common requirement of an adaptive procedure is to keep the relative global error below an acceptable small value, *i.e.*

$$\eta_t \leq \eta_{max} \tag{4.51}$$

where η_{max} is the maximum permissible error at any load level t.

For linear elliptic problems, an *optimal mesh* is commonly assumed to be the mesh in which some quantity be constant over certain regions [42]. Mesh optimality criterion based on the equal distribution of the discretization error was recently investigated by Oñate and Bugeda [125]. Accordingly, for a mesh with m elements, the optimality condition may be stated as follows

$$\eta_{e,t}^2 \leq \frac{\eta_{max}^2}{m} \tag{4.52}$$

It should be noted that only the square of the error norm is additive as demonstrated by Eq. (4.46). Therefore, the quantity to be equidistributed over the elements is the square of the relative error as shown in Eq. (4.52).

Defining e_m as the maximum permissible error at any load level t and for a finite element e, one obtains a local error parameter $\xi_{e,t}$ and conditions of mesh refinement as follows

$$\xi_{e,t} = \frac{\|\mathcal{E}\|_{e,t}}{e_m} \begin{cases} > 1 \Longrightarrow & \text{refine mesh} \\ = 1 \Longrightarrow & \text{optimum mesh} \\ < 1 \Longrightarrow & \text{coarsen mesh} \end{cases} \tag{4.53}$$

Using Eq. (4.50) and the inequality (4.52)

$$e_m = \eta_{max} \left(\frac{\|\mathcal{U}\|_t^2 + \|\mathcal{E}\|_t^2}{m} \right)^{1/2} \tag{4.54}$$

In Eq. (4.53), the condition for coarsening implies that in some regions of the mesh, coarser subdivisions are permitted. This situation is not considered in the present study. For the condition that necessitates the refinement of the mesh, a certain rate of convergence is assumed. In general, a rate of convergence of the error is assumed to be $\mathcal{O}(h^p)$ where h is a generic element size in the area covered by the finite elements which are of order p. Considering h_i and h_f to be the initial and final element sizes, respectively, one may write

$$h_f = \frac{h_i}{\xi_i^{1/p}} \tag{4.55}$$

The implementation of this criterion to calculate the required element size is followed by subsequent execution of either mesh regeneration or mesh enrichment algorithms. For simplicity, the subscripts t and e have been dropped from some of the previous equations. These subscripts should be understood from the context.

4.3.6 Mesh enrichment

In the present study, a simple routine for mesh enrichment is considered. The idea is based on the definition of the so-called Refinement Level (RL) as shown in Figure 4-4. This idea is suggested by Krishnamoorthy and Umesh [87]. From Figure 4-4, an expression relating the final element size h_f to the refinement level RL can be written as follows

$$h_f = \frac{h_i}{2^{RL}} \tag{4.56}$$

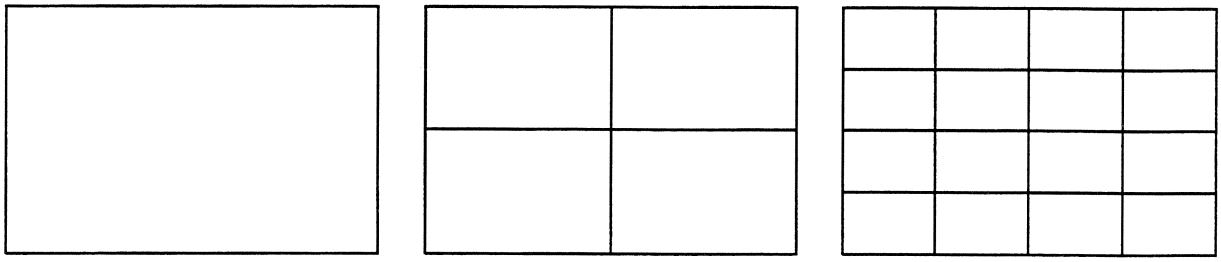

FIGURE 4-4 Refinement level used in the adaptivity procedure.

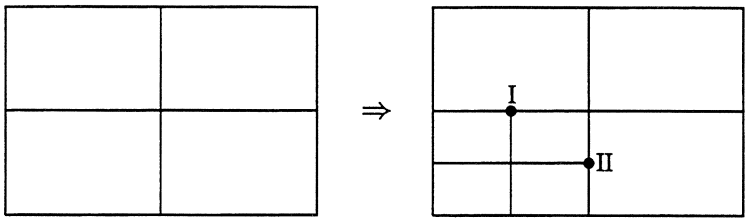

FIGURE 4-5 Identification of constraint nodes during mesh enrichment.

From Eqs. (4.55) and (4.56), RL is given by

$$RL = \frac{1}{p}\frac{\log \xi_i}{\log 2} \qquad \text{For } \xi_i > 1 \tag{4.57}$$

$$= 0 \qquad \text{For } \xi_i \leq 1 \tag{4.58}$$

The second condition, *i.e.* Eq. (4.58), is enforced because coarsening is not considered (*cf.* with Eq. (4.53)).

Two important issues related to the considered mesh enrichment technique should be emphasized. First, when only a few elements in a regular mesh[8] are refined adaptively, nodal constraints must be introduced on the boundary between the refined elements and their adjacent unrefined elements. Once these boundary nodes are identified (see nodes I and II in Figure 4-5), the required constraints are easily enforced using the TYINGS[9] of the used finite element program DIANA. Second, if two adjacent elements have large difference between their corresponding refinement levels (> 1), then smooth gradation of the mesh will *not* be achieved. To overcome such an undesirable situation, the so-called "One-level-rule"

[8]Regular meshes are those having no constraint nodes.

[9]TYINGS are user specified linear *dependencies* between degrees of freedom of the system of equations.

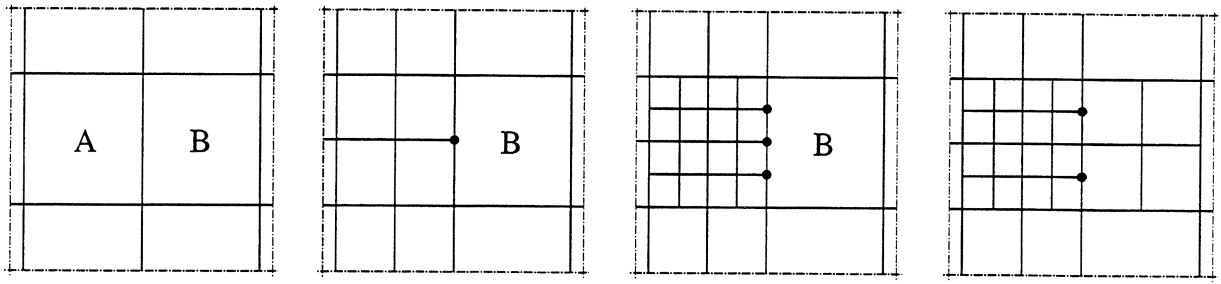

(a) RL(A) = 0, RL(B) = 0 (b) RL(A) = 1, RL(B) = 0 (c) RL(A) = 2, RL(B) = 0 (d) RL(A) = 2, RL(B) = 1

FIGURE 4-6 One-level-rule.

is enforced. This rule is suggested by Carey *et al.* [30] and states that the difference between the refinement levels of two adjacent elements should be ≤ 1. This rule is illustrated in Figure 4-6 for the case of 4-noded quadrilateral elements. In Figures 4-6(a), 4-6(b) and 4-6(d), the rule is satisfied while in Figure 4-6(c) a violation of this rule is obvious. Therefore case (c) in Figure 4-6 mush be changed to obtain case (d) by enforcing the One-level-rule.

4.3.7 Numerical results

The adaptive strategy discussed in the previous sections is applied for the problem of a steel frame infilled with masonry walls. As mentioned earlier, the present investigation lacks the inclusion of an appropriate transfer operator to continuously map the state variables from one mesh to the other. To obtain logical meshes from the adaptive technique of this nonlinear problem where nonlinearities are not only due to wall cracking but also due to frame/wall interface conditions, the error estimator for each element is calculated from Eqs. (4.35) and (4.36). The larger of the two is considered in the refinement process. This conservative choice is essential to capture both the stress concentration at the contact between the frame members and the infill wall, and the strain localization due to smeared cracking in the walls. It may be observed from the numerical results that the error estimator based on the fracture energy release always controls once cracking occurs.

The finite element model of the infilled steel frame considers smeared cracking of homogenized masonry and also the frame/wall interface conditions. The model was described in **SECTIONS 2** and **3**. Figure 4-7 shows the deformed shape obtained from the finite element solution and the corresponding adapted meshes before cracking of infill walls. The results indicate the interaction between the frame and the infill walls in the form of contact length and wall/frame separation. The adapted mesh indicates the need for refinements in regions of stress concentrations at the corners where the wall is contacting the frame members.

After cracking, the adaptive procedure requires additional regions of mesh refinement due to material damage introduced by the smeared cracks. The crack patterns and the corre-

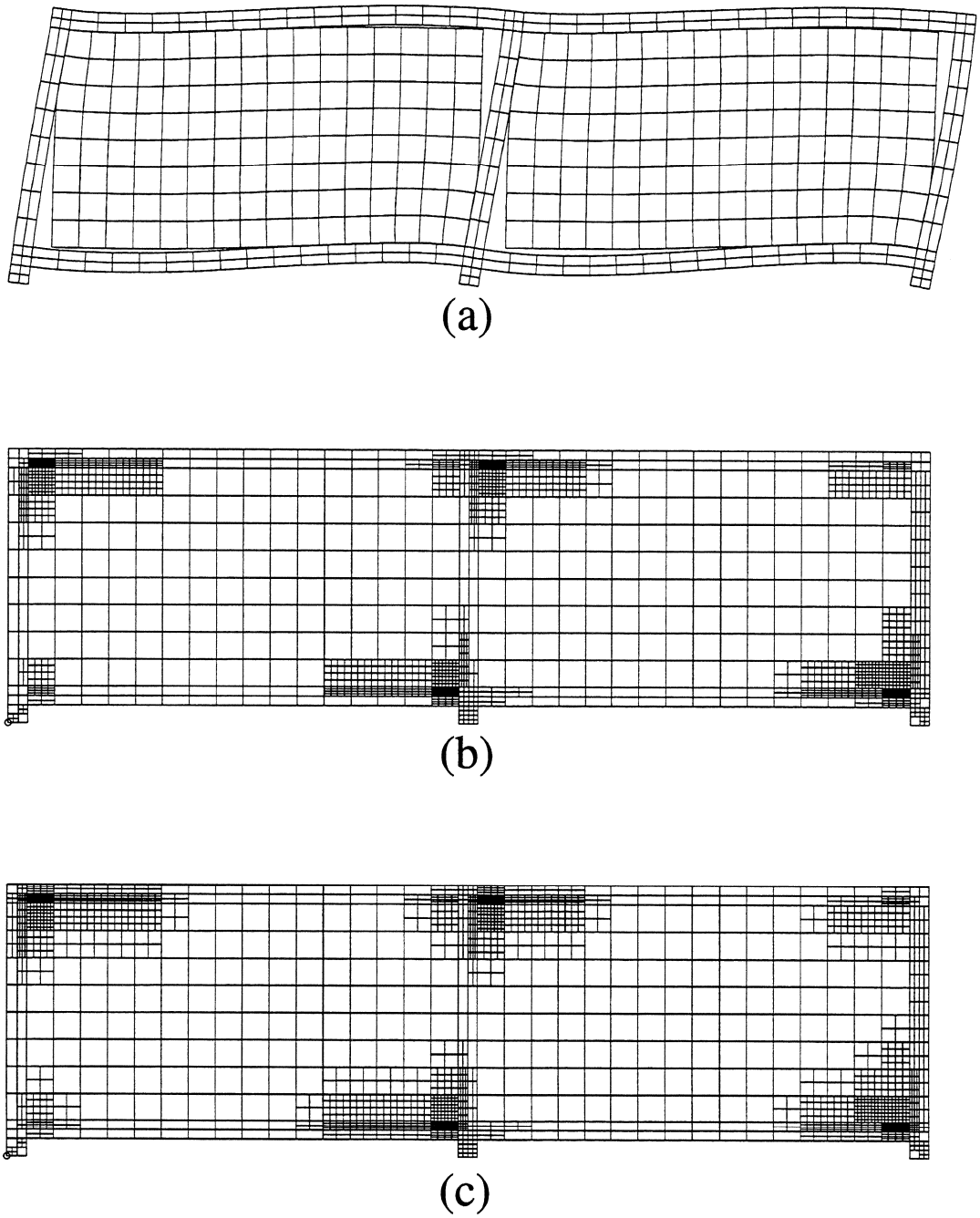

FIGURE 4-7 Results of the adaptive procedure before wall cracking; (a) Deformed shape; (b) Adapted mesh without the One-level-rule; (c) Adapted mesh enforcing the One-level-rule.

sponding adapted finite element meshes are shown in Figure 4-8. In Figures 4-7 and 4-8, the adapted meshes are shown before and after enforcing the One-level-rule. It is useful to show the adapted meshes before enforcing the One-level-rule because the physical reasons (*i.e.* stress concentration and/or cracking) dictating the need for mesh adaptation are more obvious in that case.

4.4 Evolutionary Characteristic Length Method For Smeared Cracking

The smeared cracking formulation with softening involves the introduction of the *crack band width* (Λ). Traditionally, this characteristic length has been determined using *ad hoc* rules. A systematic procedure to determine the evolution of Λ during the nonlinear finite element analysis is presented in this section. This procedure is based on the idea of nonlocal continuum which relies on spatial averaging of tensor (*e.g.* strains, stresses or inelastic strain) or scalar (*e.g.* fracture energy density or damage measures) state variables in a certain neighbourhood of a given point (for more details, see references [53], [21], or [127]). The required nonlocal forms for the apparent fracture energy density and the crack strains are obtained by means of a special SPR procedure, which makes the computations accurate and efficient for practical applications.

4.4.1 Nonlocal apparent fracture energy and systematic evaluation of Λ

The nonlocal continuum is an approach in which at least some variables are defined by *spatial averaging* [22]. Here, the *apparent fracture energy density* g^t (see Figure 4-2) is first established on the local level, *i.e.* in terms of the pointwise strains and crack band widths. Then, this form is generalized to give a nonlocal expression for g^t, which is designated by $\bar{g}^t$, in terms of nonlocal quantities which are the spatial averaging (smoothing) of their equivalent local ones. The smoothing process, required to obtain the spatially averaged quantities, is similar to the SPR technique explained in the previous section. The new features of this recovery procedure are outlined in the next section.

After simplification and assuming elastic unloading as shown in Figure 4-2, Eqs. (4.19) and (4.23) lead to

$$g^t = f_t \left(\epsilon_{cr}^t - \frac{1}{k+1} \left(\frac{k f_t}{(k+1)\mathcal{G}_f} \right)^k \sum_{i=1}^{n_t} \left[\Delta_i^k \left(\epsilon_{cr} \right) \left(\Lambda_i \right)^k \right] \right) \tag{4.59}$$

where n_t is the number of load increments up to the load level t, Λ_i is the constant crack

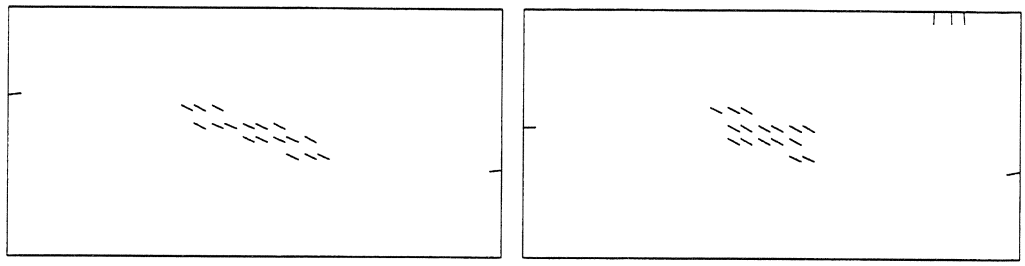

(a)

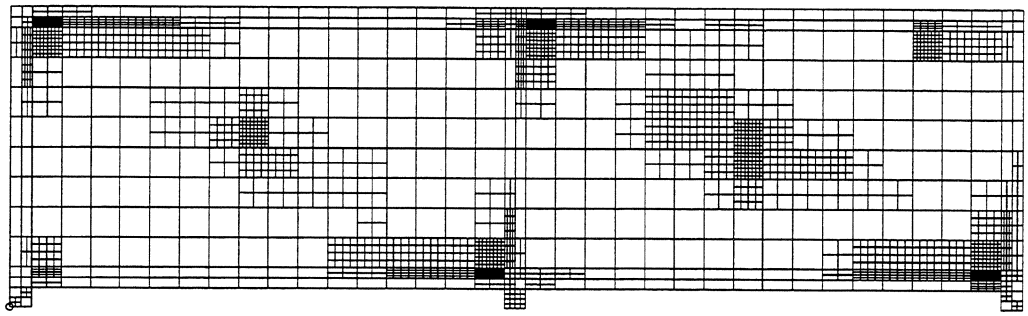

(b)

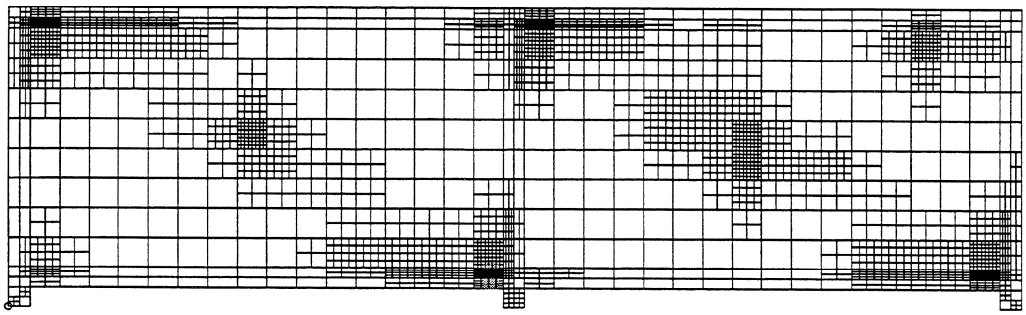

(c)

FIGURE 4-8 Results of the adaptive procedure after wall cracking; (a) Crack pattern; (b) Adapted mesh without the One-level-rule; (c) Adapted mesh enforcing the One-level-rule.

band width during the load increment number i, and the operator Δ_i^k is defined as

$$\Delta_i^k(\bullet) = \left(\bullet^i\right)^{k+1} - \left(\bullet^{i-1}\right)^{k+1} \tag{4.60}$$

Equation (4.59) gives the local form of the *apparent fracture energy density* and may be rewritten in a simpler form by using the following substitution

$$\mathcal{C} = \frac{1}{k+1}\left(\frac{k f_t}{(k+1)\mathcal{G}_f}\right)^k \tag{4.61}$$

where $\mathcal{C}$ is a material constant with $[(\text{length})^{-k}]$ dimension. Therefore, Eq. (4.59) becomes

$$g^t = f_t\left(\epsilon_{cr}^t - \mathcal{C}\sum_{i=1}^{n_t}\left[\Delta_i^k\left(\epsilon_{cr}\right)\left(\Lambda_i\right)^k\right]\right) \tag{4.62}$$

The nonlocal form of the apparent fracture energy density ($\bar{g}^t$) is defined by an expression similar to Eq. (4.62), but expressed in terms of the nonlocal crack strain ($\bar{\epsilon}_{cr}$) and a nonlocal form of the crack band width ($\bar{\Lambda}$). This definition is given by

$$\bar{g}^t \equiv f_t\left(\bar{\epsilon}_{cr}^t - \mathcal{C}\sum_{i=1}^{n_t}\left[\overline{\Delta_i^k\left(\epsilon_{cr}\right)}\left(\bar{\Lambda}_i\right)^k\right]\right) \tag{4.63}$$

Subtracting Eq. (4.62) from Eq. (4.63), one obtains

$$\mathcal{E}_g = f_t\left(\mathcal{E}_{\epsilon_{cr}} - \mathcal{C}\sum_{i=1}^{n_t}\left[\overline{\Delta_i^k\left(\epsilon_{cr}\right)}\left(\bar{\Lambda}_i\right)^k - \Delta_i^k\left(\epsilon_{cr}\right)\left(\Lambda_i\right)^k\right]\right) \tag{4.64}$$

where

$$\mathcal{E}_g = \bar{g}^t - g^t \quad \text{and} \quad \mathcal{E}_{\epsilon_{cr}} = \bar{\epsilon}_{cr}^t - \epsilon_{cr}^t \tag{4.65}$$

are measures of the *local errors* (see Section 4.3.2) for the apparent fracture energy density and the crack strain, respectively. From Eq. (4.64), an expression for the *nonlocal crack band width* after n_t load increments, *i.e.* for the new load level $(t+1)$, is readily obtained as

$$\left(\bar{\Lambda}_{t+1}\right)^k = \left(\frac{\mathcal{E}_{\epsilon_{cr}} - \mathcal{E}_g/f_t}{\mathcal{C}} - \sum_{i=1}^{t_{n-1}}\left[\overline{\Delta_i^k\left(\epsilon_{cr}\right)}\left(\bar{\Lambda}_i\right)^k\right] + \sum_{i=1}^{n_t}\left[\Delta_i^k\left(\epsilon_{cr}\right)\left(\Lambda_i\right)^k\right]\right) \Big/ \overline{\Delta_{n_t}^k\left(\epsilon_{cr}\right)} \tag{4.66}$$

which is the evolution equation for the crack band width.

Regarding the application of the evolution equation of the crack band width, the following remarks can be made:

- Continuous adaptation of Λ is performed at the sampling points level, *i.e.* Λ is varied from one Gauss point to the other even within the same finite element.

- Only cracks in the evolving status, *i.e.* cracks where crack strains are located on the descending branch of the stress-crack strain relation, should have their crack band width adapted.

- Fully developed cracks, *i.e.* cracks with their crack strain beyond the descending branch of the stress-crack strain relation, have their crack band width kept constant and equal to the last value reached before the crack became fully developed.

- For numerical stability of the application of Eq. (4.66), the terms $\overline{\Delta_i^k(\epsilon_{cr})}$ should be calculated by first operating on the finite element solution ϵ_{cr} with the operator Δ_i^k (see its definition in Eq. (4.60)) and then smoothing the result using the SPR.

- The physical implication of the continuous adaptation of the crack band width is that the softening branch of the stress-crack strain curve is continuously adjusted to satisfy the definition given by Eq. (4.63).

- The application of the evolution equation of Λ is conducted in a predictor without corrector scheme. Expressing this evolution equation in terms of the local error quantities given by Eqs. (4.65) avoids continuous drift from the constitutive model. In other words, any violation of the constitutive model at a particular load level, *i.e.* violation of the equality in Eq. (4.62), will be corrected for in the next load increment.

4.4.2 Convergence property

Equation (4.66) is convergent upon successive mesh refinement, and, in the limit of mesh refinement, leads to the following relationship

$$\Lambda_{t+1} = \Lambda_t \tag{4.67}$$

This is shown next.

In the limit of mesh refinement, $h \to 0$, where h refers to the element size. Thus,

$$\mathcal{E}_g \to 0 \quad \text{and} \quad \mathcal{E}_{\epsilon_{cr}} \to 0$$

From the error definitions in Eq. (4.65), the above expressions imply that in the limit of mesh refinement

$$\bar{g}^t = g^t \quad \text{and} \quad \bar{\epsilon}_{cr}^t = \epsilon_{cr}^t$$

respectively. Using this information in Eq. (4.66), one obtains

$$\left(\bar{\Lambda}_{t+1}\right)^k = \left(0 - \sum_{i=1}^{t_{n-1}} \left[\overline{\Delta_i^k\left(\epsilon_{cr}\right)}\left(\bar{\Lambda}_i\right)^k\right] + \sum_{i=1}^{n_t}\left[\Delta_i^k\left(\epsilon_{cr}\right)\left(\Lambda_i\right)^k\right]\right) \Big/ \overline{\Delta_{n_t}^k\left(\epsilon_{cr}\right)} \tag{4.68}$$

Since, in the limit, the nonlocal quantities approach the local ones, the right hand side of Eq. (4.68) becomes Λ_t. Thus, Eq. (4.67) is readily obtained, which is the announced result.

4.4.3 Simplified forms for the evolution equation

Two simplified forms for the evolution equation of the characteristic length are given here. These forms are directly derived from Eq. (4.66). Although the alternative equations are less accurate, they are simpler to implement and computationally less intensive than the full equation (4.66).

1st. Simplified Form: Assuming $\Delta_i^k\left(\epsilon_{cr}\right) \approx \overline{\Delta_{i-1}^k\left(\epsilon_{cr}\right)}$ and setting $\Lambda_t = \bar{\Lambda}_{t-1}$, one obtains the following simplified form for the evolution of the characteristic length

$$\left(\bar{\Lambda}_{t+1}\right)^k = \left(\frac{\mathcal{E}_{\epsilon_{cr}} - \mathcal{E}_g/f_t}{\mathcal{C}} + \Delta_1^k\left(\epsilon_{cr}\right)\left(\Lambda_1\right)^k\right) \Big/ \overline{\Delta_{n_t}^k\left(\epsilon_{cr}\right)} \tag{4.69}$$

This equation has been used by Mosalam and Paulino [117]; therefore, results reported in this reference will not be repeated here. All results reported herein are based on the complete form given by Eq. (4.66).

2nd. Simplified Form: Note that, in Eq. (4.69), $\Delta_1^k\left(\epsilon_{cr}\right) = \left(\epsilon_{cr}^1\right)^{k+1}$, which comes from the fact that the counter i in Eq. (4.60) starts at the onset of cracking. Taking into account the fact that $\left(\epsilon_{cr}^1\right)^{k+1} \approx 0$, and substituting this approximation into Eq. (4.69), one obtains

$$\left(\bar{\Lambda}_{t+1}\right)^k = \frac{\mathcal{E}_{\epsilon_{cr}} - \mathcal{E}_g/f_t}{\mathcal{C}\,\overline{\Delta_{n_t}^k\left(\epsilon_{cr}\right)}} \tag{4.70}$$

which is a further simplification of Eq. 4.66.

4.4.4 Nonlocal forms and superconvergent patch recoveries

The nonlocal forms for the apparent fracture energy density, the crack strain and the incremental crack strain, denoted by $\bar{g}^t$, $\bar{\epsilon}^t_{cr}$ and $\overline{\Delta^k_i(\epsilon_{cr})}$, respectively, are obtained from spatial averaging of their local forms. For simplicity of notation, in the following equations, the subscript *cr* is dropped. To obtain these nonlocal forms, a special form of the previously discussed SPR technique is employed.

The fields $\bar{g}^t$, $\bar{\epsilon}^t$ and $\overline{\Delta^k_i(\epsilon)}$ can be approximated by the *polynomial expansions*

$$\bar{g}^t = \boldsymbol{\mathcal{P}}\boldsymbol{a}\,, \quad \bar{\epsilon}^t = \boldsymbol{\mathcal{P}}\boldsymbol{c} \quad \text{and} \quad \overline{\Delta^k_i(\epsilon)} = \boldsymbol{\mathcal{P}}\boldsymbol{e} \tag{4.71}$$

where $\boldsymbol{\mathcal{P}}$ contains the appropriate polynomial terms, and $\boldsymbol{a}$, $\boldsymbol{c}$ and $\boldsymbol{e}$ are sets of unknown parameters (see Section 4.3.3). In the present SPR technique, the unknown coefficients $\boldsymbol{a}$, $\boldsymbol{c}$ and $\boldsymbol{e}$ can be obtained through *weighted least square fitting* of the *polynomial expansions* (4.71) to the respective values of g^t, ϵ^t and $\Delta^k_i(\epsilon)$ obtained from the finite element solution at the sampling points, *i.e.* g^t_h, ϵ^t_h and $\Delta^k_i(\epsilon_h)$ as in Section 4.3.3. However, a weighting parameter (w_i) is added to emphasize the relative importance of the sampling points which are closer to the patch assembly node (see Figure 4-1(a)). Thus,

$$\mathrm{w}_i = 1/\rho_i^p \tag{4.72}$$

where ρ_i is the Euclidean distance between the sampling point i and the patch assembly node, and p is an integer. In practical applications, p is generally in the range from 0 to 4. The case $p = 0$ corresponds to the original SPR (with uniform weighting). Thus, the weighted least square problem reduces to the minimization of the following functionals (refer to Section 4.3.3 for definitions of terms and relevant discussions)

$$\begin{aligned}
\mathcal{F} &= \sum_{i=1}^{n} \mathrm{w}_i^2 \left[\bar{g}^t(x_i, y_i) - g^t_h(x_i, y_i)\right]^2 \\
\mathcal{H} &= \sum_{i=1}^{n} \mathrm{w}_i^2 \left[\bar{\epsilon}^t(x_i, y_i) - \epsilon^t_h(x_i, y_i)\right]^2 \\
\mathcal{Z} &= \sum_{i=1}^{n} \mathrm{w}_i^2 \left[\overline{\Delta^k_i(\epsilon(x_i, y_i))} - \Delta^k_i(\epsilon_h(x_i, y_i))\right]^2
\end{aligned} \tag{4.73}$$

where the terms in square brackets are analogous to those given by Eqs. (4.65). Substituting Eqs. (4.71) into Eqs. (4.73), and solving the minimization problems by setting

$$\partial\mathcal{F}/\partial\boldsymbol{a} = 0\,, \quad \partial\mathcal{H}/\partial\boldsymbol{c} = 0 \quad \text{and} \quad \partial\mathcal{Z}/\partial\boldsymbol{e} = 0 \tag{4.74}$$

one obtains the following sets of linear algebraic equations

$$\boldsymbol{A}\boldsymbol{a} = \boldsymbol{b}\,, \quad \boldsymbol{A}\boldsymbol{c} = \boldsymbol{d} \quad \text{and} \quad \boldsymbol{A}\boldsymbol{e} = \boldsymbol{f} \tag{4.75}$$

where

$$\boldsymbol{A} = \sum_{i=1}^{n} \mathrm{w}_i^2 \, \boldsymbol{\mathcal{P}}^T(x_i, y_i) \, \boldsymbol{\mathcal{P}}(x_i, y_i) \tag{4.76}$$

$$\boldsymbol{b} = \sum_{i=1}^{n} \mathrm{w}_i^2 \, \boldsymbol{\mathcal{P}}^T(x_i, y_i) \, g_h^t(x_i, y_i) \tag{4.77}$$

$$\boldsymbol{d} = \sum_{i=1}^{n} \mathrm{w}_i^2 \, \boldsymbol{\mathcal{P}}^T(x_i, y_i) \, \epsilon_h^t(x_i, y_i) \tag{4.78}$$

$$\boldsymbol{f} = \sum_{i=1}^{n} \mathrm{w}_i^2 \, \boldsymbol{\mathcal{P}}^T(x_i, y_i) \, \Delta_i^k \left(\epsilon_h(x_i, y_i)\right) \tag{4.79}$$

Note that the system matrix $\boldsymbol{A}$ is the same for all the linear systems of Eqs. (4.75). This contributes to the computational efficiency in the calculations of the required nonlocal forms.

4.4.5 Numerical implementation

The method for adapting the crack band width in the smeared cracking model has been implemented in the DIANA system. The main steps for this specific implementation are summarized as follows:

1. Determine the mesh and initialize the material parameters.
2. Compute the finite element solution of ϵ_{cr}^t and $\Delta_i^k\left(\epsilon_{cr}\right)$ at the load level t (*i.e.* the i^{th} increment).
3. Calculate the finite element solution of g^t (Eq. (4.59)) using the history of both, the crack strain (ϵ_{cr}^i) and the corresponding crack band width (Λ_i).
4. Solve the weighted least square minimization problems in the SPR procedure to obtain the fields $\bar{g}^t$, $\bar{\epsilon}_{cr}^t$ and $\overline{\Delta_i^k\left(\epsilon_{cr}\right)}$.
5. Update the crack band width at each sampling point using Eq. (4.66) or either of its simplified forms (Eqs. (4.69) or (4.70)).
6. Continue the incremental iterative solution scheme until the final load step.

4.4.6 Mesh sensitivity study

The results of the finite element analysis with the classical smeared cracking approach, *i.e.* constant Λ, are reported to be dependent on the mesh size and geometry [149]. A simple

example (4-point bending of plain concrete beam with a notch at mid-span) is selected to numerically investigate the effect of mesh size on the finite element results with and without adaptation of Λ. The notch forces the cracks to initiate from its tip and propagate in a narrow band towards the compression zone. Therefore, fracture is localized in the ligament from its onset. The ligament to depth ratio is taken here as 0.7. Making use of symmetry, one half of the beam is analyzed with *ad hoc* boundary conditions. Three meshes are considered to represent Coarse (C), Medium (M) and Fine (F) discretizations. The beam and its discretizations are illustrated in Figure 4-9 together with the material parameters. The dimensions and material parameters are the same as the beams tested by Hordijk [70].

The numerically determined load-deflection relations are shown in Figure 4-10. The standard smeared cracking indicates higher dependency on the mesh size than the smeared cracking with adapted Λ, particularly after peak load. Λ is adapted only while cracks are developing. Once a crack becomes fully developed, *i.e.* the normal stress across the cracks drops to zero, the value of Λ is kept constant. Cracking started at $\Delta = 0.0015$ inch and became fully developed at $\Delta = 0.009$ inch.

The main reason for the notched beam example is to study the distributions of the adapted crack band width along a predefined path of strain localization (*i.e.* within the ligament). The results of such distribution for the three meshes and for different loading levels are shown in Figure 4-11. For comparison between the different meshes, the adapted value of Λ in each mesh is normalized by its initial value Λ_{init} which is determined from

$$\Lambda_{init} = \sqrt{A_e} \tag{4.80}$$

where A_e is the finite element area.

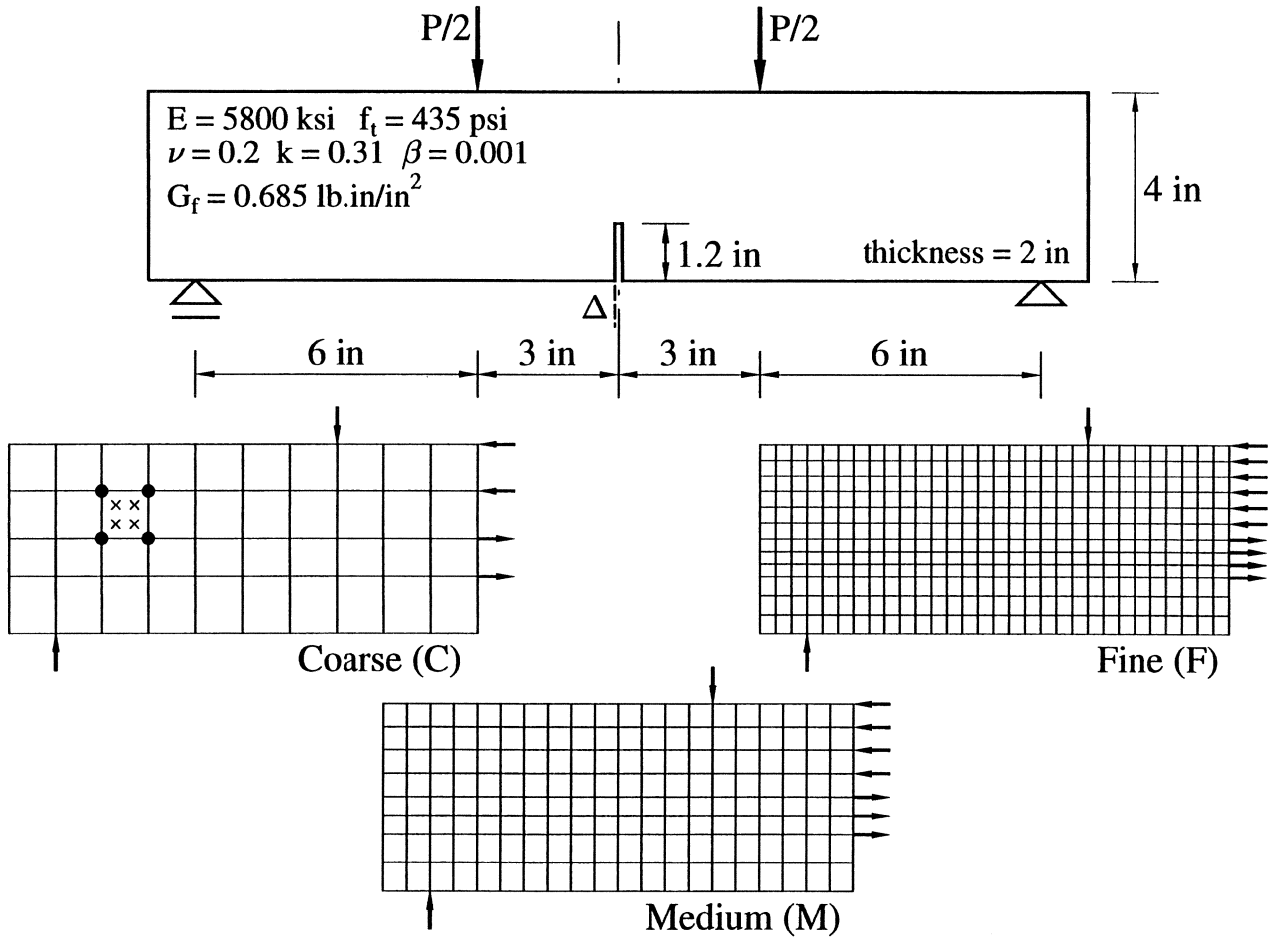

FIGURE 4-9 4-point bending notched plain concrete beam for the study of mesh sensitivity.

The following conclusions may be inferred from Figure 4-11:

1. The coarser the mesh, the larger the change of the crack band width. In this way the use of the adapted crack band width leads to an almost independent solution with respect to the mesh size.

2. The largest change in Λ occurs at the crack tip and moves with the propagation of the crack. Therefore, one may conclude that the effect of increasing damage is reflected on the adaptation of Λ.

3. For finer meshes (mesh "M" or mesh "F"), the damaged region in front of the notch occupies several sampling points. The crack strain, a measure of the material damage, is larger in some points than the others. This fact leads to an oscillatory distribution of Λ about its initial value (Λ_{init}) especially close to the crack tip.

4. Fully developed cracks are those which released all their reserved energy for fracture. At this stage, any adjustment of the crack band width will have no influence on the actual finite element solution or the recovered (smoothed) solution. Therefore, the distribution of the crack band width once the crack pattern is fully developed tend to be almost uniform.

5. The final distributions of Λ indicate that estimating it on the basis of Eq. (4.80), *i.e.* $\Lambda = \Lambda_{init}$, is an underestimation for the coarse mesh "C" while it is an overestimation for the fine mesh "F".

6. In the fine mesh "F", some *spurious* cracks occurred below the ligament, *i.e.* next to the notch. This is the reason for having values of $\Lambda/\Lambda_{\text{init}} < 1$ in the notch region for this mesh.

4.4.7 Numerical applications

Three examples are considered in this section to test the new formulation of the smeared cracking with the adaptation of the crack band width. The examples are selected to model the following situations.

1. Problems without crack initiator (*i.e.* no notch or perturbed material properties) where comparison with discrete cracking is made.

2. Problems with distributed fracture where reinforcement is present.

3. Problems with mixed-mode fracture where cracks zig-zag through the mesh.

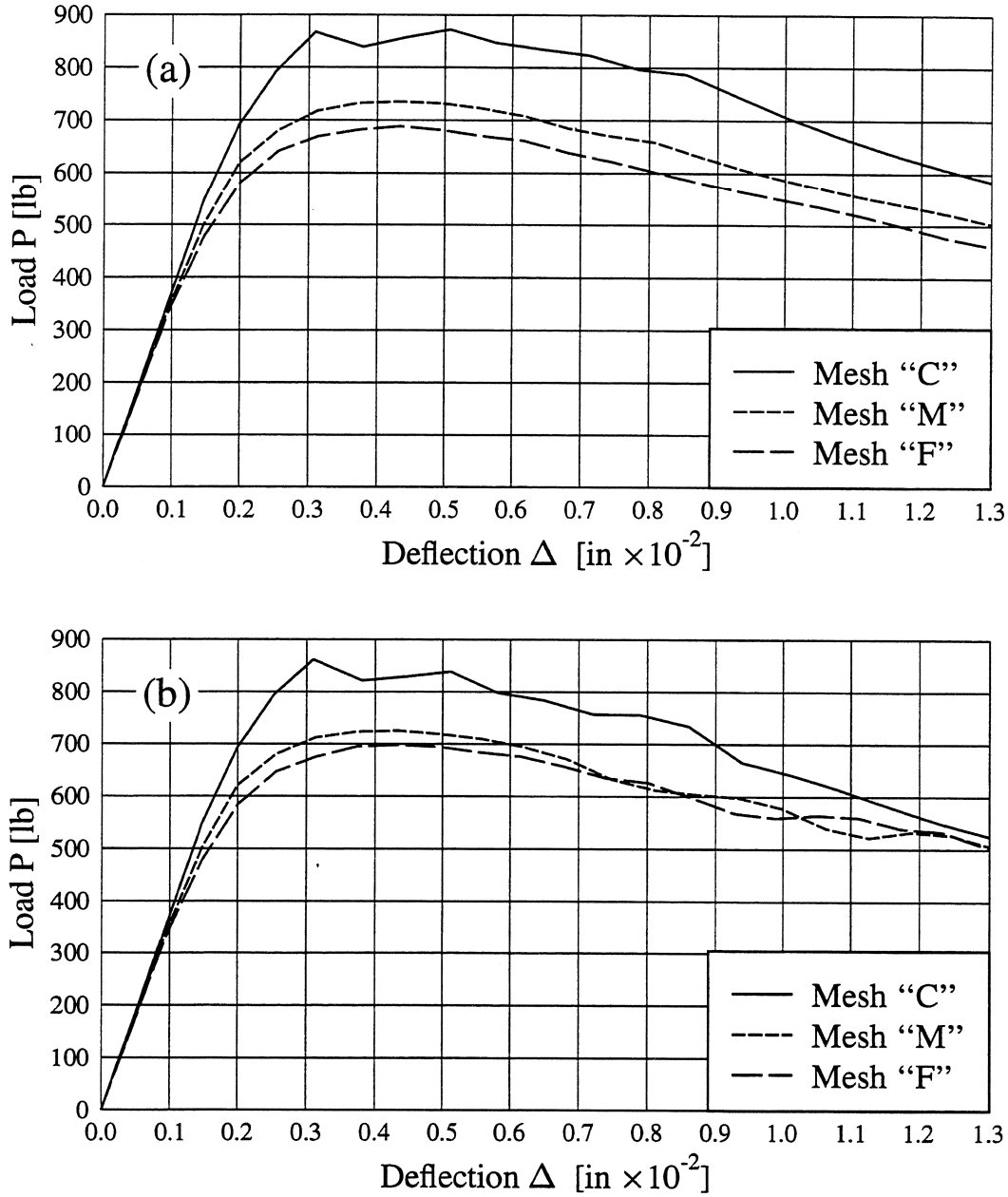

FIGURE 4-10 Results of the 4-point bending notched plain concrete beam; (a) Constant Λ; (b) Adapting Λ.

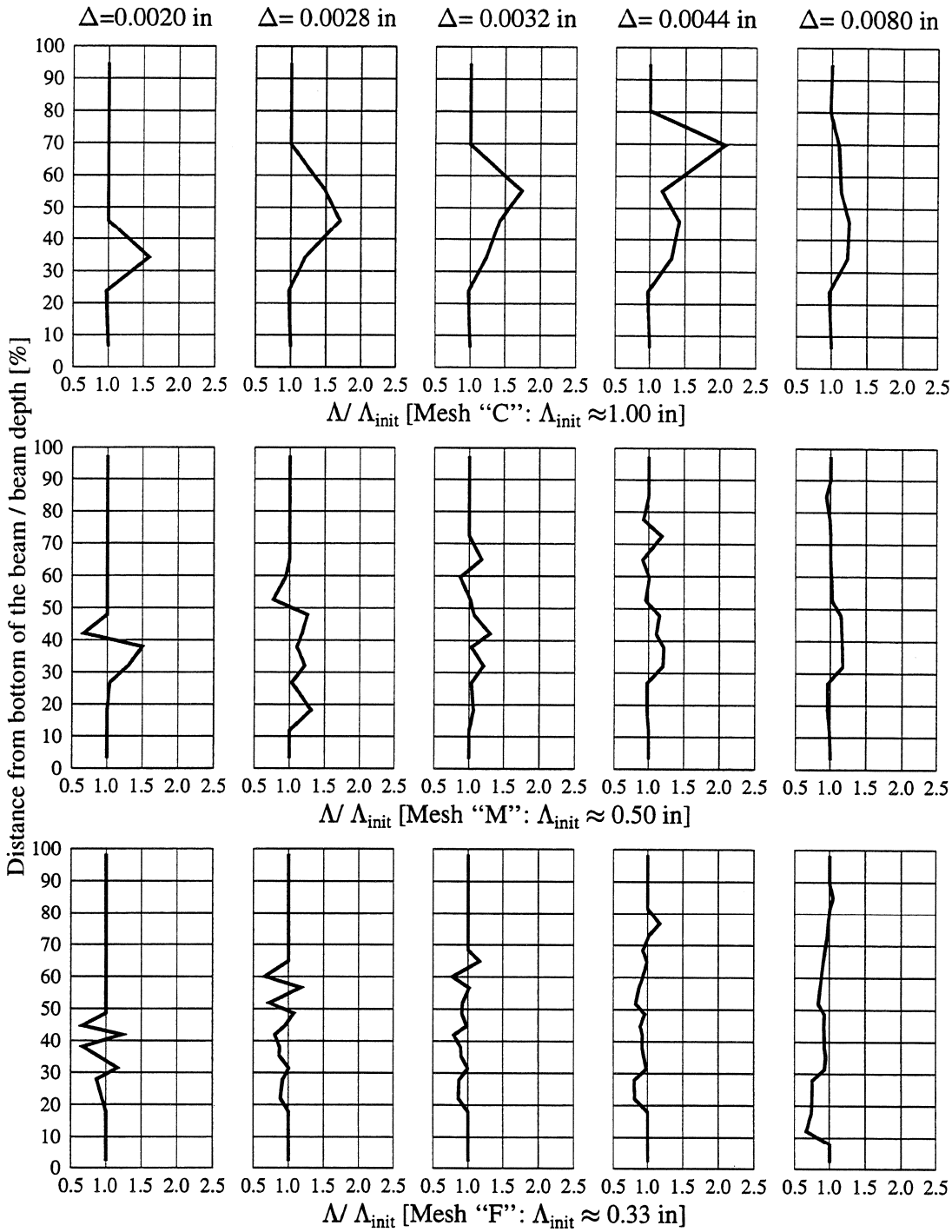

FIGURE 4-11 Distribution of the adapted crack band width along the beam ligament.

Example 1: 4-point bending plain concrete beam

This example is similar to the one used in the previous section to study the mesh sensitivity. In the present case, the beam does not have a notch. The finite element mesh of the beam and the material parameters are the same as mesh "M" in the previous example and it is shown in Figure 4-12(a) together with the obtained fully developed smeared cracks. The finite element model with interface elements introduced in the location of possible discrete cracking is shown in Figure 4-12(b). The material model for the interface element simulating discrete cracks is the same as the one used for the smeared cracks (*cf.* Eq. (4.15) with Eq. (4.19)) except that in the discrete case, an explicit relation between crack opening and stress in the normal direction of the crack can be used. Therefore, the need for the crack band width is eliminated for the discrete modeling.

The results shown in Figure 4-12 indicate that the standard smeared cracking cannot capture the shape of the descending part of the relation (*i.e.* the tail) which is reported experimentally [70]. On the contrary, adapting the crack band width in the smeared crack model captures the descending branch leading to a softer behavior. The stiffer behavior of the discrete model in comparison to the adapted smeared cracking model may be attributed to the existence of other cracks in the constant bending moment region which are represented in the smeared cracking approaches but not with the discrete model.

Example 2: 4-point bending reinforced concrete beam without shear reinforcement

The second example is a reinforced concrete beam tested in 4-point bending. This beam is the one designated 3NDB and tested by Kim [82]. The beam has a shear span to depth ratio of 3 (span = 57 inch and depth = 7.5 inch). The beam has a rectangular cross section (5 in $\times$ 9 in) and was reinforced using 2-#5 deformed bars. The concrete compressive strength is 5470 psi and the yield strength of the reinforcement is 62 ksi [82]. Other material parameters needed for the material model are assumed as follows:

$$E = 1250\,\text{ksi}\,, \qquad \nu = 0.15\,, \qquad f_t = 320\,\text{psi} \quad \& \quad G_f = 0.292\,\text{lb.in/in}^2$$

The Young's modulus E is selected to numerically obtain the same initial slope of the load-deflection relation as determined by the experimental measurements. The value of E may seem lower than what one should expect for normal strength concrete. However, it should be noted that, the actual beam deflection may have been overly large because of the flexibility of the supports. Since the flexibility of the supports is not identified in the experimental measurements, such *pseudo-modulus* is used. The tensile strength is chosen to give similar cracking load to the one reported experimentally. The assumed fracture energy is that commonly adopted for reinforced concrete structures [55].

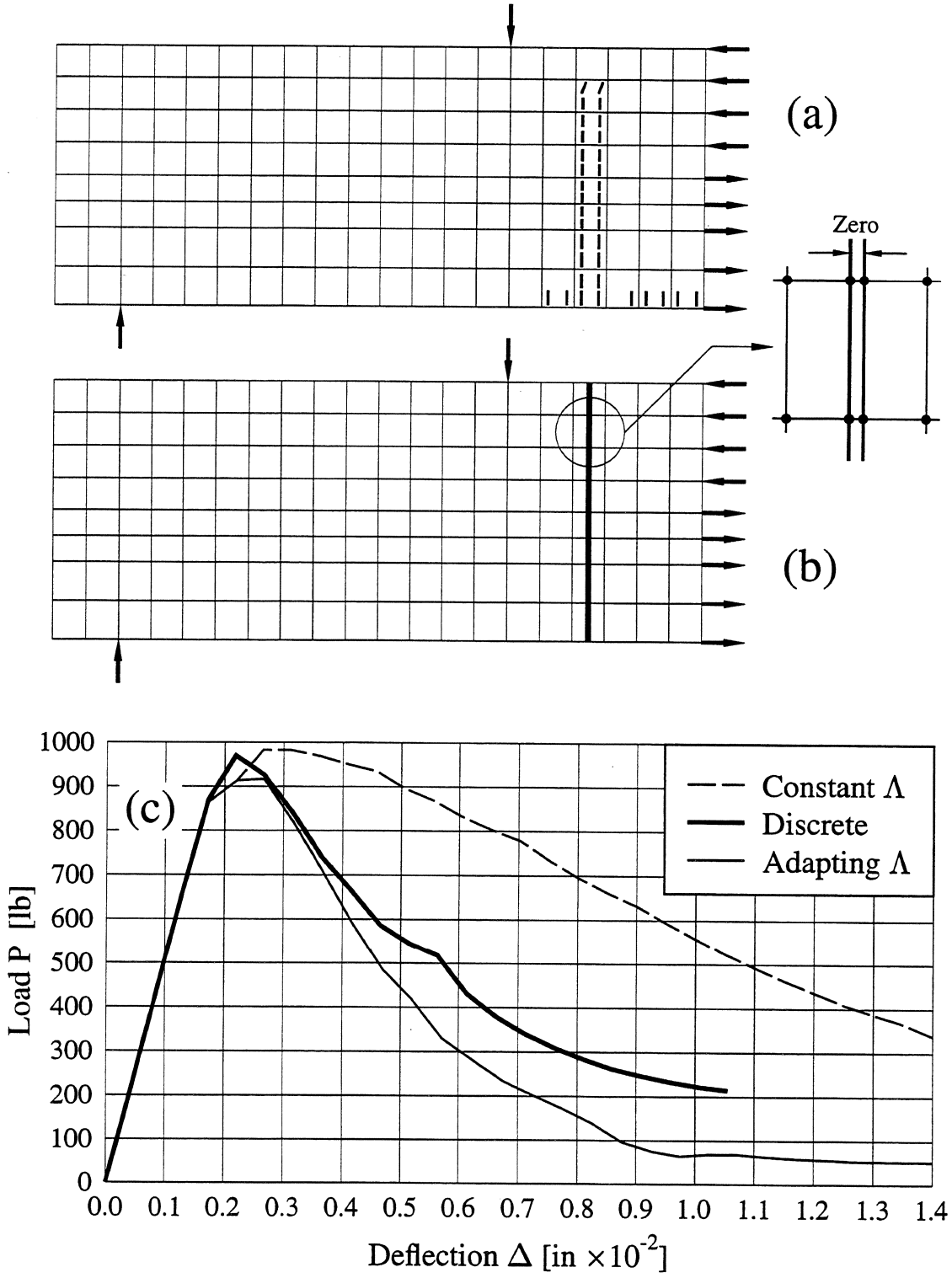

FIGURE 4-12 Results of Example 1; (a) Finite element model and fully developed smeared cracks; (b) Model for discrete cracking; (c) Comparison of load-deflection relations for different cracking approaches.

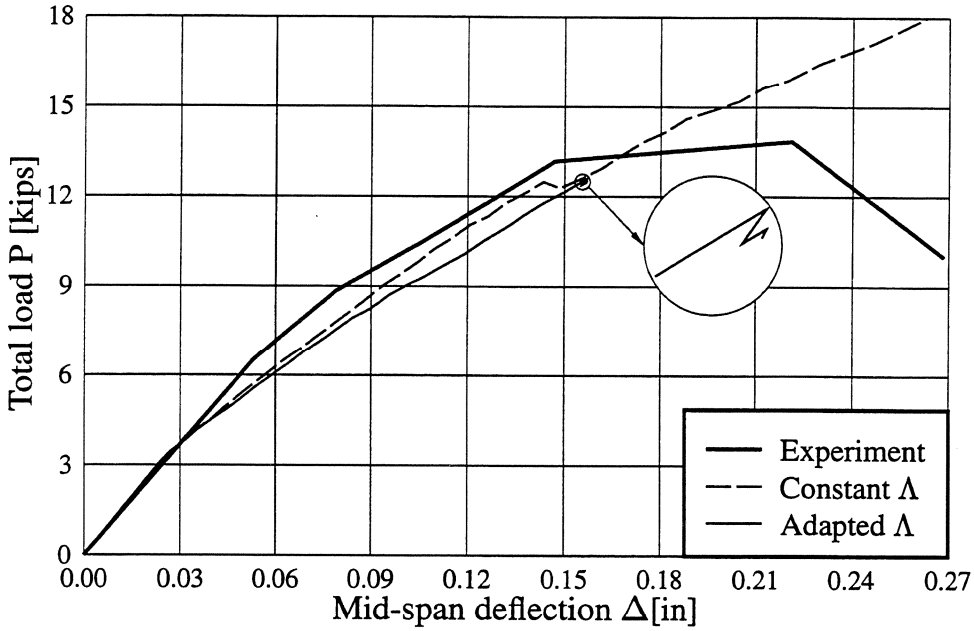

FIGURE 4-13 Load-deflection relations of Example 2.

The beam is analyzed using the smeared cracking model discussed in the beginning of this section with and without the adaptation of the crack band width. In the experiment, the beam was supported and loaded through steel platens which are included in the finite element model as well. Full bond (*i.e.* embedded reinforcement) between the reinforcing bars and the surrounding concrete is assumed. The computations are performed using the arc-length method. The numerically obtained load-deflection relations are compared with the experimentally determined curve in Figure 4-13. From these relations, it may be noticed that the results where Λ is kept constant shows snap-through close to the ultimate load but the solution is unbounded beyond this point. On the other hand, adaptation of Λ leads to a response with snap-back which caused a situation beyond which, the analysis could not be continued. This may seem as a numerical disadvantage of adapting Λ, but one may arrive at a physical explanation of the encountered numerical difficulty from the observed crack patterns with and without the adaptation of the crack band width. These patterns at a load level of about 12.5 kips together with the finite element model are shown in Figure 4-14. One clearly observes the shear crack predicted with the adaptation of Λ. This type of cracking is the experimentally determined mode of failure at the same load level ($\approx$ 13 kips). Such suddenly occurring (brittle) cracks lead to strong localization. The constraint equation used to predict the incremental load factor in the arc-length solution scheme is based on all the displacement degrees-of-freedom. Therefore, such strong localization may lead to failure of the numerical solution (more details may be found in reference [55]). A possible remedy to this numerical problem is to use the technique proposed by de Borst [26] where the number of degrees-of-freedom in the constraint equation is confined to the region of strain localization.

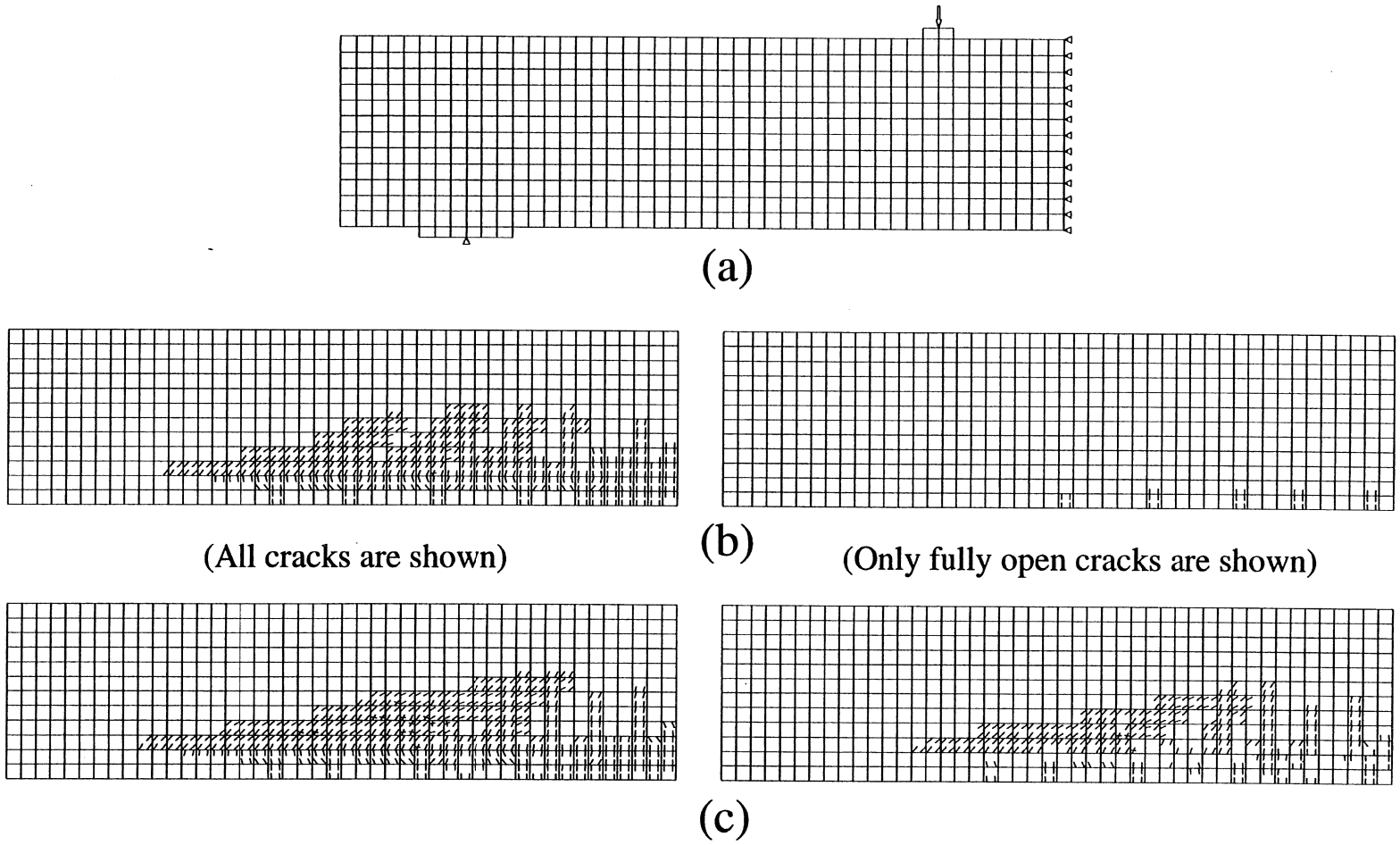

FIGURE 4-14 Example 2: finite element model and its results; (a) Model; (b) Crack patterns with constant Λ; (c) Crack patterns with adapted Λ.

From the results of the present example, one may conclude that the proposed adaptation of the crack band width leads to better prediction of the crack patterns and the ultimate load capacity than does the approach of constant crack band width. The importance of the new formulation of the smeared cracking becomes clear for problems with distributed fracture where the nonlocal continuum and the smoothing process are more natural. It is speculated that numerical difficulties may arise when Λ is adapted due to the deficiency of the numerical solver to cope with strong localization.

Example 3: Crack-Line-Wedge-Loaded Double-Cantilever-Beam (CLWL-DCB)

One of the Crack-Line-Wedge-Loaded Double-Cantilever-Beam (CLWL-DCB), tested by Kobayashi *et al.* [85] and analyzed by Rots [149], and Lotfi and Shing [101], is selected to check the validity of the proposed adaptive characteristic length method. The choice of this example is motivated by the similarity between its crack pattern and that of the infill wall cracks. In the latter, cracks appear horizontally in the middle of the panel which makes the wall panel similar to the notched plate and for both cases load is applied along the diagonal of the structure causing initial cracks to rotate towards the loaded corner.

The dimensions, material parameters and boundary conditions are illustrated in Figure 4-15(a). The specimen is assumed to be in a state of plane stress. The shear retention factor $\beta \approx 0.0$ is chosen to cause the axes of principal stress to remain *practically fixed* after crack formation. The ratio of the diagonal force (F_2) to the wedge force (F_1) is kept approximately constant at 0.6 until $F_2 = 850$ lb. Then, F_2 is kept constant and only F_1 is altered [85]. The diagonal force is applied under load control and the wedge loading under displacement control. The adopted finite element mesh is shown in Figure 4-15(b), and consists of Q4 with 2×2 Gaussian integration. Slave nodes are used along the transition line from a coarser mesh to a finer one at the upper-right corner of the plate. The reported results for this example are obtained using Eq. (4.66) and considering $p = 4$ in Eq. (4.72). The double-directional fixed smeared cracking model is adopted here, and the obtained system of nonlinear equations is solved using the *regular Newton-Raphson* method where the tangential stiffness matrix is set up before each iteration. The convergence criterion for the equilibrium iterations is based on checking the norm of the out-of-balance force vector ($\leq 10^{-3}$).

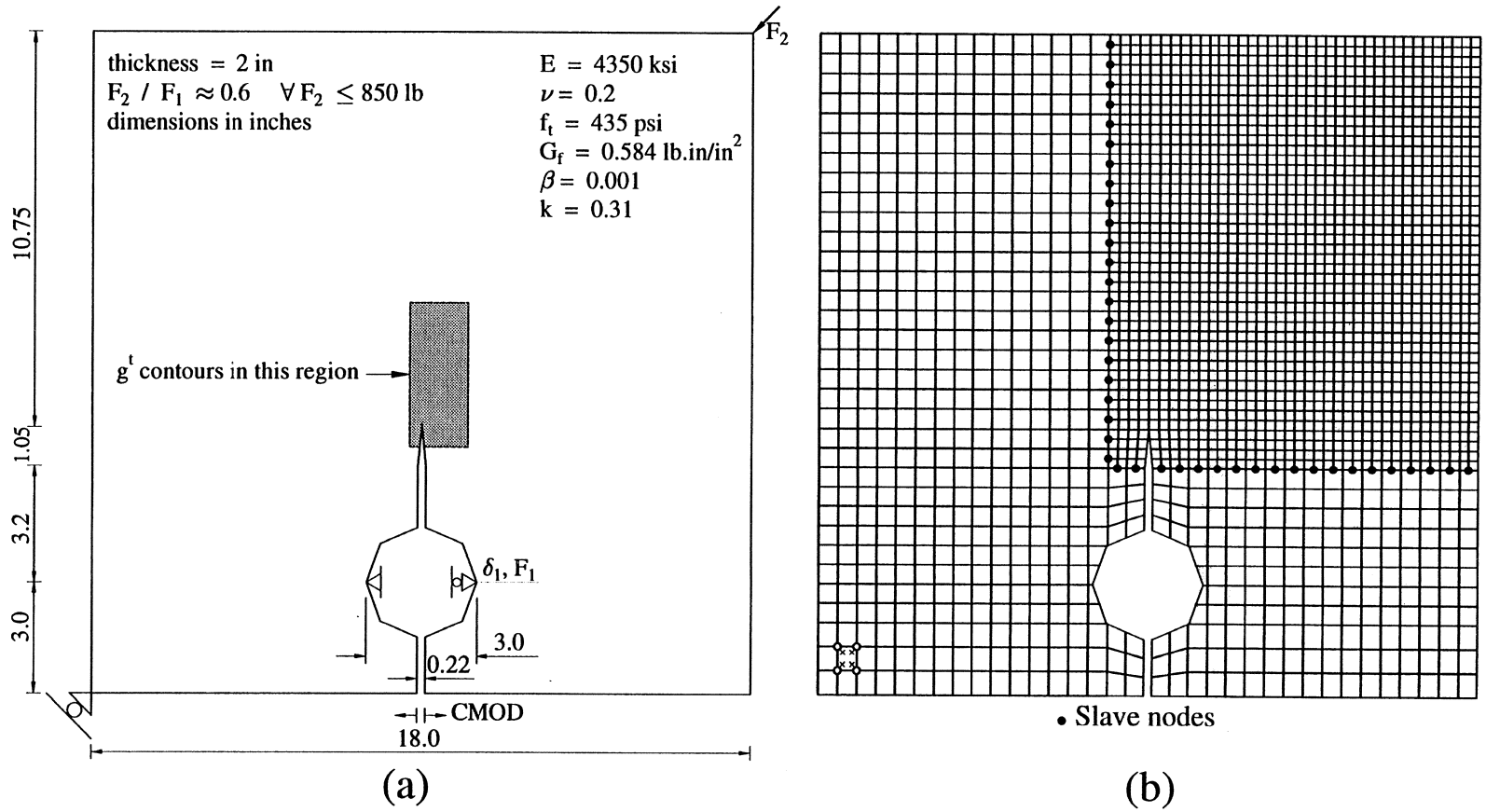

FIGURE 4-15 Crack-Line-Wedge-Loaded Double-Cantilever-Beam (CLWL-DCB) specimen; (a) Dimensions, boundary conditions and material properties; (b) Finite element mesh.

Figure 4-16(a) shows the wedge force (F_1) versus the Crack Mouth Opening Displacement (CMOD). Note that a better agreement of the descending branch with the experimental results is achieved when the evolutionary characteristic length method (adaptive Λ) is used than when Λ is kept constant throughout the analysis (standard smeared cracking). It should be noted that no attempt has been made to match the initial slope of the experimental results by adjusting the material parameters. Instead, the parameters used in reference [149] are used herein. This explains the mismatch between the experimental and numerical results of the linear part of the wedge load-CMOD relations. It is expected that the adjustment of the initial stiffness will improve the estimated ultimate load capacity of the numerical results with the adaptation of Λ. At highly damaged states, *e.g.* CMOD $\geq$ 0.008 inch in Figure 4-16(a), several cracks became fully open. Therefore, from this point on the value of Λ is kept constant at these sampling points where cracks are fully open. The corresponding results for the Crack Mouth Sliding Displacement (CMSD) versus the CMOD are illustrated in Figure 4-16(b), which shows the difference between the two approaches.

Figure 4-17 shows contour plots for the apparent fracture energy density before (Figure 4-17(a)) and after (Figure 4-17(b)) smoothing. The region considered for these plots is the shaded area in Figure 4-15(a). The contour plots are shown at the load level marked in Figure 4-16. It should be noted that these plots are shown in a distorted scale for clarity of the distributions and next to them are the same plots with the actual scale. The non-smoothed contour (Figure 4-17(a)) tends to follow the mesh pattern. This reflects one of the main deficiencies of smeared cracking models, which cannot properly capture mixed-mode cracking when the fracture zig-zags through the mesh. In this case there is a tendency for the cracks to propagate parallel to the element boundaries (mesh bias). This problem is largely circumvented by the smoother contour plot of Figure 4-17(b).

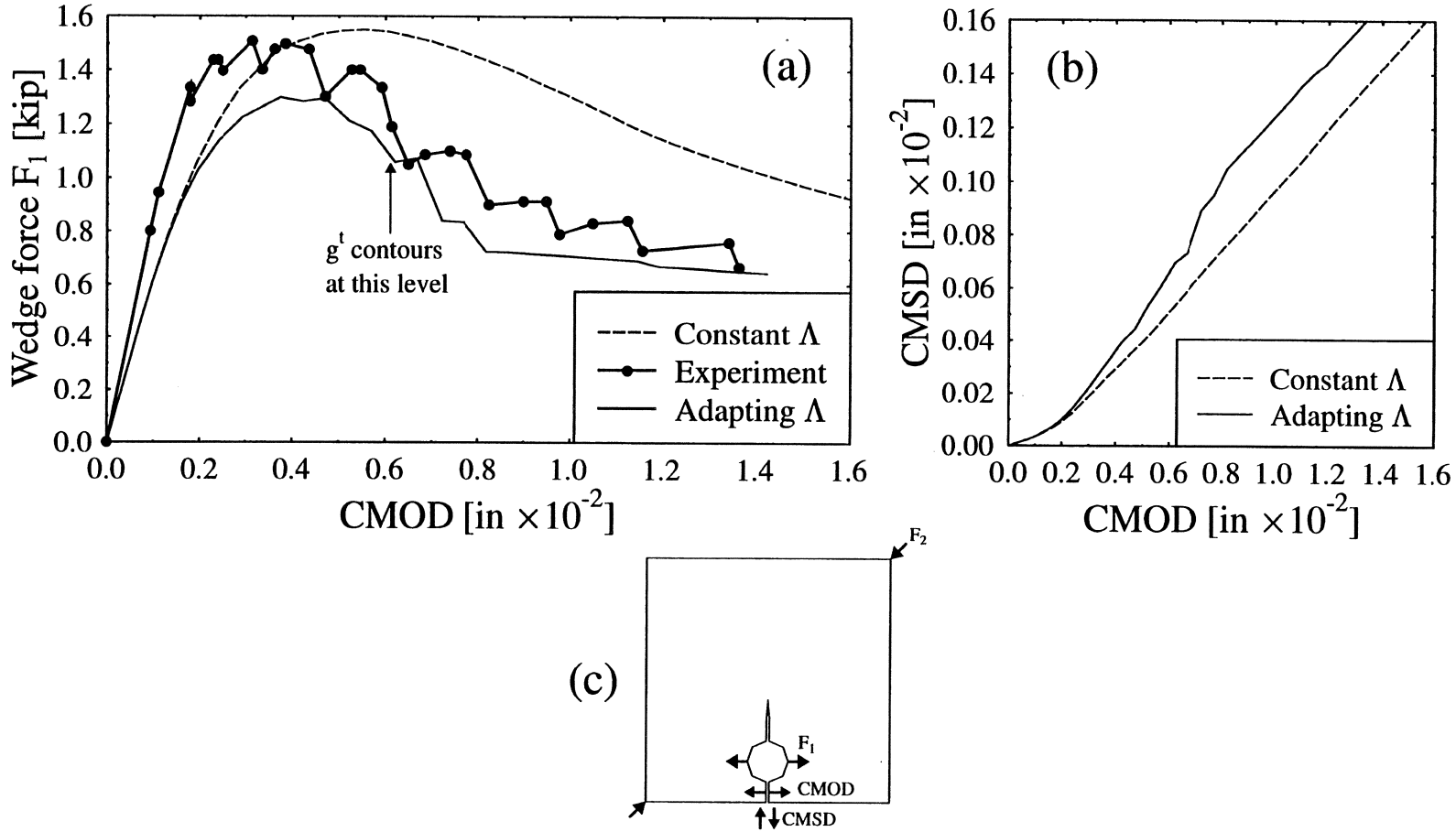

FIGURE 4-16 CLWL-DCB results; (a) Wedge force versus CMOD; (b) CMSD versus CMOD; (c) Notations.

4.5 Summary

In this section, two methods are presented to account for the evolution of material damage produced by smeared cracking. The motivation behind these methods is to be able to circumvent some of the well-known problems with smeared cracking such as mesh bias and spurious kinematic modes. Both methods are based on a nonlocal form of the so-called apparent fracture energy density which can be linked to a measure of the material damage. The first method is based on continuous change of the topology of the finite element mesh. The numerical results validated the technique where meshes were shown to be refined in regions of stress concentrations and strain localization. This method requires the introduction of transfer operators to map the state variables from the present mesh to the new one. This task is not pursued in the present study. On the other hand, a practical adaptation of the smeared crack formulation through continuous change of the so-called crack band width is presented as the second method to account for the damage evolution. The adaptation is based on the ideas of nonlocal continuum and the superconvergent patch recovery. Several examples are analyzed and the results indicate the potential of the new smeared crack formulation to capture strain localization and solve some of the inherent problems in the classical smeared cracking finite element approach.

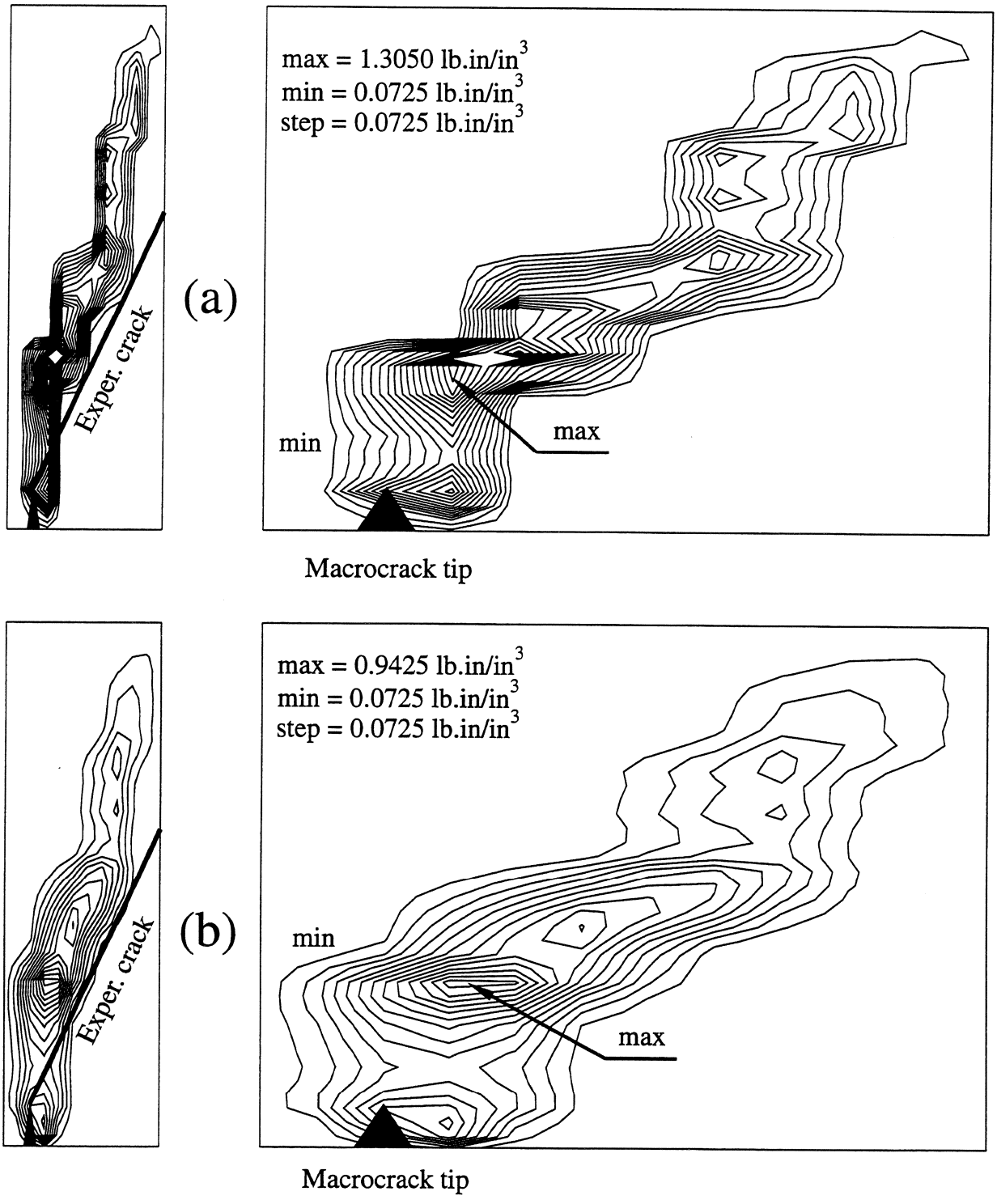

FIGURE 4-17 CLWL-DCB results; (a) Contour plot for g^t; (b) Contour plot for $\bar{g}^t$; Note: (left) actual scale and (right) distorted scale.

SECTION 5

APPROXIMATE MODELS FOR SEISMIC FRAGILITY

Estimation of the expected damage in urban areas due to severe earthquakes and its economic impact is of interest to define appropriate mitigation measures, including a rational decision-making process for resource allocation. This expected damage can be considered as a measure of seismic vulnerability. Its determination involves the investigation of the seismic performance of the numerous types of buildings normally found in a large urban region when subjected to a large variety of potential earthquakes. Due to the large size of the problem, investigations of this nature focus only on the generic types of construction. In addition, simplified structural models with random properties to account for inherent uncertainties in the structural parameters should be defined. In this way, a manageable number of simplified models for all representative building types is obtained. Unfortunately, even under these conditions, the amount of calculations involved is large and a need for simplified yet accurate methods of evaluation is evident.

As pointed out in **SECTION 1**, low-rise and mid-rise frames with infill walls represent a common type of construction in urban areas. In this section, attention is focused on this class of frames, particularly those designed mainly for gravity loads. A simplified analytical procedure for estimating the seismic performance of Lightly Reinforced Concrete (LRC) frames infilled with masonry walls is presented. This seismic performance is described by fragility curves. The procedure is based on the application of the Dynamic Plastic Hinge Method (DPHM) to an ensemble of LRC infilled frames. Several key parameters in the load-displacement relation of the structure are treated as random variables to account for the uncertainty in the material model for the analyzed ensemble. Verification of the DPHM using the FEM is also presented.

5.1 Seismic Fragility

Fragility is the proneness of an object to be easily broken or destroyed [31]. In mathematical terms, the global structural *fragility* or *vulnerability* is the probability of failure of the structure conditional on a specific hazard intensity. From the definition of fragility, the unconditional probability of failure can be obtained by integrating the fragility over the entire range of hazard intensities. Let I_j be a specific value of the hazard intensity with random details of the j^{th} excitation. Let R be the load effect due to this random event on the global *response* of the structure. Let C_i be the random structural *capacity* to withstand this load effect corresponding to the i^{th} limit state. Accordingly, the structural fragility is

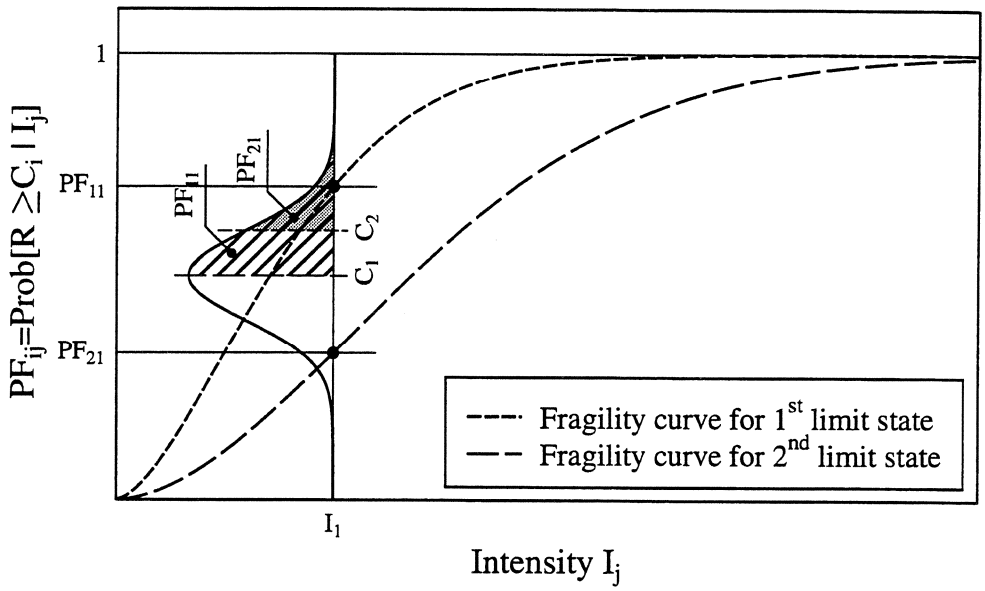

FIGURE 5-1 Definition of probability of failure for fragility analysis.

calculated as:

$$PF_{ij} = \text{Prob}\left[R \geq C_i | I_j\right] \tag{5.1}$$

where PF_{ij} denotes the probability of failure with respect to the i^{th} limit state at the j^{th} hazard intensity level. The definition given by Eq. (5.1) is schematically illustrated by Figure 5-1 where at a certain intensity level I_1, the frequency distribution of the global response of the considered ensemble of structures is shown. In the same figure, two levels of structural capacity, C_1 and C_2, are also indicated with their corresponding probability of failure (exceedance), PF_{11} and PF_{21}, respectively.

5.1.1 Seismic hazard

In the present study, fragility analysis was focused on the *seismic* hazard. In general, a complete description of the seismic hazard at a specific site should include all the variables related to earthquake occurrence, wave transmission and ground motion input to the structures. A typical site was selected for this study which is close to the University of Memphis, Tennessee. This site is in the central part of the Mississippi embayment and located close to the New Madrid Seismic Zone (NMSZ). Hwang and Huo [72] generated synthetic ground motions using probability-based scenario earthquakes established from a probabilistic seismic hazard analysis of the chosen site. Fifty acceleration time histories were generated for each specified pair of moment magnitude (M_m) and epicentral distance (R_e). Details of the technique used to generate these records can be found in reference [72].

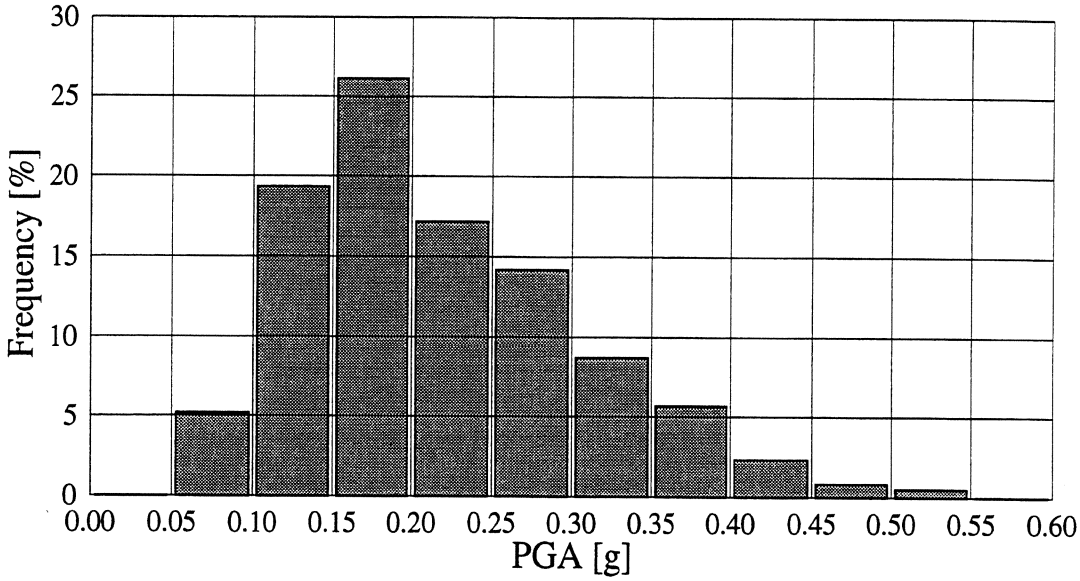

FIGURE 5-2 Distribution of the PGA of the synthetic records.

In the present fragility analysis, a total of 600 synthetic ground motion records were considered. In these records, three different values of M_m [6.5, 7.0 and 7.5] and four different values of R_e [40, 60, 80 and 100 km] were considered. The frequency distribution of the PGA of these records is shown in Figure 5-2. Here, the PGA is considered as the measure of seismic intensity. Figure 5-3 gives the time histories of a sample of the earthquake records used in the fragility analysis and their corresponding response spectra for 2% damping ratio (ξ) are shown in Figure 5-4. In Figure 5-4(a), the moment magnitude varies keeping the epicentral distance fixed whereas in Figure 5-4(b), the epicentral distance varies keeping the moment magnitude fixed. All response spectra are normalized by their PGA's. From these spectra, one may expect that short-period structures, *e.g.* low-rise to mid-rise infilled frames, will experience low seismic demand. This observation is similar to what has been concluded in the second report of this series regarding the seismic response of the two-bay, two-story SRCS infilled frame subjected to the Nahanni earthquake record.

5.1.2 Limit states

The expression "limit state" is used to denote any stage of behavior at which an undesirable response occurs. As discussed by Gergely [60], typical limit states are: cracking, yielding, drift, rupture, crushing, and buckling. Construction of the fragility curves for LRC frames with or without infills involves the determination of cumulative distribution functions of the probability that a given limit state is reached for a given seismic intensity. In this investigation, two different limit states are considered: the first includes the damage of the main structural elements, *e.g.* the frame; the second is restricted to the damage of the nonstructural elements, *e.g.* the infill walls. The need for these two limit states is

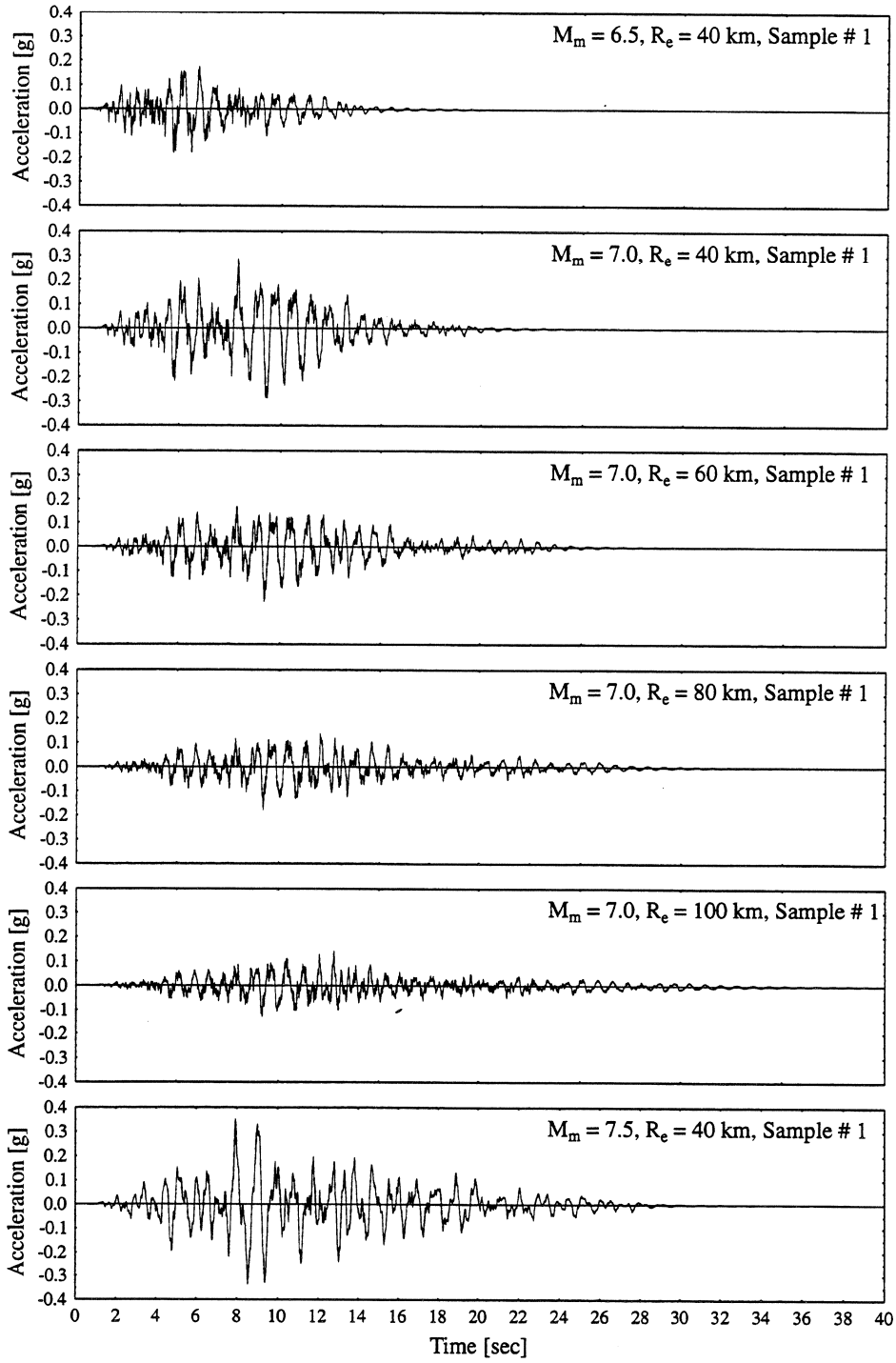

FIGURE 5-3 Time histories of a sample of earthquake records used for the fragility analysis.

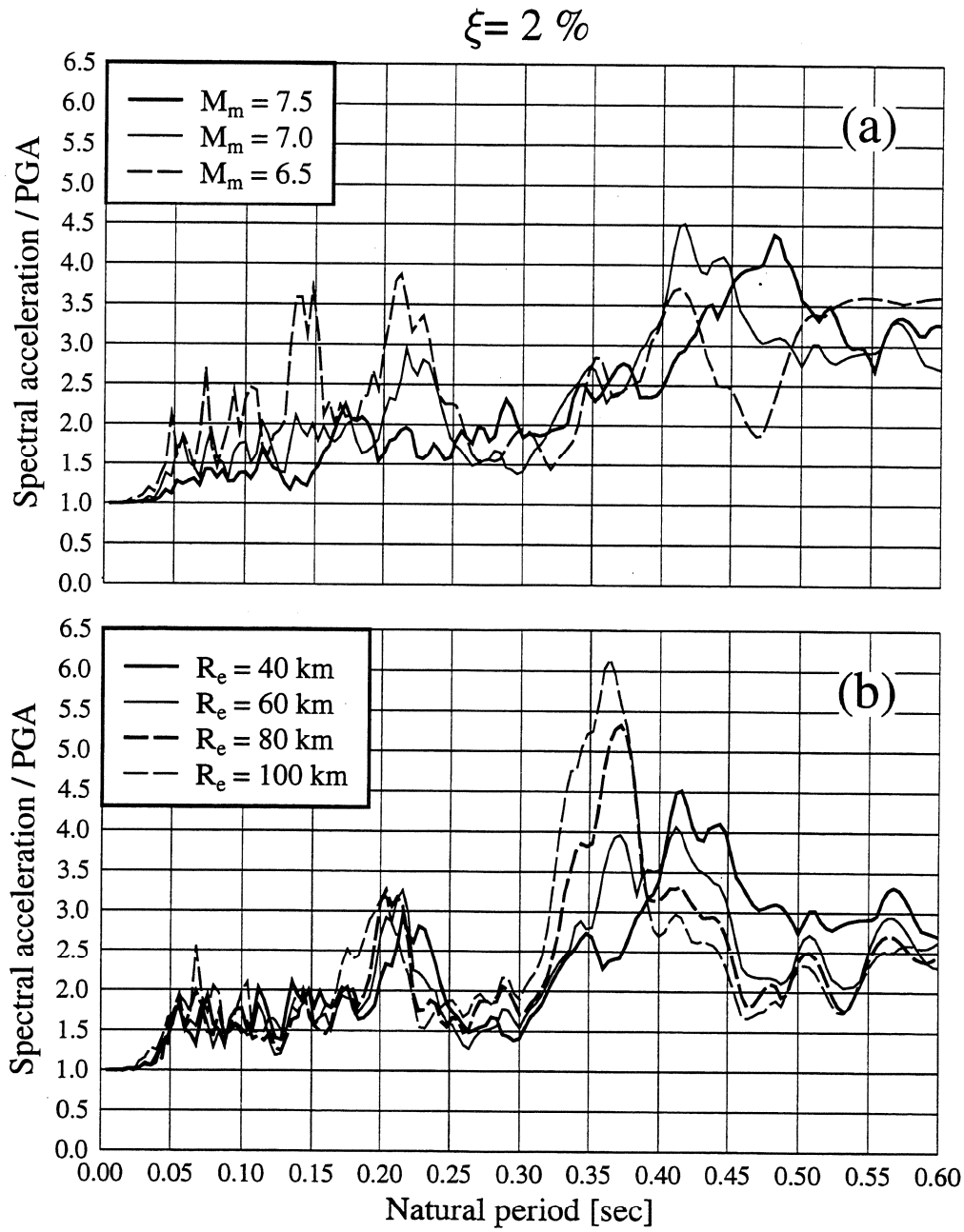

FIGURE 5-4 Response spectra of a sample of earthquake records used for the fragility analysis; (a) R_e = 40 km; (b) M_m = 7.0.

dictated by the significant differences in the seismic response between the bare and the infilled frames.

In addition to the direct seismic shaking, there exist numerous causes of seismic related structural damage, *e.g.* pounding, foundation failure and collateral effects. In the current study, only seismic shaking effects on the superstructure will be considered.

The analytical determination of seismic damage due to earthquake shaking has been the subject of research for the past few years, and has resulted in the development of a number of damage indices related to the physical state and safety of buildings and their serviceability. The recent state-of-the-art article by Williams and Sexsmith [166] reviews the seismic damage indices for concrete structures. The determination of some of these indices involve elaborate calculations which deter the aims of a vulnerability study. Ayala and Xianguo [9] have shown that some of these indices calculated for building structures correlate well with the Maximum Roof Displacement (MRD) and inter-Story Drifts (SD). The MRD and SD are structural performance parameters which may be directly obtained from equivalent pushover methods [61], or from dynamic response calculations.

In the present fragility analysis, limit states are given by the MRD obtained from the DPHM which is converted into the inter-story drift (SD_s) for story number s as follows.

$$SD_s = \left[\text{MRD} \times \frac{\phi_s - \phi_{s-1}}{\phi_r}\right] \Big/ H_s \quad [\%] \tag{5.2}$$

where H_s is the story height and ϕ_s and ϕ_r are the components of the first mode shape at floor number s and at the roof, respectively. In this way limits on the inter-story drift may be established based on engineering judgment and experimental observations as suggested in Table 5-I [48] [71]. It should be noted that the limit states depend on the structure type, *e.g.* infilled versus bare frames, reinforced concrete versus steel frames and low-rise to mid-rise versus high-rise structures.

TABLE 5-I An example of the damage states.

Damage state	Description of damage	Response level	Inter-story drift [%]
No damage	There is no damage visible in either nonstructural or structural elements.	Elastic	< 0.2
Insignificant damage	Damage requires no more than nonstructural repair. No structural repairs are necessary.	Cracking	0.2 - 0.5
Moderate damage	Repairable structural damage has occurred. The existing elements can be repaired essentially in place, without substantial demolition or replacement of elements.	Yielding	0.5 - 1.0
Heavy damage	Damage is so extensive that repair of elements is either not feasible or requires major demolition or replacement.	General yielding	> 1.0

5.2 The Dynamic Plastic Hinge Method

The determination of the nonlinear seismic response of building structures is a computationally intensive task which requires a considerable engineering effort for the data preparation as well as for the proper interpretation of the results. A fragility study involves the calculation of the nonlinear responses of a structure, with simulated structural parameters, subjected to a family of earthquakes representing the seismic hazard. The use of conventional nonlinear seismic analysis procedures would make this task practically impossible. Thus, for this type of investigations it is necessary to use simplified methods of analysis to minimize the effort and the expense involved in the determination of the responses. In this study the Dynamic Plastic Hinge Method (DPHM), as originally proposed by Wörner [34][1], is adopted. The original DPHM has the limitation of being a good approximation only for structures which respond essentially in the fundamental mode of vibration which is the case for low-rise to mid-rise regular buildings. This limitation is not of relevance in this investigation as the considered building, a two-bay, two-story LRC frame with masonry infills, is expected to respond in its first mode.

The DPHM reduces a multi-degree of freedom nonlinear structure to an equivalent Single Degree Of Freedom (SDOF) oscillator with equivalent nonlinear properties determined by the so-called Modal-Load-Deflection-Line (MLDL). The MLDL relates the change of the eigen frequency to the corresponding response acceleration. This MLDL is gradually obtained by modal analysis. The method was originally proposed for steel frames where nonlinearities under dynamic loading were due to the formation of plastic hinges. That is where the name of the method came from.

In the current implementation of the DPHM, properties of the equivalent SDOF are obtained by an adaptive pushover analysis. In this analysis, the original structure is subjected to an increasing static load with distribution along the height equivalent to the distribution the structure would experience in its first mode of vibration for different levels of structural damage. The obtained pushover curve is normally presented by spectral acceleration (Sa) versus roof displacement (Δ_r) relation. Accordingly, this pushover analysis requires the use of a nonlinear static analysis program with the capability of eigen solution evaluation each time the dynamic properties of the structure change during the loading process. The steps involved in the construction of these pushover curves are as follows:

1. Define and calibrate a nonlinear structural model for the building to be analysed. For steel structures an elasto-plastic behavioral model for the elements is acceptable. However, for concrete structures the use of more elaborate behavioral models is recommended.

2. Perform an eigen analysis for the initial fundamental mode only and obtain the eigen vector $\{\Phi^0\}$.

[1]The original reference for the DPHM is in German and is cited in reference [34].

3. Calculate the initial distribution of the equivalent static loads along the height of the structure from the following equation:

$$f_i^1 = \frac{m_i \phi_i^0 \{1\}^T [M] \{\Phi^0\}}{\{\Phi^0\}^T [M] \{\Phi^0\}} Sa^0 \tag{5.3}$$

where superscripts T and 0 refer to transpose and initial state, respectively; f_i^1, m_i and ϕ_i^0 are, respectively, the initial equivalent static load, the lumped mass and the component of the initial eigen vector, corresponding to the fundamental mode, at the i^{th} floor; Sa^0 is the initial response acceleration normalized to 1; $[M]$ is the lumped mass matrix and $\{1\}$ is a unit column vector.

4. Apply a monotonically increasing force vector $\{F^0\}$ until a significant change in the dynamic properties of the structure occurs

5. Record the roof displacement and the corresponding base shear and spectral acceleration using the current force at any floor i by the following equation:

$$Sa^n = \frac{f_i^n \{\Phi^n\}^T [M] \{\Phi^n\}}{m_i \phi_i^n \{1\}^T [M] \{\Phi^n\}} \tag{5.4}$$

where superscript n refers to the current state of the structure.

6. Repeat steps 2 and 3 for the damaged structure.

7. Modify the previous distribution of equivalent static forces adjusting their intensity to those that would give the previously recorded base shear. Subsequently, apply the new load distribution to the damaged structure monotonically increasing its intensity until a significant change in the previous dynamic properties of the structure occurs.

8. Repeat steps 6 and 7 until the maximum expected base shear is reached or until the structure cannot sustain any more lateral load.

9. Construct the pushover curve with the recorded values of the roof displacements and the corresponding spectral accelerations.

Once the pushover curve has been constructed, a dynamic step by step analysis for the equivalent SDOF oscillator is performed using as dynamic properties for each step those corresponding to the pushover curve. The global responses associated to each step in the analysis of the equivalent SDOF structure can be converted into those of the actual structure using the current fundamental mode shape and the basic equations of modal analysis (for details the reader is referred to Section 13.1 in the book by Chopra [32]).

5.3 Description of The Investigated Structure

A two-bay, two-story LRC frame with masonry infills is selected for the present investigation. This frame is similar to the one tested pseudo-dynamically and discussed in the second report of this series. At Cornell University, two identical frames are currently being tested pseudo-dynamically and on the shake table to assess the damage state and to correlate their results with computational predictions.

The finite element models of the investigated structure and of the corresponding reinforcement details are shown in Figures 5-5 and 5-6, respectively. All the features of reinforcement detailing typically found in non-seismically designed buildings in North America are captured in this finite element model. These features were identified by several researchers [133] [49] [27] [50] [24] as follows:

1. Low percentage of longitudinal reinforcement in the columns.
2. Lapped splices of column reinforcement at the maximum moment region.
3. Widely spaced column ties providing little confinement to the concrete core.
4. No transverse reinforcement within the joint region.
5. Discontinuous positive beam reinforcement with small embedment into the column.

The nonlinear analyses of this structure were carried out using the finite element system DIANA. The material model of the infill walls and the frame/wall interface were similar to those presented in **SECTIONS 3** and **4**. Homogeneous properties with smeared cracking were adopted for masonry infills. The frame/wall interface was treated using interface elements. The material modeling of the reinforced concrete frame also accounted for smeared cracking and bond-slip phenomena of the reinforcement. Smeared cracking was treated as discussed in **SECTION 4**. Regarding the bond-slip, interface elements were introduced between the reinforcing bars and the surrounding concrete elements where a nonlinear relation between shear traction and shear slip was considered. All material parameters were experimentally determined. The detailed structural configuration and the material parameters of this LRC infilled frame are given in **Appendix C**.

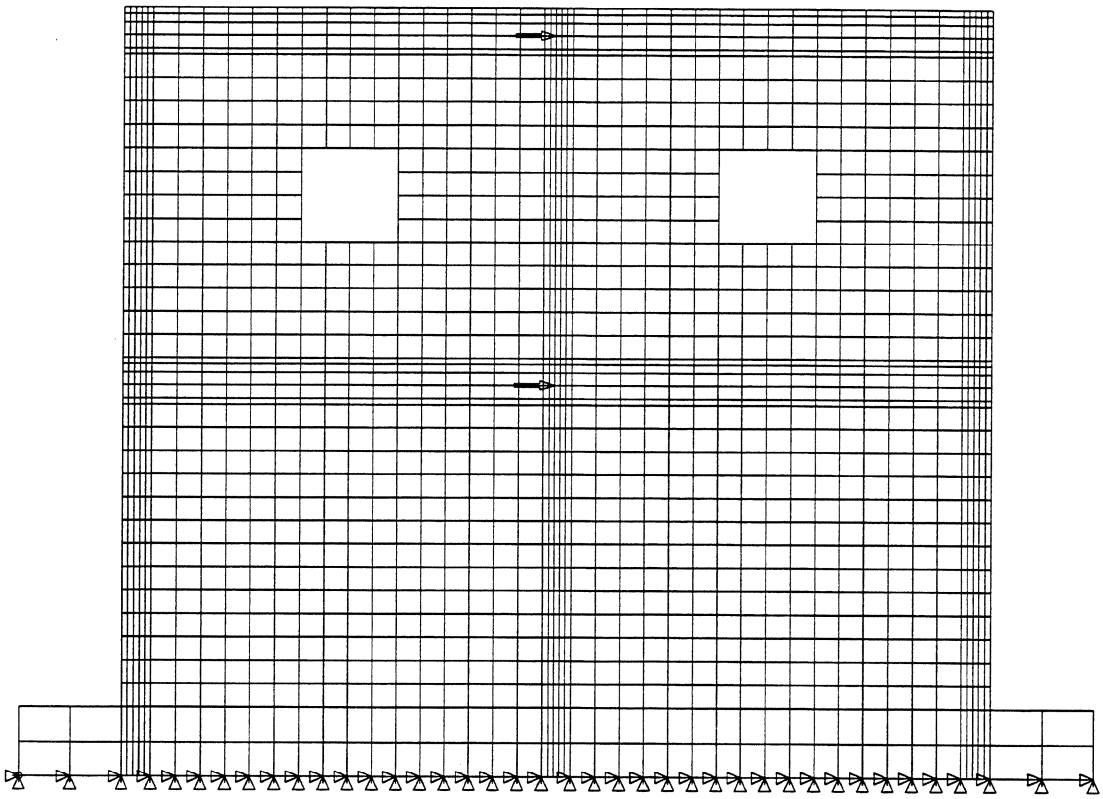

FIGURE 5-5 Finite element model of the investigated two-bay, two-story LRC infilled frame.

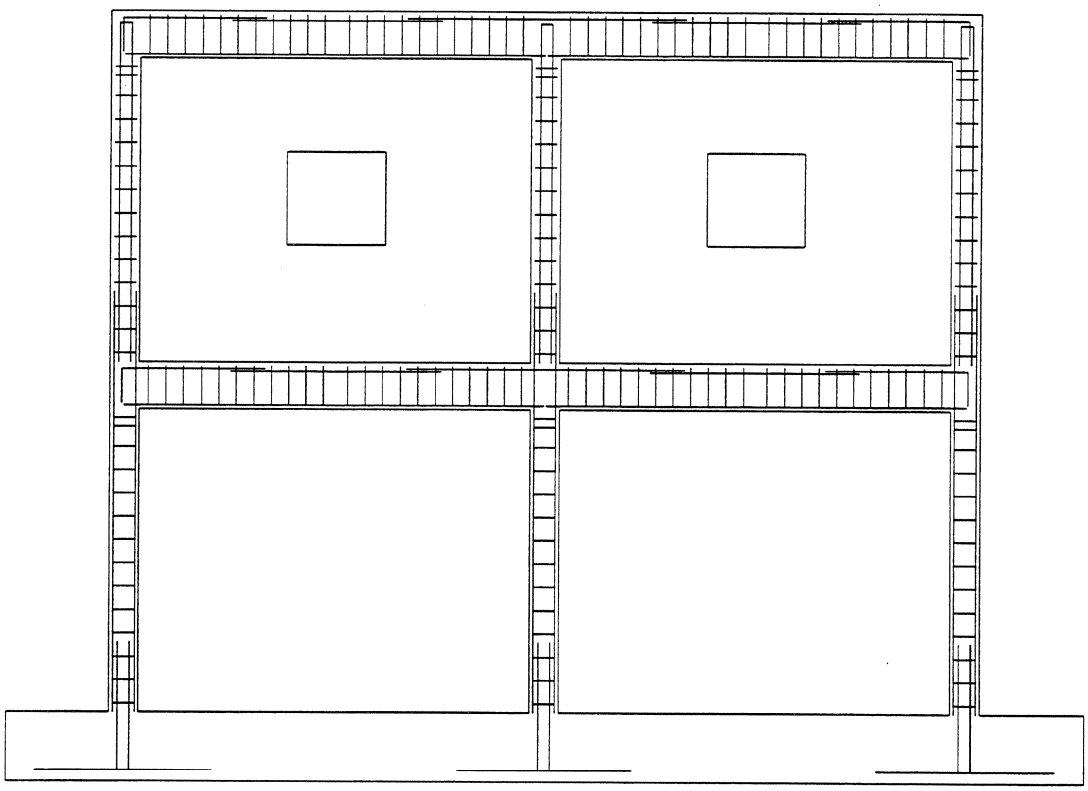

FIGURE 5-6 Reinforcement details of the finite element model of the investigated two-bay, two-story LRC infilled frame.

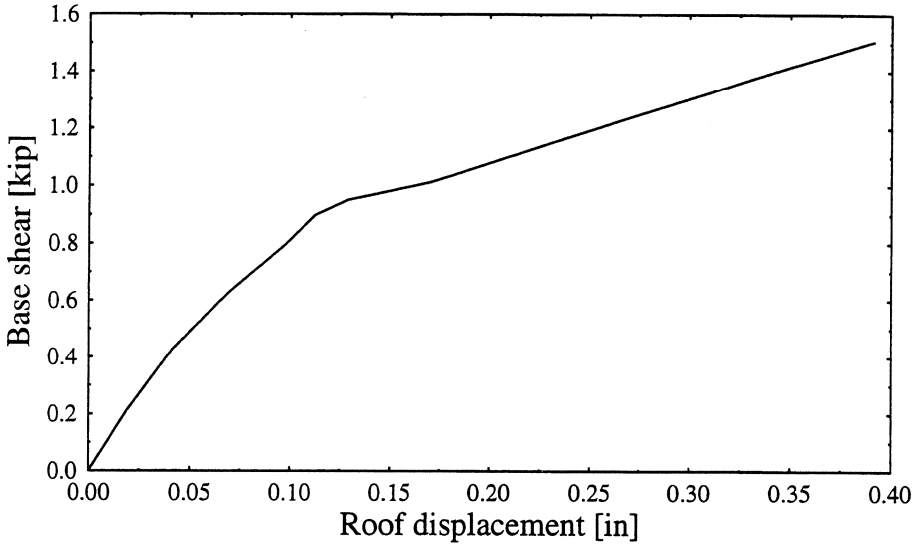

FIGURE 5-7 Pushover curve for the bare frame.

5.4 Validation of The Dynamic Plastic Hinge Method

To validate the results of the DPHM, the previously discussed LRC frame without the infills was analysed under seismic loading using the S69E component of the Taft earthquake of 1952. On the other hand, in order to use the DPHM, the pushover curve for the same frame was determined using the same finite element model and the resulting curve is plotted in Figure 5-7. In this figure, the relatively long ascending branch was due to the carrying capacity of the reinforcing bars after cracking. These bars did not show any yielding or slippage.

Nonlinear dynamic analysis for a SDOF oscillator was carried out where the constitutive model of the oscillator was based on the pushover curve shown in Figure 5-7. To account for the energy dissipated through hysteresis, secant stiffnesses from the pushover curve were considered. It should be noted that one of the major limitations of the present DPHM is that strength deterioration and stiffness degradation are not fully accounted for.

It should be noted that one of the major limitations of the present DPHM is that strength deterioration and stiffness degradation are not fully accounted for.

The time histories of the roof displacement, velocity and acceleration obtained from the nonlinear dynamic analysis using the FEM and the DPHM are shown in Figure 5-8. The comparisons in this figure indicate an excellent agreement between the finite element results and the results obtained from the simplified model using the DPHM. As long as the structure is behaving in its fundamental mode, it is expected that such agreement will always be the case.

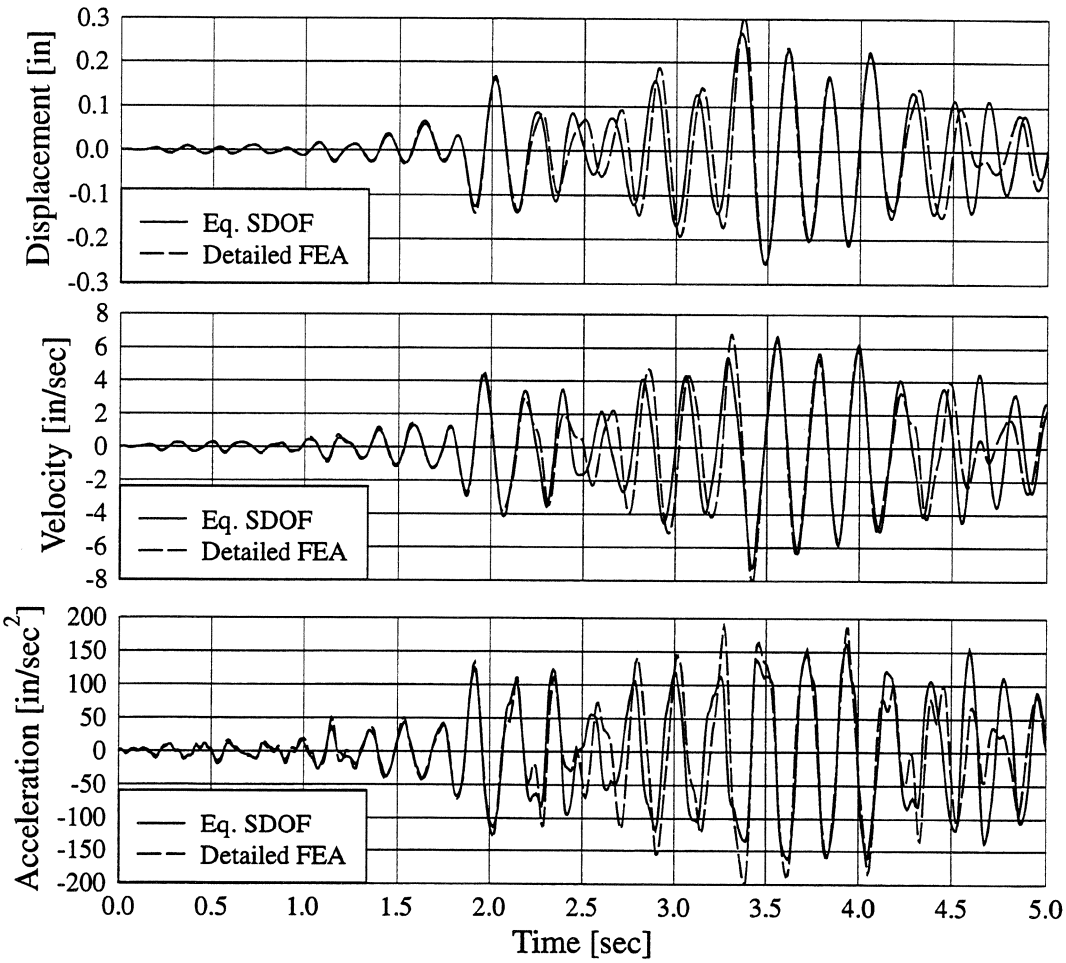

FIGURE 5-8 Comparisons between the results of finite element analysis and the equivalent SDOF based on the DPHM under Taft scaled to $0.175g$.

TABLE 5-II Random properties of the basic parameters of the analyzed LRC frames.

Random parameter	Bare frame		Infilled frame	
	μ	COV [%]	μ	COV [%]
K_1 [kip/in]	11.8	15	56.3	30
K_2 [kip/in]	6.1	20	41.5	40
K_3 [kip/in]	1.5	15	10.7	30
u_1 [in]	0.055	20	0.040	40
u_2 [in]	0.150	15	0.129	30

5.5 Random Properties

It is well known fact that the structural parameters involved in response calculations are inherently uncertain. The randomness of these parameters needs to be considered in the fragility study. Unfortunately, in this type of study, the consideration of all possible sources of uncertainty makes the involved dynamic analyses of a structure difficult if not impossible to carry out. A pragmatic approach for the DPHM is to introduce the uncertainties in the pushover curve. As this curve is the result of a series of arithmetic operations as indicated by Eqs. (5.3) and (5.4), it is valid to assume that the parameters defining it are lognormally distributed [163]. The lognormal distribution can be justified as a reasonable distribution since the statistical variation of many material parameters and seismic response variables may reasonably be represented by this distribution. This is true so long as one is not primarily concerned with the tails of the distribution which is the case for the present fragility study where the probability of exceeding a specific limit state is of interest. More elaborate methods could be implemented considering the randomness in the material properties for which scarce information [112] [52] is available.

Static loading was applied to the finite element model for the infilled frame with assumed mean value properties following the procedure outlined by the DPHM. Figure 5-9 depicts the pushover curves for both the LRC frame with and without infills obtained from such static loading. It was decided to use the curve for masonry stiffness $E_m = 300$ ksi which agrees well with the results obtained from the parameter estimation in **SECTION 3**. The curves for the bare frame and the infilled frame were idealized by tri-linear relations where the tangent stiffnesses of the three linear segments are $K_1 > K_2 > K_3 \geq 0$ and the displacements at which the slope changes are $0 < u_1 \leq u_2$. Table 5-II gives the mean values (μ) of these 5 parameters which are obtained from the pushover curves. Different values for the Coefficient Of Variation (COV) were assumed for these parameters and these assumed values are also listed in Table 5-II. The selection of higher COV for the properties of the infilled frame than those of the bare frame was due to expected higher scatter in the material parameters for masonry. Also, parameters corresponding to the cracking state are expected to be more scattered than those corresponding to the ultimate or the elastic states.

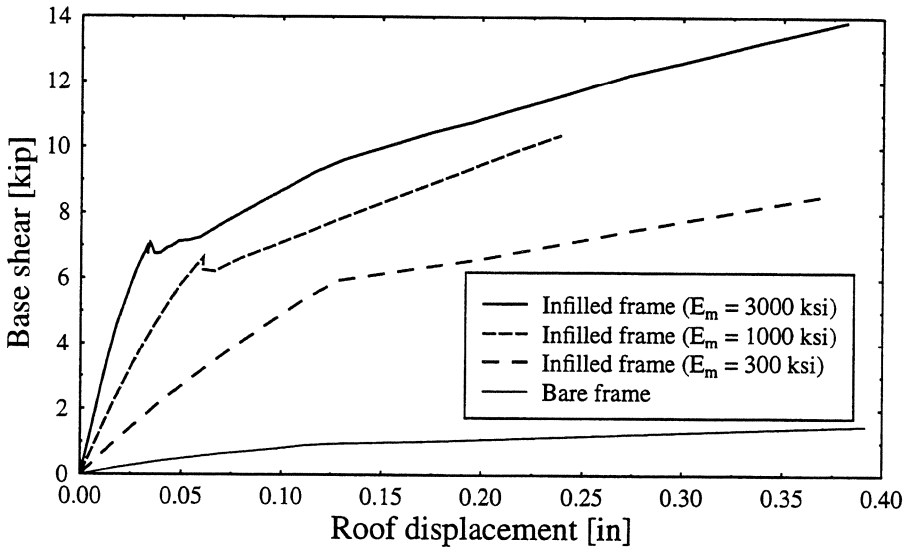

FIGURE 5-9 Pushover curves obtained from the finite element analysis.

Therefore, K_2 and u_1 were assigned higher COV than the other parameters. The ranges of variation of the pushover parameters defined by the mean (μ) $\pm$ a standard deviation (σ) for both the bare frame and the infilled frame are illustrated in Figures 5-10(a) and 5-10(b), respectively.

5.6 Simulation Method

The probability of exceedance of a certain limit state needed to construct the fragility curves can be calculated in different ways [31]. In the present study, a Monte Carlo method[2] is used. The Monte Carlo methods have the advantages of being applicable to almost any probability distribution and also of being free from complicated analytical algebra. These methods comprise the branch of experimental mathematics which is concerned with experiments on random numbers.

In the present Monte Carlo simulations, in addition to K_3 and u_1, the parameters required to fully describe a physically acceptable simulated pushover curve are the following:

$$K_{12} = K_1 - K_2\,, \qquad K_{23} = K_2 - K_3 \qquad \& \qquad u_{21} = u_2 - u_1 \tag{5.5}$$

Therefore, random samples for the 5 parameters K_{12}, K_{23}, K_3, u_1, and u_{21} of the pushover curve were generated using lognormal distribution. These 5 parameters are strictly positive which makes the choice of the lognormal distribution natural to adopt. From the mean

[2]For a complete discussion of the Monte Carlo methods, the reader is referred to the book by Kalos and Whitlock [78].

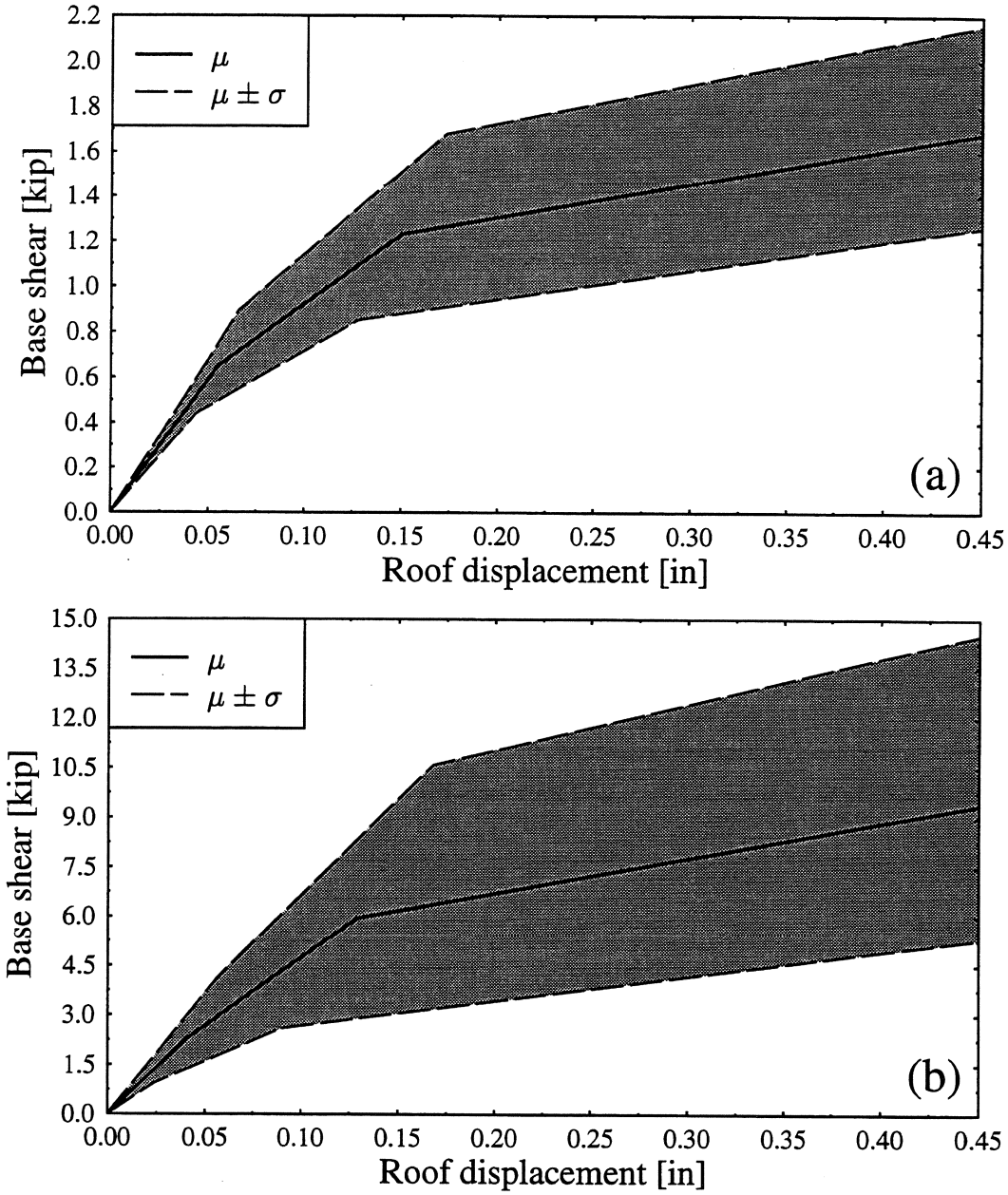

FIGURE 5-10 Range of variation of the pushover parameters for the trilinear approximate model; (a) Bare frame; (b) Infilled frame.

TABLE 5-III Random properties of additional parameters of the analyzed LRC frames.

Random parameter	Bare frame		Infilled frame	
	μ	σ	μ	σ
K_{12} [kip/in]	5.7	2.15	14.8	23.67
K_{23} [kip/in]	4.6	1.24	30.8	16.91
u_{21} [in]	0.095	0.025	0.089	0.042

values and COV's given in Table 5-II for the basic parameters K_1, K_2, K_3, u_1, and u_2 and using the definitions of the mean and variance of a linear function [4], one can easily obtain the results given in Table 5-III.

In the preliminary simulations, 4000 samples were generated, then it was realized that a much smaller number of samples was sufficient. Therefore, the results reported herein are for 200 simulations for each earthquake record.

5.7 Results

The fragility curves obtained for the bare and the infilled frames are shown in Figures 5-11(a) and 5-11(b), respectively. These curves were obtained by curve fitting the actual PF_{ij} and the obtained equations are given in the same figures. It should be noted that these fragility curves do not compromise any particular probability distribution of the results. The quality of the fitting is assessed by the coefficient r^2 which is the sum of the squares of the differences between the results of the equation and the actual data normalized by the number of data points.

Fragility curves with steep branches imply that the behavior of the structure is highly sensitive to changes in the seismic demand. On the other hand, a flat fragility curve implies a more desirable behavior. From the obtained fragility curves, the previous comments are clearly shown where flatter curves are obtained for the infilled frame than the bare one. Also, much lower values of the limit states needed to be specified for the infilled frame since the obtained roof displacements were much smaller than those of the bare frame. This implies that adding infill walls to the LRC bare frames should be an appropriate retrofitting scheme to limit the inter-story drift.

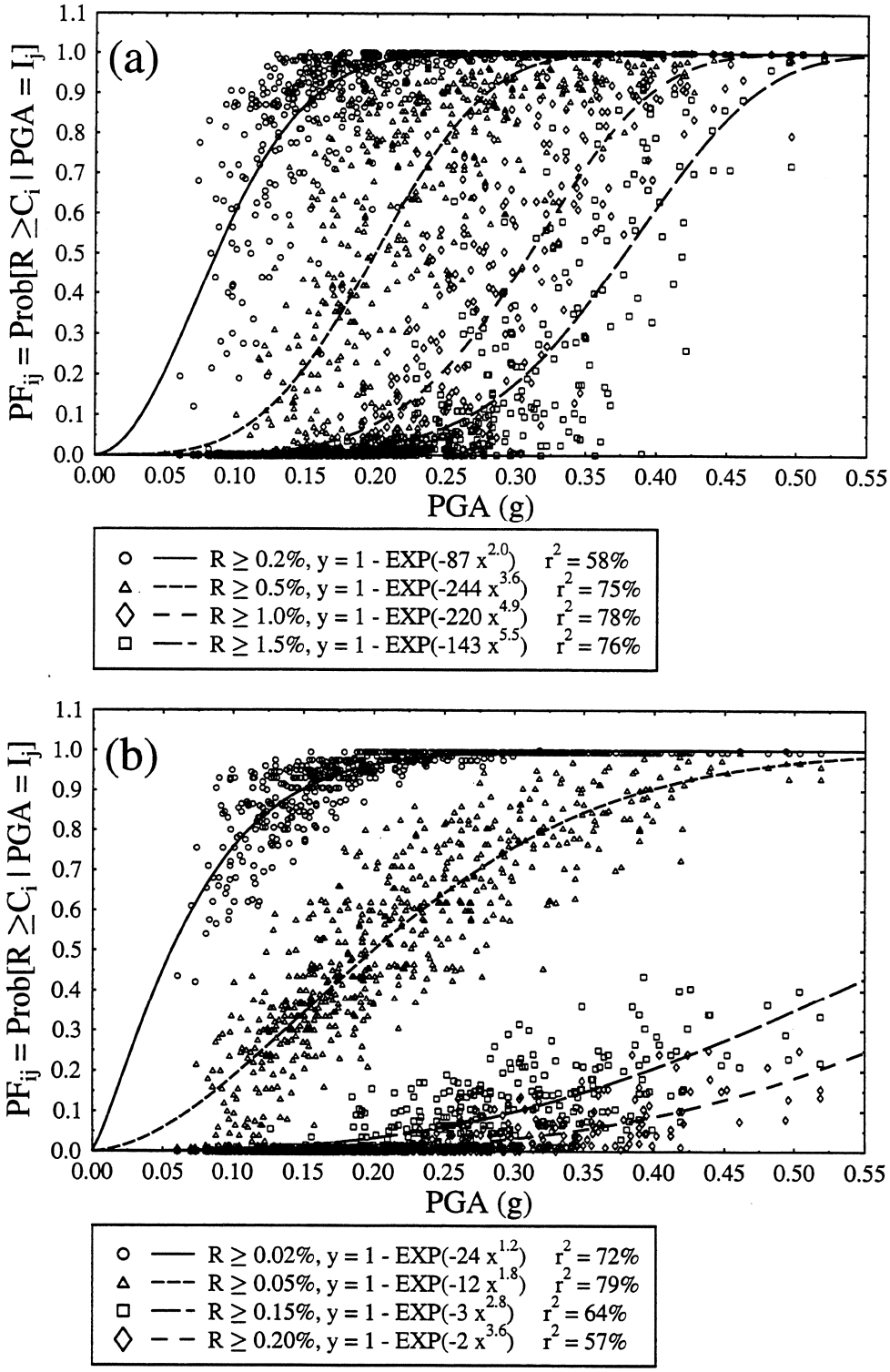

FIGURE 5-11 Fragility curves for the LRC frame; (a) Bare frame; (b) Infilled frame.

5.8 Summary

In this section, fragility analyses for the bare and the infilled LRC frames were performed. A simple computational model was adopted using the DPHM and results from a pushover analysis where the lateral load distribution is adapted to maintain the distribution which always corresponds to the first mode. This method was verified using detailed finite element analysis for the bare frame. The obtained fragility curves indicate that adding infill walls to low-rise frames reduces the likelihood of damage under the used synthetic earthquake records.

SECTION 6

CONCLUDING REMARKS

6.1 Summary and Conclusions

In this part of the study on the seismic behavior evaluation of infilled frames, improved approaches to analytical prediction of frame/wall behavior were developed. The expenditure required to experimentally investigate all the significant parameters in infilled structures is prohibitive. Motivated by this fact and without compromising any assumptions which may violate the fundamental attributes of behavior (see reports 1 and 2 of this series), attention was given to the development of appropriate computational strategies. By screening or prioritizing the different approaches in computational mechanics applied to masonry walls, three levels of details were identified and explored. The first was a micro-model where masonry was treated as a two-phase material consisting of the masonry units and the mortar joints representing planes of weakness for separation and sliding. The second was a meso-model where masonry was treated as a composite material with homogeneous properties obtained from homogenization theories, coupled with the smeared cracking approach. The third was a macro-model where equivalent trusses were used to replace the global effect of the infills on the bounding frame. All three levels were investigated and whenever applicable, comparisons were established. The major conclusions implied the superiority of the micro-models in capturing the fine details of the behavior and the capability of the meso-models to calibrate the macro-models rendering the latter an appropriate tool for accurate analysis and design purposes.

Numerical problems were encountered during the application of the meso-models to infilled frames. These problems were attributed to inherent deficiencies of the standard smeared cracking to cope with strain localization in softening media, particularly using the classical local continuum. Spurious modes were observed and obvious loss of uniqueness of the solution was detected. Two approaches were pursued to overcome these problems. In the first, an adaptive finite element technique was developed. This technique is based on the recently proposed superconvergent patch recovery method for linear problems, extended here to nonlinear problems. In these, the nonlinearities are due to smeared cracking and displacement discontinuities at the material interfaces. The second method, which is based on the evolution of the crack band width with the loading, utilizes the nonlocal character of the fracture energy density. Several problems were analyzed using this new formulation of the smeared cracking and the method proved to be superior over the standard formulation.

This study concludes with an application to improved predictions of structural fragility of infilled frames, as required in the estimation of the expected losses in urban areas due to severe earthquakes. Further simplification of the macro-model was performed using the dynamic plastic hinge method. This method was verified and its limitations identified

through detailed finite element analysis. Significant differences between the bare frames and the infilled frames were pointed out based on their fragility curves. The major conclusion was the feasibility of adding infill walls to the bare frames for the purpose of limiting the drifts, *i.e.* as a means of retrofitting.

6.2 Suggestions for Future Research

The present study (Parts I, II, and III), documented in reports 1, 2, and 3 of this series, fulfilled its objectives of establishing and evaluating the required experimental and computational strategies. Further application of the techniques should be pursued.

From a fundamental perspective, some advances may be accomplished to link the two techniques explored and developed in the present study, namely, discrete modeling and smeared crack modeling. The latter requires the use of either adaptive techniques or the evolutionary characteristic length method.

SECTION 7

REFERENCES

[1] H. Achyutha, R. Jagadish, P. S. Rao and S. S. Rahman, 'Finite element simulation of the elastic behaviour of infilled frames with openings', *Computers and Structures*, **23**, 5, 685-696 (1986).

[2] H. Achyutha, S. S. U. Rahman and Karisiddappa, 'Effect of position of openings on the behavior of infilled frames', *Proc. of the 8th Int. Brick and Block Masonry Conf.*, Dublin, Ireland, **2**, 1108-1121 (1988).

[3] American Society for Testing and Materials, *ASTM standards on masonry*, 1st edition, Philadelphia, Pennsylvania (1990).

[4] A. H-S. Ang and W. H. Tang, *Probability concepts in engineering planning and design: volume I-basic principles*, John Wiley & Sons, Inc., New York (1975).

[5] A. H-S. Ang and W. H. Tang, *Probability concepts in engineering planning and design: volume II-decision, risk, and reliability*, John Wiley & Sons, Inc., New York (1984).

[6] A. Anthoine, 'Research on unreinforced masonry at the joint research center of the European commission', *Proc. of the U.S.-Italy Workshop on Guidelines for Seismic Evaluation and Rehabilitation of Unreinforced Masonry Buildings*, D. P. Abrams and G. M. Calvi (eds.), *Technical Report NCEER-94-0021*, 3-3:3-15 (1994).

[7] A. Anthoine, 'Derivation of the in-plane elastic characteristics of masonry through homogenization theory', *Int. J. Solids Structures*, **32**, 2, 137-163 (1995).

[8] R. H. Atkinson, B. P. Amadei, S. Saeb and S. Sture, 'Response of masonry bed joints in direct shear', *J. Struct. Engrg.*, ASCE, **115**, 9, 2276-2296 (1989).

[9] G. Ayala and Y. Xianguo, 'Analytical evaluation of the structural seismic damage of reinforced concrete frames', *Proc. 7th Canadian Conf. Earthquake Engrg.*, Montreal, Quebec, Canada (1995).

[10] I. Babuška and W. C. Rheinboldt, '*A posteriori* error estimates for the finite element method', *Int. J. Numer. Methods Engrg.*, **12**, 1597-1615 (1978).

[11] I. Babuška and W. C. Rheinboldt, 'Adaptive approaches and reliability estimates in finite element analysis', *Comput. Methods Appl. Mech. Engrg.*, **17/18**, 519-540 (1979).

[12] I. Babuška, B. Szabó and I. N. Katz, 'The p-versions of the finite element method', *SIAM J. Numer. Anal.*, **18**, 515-545 (1981).

[13] I. Babuška and M. R. Dorr, 'Error estimates for the combined h and p versions of the finite element method', *Numer. Math.*, **25**, 257-277 (1981).

[14] I. Babuška, J. Chandra and J. E. Flaherty (eds.), *Adaptive computational methods for partial differential equations*, Society for Industrial and Applied Mathematics (SIAM), Philadelphia, Pennsylvania (1983).

[15] I. Babuška, O. C. Zienkiewicz, J. Gago and E. R. de A. Oliveira (eds.), *Accuracy estimates and adaptive refinements in finite element computations*, John Wiley & Sons, Chichester (1986).

[16] I. Babuška and M. Suri, 'The P and H-P versions of the finite element method, basic principle and properties', *SIAM Rev.*, **36**, 4, 578-632 (1994).

[17] K.-J. Bathe, *Finite element procedures in engineering analysis*, Prentice-Hall. Englewood Cliffs, New Jersey (1982).

[18] Z. P. Bažant and P. Gambarova, 'Rough cracks in reinforced concrete', *J. Struct. Div.*, ASCE, **106**, 4, 819-842 (1980).

[19] Z. P. Bažant, 'Crack band model for fracture of geomaterials', *Proc. 4th Int. Conf. on Numerical Methods in Geomechanics*, Edmonton, Alberta, Canada, Z. Eisenstein (ed.), **3**, 1137-1152 (1982).

[20] Z. P. Bažant and B. H. Oh, 'Crack band theory for fracture of concrete', *Material and Structures*, RILEM, **16**, 93, 155-177 (1983).

[21] Z. P. Bažant T. B. Belytschko and T.-P. Chang, 'Continuum theory for starin-softening', *J. Engrg. Mech.*, ASCE, **110**, 12, 1666-1692 (1984).

[22] Z. P. Bažant and F. Lin, 'Nonlocal smeared cracking model for concrete fracture', *J. Struct. Engrg.*, ASCE, **114**(11), 2493-2510, 1988.

[23] A. Bensoussan, J. L. Lions and G. Papanicolau, *Asymptotic analysis for periodic structures*, North Holland, Amsterdam (1978).

[24] A. B. Beres, 'Experimental and analytical evaluation of the performance of reinforced concrete frames with non-ductile details', *Ph.D. Dissertation*, Cornell University, Ithaca, New York (1994).

[25] T. Blacker and T. Belytschko, 'Superconvergent patch recovery with equilibrium and conjoint interpolant enhancements', *Int. J. Numer. Methods Engrg.*, **37**, 517-536 (1994).

[26] R. de Borst, 'Non-linear analysis of frictional materials', *Ph.D. Dissertation*, Delft Univ. of Techn., Delft, The Netherlands (1986).

[27] J. M. Bracci, 'Experimental and analytical study of seismic damage and retrofit of lightly reinforced concrete structures in low seismicity zones', *Ph.D. Dissertation* Department of Civil Engineering, State University of New York, Buffalo, New York (1992).

[28] C. A. Brebbia and M. H. Aliabadi (eds.), *Adaptive finite and boundary element methods*, Computational Mechanics Publications, Southampton, Elsevier Applied Science, London (1993).

[29] R. S. Bucy and P. D. Joseph, *Filtering for stochastic processes with applications to guidance*, Wiley (Interscience), New York, (1968).

[30] G. F. Carey, M. Sharma and K. C. Wang, 'A class of data structure for 2D and 3D adaptive mesh refinement', *Int. J. Numer. Methods Engrg.*, **26**, 2607-2622 (1988).

[31] F. Casciati and L. Faravelli, *Fragility analysis of complex structural systems*, Research Studies Press Ltd., England (1991).

[32] A. K. Chopra, *Dynamics of structures: theory and applications to earthquake engineering*, Prentice-Hall, Inc., Englewood Cliffs, New Jersy (1995).

[33] C. Z. Chrysostomou, 'Effects of degrading infill walls on the nonlinear seismic response of two-dimensional steel frames', *Ph.D. Dissertation*, Cornell University, Ithaca, New York (1991).

[34] Commission of the European Communities, 'Industrial processes, building and civil engineering, Eurocode No. 8, Structures in seismic regions, Part 2: Bridges', (draft), December (1990).

[35] Computech Engineering Services, 'COMBAT: Comprehensive Building Analysis Tool', Berkeley, California (1983).

[36] M. A. Crisfield, 'A fast incremental/iterative solution procedure that handles 'snap-through', *Computers and Structures*, **13**, 55-62 (1981).

[37] C. S. Desai, M. M. Zaman, J. G. Lightner and H. J. Siriwardane, 'Thin-layer element for interfaces and joints', *Int. J. for Numerical and Analytical Methods in Geomechanics*, **8**, 19-43 (1984).

[38] M. Dhanasekar and A. W. Page, 'Influence of brick masonry infill properties on the behaviour of infilled frames', *Proc. Instn. of Civ. Engrs.*, London, **81**, 593-605 (1986).

[39] DIANA 5.1 user's manual, TNO building and construction research, Rijswijk, The Netherlands (1993).

[40] DIANA programmer's manual, Course 5.0, TNO building and construction research, Rijswijk, The Netherlands (1993).

[41] A .R. Diaz, 'Optimization of finite element grids using interpolation error', *Ph.D. Dissertation*, The University of Michigan, Ann Arbor (1982).

[42] A. R. Diaz, N. Kikuchi and J. E. Taylor, 'A method of grid optimization for finite element methods', *Comput. Methods Appl. Mech. Engrg.*, **41**, 1, 29-45 (1983).

[43] N. J. Distéfano, 'Nonlinear processes in engineering', *Mathematics in Science and Engineering*, **110**, Academic Press, New York (1974).

[44] I. N. Doudoumis, E. N. Mitsopoulou and G. N. Nikolaidis, 'A macroelement for the simulation of the infill panels in multistorey frames under horizontal seismic actions', *Proc. 10th European Conf. on Earthquake Engrg.*, Duma (ed.), Balkema, Rotterdam, 1371-1376 (1995).

[45] R. G. Drysdale, R. V. Vanderkeyl and A. A. Hamid, 'Shear strength of brick masonry joints', *Proc. 5th Int. Brick Masonry Conf.*, Paper II-13, Washington, D. C., (1979).

[46] R. G. Drysdale, A. A. Hamid and L. R. Baker, *Masonry structures: behavior and design*, Prentice-Hall, Inc., Englewood Cliffs, New Jersy (1994).

[47] J. M. Duncan and C.-Y. Chang, 'Nonlinear analysis of stress and strain in soil', *J. Soil Mech. Found. Div.*, ASCE, **96**, SM5, 1629-1653 (1970).

[48] R. T. Eguchi and S. E. Chang, 'Losses associated with building damage in Memphis', *Proc. 11th World Conf. on Earthquake Engrg.*, Acapulco, Mexico (1996).

[49] A. G. El-Attar, 'A study on the behavior of lightly reinforced concrete buildings using small-scale models', *Ph.D. Dissertation*, Cornell University, Ithaca, New York (1991).

[50] S. El-Borgi, 'Seismic evaluation and strengthening of lightly reinforced concrete structures', *Ph.D. Dissertation*, Cornell University, Ithaca, New York (1993).

[51] M. H. El Hadad, 'Finite element analysis of infilled frames considering cracking and separation phenomena', *Computers and Structures*, **41**, 3, 439-447 (1991).

[52] B. Ellingwood and H. Hwang, 'Probabilistic descriptions of resistance of safety-related structures in nuclear plants', *Nuclear engineering and design*, **88**, 169-178 (1985).

[53] A. C. Eringen and D. G. B. Edelen, 'On nonlocal elasticity', *Int. J. Engng. Sci.*, **10**, 233-248 (1972).

[54] J. D. Eshelby, 'The determination of elastic field of an ellipsoidal inclusion and related problems', *Proc. Roy. Soc.*, **A241**, 376-396 (1957).

[55] P. H. Feenstra, 'Computational aspects of biaxial stress in plain and reinforced concrete', *Ph.D. Dissertation*, Delft Univ. of Techn., Delft, The Netherlands (1993).

[56] R. C. Fenwick and T. Paulay, 'Mechanisms of shear resistance of concrete beams', *J. Struct. Engrg.*, ASCE, **94**, ST10, 2325-2350 (1968).

[57] J. Fish, 'The s-version of the finite element method', *Computers and Structures*, **43**, 3, 539-547 (1992).

[58] G. H. Golub and C. F. van Loan, *Matrix computations*, 2nd edition, Johns Hopkins University Press (1989).

[59] L. Gambarotta and S. Lagomarsino, 'A microcrack damage model for brittle materials', *Int. J. Solids and Structures*, **30**, 2, 177-198 (1993).

[60] P. Gergely, 'Seismic fragility of reinforced concrete structures and components for application to nuclear facilities', *Technical report NUREG/CR-4123 UCID-20164*, Lawrence Livermore National Laboratory, Livermore, California (1985).

[61] P. Gergely and R. O. Hamburger, 'Simplified methods for evaluation of rehabilitated buildings', *Proc. of the U.S.-Italy Workshop on Guidelines for Seismic Evaluation and Rehabilitation of Unreinforced Masonry Buildings*, D. P. Abrams and G. M. Calvi (eds.), *Technical Report NCEER-94-0021*, 4-3:4-16 (1994).

[62] J. Ghaboussi, E. L. Wilson and J. Isenberg, 'Finite element for rock joints and interfaces', *J. Soil Mech. and Found. Div.*, ASCE, **99**, SM10, 833-848 (1973).

[63] R. E. Goodman, R. L. Taylor and T. L. Brekke, 'A model for the mechanics of jointed rock', *J. Soil Mech. and Found. Div.*, ASCE, **94**, SM3, 637-659 (1968).

[64] P. Guo, 'Investigation and modelling of the mechanical properties of masonry', *Ph.D. Dissertation*, McMaster University, Hamilton, Canada (1991).

[65] G. A. Hegemier, S. K. Arya, G. Krishnamoorthy, W. Nachbar and R. Furgerson, 'On the behavior of joints in concrete masonry', *Proc. North Amer. Masonry Conf.*, Boulder, Colorado, 4-1:4-22, August (1978).

[66] M. A. N. Hendriks, 'Identification of elastic properties by numerical-experimental method', *Heron*, **36**, 2, 17-26 (1991).

[67] A. Hillerborg, M. Modéer and P. E. Petersson, 'Analysis of crack formation and crack growth in concrete by means of fracture mechanics and finite elements', *Cement and Concrete Research*, **6**, 6, 773-782 (1976).

[68] H. K. Hilsdorf and W. Brameshuber, 'Size effects in the experimental determination of fracture mechanics parameters', *Application of Fracture Mechanics to Cementitious Composites*, S. P. Shah (ed.), Martinus Nijhoff Publ., Dordrecht, 361-397 (1985).

[69] E. Hinton and J. S. Campbell, 'Local and global smoothing of discontinuous finite element functions using a least squares method', *Int. J. Numer. Methods Engrg.*, **8**, 461-480 (1974).

[70] D. A. Hordijk, 'Tensile and tensile fatigue behaviour of concrete; experiments, modelling and analyses', *Heron*, **37**, 1 (1992).

[71] J.-R. Huo and H. Hwang, 'Fragility of Memphis buildings', *Proc. 11th World Conf. on Earthquake Engrg.*, Acapulco, Mexico (1996).

[72] H. H. Hwang and J-R. Huo, 'Generation of hazard consistent fragility curves for seismic loss estimation studies', *Technical Report NCEER-94-0015*, State University of New York at Buffalo (1994).

[73] R. H. Iding, K. S. Pister and R. L. Taylor, 'Identification of non-linear elastic solids by a finite element method', *Comput. Methods Appl. Mech. Engrg.*, **4**, 121-142 (1974).

[74] C. Johnson and P. Hansbo, 'Adaptive finite element methods in computational mechanics', *Comput. Methods Appl. Mech. Engrg.*, **101**, 143-181 (1992).

[75] C. Johnson and P. Hansbo, 'Adaptive finite element methods for small strain elastoplasticity', *Finite inelastic deformations - Theory and applications*, D. Besdo and S. Stein (eds.), Springer, Berlin, 273-288 (1992).

[76] R. E. Kalman, 'A new approach to linear filtering and prediction', *Trans. ASME. Ser. D, J. Basic. Engrg.*, **82**, 35-45 (1960).

[77] R. E. Kalman and R. S. Bucy, 'New results in linear filtering and prediction theory', *Trans. ASME. Ser. D, J. Basic. Engrg.*, **83**, 95-107 (1961).

[78] M. H. Kalos and P. A. Whitlock, *Monte Carlo methods volume I: basics*, John Wiley & Sons, Inc., New York (1986).

[79] M. F. Kanninen and C. H. Popelar, *Advanced fracture mechanics*, Oxford University Press, New York (1985).

[80] T. Karamanski, 'Calculating infilled frames by the method of finite elements', *Symposium on tall buildings*, A. Coull and B. Stafford-Smith (eds.), Pergamon Press (1967).

[81] K. T. Kavanagh and R. W. Clough, 'Finite element applications in the characterization of elastic solids', *Int. J. Solids Structures*, **7**, 11-23 (1971).

[82] W. Kim, 'Shear-critical cracks in reinforced concrete beams without web reinforcement: their initiation and propagation', *Ph.D. Dissertation*, Cornell University, Ithaca, New York (1987).

[83] G. J. W. King and P. C. Pandey, 'The analysis of infilled frames using finite elements', *Proc. Instn. of Civ. Engrs.*, London, **65**, 749-760 (1978).

[84] R. E. Klingner, 'Mathematical modeling of infilled frames', *Reinforced Concrete Structures Subjected to Wind and Earthquake Forces*, Amer. Concrete Inst., SP-63, 1-25 (1980).

[85] A. S. Kobayashi, N. M. Hawkins, D. B. Barker and B. M. Liaw, 'Fracture process zone of concrete', *Application of Fracture Mechanics to Cementitious Composites*, S. P. Shah (ed.), Martinus Nijhoff Publ., Dordrecht, 25-50 (1985).

[86] G. Kost and W. Weaver, Jr., 'Nonlinear dynamic analysis of frames with filler panels', *J. Struct. Engrg.*, ASCE, **100**, ST4, 743-757 (1974).

[87] C. S. Krishnamoorthy and K. R. Umesh, 'Adaptive mesh refinement for two-dimensional finite element stress analysis', *Computers and Structures*, **48**, 1, 121-133 (1993).

[88] M. Krizek and P. Neittaanmakior, 'On superconvergence techniques', *Acta Appl. Meth.*, **9**, 175-198 (1987).

[89] F. H. Kulhawy, 'Stress deformation properties of rock and rock discontinuities', *Engrg. geol.*, **9**, 327-350 (1975).

[90] P. Ladeveze, G. Coffignal and J. P. Pelle, 'Accuracy of elastoplastic and dynamic analysis', *Accuracy estimates and adaptive refinements in finite element computations*, I. Babuška, O. C. Zienkiewicz, J. Gago and E. R. de A. Oliveira (eds.), John Wiley & Sons, Chichester, 181-203 (1986).

[91] N.-S. Lee and K.-J. Bathe, 'Error indicators and adaptive remeshing in large deformation finite element analysis', *Finite Elem. Anal. Design*, **16**, 99-139 (1994).

[92] M. Lafuente and C. Genatios, 'Analytical studies of masonry walls subjected to monotonic lateral loads', *Proc. 10th European Conf. on Earthquake Engrg.*, Duma (ed.), Balkema, Rotterdam, 1751-1756 (1995).

[93] J. X. Liang, G. N. Pande and J. Middleton, 'Derivation of elastic parameters for masonry', *Numerical Methods in Engineering: Theory and Applications (NUMETA90)*, G. N. Pande and J. Middleton (eds.), **2**, Elsevier Applied Science, London, 844-853 (1990).

[94] T. C. Liauw, 'Elastic behavior of infilled frames', *Proc. Instn. of Civ. Engrs.*, London, **46**, 343-349 (1970).

[95] T. C. Liauw and K. H. Kwan, 'Non-linear analysis of multistory infilled frames', *Proc. Instn. of Civ. Engrs.*, Part 2, **73**, 441-454 (1982).

[96] T. C. Liauw and K. H. Kwan, 'Nonlinear behaviour of non-integral infilled frames', *Computers and Structures*, **18**, 3, 551-560 (1984).

[97] T. C. Liauw and K. H. Kwan, 'Plastic design of infilled frames', *Proc. Instn. of Civ. Engrs.*, Part 2, Technical Note, **77**, 367-377 (1984).

[98] T. C. Liauw and K. H. Kwan, 'Static and cyclic behaviours of multistory infilled frames with different interface conditions', *Journal of Sounds and Vibrations*, **99**, 2, 275-283 (1985).

[99] R. W. Litton, 'A contribution to the analysis of concrete structures under cyclic loading', *Ph.D. Dissertation*, Univ. of California, Berkeley (1974).

[100] H. R. Lotfi and P. B. Shing, 'Interface model applied to fracture of masonry structures', *J. Struct. Engrg.*, ASCE, **120**, 1, 63-80 (1994).

[101] H. R. Lotfi and P. B. Shing, 'Embedded representation of fracture in concrete with mixed finite elements', *Int. J. Numer. Methods Engrg.*, **38**, 1307-1325 (1995).

[102] P. B. Lourenço, 'Computational strategies for masonry structures', *Ph.D. Dissertation*, Delft Univ. of Techn., Delft, The Netherlands (1996).

[103] J. Mackerle, 'Mesh generation and refinement for FEM and BEM - A bibliography (1990-1993)', *Finite Elem. Anal. Design*, **15**, 2, 177-188 (1993).

[104] J. Mackerle, 'Error analysis, adaptive techniques and finite and boundary elements - A bibliography (1992-1993)', *Finite Elem. Anal. Design*, **17**, 3, 231-246 (1994).

[105] G. Maier, A. Nappi and E. Papa, 'Damage models for masonry as a composite material: a numerical and experimental analysis', *Constitutive laws for engineering materials*, C. S. Desai, E. Krempl, G. Frantziskonis and H. Saadatmanesh (eds.), ASME Press, New York, 427-432 (1991).

[106] D. V. Mallick and R. T. Severn, 'The behavior of infilled frames under static loading', *Proc. Instn. of Civ. Engrs.*, London, England, **38**, 639-656 (1967).

[107] D. V. Mallick and R. P. Garg, 'Effect of openings on the lateral stiffness of infilled frames', *Proc. Instn. of Civ. Engrs.*, London, England, **49**, 193-209 (1971).

[108] H. D. McNiven and Y. Mengi, 'A mathematical model for the linear dynamic behavior of two phase periodic materials', *Int. J. Solids Structures*, **15**, 271-280 (1979).

[109] H. D. McNiven and Y. Mengi, 'A mixture theory for elastic laminated composites', *Int. J. Solids Structures*, **15**, 281-302 (1979).

[110] H. D. McNiven and Y. Mengi, 'Propagation of transient waves in elastic laminated composites', *Int. J. Solids Structures*, **15**, 303-318 (1979).

[111] A. B. Mehrabi, P. B. Shing, M. P. Schuller and J. L Noland, 'Performance of masonry-infilled R/C frames under in-plane lateral loads', *Report CU/SR-94/6 Struct. Engrg. and Struct. Mech. Research Series*, Dept. of Civil, Environ. and Arch. Engrg., University of Colorado at Boulder (1994).

[112] R. Meli, 'Seismic behavior of masonry walls' (in Spanish), *Research Report*, Institute of Engineering, UNAM, Mexico (1979).

[113] R. J. Melosh and P. V. Marcal, 'An energy basis for mesh refinement of structural continua', *Int. J. Numer. Methods Engrg.*, **11**, 1083-1091 (1977).

[114] Y. Mengi, H. Sucuoglu and H. D. McNiven, 'A linear mathematical model for the seismic inplane behaviour of brick masonry walls part 1: Theoretical consideration', *Earthquake Engrg. Struct. Dyn.*, **12**, 313-326 (1984).

[115] J. G. M. van Mier, M. B. Nooru-Mohamed and G. Timmers, 'An experimental study of shear fracture and aggregate interlock in cementbased composites', *Heron*, **36**, 4 (1991).

[116] T. Mori and K. Tanaka, 'Average stress in the matrix and average elastic energy of materials with misfitting inclusions', *Acta Metallurgica*, **21**, 571-574 (1973).

[117] K. M. Mosalam and G. H. Paulino, 'Evolutionary characteristic length method for smeared cracking finite element models', *Finite Elem. Anal. Design* (in press).

[118] P. S. Natarajan and R. K. Wen, 'Effect of walls on structural response to earthquakes', *ASCE National Structural Engineering Meeting*, Portland, Oregon, Preprint 1155, 1-24 (1970).

[119] H. G. Natke (ed.), *Applications of system identification in engineering*, Springer-Verlag, Berlin (1988).

[120] A. H. Nilson *et al.* (eds.), *State-of-the-art report: Finite element analysis of reinforced concrete*, ASCE, New York (1982).

[121] A. K. Noor and I. Babuška, 'Quality assessment and control of finite element solutions', *Finite Elem. Anal. Design*, **3**, 1, 1-26 (1994).

[122] J. P. Norton, *An introduction to identification*, Academic Press, New York (1986).

[123] J. T. Oden and L. Demkowicz, 'Chapter 13: Advances in adaptive improvements - A survey of adaptive finite element methods in computational mechanics', In *State-of-the-art surveys on computational mechanics*, A. K. Noor and T. J. Oden (eds.), The American Society of Mechanical Engineers (ASME), New York, 441-467 (1989).

[124] J. Oliver, 'Consistent characteristic length for smeared cracking models', *Int. J. Numer. Methods Engrg.*, **28**, 461-474 (1989).

[125] E. Oñate and G. Bugeda, 'A study of mesh optimality criteria in adaptive finite element analysis', *Engng. Computations*, **10**, 4, 307-321 (1993).

[126] D. R. J. Owen, D. Perić, E. A. de Souza Neto, Jianguo Yu and M. Dutko, 'Advanced computational strategies for 3-D large scale metal forming simulations', *Proc. 5th Int. Conf. on Numer. Methods in Industrial Forming Processes - NUMIFORM'95*, S.-F. Shen and P. R. Dawson (eds.), Ithaca, New York, 18-21 June, 7-22 (1995).

[127] J. Pamin, 'Gradient-dependent plasticity in numerical simulation of localization phenomena', *Ph.D. Dissertation*, Delft Univ. of Techn., Delft, The Netherlands (1994).

[128] G. N. Pande, J. X. Liang and J. Middleton, 'Equivalent elastic moduli for brick masonry', *Comp. Geothec.*, **8**, 243-265 (1989).

[129] E. Papa, 'About damage mechanics with particular reference to masonry' (in Italian), *Ph.D. Dissertation*, Politecnico di Milan, Italy (1990).

[130] T. Paulay and P. J. Loeber, 'Shear transfer by aggregate interlock', *ACI special publ.*, SP-42, **I**, Shear in reinforced concrete, 1-16 (1974).

[131] G. H. Paulino, 'Novel formulations of the boundary element method for fracture mechanics and error estimation', *Ph.D. Dissertation*, Cornell University, Ithaca, New York (1995).

[132] D. Perić, J. Yu and D. R. J. Owen, 'On error estimates and adaptivity in elastoplastic solids: Applications to the numerical simulation of strain localization in classical and Cosserat continua', *Int. J. Numer. Methods Engrg.*, **37**, 1351-1379 (1994).

[133] S. P. Pessiki, Experimental investigation of the behavior of lightly-reinforced concrete column and beam-column joint details subjected to seismic loading, *Ph.D. Dissertation*, Cornell University, Ithaca, New York (1990).

[134] S. Pietruszczak, 'On mechanics of jointed media: Masonry and related problems', *Computer Methods and Advances in Geomechanics*, G. Beer, J. R. Booker and J. P. Carter (eds.), **1**, Brookfield, 407-413 (1991).

[135] S. Pietruszczak and X. Niu, 'A mathematical description of macroscopic behaviour of brick masonry', *Int. J. Solids Structures*, **29**, 5, 531-546 (1992).

[136] M. E. Plesha, R. Ballarini and A. Parulekar, 'Constitutive model and finite element procedure for dilatant contact problems', *J. Engrg. Mech.*, ASCE, **115**, 12, 2649-2668 (1989).

[137] R. van der Pluijm, 'Shear behaviour of bed joints', *Proc. 6th North American Masonry Conf.*, Philadelphia, Pennsylvania, **1**, 125-136 (1993).

[138] R. L. Pook, M. A. Stylianou and J. L. Dawe, 'Experimental investigation of the influence of compression on the shear strength of masonry joints', *Proc. 4th Conc. Masonry Symp.*, Fredericton, NB, Canada (1986).

[139] Y. R. Rashid, 'Analysis of prestressed concrete pressure vessels', *Nuclear Engineering and Design*, **29**, 4, 334-344 (1968).

[140] H. E. Read and G. A. Hegemier, 'Strain softening of rock, soil and concrete - A review article', *Mechanics of Materials*, **3**, 4, 271-294 (1984).

[141] J. Reflak and P. Fajfar, 'Elastic analysis of infilled frames using substructures', *Proc. 6th Canadian Conf. Earthquake Engrg.*, Toronto, 285-292 (1991).

[142] H. W. Reinhardt, 'Fracture mechanics of an elastic softening material like concrete', *Heron*, **29**, 2 (1984).

[143] W. C. Rheinboldt, 'Error estimates for nonlinear finite element computations', *Computers and Structures*, **17**, 1-3, 91-98 (1985).

[144] J. R. Riddington and B. Stafford-Smith, 'Analysis of infilled frames subjected to racking with design recommendations', *Structural Engineer*, **55**, 6, 263-268 (1977).

[145] J. R. Riddington, 'The influence of initial gaps on infilled frame behaviour', *Proc. Instn. of Civ. Engrs.*, Part 2, **77**, 295-310 (1984).

[146] H. R. Riggs and G. H. Powell, 'Rough crack model for analysis of concrete', *J. Engrg. Mech.*, ASCE, **112**, 5, 448-464 (1986).

[147] E. Riks, 'An incremental approach to the solution of snapping and buckling problems', *Int. J. Solids and Structures*, **15**, 529-551 (1979).

[148] C. E. Rivero and W. H. Walker, 'A model to study the interaction of frames and infill masonry walls', *Proc. of the 3rd North American Masonry Conf.*, 76:1-76:14 (1982).

[149] J. G. Rots, 'Computational modeling of concrete fracture', *Ph.D. Dissertation*, Delft Univ. of Techn., Delft, The Netherlands (1988).

[150] J. G. Rots, 'Numerical simulation of cracking in structural masonry', *Heron*, **36**, 2, 49-63 (1991).

[151] E. Sanchez-Palencia, 'Local and macroscopic behavior of a physical and hetrogeneous type of media' (in French), *Int. J. Engng. Sci.*, **12**, 331-351 (1974).

[152] E. Sanchez-Palencia, 'Non-homogeneous media and vibration theory', Homogenization techniques for composite media, *Lecture notes in physics, no. 127*, Springer-Verlag, Berlin (1980).

[153] T. Stankowski, K. Runesson and S. Sture, 'Fracture and slip of interfaces in cementitious composites. I: Characteristics', *J. Engrg. Mech.*, ASCE, **119**, 2, 292-314 (1993).

[154] T. Stankowski, K. Runesson and S. Sture, 'Fracture and slip of interfaces in cementitious composites. II: Implementation', *J. Engrg. Mech.*, ASCE, **119**, 2, 315-327 (1993).

[155] T. Strouboulis and K. A. Haque, 'Recent experiences with error estimation and adaptivity, Part I: Review of error estimators for scalar elliptic problems', *Comput. Methods Appl. Mech. Engrg.*, **97**, 3, 399-436 (1992).

[156] T. Strouboulis and K. A. Haque, 'Recent experiences with error estimation and adaptivity, Part II: Error estimation for h-adaptive approximations on grids of triangles and quadrilaterals', *Comput. Methods Appl. Mech. Engrg.*, **100**, 3, 359-430 (1992).

[157] H. Sucuoglu, Y. Mengi and H. D. McNiven, 'A linear mathematical model for the seismic inplane behaviour of brick masonry walls part 2: Determination of model parameters through optimization using experimental data', *Earthquake Engrg. Struct. Dyn.*, **12**, 327-346 (1984).

[158] P.-M. Suquet, 'Elements of homogenization for inelastic solid mechanics', In *Homogenization techniques for composite medias*, E. Sanchez-Palencia and A. Zaoui (eds.), Springer, 193-279 (1987).

[159] B. Szabó and I. Babuška, *Finite Element Analysis*, John Wiley & Sons, New York (1991).

[160] H. P. J. Taylor, 'The fundamental behavior of reinforced concrete beams in bending and shear', *ACI special publ.*, SP-42, **I**, Shear in reinforced concrete, 42-3, 43-78 (1974).

[161] V. Thiruvengadam, 'On the natural frequency of infilled frames', *Earthquake Engrg. Struct. Dyn.*, **13**, 401-419 (1985).

[162] M. E. Thurston, 'Influence of residual stresses on ceramic-metal interfacial toughness', *Ph.D. Dissertation*, Cornell University, Ithaca, New York (1994).

[163] D. A. Wesley and P. S. Hashimoto, 'Seismic structural fragility investigation for the Zion nuclear power plant', *Technical report NUREG/CR-2320 UCID-15380*, Lawrence Livermore National Laboratory, Livermore, California (1981).

[164] R. N. White and M. J. Holley, 'Experimental study of membrane shear transfer + discussion', *J. Struct. Engrg.*, ASCE, **98/99**, ST8/7, 1835-1852/1664-1665 (1972/1973).

[165] N.-E. Wiberg and F. Abdulwahab, 'Patch recovery based on superconvergent derivatives and equilibrium', *Int. J. Numer. Methods Engrg.*, **36**, 2703-2724 (1993).

[166] M. S. Williams and R. G. Sexsmith, 'Seismic damage indices for concrete structures: A state-of-the-art review', *Earthquake SPECTRA*, **11**, 2, 319-349 (1995).

[167] T. C. Yong, 'Shear strength of masonry infilled panels in steel frames', *M.Sc. Thesis*, University of New Brunswick, Canada (1984).

[168] J. Z. Zhu, E. Hinton and O. C. Zienkiewicz, 'Mesh enrichment against mesh regeneration using quadrilateral elements', *Comm. Numer. Methods Engrg.*, **9**, 547-554 (1993).

[169] O. C. Zienkiewicz and J. Z. Zhu, 'A simple error estimator and adaptive procedure for practical engineering analysis', *Int. J. Numer. Methods Engrg.*, **24**, 337-357 (1987).

[170] O. C. Zienkiewicz and R. L. Taylor, *The finite element method (4th edition): Volume 1, Basic formulation and linear problems*, Mc-Graw Hill, Berkshire, England, UK (1989).

[171] O. C. Zienkiewicz and R. L. Taylor, *The Finite Element Method (4th edition): Volume 2, Solid and fluid mechanics, dynamics and non-linearity*, Mc-Graw Hill, Berkshire, England (1991).

[172] O. C. Zienkiewicz and J. Z. Zhu, 'The superconvergent patch recovery and *a posteriori* error estimates. Part 1: The recovery technique', *Int. J. Numer. Methods Engrg.*, **33**, 7, 1331-1364 (1992).

[173] O. C. Zienkiewicz and J. Z. Zhu, 'The superconvergent patch recovery and *a posteriori* error estimates. Part 2: Error estimates and adaptivity', *Int. J. Numer. Methods Engrg.*, **33**, 7, 1365-1382 (1992).

[174] O. C. Zienkiewicz and J. Z. Zhu, 'Letter to the editor: the SPR recovery and boundaries', *Int. J. Numer. Methods Engrg.*, **37**, 18, 3195-3196 (1994).

Appendix A

Derivation of Equivalent Elastic Properties of Masonry

A.1 Vertical Direction

From Figure 3-2(c), one can write

$$\epsilon_{com} = \frac{\sigma_{com}}{E_{com}} = \frac{\Delta_{com}}{h_b + t_{mb}} \tag{A.1}$$

where subscript (com) stands for the composite material and Δ is the deformation of the unit under the applied load. The stresses, strains and modulus of elasticity are denoted by σ, ϵ, and E, respectively. The first equality in the previous equation comes from Hooke's law where lateral stresses from Poisson's effect are ignored. Defining an apparent cross sectional area A_{com} of the composite, one has

$$E_{com} = \frac{h_b + t_{mb}}{A_{com}} \frac{F_v}{\Delta_{com}} \tag{A.2}$$

For *equilibrium*

$$F_v = \sigma_{mb}(l_b + t_{mh})t_b = \frac{\Delta_{mb}}{t_{mb}} E_m (l_b + t_{mh})t_b$$

where E_m is the modulus of elasticity for mortar and Δ_{mb} is the shortening of the mortar bed joint due to the vertical load F_v. Substituting in Eq. (A.2), one obtains

$$E_{com} = \frac{(h_b + t_{mb})(l_b + t_{mh})t_b E_m}{A_{com}} \frac{\Delta_{mb}}{t_{mb}\Delta_{com}} \tag{A.3}$$

Once again, for equilibrium

$$F_v = \sigma_{mb}(l_b + t_{mh})t_b = \sigma_{mh} t_{mh} l_{mh} + \sigma_b l_b t_b$$

For *compatibility*, we have $\epsilon_b = \epsilon_{mh}$. Therefore, from Hooke's law and considering that E_b is the modulus of elasticity for blocks, we obtain

$$E_m \epsilon_{mb}(l_b + t_{mh})t_b = \epsilon_{mh}\left[E_m t_{mh} l_{mh} + E_b l_b t_b\right]$$

Accordingly,

$$\frac{\epsilon_{mb}}{\epsilon_{mh}} = \frac{E_m t_{mh} l_{mh} + E_b l_b t_b}{E_m (l_b + t_{mh}) t_b}$$

Since,

$$\frac{\Delta_{com}}{\Delta_{mb}} = \frac{\Delta_{mb} + \Delta_{mh}}{\Delta_{mb}} = 1 + \frac{\epsilon_{mh}}{\epsilon_{mb}} \frac{h_b}{t_{mb}}$$

therefore,

$$\frac{\Delta_{com}}{\Delta_{mb}} = \frac{E_m t_{mh} l_{mh} t_{mb} + E_b l_b t_b t_{mb} + E_m t_b (l_b + t_{mh}) h_b}{t_{mb} \left[E_m t_{mh} l_{mh} + E_b l_b t_b \right]}$$

Substituting in Eq. (A.3), one obtains the expression given by Eq. (3.2) for the equivalent Young's modulus in the vertical direction.

A_{com} can be obtained from Eq. (3.2) by the following substitution

$$E_{com} = E_m = E_b$$

A.2 Horizontal direction

Considering the horizontal direction which is shown in Figure 3-2(d), we can write

$$\epsilon_{com} = \frac{\sigma_{com}}{E_{com}} = \frac{\Delta_{com}}{l_b + t_{mh}}$$

Similar assumptions and notations as for the vertical direction are adopted for the horizontal direction. Accordingly,

$$E_{com} = \frac{l_b + t_{mh}}{A_{com}} \frac{F_h}{\Delta_{com}} \tag{A.4}$$

For *equilibrium*,

$$F_h = \sigma_{mb} t_{mb} t_b + \sigma_{mh} h_b l_{mh} = \frac{\Delta_{mb}}{l_b + t_{mh}} E_m t_{mb} t_b + \frac{\Delta_{mh}}{h_b} E_m h_b l_{mh}$$

Substituting in Eq. (A.4),

$$E_{com} = \frac{(l_b + t_{mh})E_m}{A_{com}} \left[\frac{t_{mb}t_b}{l_b + t_{mh}} + \frac{\Delta_{mh}h_b l_{mh}}{t_{mh}\Delta_{com}} \right] \tag{A.5}$$

For *compatibility*,

$$\Delta_{com} = \Delta_{mb} = \Delta_{mh} + \Delta_b$$

Accordingly,

$$\frac{\Delta_{com}}{\Delta_{mh}} = 1 + \frac{\Delta_b}{\Delta_{mh}} = 1 + \frac{\epsilon_b l_b}{\epsilon_{mh} t_{mh}}$$

Once again, for equilibrium

$$\sigma_{mh} l_{mh} = \sigma_b t_b$$

From the previous relations and applying Hooke's law, after some simplifications, one obtains the expressions given by Eqs. (3.5) and (3.6) for the equivalent Young's modulus in the horizontal direction and the corresponding apparent cross sectional area.

Appendix B

Fracture Energy and Damage Mechanics

In this appendix, a relation between the apparent fracture energy density (g^t) and a measure of the material damage (ω) introduced by smeared cracking is presented. Assuming elastic unloading (Eq. (4.22)) and using the stress-crack strain relation given by Eq. (4.19) with the definition of Eq. (4.61), one may easily show that

$$g^t = f_t \epsilon_{cr}^t - C\Lambda^k \left(\epsilon_{cr}^t\right)^{k+1} \tag{B.1}$$

For simplicity and without loss of generality, k is assumed to be 1, *i.e.* linear softening. Accordingly

$$g^t = \epsilon_{cr}^t f_t \left(1 - \frac{f_t \Lambda}{4\mathcal{G}_f} \epsilon_{cr}^t\right) \tag{B.2}$$

The local form of the stress-strain law in the principal direction (1, 2), with direction 1 being normal to the cracking plane, can be written for plain stress idealization as

$$\begin{Bmatrix} \epsilon_{11} \\ \epsilon_{22} \\ \gamma_{12} \end{Bmatrix} = \frac{1}{E} \begin{bmatrix} 1 & -\nu & 0 \\ -\nu & 1 & 0 \\ 0 & 0 & 2(1+\nu)/\beta \end{bmatrix} \begin{Bmatrix} \sigma_{11} \\ \sigma_{22} \\ \tau_{12} \end{Bmatrix} + \begin{Bmatrix} \epsilon_{cr} \\ 0 \\ 0 \end{Bmatrix} \tag{B.3}$$

$$= \frac{1}{E} \begin{bmatrix} 1/(1-\omega) & -\nu & 0 \\ -\nu & 1 & 0 \\ 0 & 0 & 2(1+\nu)/\beta \end{bmatrix} \begin{Bmatrix} \sigma_{11} \\ \sigma_{22} \\ \tau_{12} \end{Bmatrix} \tag{B.4}$$

where E is Young's modulus, ν is Poisson's ratio and ϵ_{cr} is the crack strain. The superscript t indicating the load level is dropped for simplicity but should be understood from the context. The parameters ω and β are measures of the degree of damage in the normal and tangential directions of the crack. β is the well-know shear retention factor and is not of any concern in the present derivation. On the other hand, ω varies according to the level of damage introduced by smeared cracking from $\omega = 0$ (no damage) to $\omega = 1$ (complete damage). Focusing our attention only to the normal direction of the crack, one obtains from Eqs. (B.3) and (B.4)

$$\epsilon_{cr} = \frac{\sigma_{11}}{E} \left(\frac{\omega}{1-\omega}\right) \tag{B.5}$$

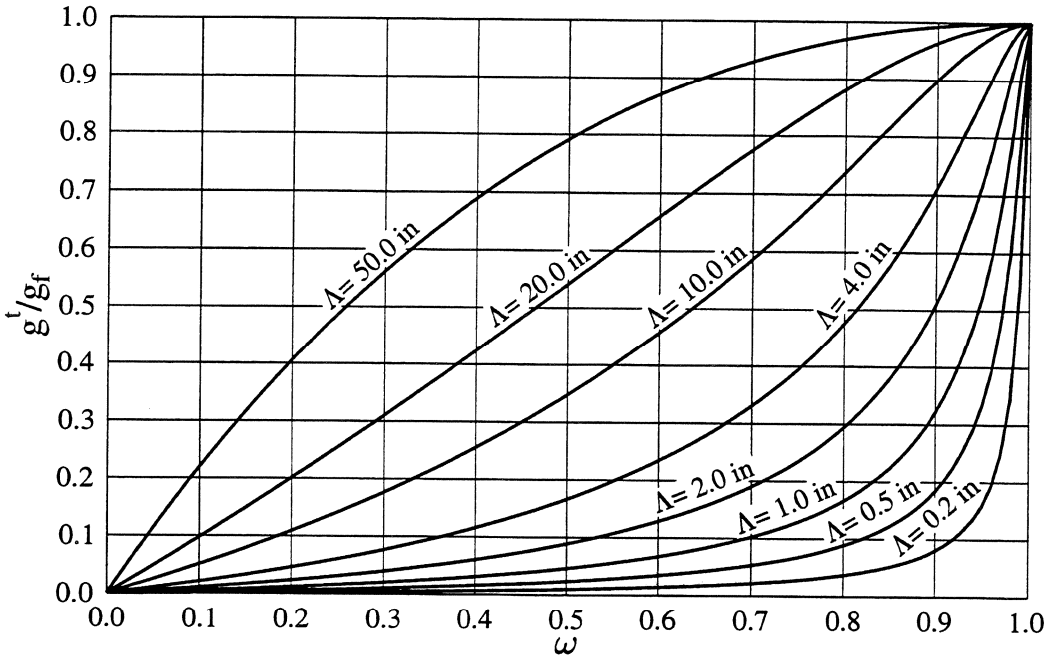

FIGURE B-1 Relation between damage parameter and apparent fracture energy density for different value of the crack band width.

It is assumed that the relation s-ϵ_{cr} is almost the same as the relation σ_{11}-ϵ_{cr} which implies that $\beta \approx 0.0$. Accordingly using Eq. (4.19) for $k = 1$ one may rewrite Eq. (B.5) as

$$\epsilon_{cr} = \left(\frac{f_t \omega}{E(1-\omega)}\right)\left[1 - \frac{f_t \Lambda}{2\mathcal{G}_f}\epsilon_{cr}\right] \tag{B.6}$$

Solving Eq. (B.6) for ϵ_{cr} and then substituting in Eq. (B.2), one obtains a relation between g^t and ω. This relation is plotted in Figure B-1 for different values of Λ. In this figure the apparent fracture energy density is normalized by its total value g_f which is defined by Eq. (4.21). One may clearly observe that the correlation of the apparent fracture energy density and the damage parameter increases with the increase of the crack band width. Another important observation may be inferred from Figure B-1 which is the need to impose upper and lower bounds on the crack band width to ensure reasonable variation of the damage with the release of the fracture energy.

Appendix C

Characteristics of LRC Frame

The structure considered for the fragility analysis is a 1/4-scale, two-bay, two-story LRC frame with details as shown in Figure C-1. A typical stress-strain relation for the concrete used in the model is shown in Figure C-2. The best linear fit of the variations of the splitting tensile strength, the modulus of rupture and the modulus of elasticity with the compressive strength are shown in Figures C-3, C-4, and C-5, respectively.

Since the embedment of the bottom reinforcement of the beam into the column is 1.5 inch, cylinders of 1.5 inch length with embedded reinforcing bars were tested in a standard bond slip experiment. A typical variation of the traction along the bar with the unit slip is shown in Figure C-6.

The fracture properties of the concrete material were determined from the results of the three point bending tests, measuring the width of the crack initiating and propagating at mid-span. The range of the experimental results is shown in Figure C-7. From this figure, one may determine the fracture energy release and the shape of the descending branch required by the smeared cracking model.

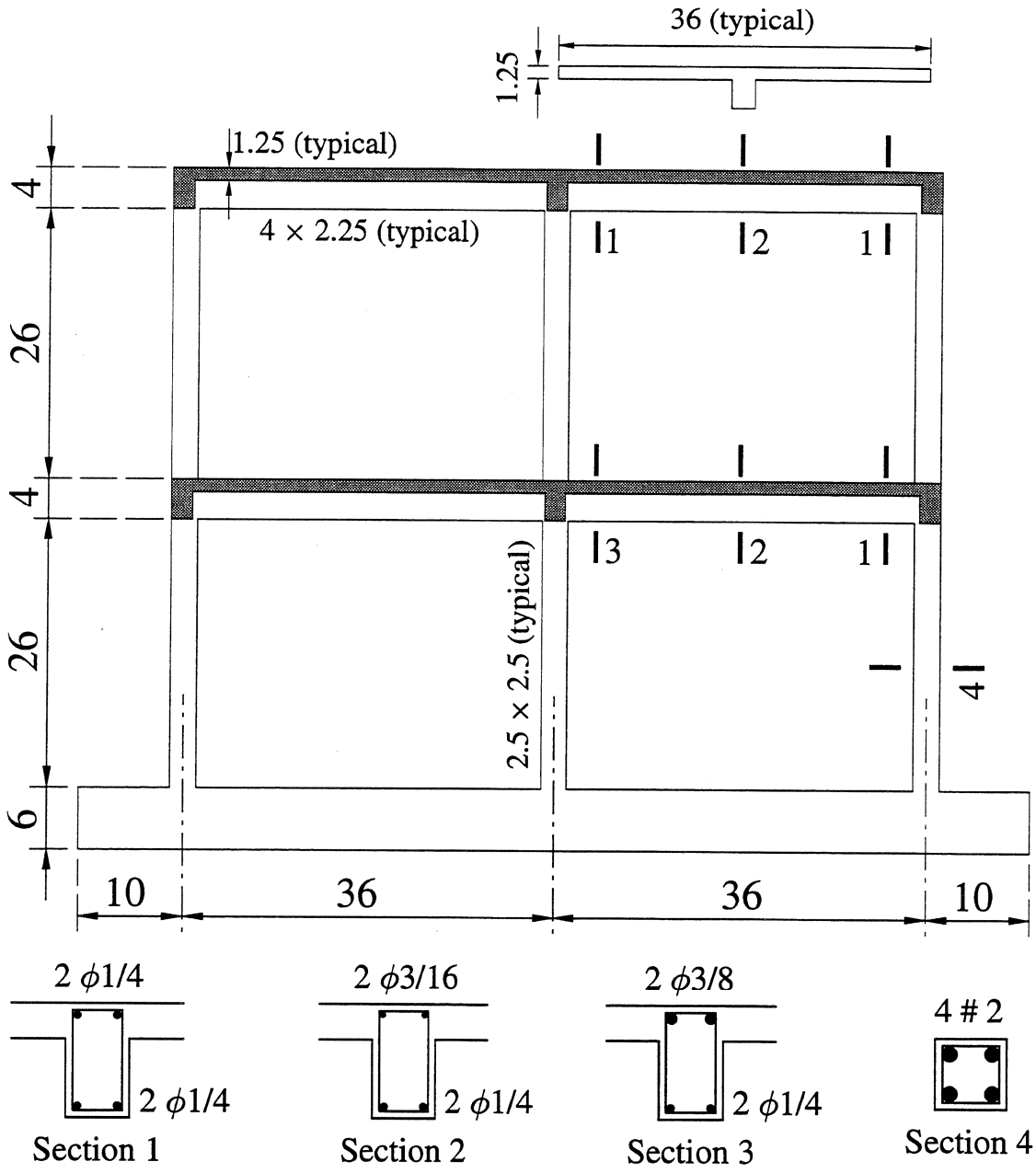

Notes: All dimensions are in inches

All beam stirrups and column ties are deformed bars of diameter 3/32 in

Reinforcement sizes of Sections 1-3 are for standard threaded rods with 24 threads/in

Reinforcement sizes of Section 4 are for standard deformed bars

FIGURE C-1 Concrete dimensions and reinforcement details of the LRC frame.

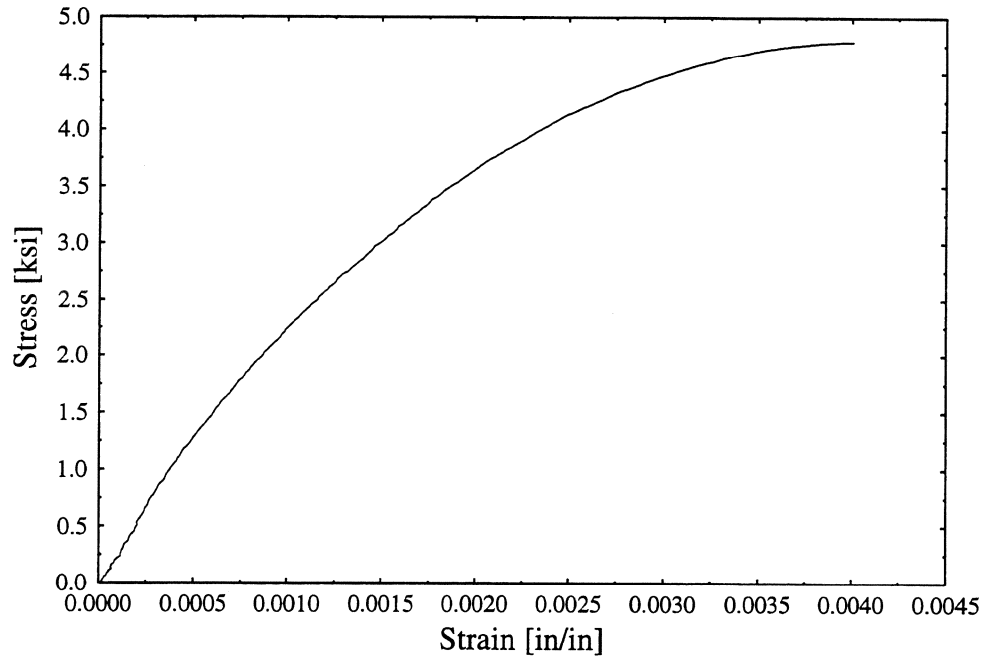

FIGURE C-2 Typical stress-strain relation of the concrete used in constructing the LRC frame.

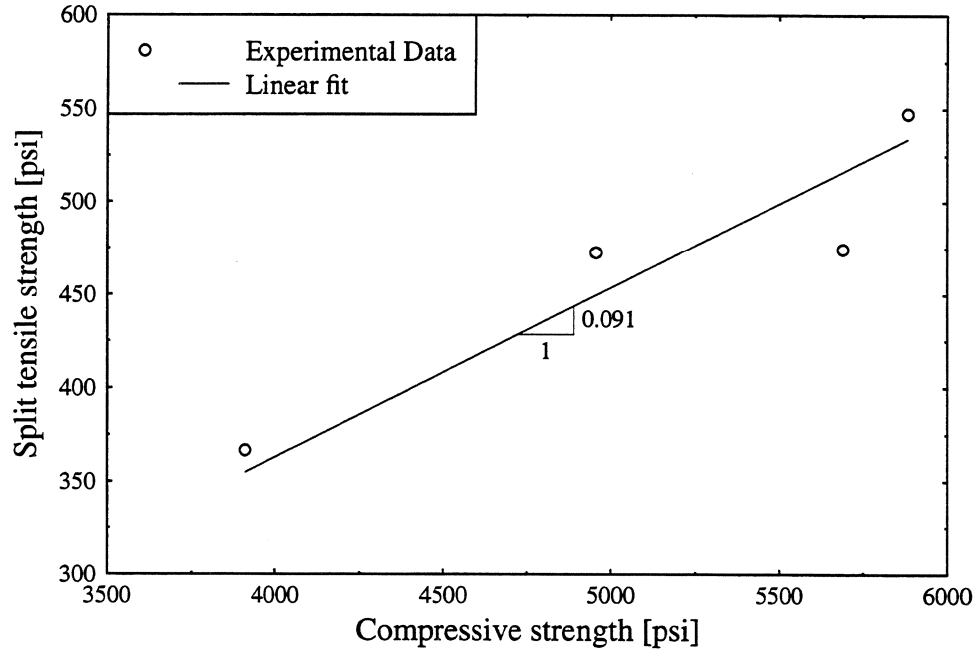

FIGURE C-3 Variation of the splitting tensile strength with the compressive strength.

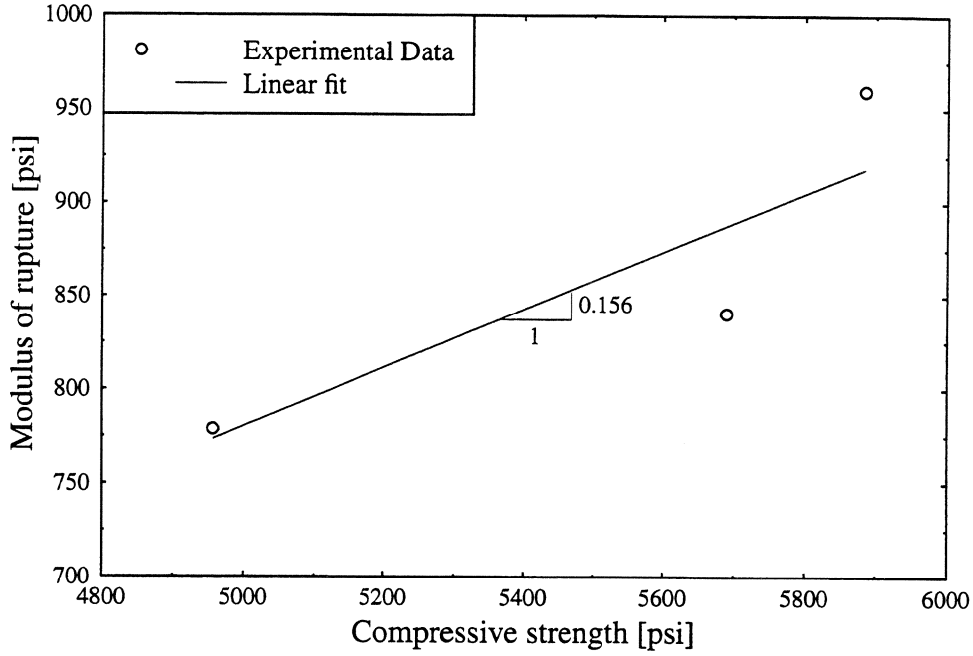

FIGURE C-4 Variation of the modulus of rupture with the compressive strength.

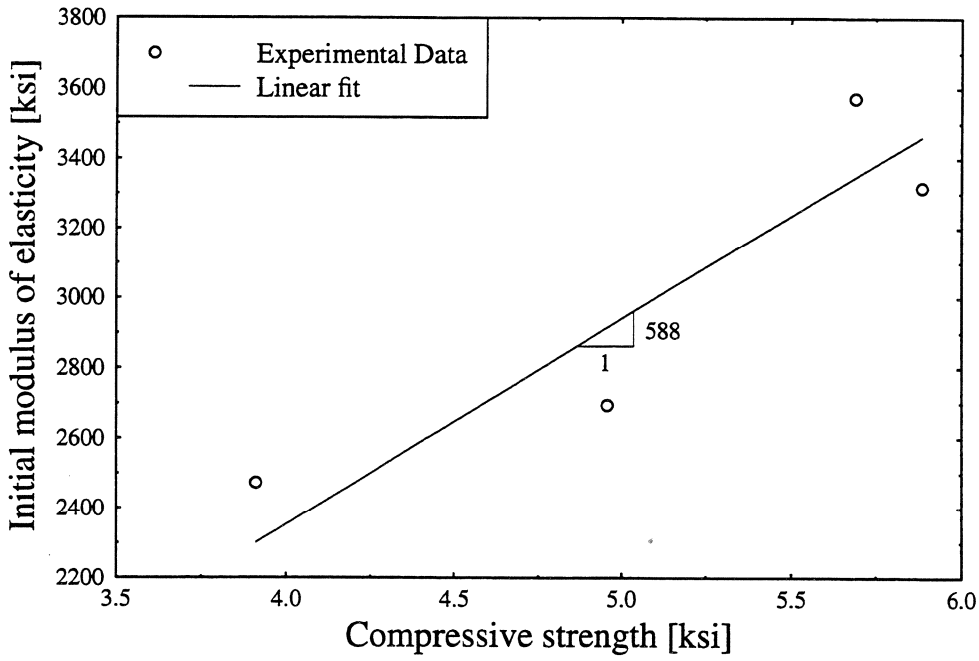

FIGURE C-5 Variation of the modulus of elasticity with the compressive strength.

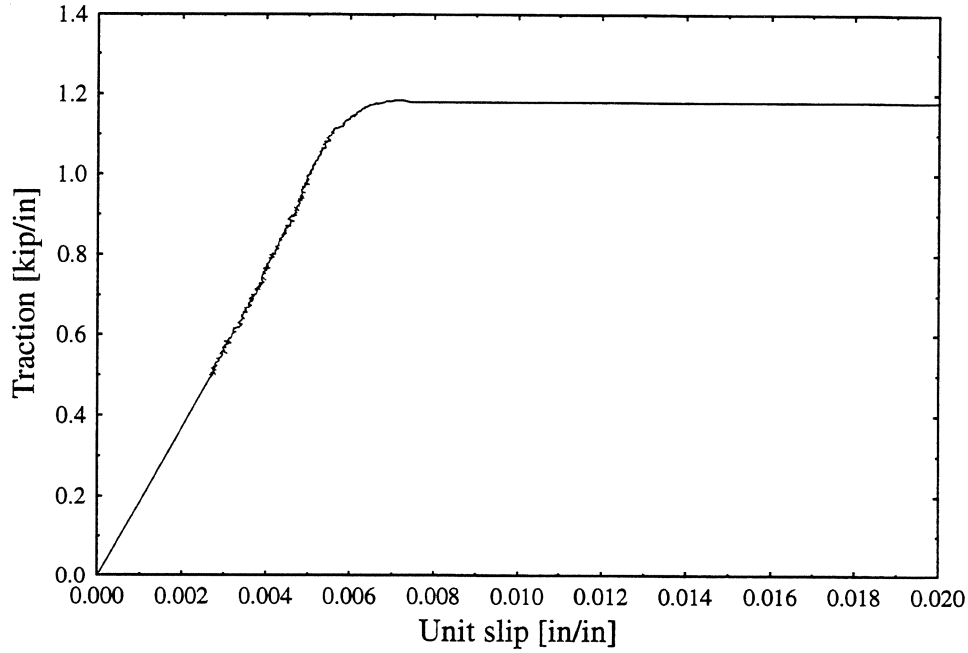

FIGURE C-6 Typical result of a bond slip test.

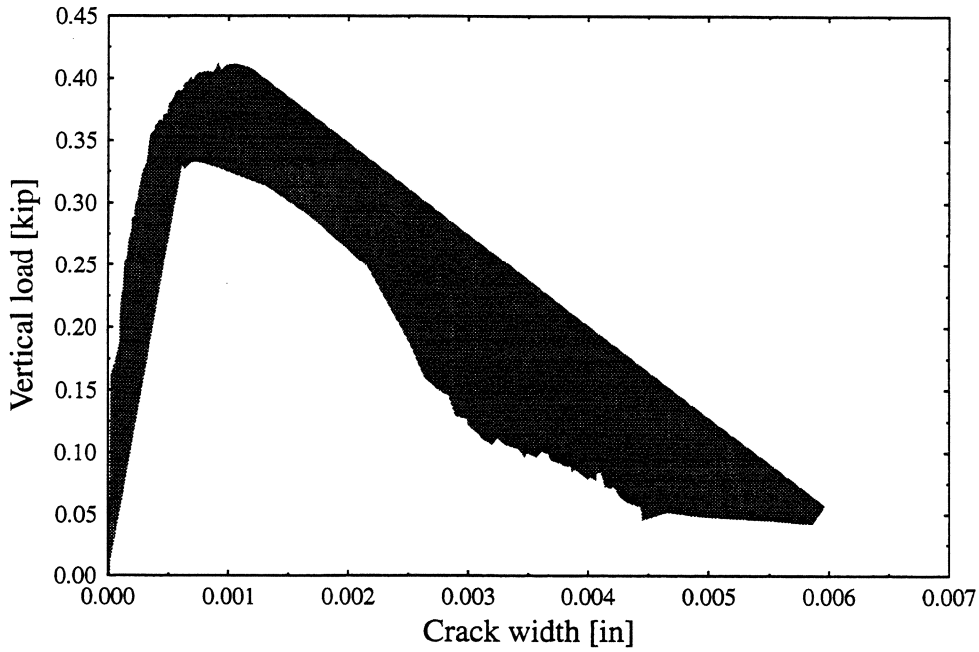

FIGURE C-7 Experimental results of the crack width versus the applied vertical load in three point bending experiments.

NATIONAL CENTER FOR EARTHQUAKE ENGINEERING RESEARCH
LIST OF TECHNICAL REPORTS

The National Center for Earthquake Engineering Research (NCEER) publishes technical reports on a variety of subjects related to earthquake engineering written by authors funded through NCEER. These reports are available from both NCEER Publications and the National Technical Information Service (NTIS). Requests for reports should be directed to NCEER Publications, National Center for Earthquake Engineering Research, State University of New York at Buffalo, Red Jacket Quadrangle, Buffalo, New York 14261. Reports can also be requested through NTIS, 5285 Port Royal Road, Springfield, Virginia 22161. NTIS accession numbers are shown in parenthesis, if available.

NCEER-87-0001 "First-Year Program in Research, Education and Technology Transfer," 3/5/87, (PB88-134275, A04, MF-A01).

NCEER-87-0002 "Experimental Evaluation of Instantaneous Optimal Algorithms for Structural Control," by R.C. Lin, T.T. Soong and A.M. Reinhorn, 4/20/87, (PB88-134341, A04, MF-A01).

NCEER-87-0003 "Experimentation Using the Earthquake Simulation Facilities at University at Buffalo," by A.M. Reinhorn and R.L. Ketter, to be published.

NCEER-87-0004 "The System Characteristics and Performance of a Shaking Table," by J.S. Hwang, K.C. Chang and G.C. Lee, 6/1/87, (PB88-134259, A03, MF-A01). This report is available only through NTIS (see address given above).

NCEER-87-0005 "A Finite Element Formulation for Nonlinear Viscoplastic Material Using a Q Model," by O. Gyebi and G. Dasgupta, 11/2/87, (PB88-213764, A08, MF-A01).

NCEER-87-0006 "Symbolic Manipulation Program (SMP) - Algebraic Codes for Two and Three Dimensional Finite Element Formulations," by X. Lee and G. Dasgupta, 11/9/87, (PB88-218522, A05, MF-A01).

NCEER-87-0007 "Instantaneous Optimal Control Laws for Tall Buildings Under Seismic Excitations," by J.N. Yang, A. Akbarpour and P. Ghaemmaghami, 6/10/87, (PB88-134333, A06, MF-A01). This report is only available through NTIS (see address given above).

NCEER-87-0008 "IDARC: Inelastic Damage Analysis of Reinforced Concrete Frame - Shear-Wall Structures," by Y.J. Park, A.M. Reinhorn and S.K. Kunnath, 7/20/87, (PB88-134325, A09, MF-A01). This report is only available through NTIS (see address given above).

NCEER-87-0009 "Liquefaction Potential for New York State: A Preliminary Report on Sites in Manhattan and Buffalo," by M. Budhu, V. Vijayakumar, R.F. Giese and L. Baumgras, 8/31/87, (PB88-163704, A03, MF-A01). This report is available only through NTIS (see address given above).

NCEER-87-0010 "Vertical and Torsional Vibration of Foundations in Inhomogeneous Media," by A.S. Veletsos and K.W. Dotson, 6/1/87, (PB88-134291, A03, MF-A01). This report is only available through NTIS (see address given above).

NCEER-87-0011 "Seismic Probabilistic Risk Assessment and Seismic Margins Studies for Nuclear Power Plants," by Howard H.M. Hwang, 6/15/87, (PB88-134267, A03, MF-A01). This report is only available through NTIS (see address given above).

NCEER-87-0012 "Parametric Studies of Frequency Response of Secondary Systems Under Ground-Acceleration Excitations," by Y. Yong and Y.K. Lin, 6/10/87, (PB88-134309, A03, MF-A01). This report is only available through NTIS (see address given above).

NCEER-87-0013 "Frequency Response of Secondary Systems Under Seismic Excitation," by J.A. HoLung, J. Cai and Y.K. Lin, 7/31/87, (PB88-134317, A05, MF-A01). This report is only available through NTIS (see address given above).

NCEER-87-0014 "Modelling Earthquake Ground Motions in Seismically Active Regions Using Parametric Time Series Methods," by G.W. Ellis and A.S. Cakmak, 8/25/87, (PB88-134283, A08, MF-A01). This report is only available through NTIS (see address given above).

NCEER-87-0015 "Detection and Assessment of Seismic Structural Damage," by E. DiPasquale and A.S. Cakmak, 8/25/87, (PB88-163712, A05, MF-A01). This report is only available through NTIS (see address given above).

NCEER-87-0016 "Pipeline Experiment at Parkfield, California," by J. Isenberg and E. Richardson, 9/15/87, (PB88-163720, A03, MF-A01). This report is available only through NTIS (see address given above).

NCEER-87-0017 "Digital Simulation of Seismic Ground Motion," by M. Shinozuka, G. Deodatis and T. Harada, 8/31/87, (PB88-155197, A04, MF-A01). This report is available only through NTIS (see address given above).

NCEER-87-0018 "Practical Considerations for Structural Control: System Uncertainty, System Time Delay and Truncation of Small Control Forces," J.N. Yang and A. Akbarpour, 8/10/87, (PB88-163738, A08, MF-A01). This report is only available through NTIS (see address given above).

NCEER-87-0019 "Modal Analysis of Nonclassically Damped Structural Systems Using Canonical Transformation," by J.N. Yang, S. Sarkani and F.X. Long, 9/27/87, (PB88-187851, A04, MF-A01).

NCEER-87-0020 "A Nonstationary Solution in Random Vibration Theory," by J.R. Red-Horse and P.D. Spanos, 11/3/87, (PB88-163746, A03, MF-A01).

NCEER-87-0021 "Horizontal Impedances for Radially Inhomogeneous Viscoelastic Soil Layers," by A.S. Veletsos and K.W. Dotson, 10/15/87, (PB88-150859, A04, MF-A01).

NCEER-87-0022 "Seismic Damage Assessment of Reinforced Concrete Members," by Y.S. Chung, C. Meyer and M. Shinozuka, 10/9/87, (PB88-150867, A05, MF-A01). This report is available only through NTIS (see address given above).

NCEER-87-0023 "Active Structural Control in Civil Engineering," by T.T. Soong, 11/11/87, (PB88-187778, A03, MF-A01).

NCEER-87-0024 "Vertical and Torsional Impedances for Radially Inhomogeneous Viscoelastic Soil Layers," by K.W. Dotson and A.S. Veletsos, 12/87, (PB88-187786, A03, MF-A01).

NCEER-87-0025 "Proceedings from the Symposium on Seismic Hazards, Ground Motions, Soil-Liquefaction and Engineering Practice in Eastern North America," October 20-22, 1987, edited by K.H. Jacob, 12/87, (PB88-188115, A23, MF-A01).

NCEER-87-0026 "Report on the Whittier-Narrows, California, Earthquake of October 1, 1987," by J. Pantelic and A. Reinhorn, 11/87, (PB88-187752, A03, MF-A01). This report is available only through NTIS (see address given above).

NCEER-87-0027 "Design of a Modular Program for Transient Nonlinear Analysis of Large 3-D Building Structures," by S. Srivastav and J.F. Abel, 12/30/87, (PB88-187950, A05, MF-A01). This report is only available through NTIS (see address given above).

NCEER-87-0028 "Second-Year Program in Research, Education and Technology Transfer," 3/8/88, (PB88-219480, A04, MF-A01).

NCEER-88-0001 "Workshop on Seismic Computer Analysis and Design of Buildings With Interactive Graphics," by W. McGuire, J.F. Abel and C.H. Conley, 1/18/88, (PB88-187760, A03, MF-A01). This report is only available through NTIS (see address given above).

NCEER-88-0002 "Optimal Control of Nonlinear Flexible Structures," by J.N. Yang, F.X. Long and D. Wong, 1/22/88, (PB88-213772, A06, MF-A01).

NCEER-88-0003 "Substructuring Techniques in the Time Domain for Primary-Secondary Structural Systems," by G.D. Manolis and G. Juhn, 2/10/88, (PB88-213780, A04, MF-A01).

NCEER-88-0004 "Iterative Seismic Analysis of Primary-Secondary Systems," by A. Singhal, L.D. Lutes and P.D. Spanos, 2/23/88, (PB88-213798, A04, MF-A01).

NCEER-88-0005 "Stochastic Finite Element Expansion for Random Media," by P.D. Spanos and R. Ghanem, 3/14/88, (PB88-213806, A03, MF-A01).

NCEER-88-0006 "Combining Structural Optimization and Structural Control," by F.Y. Cheng and C.P. Pantelides, 1/10/88, (PB88-213814, A05, MF-A01).

NCEER-88-0007 "Seismic Performance Assessment of Code-Designed Structures," by H.H-M. Hwang, J-W. Jaw and H-J. Shau, 3/20/88, (PB88-219423, A04, MF-A01). This report is only available through NTIS (see address given above).

NCEER-88-0008 "Reliability Analysis of Code-Designed Structures Under Natural Hazards," by H.H-M. Hwang, H. Ushiba and M. Shinozuka, 2/29/88, (PB88-229471, A07, MF-A01). This report is only available through NTIS (see address given above).

NCEER-88-0009 "Seismic Fragility Analysis of Shear Wall Structures," by J-W Jaw and H.H-M. Hwang, 4/30/88, (PB89-102867, A04, MF-A01).

NCEER-88-0010 "Base Isolation of a Multi-Story Building Under a Harmonic Ground Motion - A Comparison of Performances of Various Systems," by F-G Fan, G. Ahmadi and I.G. Tadjbakhsh, 5/18/88, (PB89-122238, A06, MF-A01). This report is only available through NTIS (see address given above).

NCEER-88-0011 "Seismic Floor Response Spectra for a Combined System by Green's Functions," by F.M. Lavelle, L.A. Bergman and P.D. Spanos, 5/1/88, (PB89-102875, A03, MF-A01).

NCEER-88-0012 "A New Solution Technique for Randomly Excited Hysteretic Structures," by G.Q. Cai and Y.K. Lin, 5/16/88, (PB89-102883, A03, MF-A01).

NCEER-88-0013 "A Study of Radiation Damping and Soil-Structure Interaction Effects in the Centrifuge," by K. Weissman, supervised by J.H. Prevost, 5/24/88, (PB89-144703, A06, MF-A01).

NCEER-88-0014 "Parameter Identification and Implementation of a Kinematic Plasticity Model for Frictional Soils," by J.H. Prevost and D.V. Griffiths, to be published.

NCEER-88-0015 "Two- and Three- Dimensional Dynamic Finite Element Analyses of the Long Valley Dam," by D.V. Griffiths and J.H. Prevost, 6/17/88, (PB89-144711, A04, MF-A01).

NCEER-88-0016 "Damage Assessment of Reinforced Concrete Structures in Eastern United States," by A.M. Reinhorn, M.J. Seidel, S.K. Kunnath and Y.J. Park, 6/15/88, (PB89-122220, A04, MF-A01). This report is only available through NTIS (see address given above).

NCEER-88-0017 "Dynamic Compliance of Vertically Loaded Strip Foundations in Multilayered Viscoelastic Soils," by S. Ahmad and A.S.M. Israil, 6/17/88, (PB89-102891, A04, MF-A01).

NCEER-88-0018 "An Experimental Study of Seismic Structural Response With Added Viscoelastic Dampers," by R.C. Lin, Z. Liang, T.T. Soong and R.H. Zhang, 6/30/88, (PB89-122212, A05, MF-A01). This report is available only through NTIS (see address given above).

NCEER-88-0019 "Experimental Investigation of Primary - Secondary System Interaction," by G.D. Manolis, G. Juhn and A.M. Reinhorn, 5/27/88, (PB89-122204, A04, MF-A01).

NCEER-88-0020 "A Response Spectrum Approach For Analysis of Nonclassically Damped Structures," by J.N. Yang, S. Sarkani and F.X. Long, 4/22/88, (PB89-102909, A04, MF-A01).

NCEER-88-0021 "Seismic Interaction of Structures and Soils: Stochastic Approach," by A.S. Veletsos and A.M. Prasad, 7/21/88, (PB89-122196, A04, MF-A01). This report is only available through NTIS (see address given above).

NCEER-88-0022 "Identification of the Serviceability Limit State and Detection of Seismic Structural Damage," by E. DiPasquale and A.S. Cakmak, 6/15/88, (PB89-122188, A05, MF-A01). This report is available only through NTIS (see address given above).

NCEER-88-0023 "Multi-Hazard Risk Analysis: Case of a Simple Offshore Structure," by B.K. Bhartia and E.H. Vanmarcke, 7/21/88, (PB89-145213, A05, MF-A01).

NCEER-88-0024 "Automated Seismic Design of Reinforced Concrete Buildings," by Y.S. Chung, C. Meyer and M. Shinozuka, 7/5/88, (PB89-122170, A06, MF-A01). This report is available only through NTIS (see address given above).

NCEER-88-0025 "Experimental Study of Active Control of MDOF Structures Under Seismic Excitations," by L.L. Chung, R.C. Lin, T.T. Soong and A.M. Reinhorn, 7/10/88, (PB89-122600, A04, MF-A01).

NCEER-88-0026 "Earthquake Simulation Tests of a Low-Rise Metal Structure," by J.S. Hwang, K.C. Chang, G.C. Lee and R.L. Ketter, 8/1/88, (PB89-102917, A04, MF-A01).

NCEER-88-0027 "Systems Study of Urban Response and Reconstruction Due to Catastrophic Earthquakes," by F. Kozin and H.K. Zhou, 9/22/88, (PB90-162348, A04, MF-A01).

NCEER-88-0028 "Seismic Fragility Analysis of Plane Frame Structures," by H.H-M. Hwang and Y.K. Low, 7/31/88, (PB89-131445, A06, MF-A01).

NCEER-88-0029 "Response Analysis of Stochastic Structures," by A. Kardara, C. Bucher and M. Shinozuka, 9/22/88, (PB89-174429, A04, MF-A01).

NCEER-88-0030 "Nonnormal Accelerations Due to Yielding in a Primary Structure," by D.C.K. Chen and L.D. Lutes, 9/19/88, (PB89-131437, A04, MF-A01).

NCEER-88-0031 "Design Approaches for Soil-Structure Interaction," by A.S. Veletsos, A.M. Prasad and Y. Tang, 12/30/88, (PB89-174437, A03, MF-A01). This report is available only through NTIS (see address given above).

NCEER-88-0032 "A Re-evaluation of Design Spectra for Seismic Damage Control," by C.J. Turkstra and A.G. Tallin, 11/7/88, (PB89-145221, A05, MF-A01).

NCEER-88-0033 "The Behavior and Design of Noncontact Lap Splices Subjected to Repeated Inelastic Tensile Loading," by V.E. Sagan, P. Gergely and R.N. White, 12/8/88, (PB89-163737, A08, MF-A01).

NCEER-88-0034 "Seismic Response of Pile Foundations," by S.M. Mamoon, P.K. Banerjee and S. Ahmad, 11/1/88, (PB89-145239, A04, MF-A01).

NCEER-88-0035 "Modeling of R/C Building Structures With Flexible Floor Diaphragms (IDARC2)," by A.M. Reinhorn, S.K. Kunnath and N. Panahshahi, 9/7/88, (PB89-207153, A07, MF-A01).

NCEER-88-0036 "Solution of the Dam-Reservoir Interaction Problem Using a Combination of FEM, BEM with Particular Integrals, Modal Analysis, and Substructuring," by C-S. Tsai, G.C. Lee and R.L. Ketter, 12/31/88, (PB89-207146, A04, MF-A01).

NCEER-88-0037 "Optimal Placement of Actuators for Structural Control," by F.Y. Cheng and C.P. Pantelides, 8/15/88, (PB89-162846, A05, MF-A01).

NCEER-88-0038 "Teflon Bearings in Aseismic Base Isolation: Experimental Studies and Mathematical Modeling," by A. Mokha, M.C. Constantinou and A.M. Reinhorn, 12/5/88, (PB89-218457, A10, MF-A01). This report is available only through NTIS (see address given above).

NCEER-88-0039 "Seismic Behavior of Flat Slab High-Rise Buildings in the New York City Area," by P. Weidlinger and M. Ettouney, 10/15/88, (PB90-145681, A04, MF-A01).

NCEER-88-0040 "Evaluation of the Earthquake Resistance of Existing Buildings in New York City," by P. Weidlinger and M. Ettouney, 10/15/88, to be published.

NCEER-88-0041 "Small-Scale Modeling Techniques for Reinforced Concrete Structures Subjected to Seismic Loads," by W. Kim, A. El-Attar and R.N. White, 11/22/88, (PB89-189625, A05, MF-A01).

NCEER-88-0042 "Modeling Strong Ground Motion from Multiple Event Earthquakes," by G.W. Ellis and A.S. Cakmak, 10/15/88, (PB89-174445, A03, MF-A01).

NCEER-88-0043 "Nonstationary Models of Seismic Ground Acceleration," by M. Grigoriu, S.E. Ruiz and E. Rosenblueth, 7/15/88, (PB89-189617, A04, MF-A01).

NCEER-88-0044 "SARCF User's Guide: Seismic Analysis of Reinforced Concrete Frames," by Y.S. Chung, C. Meyer and M. Shinozuka, 11/9/88, (PB89-174452, A08, MF-A01).

NCEER-88-0045 "First Expert Panel Meeting on Disaster Research and Planning," edited by J. Pantelic and J. Stoyle, 9/15/88, (PB89-174460, A05, MF-A01). This report is only available through NTIS (see address given above).

NCEER-88-0046 "Preliminary Studies of the Effect of Degrading Infill Walls on the Nonlinear Seismic Response of Steel Frames," by C.Z. Chrysostomou, P. Gergely and J.F. Abel, 12/19/88, (PB89-208383, A05, MF-A01).

NCEER-88-0047 "Reinforced Concrete Frame Component Testing Facility - Design, Construction, Instrumentation and Operation," by S.P. Pessiki, C. Conley, T. Bond, P. Gergely and R.N. White, 12/16/88, (PB89-174478, A04, MF-A01).

NCEER-89-0001 "Effects of Protective Cushion and Soil Compliancy on the Response of Equipment Within a Seismically Excited Building," by J.A. HoLung, 2/16/89, (PB89-207179, A04, MF-A01).

NCEER-89-0002 "Statistical Evaluation of Response Modification Factors for Reinforced Concrete Structures," by H.H-M. Hwang and J-W. Jaw, 2/17/89, (PB89-207187, A05, MF-A01).

NCEER-89-0003 "Hysteretic Columns Under Random Excitation," by G-Q. Cai and Y.K. Lin, 1/9/89, (PB89-196513, A03, MF-A01).

NCEER-89-0004 "Experimental Study of `Elephant Foot Bulge' Instability of Thin-Walled Metal Tanks," by Z-H. Jia and R.L. Ketter, 2/22/89, (PB89-207195, A03, MF-A01).

NCEER-89-0005 "Experiment on Performance of Buried Pipelines Across San Andreas Fault," by J. Isenberg, E. Richardson and T.D. O'Rourke, 3/10/89, (PB89-218440, A04, MF-A01). This report is available only through NTIS (see address given above).

NCEER-89-0006 "A Knowledge-Based Approach to Structural Design of Earthquake-Resistant Buildings," by M. Subramani, P. Gergely, C.H. Conley, J.F. Abel and A.H. Zaghw, 1/15/89, (PB89-218465, A06, MF-A01).

NCEER-89-0007 "Liquefaction Hazards and Their Effects on Buried Pipelines," by T.D. O'Rourke and P.A. Lane, 2/1/89, (PB89-218481, A09, MF-A01).

NCEER-89-0008 "Fundamentals of System Identification in Structural Dynamics," by H. Imai, C-B. Yun, O. Maruyama and M. Shinozuka, 1/26/89, (PB89-207211, A04, MF-A01).

NCEER-89-0009 "Effects of the 1985 Michoacan Earthquake on Water Systems and Other Buried Lifelines in Mexico," by A.G. Ayala and M.J. O'Rourke, 3/8/89, (PB89-207229, A06, MF-A01).

NCEER-89-R010 "NCEER Bibliography of Earthquake Education Materials," by K.E.K. Ross, Second Revision, 9/1/89, (PB90-125352, A05, MF-A01). This report is replaced by NCEER-92-0018.

NCEER-89-0011 "Inelastic Three-Dimensional Response Analysis of Reinforced Concrete Building Structures (IDARC-3D), Part I - Modeling," by S.K. Kunnath and A.M. Reinhorn, 4/17/89, (PB90-114612, A07, MF-A01).

NCEER-89-0012 "Recommended Modifications to ATC-14," by C.D. Poland and J.O. Malley, 4/12/89, (PB90-108648, A15, MF-A01).

NCEER-89-0013 "Repair and Strengthening of Beam-to-Column Connections Subjected to Earthquake Loading," by M. Corazao and A.J. Durrani, 2/28/89, (PB90-109885, A06, MF-A01).

NCEER-89-0014 "Program EXKAL2 for Identification of Structural Dynamic Systems," by O. Maruyama, C-B. Yun, M. Hoshiya and M. Shinozuka, 5/19/89, (PB90-109877, A09, MF-A01).

NCEER-89-0015 "Response of Frames With Bolted Semi-Rigid Connections, Part I - Experimental Study and Analytical Predictions," by P.J. DiCorso, A.M. Reinhorn, J.R. Dickerson, J.B. Radziminski and W.L. Harper, 6/1/89, to be published.

NCEER-89-0016 "ARMA Monte Carlo Simulation in Probabilistic Structural Analysis," by P.D. Spanos and M.P. Mignolet, 7/10/89, (PB90-109893, A03, MF-A01).

NCEER-89-P017 "Preliminary Proceedings from the Conference on Disaster Preparedness - The Place of Earthquake Education in Our Schools," Edited by K.E.K. Ross, 6/23/89, (PB90-108606, A03, MF-A01).

NCEER-89-0017 "Proceedings from the Conference on Disaster Preparedness - The Place of Earthquake Education in Our Schools," Edited by K.E.K. Ross, 12/31/89, (PB90-207895, A012, MF-A02). This report is available only through NTIS (see address given above).

NCEER-89-0018 "Multidimensional Models of Hysteretic Material Behavior for Vibration Analysis of Shape Memory Energy Absorbing Devices, by E.J. Graesser and F.A. Cozzarelli, 6/7/89, (PB90-164146, A04, MF-A01).

NCEER-89-0019 "Nonlinear Dynamic Analysis of Three-Dimensional Base Isolated Structures (3D-BASIS)," by S. Nagarajaiah, A.M. Reinhorn and M.C. Constantinou, 8/3/89, (PB90-161936, A06, MF-A01). This report has been replaced by NCEER-93-0011.

NCEER-89-0020 "Structural Control Considering Time-Rate of Control Forces and Control Rate Constraints," by F.Y. Cheng and C.P. Pantelides, 8/3/89, (PB90-120445, A04, MF-A01).

NCEER-89-0021 "Subsurface Conditions of Memphis and Shelby County," by K.W. Ng, T-S. Chang and H-H.M. Hwang, 7/26/89, (PB90-120437, A03, MF-A01).

NCEER-89-0022 "Seismic Wave Propagation Effects on Straight Jointed Buried Pipelines," by K. Elhmadi and M.J. O'Rourke, 8/24/89, (PB90-162322, A10, MF-A02).

NCEER-89-0023 "Workshop on Serviceability Analysis of Water Delivery Systems," edited by M. Grigoriu, 3/6/89, (PB90-127424, A03, MF-A01).

NCEER-89-0024 "Shaking Table Study of a 1/5 Scale Steel Frame Composed of Tapered Members," by K.C. Chang, J.S. Hwang and G.C. Lee, 9/18/89, (PB90-160169, A04, MF-A01).

NCEER-89-0025 "DYNA1D: A Computer Program for Nonlinear Seismic Site Response Analysis - Technical Documentation," by Jean H. Prevost, 9/14/89, (PB90-161944, A07, MF-A01). This report is available only through NTIS (see address given above).

NCEER-89-0026 "1:4 Scale Model Studies of Active Tendon Systems and Active Mass Dampers for Aseismic Protection," by A.M. Reinhorn, T.T. Soong, R.C. Lin, Y.P. Yang, Y. Fukao, H. Abe and M. Nakai, 9/15/89, (PB90-173246, A10, MF-A02).

NCEER-89-0027 "Scattering of Waves by Inclusions in a Nonhomogeneous Elastic Half Space Solved by Boundary Element Methods," by P.K. Hadley, A. Askar and A.S. Cakmak, 6/15/89, (PB90-145699, A07, MF-A01).

NCEER-89-0028 "Statistical Evaluation of Deflection Amplification Factors for Reinforced Concrete Structures," by H.H.M. Hwang, J-W. Jaw and A.L. Ch'ng, 8/31/89, (PB90-164633, A05, MF-A01).

NCEER-89-0029 "Bedrock Accelerations in Memphis Area Due to Large New Madrid Earthquakes," by H.H.M. Hwang, C.H.S. Chen and G. Yu, 11/7/89, (PB90-162330, A04, MF-A01).

NCEER-89-0030 "Seismic Behavior and Response Sensitivity of Secondary Structural Systems," by Y.Q. Chen and T.T. Soong, 10/23/89, (PB90-164658, A08, MF-A01).

NCEER-89-0031 "Random Vibration and Reliability Analysis of Primary-Secondary Structural Systems," by Y. Ibrahim, M. Grigoriu and T.T. Soong, 11/10/89, (PB90-161951, A04, MF-A01).

NCEER-89-0032 "Proceedings from the Second U.S. - Japan Workshop on Liquefaction, Large Ground Deformation and Their Effects on Lifelines, September 26-29, 1989," Edited by T.D. O'Rourke and M. Hamada, 12/1/89, (PB90-209388, A22, MF-A03).

NCEER-89-0033 "Deterministic Model for Seismic Damage Evaluation of Reinforced Concrete Structures," by J.M. Bracci, A.M. Reinhorn, J.B. Mander and S.K. Kunnath, 9/27/89, (PB91-108803, A06, MF-A01).

NCEER-89-0034 "On the Relation Between Local and Global Damage Indices," by E. DiPasquale and A.S. Cakmak, 8/15/89, (PB90-173865, A05, MF-A01).

NCEER-89-0035 "Cyclic Undrained Behavior of Nonplastic and Low Plasticity Silts," by A.J. Walker and H.E. Stewart, 7/26/89, (PB90-183518, A10, MF-A01).

NCEER-89-0036 "Liquefaction Potential of Surficial Deposits in the City of Buffalo, New York," by M. Budhu, R. Giese and L. Baumgrass, 1/17/89, (PB90-208455, A04, MF-A01).

NCEER-89-0037 "A Deterministic Assessment of Effects of Ground Motion Incoherence," by A.S. Veletsos and Y. Tang, 7/15/89, (PB90-164294, A03, MF-A01).

NCEER-89-0038 "Workshop on Ground Motion Parameters for Seismic Hazard Mapping," July 17-18, 1989, edited by R.V. Whitman, 12/1/89, (PB90-173923, A04, MF-A01).

NCEER-89-0039 "Seismic Effects on Elevated Transit Lines of the New York City Transit Authority," by C.J. Costantino, C.A. Miller and E. Heymsfield, 12/26/89, (PB90-207887, A06, MF-A01).

NCEER-89-0040 "Centrifugal Modeling of Dynamic Soil-Structure Interaction," by K. Weissman, Supervised by J.H. Prevost, 5/10/89, (PB90-207879, A07, MF-A01).

NCEER-89-0041 "Linearized Identification of Buildings With Cores for Seismic Vulnerability Assessment," by I-K. Ho and A.E. Aktan, 11/1/89, (PB90-251943, A07, MF-A01).

NCEER-90-0001 "Geotechnical and Lifeline Aspects of the October 17, 1989 Loma Prieta Earthquake in San Francisco," by T.D. O'Rourke, H.E. Stewart, F.T. Blackburn and T.S. Dickerman, 1/90, (PB90-208596, A05, MF-A01).

NCEER-90-0002 "Nonnormal Secondary Response Due to Yielding in a Primary Structure," by D.C.K. Chen and L.D. Lutes, 2/28/90, (PB90-251976, A07, MF-A01).

NCEER-90-0003 "Earthquake Education Materials for Grades K-12," by K.E.K. Ross, 4/16/90, (PB91-251984, A05, MF-A05). This report has been replaced by NCEER-92-0018.

NCEER-90-0004 "Catalog of Strong Motion Stations in Eastern North America," by R.W. Busby, 4/3/90, (PB90-251984, A05, MF-A01).

NCEER-90-0005 "NCEER Strong-Motion Data Base: A User Manual for the GeoBase Release (Version 1.0 for the Sun3)," by P. Friberg and K. Jacob, 3/31/90 (PB90-258062, A04, MF-A01).

NCEER-90-0006 "Seismic Hazard Along a Crude Oil Pipeline in the Event of an 1811-1812 Type New Madrid Earthquake," by H.H.M. Hwang and C-H.S. Chen, 4/16/90, (PB90-258054, A04, MF-A01).

NCEER-90-0007 "Site-Specific Response Spectra for Memphis Sheahan Pumping Station," by H.H.M. Hwang and C.S. Lee, 5/15/90, (PB91-108811, A05, MF-A01).

NCEER-90-0008 "Pilot Study on Seismic Vulnerability of Crude Oil Transmission Systems," by T. Ariman, R. Dobry, M. Grigoriu, F. Kozin, M. O'Rourke, T. O'Rourke and M. Shinozuka, 5/25/90, (PB91-108837, A06, MF-A01).

NCEER-90-0009 "A Program to Generate Site Dependent Time Histories: EQGEN," by G.W. Ellis, M. Srinivasan and A.S. Cakmak, 1/30/90, (PB91-108829, A04, MF-A01).

NCEER-90-0010 "Active Isolation for Seismic Protection of Operating Rooms," by M.E. Talbott, Supervised by M. Shinozuka, 6/8/9, (PB91-110205, A05, MF-A01).

NCEER-90-0011 "Program LINEARID for Identification of Linear Structural Dynamic Systems," by C-B. Yun and M. Shinozuka, 6/25/90, (PB91-110312, A08, MF-A01).

NCEER-90-0012 "Two-Dimensional Two-Phase Elasto-Plastic Seismic Response of Earth Dams," by A.N. Yiagos, Supervised by J.H. Prevost, 6/20/90, (PB91-110197, A13, MF-A02).

NCEER-90-0013 "Secondary Systems in Base-Isolated Structures: Experimental Investigation, Stochastic Response and Stochastic Sensitivity," by G.D. Manolis, G. Juhn, M.C. Constantinou and A.M. Reinhorn, 7/1/90, (PB91-110320, A08, MF-A01).

NCEER-90-0014 "Seismic Behavior of Lightly-Reinforced Concrete Column and Beam-Column Joint Details," by S.P. Pessiki, C.H. Conley, P. Gergely and R.N. White, 8/22/90, (PB91-108795, A11, MF-A02).

NCEER-90-0015 "Two Hybrid Control Systems for Building Structures Under Strong Earthquakes," by J.N. Yang and A. Danielians, 6/29/90, (PB91-125393, A04, MF-A01).

NCEER-90-0016 "Instantaneous Optimal Control with Acceleration and Velocity Feedback," by J.N. Yang and Z. Li, 6/29/90, (PB91-125401, A03, MF-A01).

NCEER-90-0017 "Reconnaissance Report on the Northern Iran Earthquake of June 21, 1990," by M. Mehrain, 10/4/90, (PB91-125377, A03, MF-A01).

NCEER-90-0018 "Evaluation of Liquefaction Potential in Memphis and Shelby County," by T.S. Chang, P.S. Tang, C.S. Lee and H. Hwang, 8/10/90, (PB91-125427, A09, MF-A01).

NCEER-90-0019 "Experimental and Analytical Study of a Combined Sliding Disc Bearing and Helical Steel Spring Isolation System," by M.C. Constantinou, A.S. Mokha and A.M. Reinhorn, 10/4/90, (PB91-125385, A06, MF-A01). This report is available only through NTIS (see address given above).

NCEER-90-0020 "Experimental Study and Analytical Prediction of Earthquake Response of a Sliding Isolation System with a Spherical Surface," by A.S. Mokha, M.C. Constantinou and A.M. Reinhorn, 10/11/90, (PB91-125419, A05, MF-A01).

NCEER-90-0021 "Dynamic Interaction Factors for Floating Pile Groups," by G. Gazetas, K. Fan, A. Kaynia and E. Kausel, 9/10/90, (PB91-170381, A05, MF-A01).

NCEER-90-0022 "Evaluation of Seismic Damage Indices for Reinforced Concrete Structures," by S. Rodriguez-Gomez and A.S. Cakmak, 9/30/90, PB91-171322, A06, MF-A01).

NCEER-90-0023 "Study of Site Response at a Selected Memphis Site," by H. Desai, S. Ahmad, E.S. Gazetas and M.R. Oh, 10/11/90, (PB91-196857, A03, MF-A01).

NCEER-90-0024 "A User's Guide to Strongmo: Version 1.0 of NCEER's Strong-Motion Data Access Tool for PCs and Terminals," by P.A. Friberg and C.A.T. Susch, 11/15/90, (PB91-171272, A03, MF-A01).

NCEER-90-0025 "A Three-Dimensional Analytical Study of Spatial Variability of Seismic Ground Motions," by L-L. Hong and A.H.-S. Ang, 10/30/90, (PB91-170399, A09, MF-A01).

NCEER-90-0026 "MUMOID User's Guide - A Program for the Identification of Modal Parameters," by S. Rodriguez-Gomez and E. DiPasquale, 9/30/90, (PB91-171298, A04, MF-A01).

NCEER-90-0027 "SARCF-II User's Guide - Seismic Analysis of Reinforced Concrete Frames," by S. Rodriguez-Gomez, Y.S. Chung and C. Meyer, 9/30/90, (PB91-171280, A05, MF-A01).

NCEER-90-0028 "Viscous Dampers: Testing, Modeling and Application in Vibration and Seismic Isolation," by N. Makris and M.C. Constantinou, 12/20/90 (PB91-190561, A06, MF-A01).

NCEER-90-0029 "Soil Effects on Earthquake Ground Motions in the Memphis Area," by H. Hwang, C.S. Lee, K.W. Ng and T.S. Chang, 8/2/90, (PB91-190751, A05, MF-A01).

NCEER-91-0001 "Proceedings from the Third Japan-U.S. Workshop on Earthquake Resistant Design of Lifeline Facilities and Countermeasures for Soil Liquefaction, December 17-19, 1990," edited by T.D. O'Rourke and M. Hamada, 2/1/91, (PB91-179259, A99, MF-A04).

NCEER-91-0002 "Physical Space Solutions of Non-Proportionally Damped Systems," by M. Tong, Z. Liang and G.C. Lee, 1/15/91, (PB91-179242, A04, MF-A01).

NCEER-91-0003 "Seismic Response of Single Piles and Pile Groups," by K. Fan and G. Gazetas, 1/10/91, (PB92-174994, A04, MF-A01).

NCEER-91-0004 "Damping of Structures: Part 1 - Theory of Complex Damping," by Z. Liang and G. Lee, 10/10/91, (PB92-197235, A12, MF-A03).

NCEER-91-0005 "3D-BASIS - Nonlinear Dynamic Analysis of Three Dimensional Base Isolated Structures: Part II," by S. Nagarajaiah, A.M. Reinhorn and M.C. Constantinou, 2/28/91, (PB91-190553, A07, MF-A01). This report has been replaced by NCEER-93-0011.

NCEER-91-0006 "A Multidimensional Hysteretic Model for Plasticity Deforming Metals in Energy Absorbing Devices," by E.J. Graesser and F.A. Cozzarelli, 4/9/91, (PB92-108364, A04, MF-A01).

NCEER-91-0007 "A Framework for Customizable Knowledge-Based Expert Systems with an Application to a KBES for Evaluating the Seismic Resistance of Existing Buildings," by E.G. Ibarra-Anaya and S.J. Fenves, 4/9/91, (PB91-210930, A08, MF-A01).

NCEER-91-0008 "Nonlinear Analysis of Steel Frames with Semi-Rigid Connections Using the Capacity Spectrum Method," by G.G. Deierlein, S-H. Hsieh, Y-J. Shen and J.F. Abel, 7/2/91, (PB92-113828, A05, MF-A01).

NCEER-91-0009 "Earthquake Education Materials for Grades K-12," by K.E.K. Ross, 4/30/91, (PB91-212142, A06, MF-A01). This report has been replaced by NCEER-92-0018.

NCEER-91-0010 "Phase Wave Velocities and Displacement Phase Differences in a Harmonically Oscillating Pile," by N. Makris and G. Gazetas, 7/8/91, (PB92-108356, A04, MF-A01).

NCEER-91-0011 "Dynamic Characteristics of a Full-Size Five-Story Steel Structure and a 2/5 Scale Model," by K.C. Chang, G.C. Yao, G.C. Lee, D.S. Hao and Y.C. Yeh," 7/2/91, (PB93-116648, A06, MF-A02).

NCEER-91-0012 "Seismic Response of a 2/5 Scale Steel Structure with Added Viscoelastic Dampers," by K.C. Chang, T.T. Soong, S-T. Oh and M.L. Lai, 5/17/91, (PB92-110816, A05, MF-A01).

NCEER-91-0013 "Earthquake Response of Retaining Walls; Full-Scale Testing and Computational Modeling," by S. Alampalli and A-W.M. Elgamal, 6/20/91, to be published.

NCEER-91-0014 "3D-BASIS-M: Nonlinear Dynamic Analysis of Multiple Building Base Isolated Structures," by P.C. Tsopelas, S. Nagarajaiah, M.C. Constantinou and A.M. Reinhorn, 5/28/91, (PB92-113885, A09, MF-A02).

NCEER-91-0015 "Evaluation of SEAOC Design Requirements for Sliding Isolated Structures," by D. Theodossiou and M.C. Constantinou, 6/10/91, (PB92-114602, A11, MF-A03).

NCEER-91-0016 "Closed-Loop Modal Testing of a 27-Story Reinforced Concrete Flat Plate-Core Building," by H.R. Somaprasad, T. Toksoy, H. Yoshiyuki and A.E. Aktan, 7/15/91, (PB92-129980, A07, MF-A02).

NCEER-91-0017 "Shake Table Test of a 1/6 Scale Two-Story Lightly Reinforced Concrete Building," by A.G. El-Attar, R.N. White and P. Gergely, 2/28/91, (PB92-222447, A06, MF-A02).

NCEER-91-0018 "Shake Table Test of a 1/8 Scale Three-Story Lightly Reinforced Concrete Building," by A.G. El-Attar, R.N. White and P. Gergely, 2/28/91, (PB93-116630, A08, MF-A02).

NCEER-91-0019 "Transfer Functions for Rigid Rectangular Foundations," by A.S. Veletsos, A.M. Prasad and W.H. Wu, 7/31/91, to be published.

NCEER-91-0020 "Hybrid Control of Seismic-Excited Nonlinear and Inelastic Structural Systems," by J.N. Yang, Z. Li and A. Danielians, 8/1/91, (PB92-143171, A06, MF-A02).

NCEER-91-0021 "The NCEER-91 Earthquake Catalog: Improved Intensity-Based Magnitudes and Recurrence Relations for U.S. Earthquakes East of New Madrid," by L. Seeber and J.G. Armbruster, 8/28/91, (PB92-176742, A06, MF-A02).

NCEER-91-0022 "Proceedings from the Implementation of Earthquake Planning and Education in Schools: The Need for Change - The Roles of the Changemakers," by K.E.K. Ross and F. Winslow, 7/23/91, (PB92-129998, A12, MF-A03).

NCEER-91-0023 "A Study of Reliability-Based Criteria for Seismic Design of Reinforced Concrete Frame Buildings," by H.H.M. Hwang and H-M. Hsu, 8/10/91, (PB92-140235, A09, MF-A02).

NCEER-91-0024 "Experimental Verification of a Number of Structural System Identification Algorithms," by R.G. Ghanem, H. Gavin and M. Shinozuka, 9/18/91, (PB92-176577, A18, MF-A04).

NCEER-91-0025 "Probabilistic Evaluation of Liquefaction Potential," by H.H.M. Hwang and C.S. Lee," 11/25/91, (PB92-143429, A05, MF-A01).

NCEER-91-0026 "Instantaneous Optimal Control for Linear, Nonlinear and Hysteretic Structures - Stable Controllers," by J.N. Yang and Z. Li, 11/15/91, (PB92-163807, A04, MF-A01).

NCEER-91-0027 "Experimental and Theoretical Study of a Sliding Isolation System for Bridges," by M.C. Constantinou, A. Kartoum, A.M. Reinhorn and P. Bradford, 11/15/91, (PB92-176973, A10, MF-A03).

NCEER-92-0001 "Case Studies of Liquefaction and Lifeline Performance During Past Earthquakes, Volume 1: Japanese Case Studies," Edited by M. Hamada and T. O'Rourke, 2/17/92, (PB92-197243, A18, MF-A04).

NCEER-92-0002 "Case Studies of Liquefaction and Lifeline Performance During Past Earthquakes, Volume 2: United States Case Studies," Edited by T. O'Rourke and M. Hamada, 2/17/92, (PB92-197250, A20, MF-A04).

NCEER-92-0003 "Issues in Earthquake Education," Edited by K. Ross, 2/3/92, (PB92-222389, A07, MF-A02).

NCEER-92-0004 "Proceedings from the First U.S. - Japan Workshop on Earthquake Protective Systems for Bridges," Edited by I.G. Buckle, 2/4/92, (PB94-142239, A99, MF-A06).

NCEER-92-0005 "Seismic Ground Motion from a Haskell-Type Source in a Multiple-Layered Half-Space," A.P. Theoharis, G. Deodatis and M. Shinozuka, 1/2/92, to be published.

NCEER-92-0006 "Proceedings from the Site Effects Workshop," Edited by R. Whitman, 2/29/92, (PB92-197201, A04, MF-A01).

NCEER-92-0007 "Engineering Evaluation of Permanent Ground Deformations Due to Seismically-Induced Liquefaction," by M.H. Baziar, R. Dobry and A-W.M. Elgamal, 3/24/92, (PB92-222421, A13, MF-A03).

NCEER-92-0008 "A Procedure for the Seismic Evaluation of Buildings in the Central and Eastern United States," by C.D. Poland and J.O. Malley, 4/2/92, (PB92-222439, A20, MF-A04).

NCEER-92-0009 "Experimental and Analytical Study of a Hybrid Isolation System Using Friction Controllable Sliding Bearings," by M.Q. Feng, S. Fujii and M. Shinozuka, 5/15/92, (PB93-150282, A06, MF-A02).

NCEER-92-0010 "Seismic Resistance of Slab-Column Connections in Existing Non-Ductile Flat-Plate Buildings," by A.J. Durrani and Y. Du, 5/18/92, (PB93-116812, A06, MF-A02).

NCEER-92-0011 "The Hysteretic and Dynamic Behavior of Brick Masonry Walls Upgraded by Ferrocement Coatings Under Cyclic Loading and Strong Simulated Ground Motion," by H. Lee and S.P. Prawel, 5/11/92, to be published.

NCEER-92-0012 "Study of Wire Rope Systems for Seismic Protection of Equipment in Buildings," by G.F. Demetriades, M.C. Constantinou and A.M. Reinhorn, 5/20/92, (PB93-116655, A08, MF-A02).

NCEER-92-0013 "Shape Memory Structural Dampers: Material Properties, Design and Seismic Testing," by P.R. Witting and F.A. Cozzarelli, 5/26/92, (PB93-116663, A05, MF-A01).

NCEER-92-0014 "Longitudinal Permanent Ground Deformation Effects on Buried Continuous Pipelines," by M.J. O'Rourke, and C. Nordberg, 6/15/92, (PB93-116671, A08, MF-A02).

NCEER-92-0015 "A Simulation Method for Stationary Gaussian Random Functions Based on the Sampling Theorem," by M. Grigoriu and S. Balopoulou, 6/11/92, (PB93-127496, A05, MF-A01).

NCEER-92-0016 "Gravity-Load-Designed Reinforced Concrete Buildings: Seismic Evaluation of Existing Construction and Detailing Strategies for Improved Seismic Resistance," by G.W. Hoffmann, S.K. Kunnath, A.M. Reinhorn and J.B. Mander, 7/15/92, (PB94-142007, A08, MF-A02).

NCEER-92-0017 "Observations on Water System and Pipeline Performance in the Limón Area of Costa Rica Due to the April 22, 1991 Earthquake," by M. O'Rourke and D. Ballantyne, 6/30/92, (PB93-126811, A06, MF-A02).

NCEER-92-0018 "Fourth Edition of Earthquake Education Materials for Grades K-12," Edited by K.E.K. Ross, 8/10/92, (PB93-114023, A07, MF-A02).

NCEER-92-0019 "Proceedings from the Fourth Japan-U.S. Workshop on Earthquake Resistant Design of Lifeline Facilities and Countermeasures for Soil Liquefaction," Edited by M. Hamada and T.D. O'Rourke, 8/12/92, (PB93-163939, A99, MF-E11).

NCEER-92-0020 "Active Bracing System: A Full Scale Implementation of Active Control," by A.M. Reinhorn, T.T. Soong, R.C. Lin, M.A. Riley, Y.P. Wang, S. Aizawa and M. Higashino, 8/14/92, (PB93-127512, A06, MF-A02).

NCEER-92-0021 "Empirical Analysis of Horizontal Ground Displacement Generated by Liquefaction-Induced Lateral Spreads," by S.F. Bartlett and T.L. Youd, 8/17/92, (PB93-188241, A06, MF-A02).

NCEER-92-0022 "IDARC Version 3.0: Inelastic Damage Analysis of Reinforced Concrete Structures," by S.K. Kunnath, A.M. Reinhorn and R.F. Lobo, 8/31/92, (PB93-227502, A07, MF-A02).

NCEER-92-0023 "A Semi-Empirical Analysis of Strong-Motion Peaks in Terms of Seismic Source, Propagation Path and Local Site Conditions, by M. Kamiyama, M.J. O'Rourke and R. Flores-Berrones, 9/9/92, (PB93-150266, A08, MF-A02).

NCEER-92-0024 "Seismic Behavior of Reinforced Concrete Frame Structures with Nonductile Details, Part I: Summary of Experimental Findings of Full Scale Beam-Column Joint Tests," by A. Beres, R.N. White and P. Gergely, 9/30/92, (PB93-227783, A05, MF-A01).

NCEER-92-0025 "Experimental Results of Repaired and Retrofitted Beam-Column Joint Tests in Lightly Reinforced Concrete Frame Buildings," by A. Beres, S. El-Borgi, R.N. White and P. Gergely, 10/29/92, (PB93-227791, A05, MF-A01).

NCEER-92-0026 "A Generalization of Optimal Control Theory: Linear and Nonlinear Structures," by J.N. Yang, Z. Li and S. Vongchavalitkul, 11/2/92, (PB93-188621, A05, MF-A01).

NCEER-92-0027 "Seismic Resistance of Reinforced Concrete Frame Structures Designed Only for Gravity Loads: Part I - Design and Properties of a One-Third Scale Model Structure," by J.M. Bracci, A.M. Reinhorn and J.B. Mander, 12/1/92, (PB94-104502, A08, MF-A02).

NCEER-92-0028 "Seismic Resistance of Reinforced Concrete Frame Structures Designed Only for Gravity Loads: Part II - Experimental Performance of Subassemblages," by L.E. Aycardi, J.B. Mander and A.M. Reinhorn, 12/1/92, (PB94-104510, A08, MF-A02).

NCEER-92-0029 "Seismic Resistance of Reinforced Concrete Frame Structures Designed Only for Gravity Loads: Part III - Experimental Performance and Analytical Study of a Structural Model," by J.M. Bracci, A.M. Reinhorn and J.B. Mander, 12/1/92, (PB93-227528, A09, MF-A01).

NCEER-92-0030 "Evaluation of Seismic Retrofit of Reinforced Concrete Frame Structures: Part I - Experimental Performance of Retrofitted Subassemblages," by D. Choudhuri, J.B. Mander and A.M. Reinhorn, 12/8/92, (PB93-198307, A07, MF-A02).

NCEER-92-0031 "Evaluation of Seismic Retrofit of Reinforced Concrete Frame Structures: Part II - Experimental Performance and Analytical Study of a Retrofitted Structural Model," by J.M. Bracci, A.M. Reinhorn and J.B. Mander, 12/8/92, (PB93-198315, A09, MF-A03).

NCEER-92-0032 "Experimental and Analytical Investigation of Seismic Response of Structures with Supplemental Fluid Viscous Dampers," by M.C. Constantinou and M.D. Symans, 12/21/92, (PB93-191435, A10, MF-A03).

NCEER-92-0033 "Reconnaissance Report on the Cairo, Egypt Earthquake of October 12, 1992," by M. Khater, 12/23/92, (PB93-188621, A03, MF-A01).

NCEER-92-0034 "Low-Level Dynamic Characteristics of Four Tall Flat-Plate Buildings in New York City," by H. Gavin, S. Yuan, J. Grossman, E. Pekelis and K. Jacob, 12/28/92, (PB93-188217, A07, MF-A02).

NCEER-93-0001 "An Experimental Study on the Seismic Performance of Brick-Infilled Steel Frames With and Without Retrofit," by J.B. Mander, B. Nair, K. Wojtkowski and J. Ma, 1/29/93, (PB93-227510, A07, MF-A02).

NCEER-93-0002 "Social Accounting for Disaster Preparedness and Recovery Planning," by S. Cole, E. Pantoja and V. Razak, 2/22/93, (PB94-142114, A12, MF-A03).

NCEER-93-0003 "Assessment of 1991 NEHRP Provisions for Nonstructural Components and Recommended Revisions," by T.T. Soong, G. Chen, Z. Wu, R-H. Zhang and M. Grigoriu, 3/1/93, (PB93-188639, A06, MF-A02).

NCEER-93-0004 "Evaluation of Static and Response Spectrum Analysis Procedures of SEAOC/UBC for Seismic Isolated Structures," by C.W. Winters and M.C. Constantinou, 3/23/93, (PB93-198299, A10, MF-A03).

NCEER-93-0005 "Earthquakes in the Northeast - Are We Ignoring the Hazard? A Workshop on Earthquake Science and Safety for Educators," edited by K.E.K. Ross, 4/2/93, (PB94-103066, A09, MF-A02).

NCEER-93-0006 "Inelastic Response of Reinforced Concrete Structures with Viscoelastic Braces," by R.F. Lobo, J.M. Bracci, K.L. Shen, A.M. Reinhorn and T.T. Soong, 4/5/93, (PB93-227486, A05, MF-A02).

NCEER-93-0007 "Seismic Testing of Installation Methods for Computers and Data Processing Equipment," by K. Kosar, T.T. Soong, K.L. Shen, J.A. HoLung and Y.K. Lin, 4/12/93, (PB93-198299, A07, MF-A02).

NCEER-93-0008 "Retrofit of Reinforced Concrete Frames Using Added Dampers," by A. Reinhorn, M. Constantinou and C. Li, to be published.

NCEER-93-0009 "Seismic Behavior and Design Guidelines for Steel Frame Structures with Added Viscoelastic Dampers," by K.C. Chang, M.L. Lai, T.T. Soong, D.S. Hao and Y.C. Yeh, 5/1/93, (PB94-141959, A07, MF-A02).

NCEER-93-0010 "Seismic Performance of Shear-Critical Reinforced Concrete Bridge Piers," by J.B. Mander, S.M. Waheed, M.T.A. Chaudhary and S.S. Chen, 5/12/93, (PB93-227494, A08, MF-A02).

NCEER-93-0011 "3D-BASIS-TABS: Computer Program for Nonlinear Dynamic Analysis of Three Dimensional Base Isolated Structures," by S. Nagarajaiah, C. Li, A.M. Reinhorn and M.C. Constantinou, 8/2/93, (PB94-141819, A09, MF-A02).

NCEER-93-0012 "Effects of Hydrocarbon Spills from an Oil Pipeline Break on Ground Water," by O.J. Helweg and H.H.M. Hwang, 8/3/93, (PB94-141942, A06, MF-A02).

NCEER-93-0013 "Simplified Procedures for Seismic Design of Nonstructural Components and Assessment of Current Code Provisions," by M.P. Singh, L.E. Suarez, E.E. Matheu and G.O. Maldonado, 8/4/93, (PB94-141827, A09, MF-A02).

NCEER-93-0014 "An Energy Approach to Seismic Analysis and Design of Secondary Systems," by G. Chen and T.T. Soong, 8/6/93, (PB94-142767, A11, MF-A03).

NCEER-93-0015 "Proceedings from School Sites: Becoming Prepared for Earthquakes - Commemorating the Third Anniversary of the Loma Prieta Earthquake," Edited by F.E. Winslow and K.E.K. Ross, 8/16/93, (PB94-154275, A16, MF-A02).

NCEER-93-0016 "Reconnaissance Report of Damage to Historic Monuments in Cairo, Egypt Following the October 12, 1992 Dahshur Earthquake," by D. Sykora, D. Look, G. Croci, E. Karaesmen and E. Karaesmen, 8/19/93, (PB94-142221, A08, MF-A02).

NCEER-93-0017 "The Island of Guam Earthquake of August 8, 1993," by S.W. Swan and S.K. Harris, 9/30/93, (PB94-141843, A04, MF-A01).

NCEER-93-0018 "Engineering Aspects of the October 12, 1992 Egyptian Earthquake," by A.W. Elgamal, M. Amer, K. Adalier and A. Abul-Fadl, 10/7/93, (PB94-141983, A05, MF-A01).

NCEER-93-0019 "Development of an Earthquake Motion Simulator and its Application in Dynamic Centrifuge Testing," by I. Krstelj, Supervised by J.H. Prevost, 10/23/93, (PB94-181773, A-10, MF-A03).

NCEER-93-0020 "NCEER-Taisei Corporation Research Program on Sliding Seismic Isolation Systems for Bridges: Experimental and Analytical Study of a Friction Pendulum System (FPS)," by M.C. Constantinou, P. Tsopelas, Y-S. Kim and S. Okamoto, 11/1/93, (PB94-142775, A08, MF-A02).

NCEER-93-0021 "Finite Element Modeling of Elastomeric Seismic Isolation Bearings," by L.J. Billings, Supervised by R. Shepherd, 11/8/93, to be published.

NCEER-93-0022 "Seismic Vulnerability of Equipment in Critical Facilities: Life-Safety and Operational Consequences," by K. Porter, G.S. Johnson, M.M. Zadeh, C. Scawthorn and S. Eder, 11/24/93, (PB94-181765, A16, MF-A03).

NCEER-93-0023 "Hokkaido Nansei-oki, Japan Earthquake of July 12, 1993, by P.I. Yanev and C.R. Scawthorn, 12/23/93, (PB94-181500, A07, MF-A01).

NCEER-94-0001 "An Evaluation of Seismic Serviceability of Water Supply Networks with Application to the San Francisco Auxiliary Water Supply System," by I. Markov, Supervised by M. Grigoriu and T. O'Rourke, 1/21/94, (PB94-204013, A07, MF-A02).

NCEER-94-0002 "NCEER-Taisei Corporation Research Program on Sliding Seismic Isolation Systems for Bridges: Experimental and Analytical Study of Systems Consisting of Sliding Bearings, Rubber Restoring Force Devices and Fluid Dampers," Volumes I and II, by P. Tsopelas, S. Okamoto, M.C. Constantinou, D. Ozaki and S. Fujii, 2/4/94, (PB94-181740, A09, MF-A02 and PB94-181757, A12, MF-A03).

NCEER-94-0003 "A Markov Model for Local and Global Damage Indices in Seismic Analysis," by S. Rahman and M. Grigoriu, 2/18/94, (PB94-206000, A12, MF-A03).

NCEER-94-0004 "Proceedings from the NCEER Workshop on Seismic Response of Masonry Infills," edited by D.P. Abrams, 3/1/94, (PB94-180783, A07, MF-A02).

NCEER-94-0005 "The Northridge, California Earthquake of January 17, 1994: General Reconnaissance Report," edited by J.D. Goltz, 3/11/94, (PB193943, A10, MF-A03).

NCEER-94-0006 "Seismic Energy Based Fatigue Damage Analysis of Bridge Columns: Part I - Evaluation of Seismic Capacity," by G.A. Chang and J.B. Mander, 3/14/94, (PB94-219185, A11, MF-A03).

NCEER-94-0007 "Seismic Isolation of Multi-Story Frame Structures Using Spherical Sliding Isolation Systems," by T.M. Al-Hussaini, V.A. Zayas and M.C. Constantinou, 3/17/94, (PB193745, A09, MF-A02).

NCEER-94-0008 "The Northridge, California Earthquake of January 17, 1994: Performance of Highway Bridges," edited by I.G. Buckle, 3/24/94, (PB94-193851, A06, MF-A02).

NCEER-94-0009 "Proceedings of the Third U.S.-Japan Workshop on Earthquake Protective Systems for Bridges," edited by I.G. Buckle and I. Friedland, 3/31/94, (PB94-195815, A99, MF-A06).

NCEER-94-0010 "3D-BASIS-ME: Computer Program for Nonlinear Dynamic Analysis of Seismically Isolated Single and Multiple Structures and Liquid Storage Tanks," by P.C. Tsopelas, M.C. Constantinou and A.M. Reinhorn, 4/12/94, (PB94-204922, A09, MF-A02).

NCEER-94-0011 "The Northridge, California Earthquake of January 17, 1994: Performance of Gas Transmission Pipelines," by T.D. O'Rourke and M.C. Palmer, 5/16/94, (PB94-204989, A05, MF-A01).

NCEER-94-0012 "Feasibility Study of Replacement Procedures and Earthquake Performance Related to Gas Transmission Pipelines," by T.D. O'Rourke and M.C. Palmer, 5/25/94, (PB94-206638, A09, MF-A02).

NCEER-94-0013 "Seismic Energy Based Fatigue Damage Analysis of Bridge Columns: Part II - Evaluation of Seismic Demand," by G.A. Chang and J.B. Mander, 6/1/94, (PB95-18106, A08, MF-A02).

NCEER-94-0014 "NCEER-Taisei Corporation Research Program on Sliding Seismic Isolation Systems for Bridges: Experimental and Analytical Study of a System Consisting of Sliding Bearings and Fluid Restoring Force/Damping Devices," by P. Tsopelas and M.C. Constantinou, 6/13/94, (PB94-219144, A10, MF-A03).

NCEER-94-0015 "Generation of Hazard-Consistent Fragility Curves for Seismic Loss Estimation Studies," by H. Hwang and J-R. Huo, 6/14/94, (PB95-181996, A09, MF-A02).

NCEER-94-0016 "Seismic Study of Building Frames with Added Energy-Absorbing Devices," by W.S. Pong, C.S. Tsai and G.C. Lee, 6/20/94, (PB94-219136, A10, A03).

NCEER-94-0017 "Sliding Mode Control for Seismic-Excited Linear and Nonlinear Civil Engineering Structures," by J. Yang, J. Wu, A. Agrawal and Z. Li, 6/21/94, (PB95-138483, A06, MF-A02).

NCEER-94-0018 "3D-BASIS-TABS Version 2.0: Computer Program for Nonlinear Dynamic Analysis of Three Dimensional Base Isolated Structures," by A.M. Reinhorn, S. Nagarajaiah, M.C. Constantinou, P. Tsopelas and R. Li, 6/22/94, (PB95-182176, A08, MF-A02).

NCEER-94-0019 "Proceedings of the International Workshop on Civil Infrastructure Systems: Application of Intelligent Systems and Advanced Materials on Bridge Systems," Edited by G.C. Lee and K.C. Chang, 7/18/94, (PB95-252474, A20, MF-A04).

NCEER-94-0020 "Study of Seismic Isolation Systems for Computer Floors," by V. Lambrou and M.C. Constantinou, 7/19/94, (PB95-138533, A10, MF-A03).

NCEER-94-0021 "Proceedings of the U.S.-Italian Workshop on Guidelines for Seismic Evaluation and Rehabilitation of Unreinforced Masonry Buildings," Edited by D.P. Abrams and G.M. Calvi, 7/20/94, (PB95-138749, A13, MF-A03).

NCEER-94-0022 "NCEER-Taisei Corporation Research Program on Sliding Seismic Isolation Systems for Bridges: Experimental and Analytical Study of a System Consisting of Lubricated PTFE Sliding Bearings and Mild Steel Dampers," by P. Tsopelas and M.C. Constantinou, 7/22/94, (PB95-182184, A08, MF-A02).

NCEER-94-0023 "Development of Reliability-Based Design Criteria for Buildings Under Seismic Load," by Y.K. Wen, H. Hwang and M. Shinozuka, 8/1/94, (PB95-211934, A08, MF-A02).

NCEER-94-0024 "Experimental Verification of Acceleration Feedback Control Strategies for an Active Tendon System," by S.J. Dyke, B.F. Spencer, Jr., P. Quast, M.K. Sain, D.C. Kaspari, Jr. and T.T. Soong, 8/29/94, (PB95-212320, A05, MF-A01).

NCEER-94-0025 "Seismic Retrofitting Manual for Highway Bridges," Edited by I.G. Buckle and I.F. Friedland, published by the Federal Highway Administration (PB95-212676, A15, MF-A03).

NCEER-94-0026 "Proceedings from the Fifth U.S.-Japan Workshop on Earthquake Resistant Design of Lifeline Facilities and Countermeasures Against Soil Liquefaction," Edited by T.D. O'Rourke and M. Hamada, 11/7/94, (PB95-220802, A99, MF-E08).

NCEER-95-0001 "Experimental and Analytical Investigation of Seismic Retrofit of Structures with Supplemental Damping: Part 1 - Fluid Viscous Damping Devices," by A.M. Reinhorn, C. Li and M.C. Constantinou, 1/3/95, (PB95-266599, A09, MF-A02).

NCEER-95-0002 "Experimental and Analytical Study of Low-Cycle Fatigue Behavior of Semi-Rigid Top-And-Seat Angle Connections," by G. Pekcan, J.B. Mander and S.S. Chen, 1/5/95, (PB95-220042, A07, MF-A02).

NCEER-95-0003 "NCEER-ATC Joint Study on Fragility of Buildings," by T. Anagnos, C. Rojahn and A.S. Kiremidjian, 1/20/95, (PB95-220026, A06, MF-A02).

NCEER-95-0004 "Nonlinear Control Algorithms for Peak Response Reduction," by Z. Wu, T.T. Soong, V. Gattulli and R.C. Lin, 2/16/95, (PB95-220349, A05, MF-A01).

NCEER-95-0005 "Pipeline Replacement Feasibility Study: A Methodology for Minimizing Seismic and Corrosion Risks to Underground Natural Gas Pipelines," by R.T. Eguchi, H.A. Seligson and D.G. Honegger, 3/2/95, (PB95-252326, A06, MF-A02).

NCEER-95-0006 "Evaluation of Seismic Performance of an 11-Story Frame Building During the 1994 Northridge Earthquake," by F. Naeim, R. DiSulio, K. Benuska, A. Reinhorn and C. Li, to be published.

NCEER-95-0007 "Prioritization of Bridges for Seismic Retrofitting," by N. Basöz and A.S. Kiremidjian, 4/24/95, (PB95-252300, A08, MF-A02).

NCEER-95-0008 "Method for Developing Motion Damage Relationships for Reinforced Concrete Frames," by A. Singhal and A.S. Kiremidjian, 5/11/95, (PB95-266607, A06, MF-A02).

NCEER-95-0009 "Experimental and Analytical Investigation of Seismic Retrofit of Structures with Supplemental Damping: Part II - Friction Devices," by C. Li and A.M. Reinhorn, 7/6/95, (PB96-128087, A11, MF-A03).

NCEER-95-0010 "Experimental Performance and Analytical Study of a Non-Ductile Reinforced Concrete Frame Structure Retrofitted with Elastomeric Spring Dampers," by G. Pekcan, J.B. Mander and S.S. Chen, 7/14/95, (PB96-137161, A08, MF-A02).

NCEER-95-0011 "Development and Experimental Study of Semi-Active Fluid Damping Devices for Seismic Protection of Structures," by M.D. Symans and M.C. Constantinou, 8/3/95, (PB96-136940, A23, MF-A04).

NCEER-95-0012 "Real-Time Structural Parameter Modification (RSPM): Development of Innervated Structures," by Z. Liang, M. Tong and G.C. Lee, 4/11/95, (PB96-137153, A06, MF-A01).

NCEER-95-0013 "Experimental and Analytical Investigation of Seismic Retrofit of Structures with Supplemental Damping: Part III - Viscous Damping Walls," by A.M. Reinhorn and C. Li, 10/1/95, (PB96-176409, A11, MF-A03).

NCEER-95-0014 "Seismic Fragility Analysis of Equipment and Structures in a Memphis Electric Substation," by J-R. Huo and H.H.M. Hwang, (PB96-128087, A09, MF-A02), 8/10/95.

NCEER-95-0015 "The Hanshin-Awaji Earthquake of January 17, 1995: Performance of Lifelines," Edited by M. Shinozuka, 11/3/95, (PB96-176383, A15, MF-A03).

NCEER-95-0016 "Highway Culvert Performance During Earthquakes," by T.L. Youd and C.J. Beckman, available as NCEER-96-0015.

NCEER-95-0017 "The Hanshin-Awaji Earthquake of January 17, 1995: Performance of Highway Bridges," Edited by I.G. Buckle, 12/1/95, to be published.

NCEER-95-0018 "Modeling of Masonry Infill Panels for Structural Analysis," by A.M. Reinhorn, A. Madan, R.E. Valles, Y. Reichmann and J.B. Mander, 12/8/95.

NCEER-95-0019 "Optimal Polynomial Control for Linear and Nonlinear Structures," by A.K. Agrawal and J.N. Yang, 12/11/95, (PB96-168737, A07, MF-A02).

NCEER-95-0020 "Retrofit of Non-Ductile Reinforced Concrete Frames Using Friction Dampers," by R.S. Rao, P. Gergely and R.N. White, 12/22/95, (PB97-133508, A10, MF-A02).

NCEER-95-0021 "Parametric Results for Seismic Response of Pile-Supported Bridge Bents," by G. Mylonakis, A. Nikolaou and G. Gazetas, 12/22/95, (PB97-100242, A12, MF-A03).

NCEER-95-0022 "Kinematic Bending Moments in Seismically Stressed Piles," by A. Nikolaou, G. Mylonakis and G. Gazetas, 12/23/95.

NCEER-96-0001 "Dynamic Response of Unreinforced Masonry Buildings with Flexible Diaphragms," by A.C. Costley and D.P. Abrams," 10/10/96.

NCEER-96-0002 "State of the Art Review: Foundations and Retaining Structures," by I. Po Lam, to be published.

NCEER-96-0003 "Ductility of Rectangular Reinforced Concrete Bridge Columns with Moderate Confinement," by N. Wehbe, M. Saiidi, D. Sanders and B. Douglas, 11/7/96, (PB97-133557, A06, MF-A02).

NCEER-96-0004 "Proceedings of the Long-Span Bridge Seismic Research Workshop," edited by I.G. Buckle and I.M. Friedland, to be published.

NCEER-96-0005 "Establish Representative Pier Types for Comprehensive Study: Eastern United States," by J. Kulicki and Z. Prucz, 5/28/96.

NCEER-96-0006 "Establish Representative Pier Types for Comprehensive Study: Western United States," by R. Imbsen, R.A. Schamber and T.A. Osterkamp, 5/28/96.

NCEER-96-0007 "Nonlinear Control Techniques for Dynamical Systems with Uncertain Parameters," by R.G. Ghanem and M.I. Bujakov, 5/27/96, (PB97-100259, A17, MF-A03).

NCEER-96-0008 "Seismic Evaluation of a 30-Year Old Non-Ductile Highway Bridge Pier and Its Retrofit," by J.B. Mander, B. Mahmoodzadegan, S. Bhadra and S.S. Chen, 5/31/96.

NCEER-96-0009 "Seismic Performance of a Model Reinforced Concrete Bridge Pier Before and After Retrofit," by J.B. Mander, J.H. Kim and C.A. Ligozio, 5/31/96.

NCEER-96-0010 "IDARC2D Version 4.0: A Computer Program for the Inelastic Damage Analysis of Buildings," by R.E. Valles, A.M. Reinhorn, S.K. Kunnath, C. Li and A. Madan, 6/3/96, (PB97-100234, A17, MF-A03).

NCEER-96-0011 "Estimation of the Economic Impact of Multiple Lifeline Disruption: Memphis Light, Gas and Water Division Case Study," by S.E. Chang, H.A. Seligson and R.T. Eguchi, 8/16/96, (PB97-133490, A11, MF-A03).

NCEER-96-0012 "Proceedings from the Sixth Japan-U.S. Workshop on Earthquake Resistant Design of Lifeline Facilities and Countermeasures Against Soil Liquefaction, Edited by M. Hamada and T. O'Rourke, 9/11/96, (PB97-133581, A99, MF-A06).

NCEER-96-0013 "Chemical Hazards, Mitigation and Preparedness in Areas of High Seismic Risk: A Methodology for Estimating the Risk of Post-Earthquake Hazardous Materials Release," by H.A. Seligson, R.T. Eguchi, K.J. Tierney and K. Richmond, 11/7/96.

NCEER-96-0014 "Response of Steel Bridge Bearings to Reversed Cyclic Loading," by J.B. Mander, D-K. Kim, S.S. Chen and G.J. Premus, 11/13/96, (PB97-140735, A12, MF-A03).

NCEER-96-0015 "Highway Culvert Performance During Past Earthquakes," by T.L. Youd and C.J. Beckman, 11/25/96, (PB97-133532, A06, MF-A01).

NCEER-97-0001 "Evaluation, Prevention and Mitigation of Pounding Effects in Building Structures," by R.E. Valles and A.M. Reinhorn, 2/20/97, (PB97-159552, A14, MF-A03).

NCEER-97-0002 "Seismic Design Criteria for Bridges and Other Highway Structures," by C. Rojahn, R. Mayes, D.G. Anderson, J. Clark, J.H. Hom, R.V. Nutt and M.J. O'Rourke, 4/30/97, (PB97-194658, A06, MF-A03).

NCEER-97-0003 "Proceedings of the U.S.-Italian Workshop on Seismic Evaluation and Retrofit," Edited by D.P. Abrams and G.M. Calvi, 3/19/97, (PB97-194666, A13, MF-A03).

NCEER-97-0004 "Investigation of Seismic Response of Buildings with Linear and Nonlinear Fluid Viscous Dampers," by A.A. Seleemah and M.C. Constantinou, 5/21/97, (PB98-109002, A15, MF-A03).

NCEER-97-0005 "Proceedings of the Workshop on Earthquake Engineering Frontiers in Transportation Facilities," edited by G.C. Lee and I.M. Friedland, 8/29/97, (PB98-128911, A25, MR-A04).

NCEER-97-0006 "Cumulative Seismic Damage of Reinforced Concrete Bridge Piers," by S.K. Kunnath, A. El-Bahy, A. Taylor and W. Stone, 9/2/97, (PB98-108814, A11, MF-A03).

NCEER-97-0007 "Structural Details to Accommodate Seismic Movements of Highway Bridges and Retaining Walls," by R.A. Imbsen, R.A. Schamber, E. Thorkildsen, A. Kartoum, B.T. Martin, T.N. Rosser and J.M. Kulicki, 9/3/97.

NCEER-97-0008 "A Method for Earthquake Motion-Damage Relationships with Application to Reinforced Concrete Frames," by A. Singhal and A.S. Kiremidjian, 9/10/97, (PB98-108988, A13, MF-A03).

NCEER-97-0009 "Seismic Analysis and Design of Bridge Abutments Considering Sliding and Rotation," by K. Fishman and R. Richards, Jr., 9/15/97, (PB98-108897, A06, MF-A02).

NCEER-97-0010 "Proceedings of the FHWA/NCEER Workshop on the National Representation of Seismic Ground Motion for New and Existing Highway Facilities," edited by I.M. Friedland, M.S. Power and R.L. Mayes, 9/22/97.

NCEER-97-0011 "Seismic Analysis for Design or Retrofit of Gravity Bridge Abutments," by K.L. Fishman, R. Richards, Jr. and R.C. Divito, 10/2/97, (PB98-128937, A08, MF-A02).

NCEER-97-0012 "Evaluation of Simplified Methods of Analysis for Yielding Structures," by P. Tsopelas, M.C. Constantinou, C.A. Kircher and A.S. Whittaker, 10/31/97, (PB98-128929, A10, MF-A03).

NCEER-97-0013 "Seismic Design of Bridge Columns Based on Control and Repairability of Damage," by C-T. Cheng and J.B. Mander, 12/8/97.

NCEER-97-0014 "Seismic Resistance of Bridge Piers Based on Damage Avoidance Design," by J.B. Mander and C-T. Cheng, 12/10/97.

NCEER-97-0015 "Seismic Response of Nominally Symmetric Systems with Strength Uncertainty," by S. Balopoulou and M. Grigoriu, 12/23/97.

NCEER-97-0016 "Evaluation of Seismic Retrofit Methods for Reinforced Concrete Bridge Columns," by T.J. Wipf, F.W. Klaiber and F.M. Russo, 12/28/97.

NCEER-97-0017 "Seismic Fragility of Existing Conventional Reinforced Concrete Highway Bridges," by C.L. Mullen and A.S. Cakmak, 12/30/97.

NCEER-97-0018 "Loss Asssessment of Memphis Buildings," edited by D.P. Abrams and M. Shinozuka, 12/31/97.

NCEER-97-0019 "Seismic Evaluation of Frames with Infill Walls Using Quasi-static Experiments," by K.M. Mosalam, R.N. White and P. Gergely, 12/31/97.

NCEER-97-0020 "Seismic Evaluation of Frames with Infill Walls Using Pseudo-dynamic Experiments," by K.M. Mosalam, R.N. White and P. Gergely, 12/31/97.

NCEER-97-0021 "Computational Strategies for Frames with Infill Walls: Discrete and Smeared Crack Analyses and Seismic Fragility," by K.M. Mosalam, R.N. White and P. Gergely, 12/31/97.

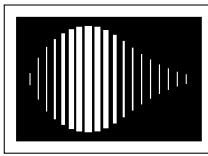

NATIONAL CENTER FOR EARTHQUAKE ENGINEERING RESEARCH

Headquartered at the State University of New York at Buffalo

State University of New York at Buffalo
Red Jacket Quadrangle
Buffalo, New York 14261
Telephone: 716/645-3391
FAX: 716/645-3399

ISSN 1088-3800